# Functional Studies of Genetic Variants in *TRPM7* and *AKAP9* – Two Candidate Genes for Stillbirth

**Mr James Cartwright**

A thesis submitted to Queen Mary University of London (Barts and the London School of Medicine and Dentistry) in partial fulfilment of the requirements for the degree of Doctor of Philosophy

CLINICAL PHARMACOLOGY,
WILLIAM HARVEY RESEARCH INSTITUTE,
BARTS AND THE LONDON SCHOOL OF MEDICINE AND DENTISTRY
CHARTERHOUSE SQUARE, LONDON EC1M 6BQ

I, James Cartwright, confirm that the research included within this thesis is my own work or that where it has been carried out in collaboration with, or supported by others, that this is duly acknowledged below and my contribution indicated. Previously published material is also acknowledged below.

I attest that I have exercised reasonable care to ensure that the work is original, and does not to the best of my knowledge break any UK law, infringe any third party's copyright or other Intellectual Property Right, or contain any confidential material.

I accept that the College has the right to use plagiarism detection software to check the electronic version of the thesis.

I confirm that this thesis has not been previously submitted for the award of a degree by this or any other university.



Signature: James Cartwright

Date: 18th of June 2018

# Abstract

For every 200 births in the UK, one will end in a stillbirth. Stillbirth is classified as a baby born dead after 24 weeks gestation. Mutations in genes that cause ion channelopathies are known to cause sudden cardiac death in adults and children. Prenatal diagnosis of LQT has been possible for decades, creating a disease spectrum where channelopathies may fatally influence pregnancy. We sequenced 35 candidate genes in 70 unexplained stillbirth cases. Thirty-nine cases harboured a predicted damaging protein missense variant. Two novel and two rare variants were observed in the transient receptor potential melastatin 7 (*TRPM7*) gene and five rare genetic variants were found in A-kinase anchor protein 9 (*AKAP9*). The aim of this PhD was to perform functional studies of these variants in *TRPM7* and *AKAP9*.

TRPM7 is an ion channel indispensable for mouse cardiogenesis. Two TRPM7 variants (p.G179V and p.T860M) showed significantly reduced current compared to wild-type channels. Conversely, cells expressing p.R494Q TRPM7, had a significant increase in current compared to WT channels, but only in CHO-K1 cells. Western blot analyses failed to detect full length TRPM7 in cells transfected with either p.G179V or p.T860M compared to wild-type expressing cells. Proteosomal inhibition using MG132 produced a small but visible band in p.T860M transfected cells. Expression of TRPM7 in iPSC-derived cardiomyocytes increases during cell maturation, and TRPM7-like current was measured in 20-23 day old cardiomyocytes.

AKAP9 is required to couple adrenergic stimulation in the heart with faster cardiac repolarisation. Cells expressing WT AKAP9 alongside the KCNQ1/KCNE1 potassium channel responded to β-adrenergic stimulation, however those transfected with p.A3043T AKAP9 did not respond to treatment with forskolin.

Our analyses supports two deleterious variants in *TRPM7* and one in *AKAP9* in unexplained stillbirth cases. These heterozygous variants could lead to haploinsufficiency and may be a cause of stillbirth.

# Table of Contents

# Acknowledgements

Foremost, my thanks are due to Professors Patricia Munroe & Andrew Tinker. Their insight, guidance and attention to detail has been a constant driving force for me throughout this thesis, and I am grateful for all the advice and help they have given me. Their willingness to always provide me with critical feedback will ensure I remember the differences between TRPM7 and *TRPM7*, and outward and inward rectifiers, hopefully.

Next, I give my thanks to the trio of Qadeer 'boss' Aziz, Stephen Harmer and Kate 'the boss' Witkowska. I truly appreciate their aid and patience during the experimental work of my PhD; few are the students with such fine advisors and colleagues. Both the Tinker and Munroe laboratories have been a fantastic group of scientists to work with on a daily basis – you have my thanks for every conversation had, reagent lent and technique taught.

To Jane, Kasia, Jamie and Emily, you were great housemates for the last four years, and I will not forget our fantastic times together. Natalie, to be with someone who volunteers to read this thesis, I am a very, very fortunate soul. Without you I am not sure how far I would have gotten in this entire endeavour – thank you.

Lastly, the British Heart Foundation charity have my sincere gratitude for the funding provided throughout my MRes and PhD project (Grant MCPG1J3R), which made this work possible.

# Abbreviations

| | |
|---|---|
| 1000G | 1000 Genomes Project |
| A | Amperes |
| AKAP9 | A-Kinase Anchoring Protein 9 |
| APD | Action Potential Duration |
| ARVC | Arrhythmogenic Right Ventricular Cardiomyopathy |
| BRS | Brugada Syndrome |
| CAD | Coronary Artery Disease |
| CHF | Congestive Heart Failure |
| CHO-K1 | Chinese Hamster Ovary K1 Cell Line |
| CICUS | Cardiac Ion Channelopathies in Unexplained Stillbirth |
| CPVT | Catecholaminergic Polymorphic Ventricular Tachycardia |
| CREBBP | cAMP Response Element Binding Protein - Binding Protein |
| ECG | Electrocardiogram |
| ERS | Early Repolarisation Syndrome |
| ESP6500 | NHLBI GO Exome Sequencing Project |
| ExAC | Exome Aggregation Consortium |
| GPCR | G-Protein Coupled Receptor |
| GWAS | Genome-Wide Association Study |
| HDF | Human Dermal Fibroblast |
| HEK293 | Human Embryonic Kidney 293 Cell Line |
| ICCD | Isolated Cardiac Conduction Defect |
| IKr | Rapid Delayed Rectifier Potassium Current |
| IKs | Slow Delayed Rectifier Potassium Current |
| iPSC | Induced Pluripotent Stem Cell |

| | |
|---|---|
| I-V | Current-Voltage |
| JLNS | Jervell and Lange-Nielsen syndrome |
| KCNE1 | Potassium Voltage-Gated Channel Subfamily E Regulatory Subunit 1 |
| KCNQ1 | Potassium Voltage-Gated Channel Subfamily Q Member 1 |
| LJP | Liquid Junction Potential |
| LQT(S) | Long QT (Syndrome) |
| MEF | Mouse Embryonic Fibroblasts |
| MI | Myocardial Infarction |
| pA | Picoamp |
| pF | Picofarad |
| PVDF | Polyvinylidene Fluoride |
| SCA | Sudden Cardiac Arrest |
| SCD | Sudden Cardiac Death |
| SDS | Sodium Dodecyl Sulfate |
| SIDS | Sudden Infant Death Syndrome |
| SQTS | Short QT Syndrome |
| SR | Sarcoplasmic Reticulum |
| SUD | Sudden Unexplained Death |
| TRPM7 | Transient Receptor Potential Melastatin 7 |
| V | Volts / Voltage |
| VF | Ventricular Fibrillation |
| WT | Wild-Type |

# List of Figures

# List of Tables

# 1 Introduction

## 1.1 Stillbirth

Over the past few decades there has been a remarkable shift in healthcare policy aimed at improving the outcome of pregnancies across the world. This involved increasing attention to maternal mortality, neonatal survival and the causes of death in children [1-3]. An approach which has received less attention however, is investigation into the causes of child loss before birth. Stillbirth is a foetal death at or later than 22 weeks of gestation. It is surprisingly common even in the developed world; in the UK there were 4.64 stillbirths per 1000 total births reported in 2013 [4]. More than 1 in every 200 births in the US ends with stillbirth despite highly-rated levels of antenatal care [5].

### 1.1.1 Epidemiology

Across the globe, there is a wide range of stillbirth rates; in countries with less antenatal care or little drive to reduce stillbirth the occurrence is alarmingly high [6]. In middle- and low-income countries recent analysis of stillbirth occurrence estimated a total of 2.6 million stillbirths in 2015, with only 2% occurring in high income countries [7]. Over half of stillbirths occur in rural sub-Saharan Africa and South Asia where in 2008 there were 29.0 and 26.7 stillbirths per 1000 births, respectively [6]. Of almost four million live births in China between 2012 and 2014 there were 37,855 stillbirths, equating to 8.8 per 1000 births [8].

### 1.1.2 Causes of Stillbirth

There have been numerous studies investigating known, probable and possible causes of stillbirth alongside work to discover factors that increase risk [9-13]. Current data produce an unclear picture, not least because of the disparate reporting methods used by clinicians to report

stillbirths. Over 30 different systems have been used to classify the causes of stillbirth, prompting Flenady et al. to test the performance of the six most robust and well known [14]. Analysis of 857 stillbirth cases across 7 countries showed significant differences in how they were classified. The 'Wigglesworth' criteria giving 50.2% as unexplained against the most stringent, CODAC, that reported 9.5%. These classification systems corroborate clinical findings, other relevant conditions and placental pathology to produce a verdict on the cause of death. The most commonly identified causes of stillbirth are obstetric complications, placental disease, genetic anomalies, umbilical cord accidents, foetal and maternal haemorrhage and infection [9,15,16].

In 2011, Bukowski et al. reported complete post-mortem examinations in 512 cases and were able to find possible causes in 390 (70%) of these, with some having more than one possible cause (Figure 1.1 & Table 1.1) [9]. The two most common causes were obstetric complications and placental insufficiency accounting for 29.3% and 23.6%, respectively.

Bukowski et al. classified all intrapartum stillbirths (occurred during delivery) as obstetric complications, which including placental abruption, multiple gestations and cervical insufficiency. An abruption occurs when the placenta separates from the uterus, leading to vaginal bleeding and abdominal pain. The higher the degree of separation, the more likely foetal demise [17]. Placental insufficiency is a progressive deterioration of function over time, leading to reduced transfer of oxygen and nutrients to the foetus [18]. This leads to growth restriction, perturbing the development of multiple organs. Genetic causes of stillbirth can include chromosomal monosomy or trisomy, while structural abnormalities denote a malformed foetus. Multiple complications can be attributed to a cord anomaly, including cord entrapment, vasa previa (vessel rupture) or evidence of vessel occlusion.

Earlier work by Varli et al. created a 'Stockholm' classification of stillbirth by evaluating 382 cases. Varli et al. noted placental insufficiency and infection as the most common cause of stillbirth [19]. This classification system identified 17 separate causes of death, each split into a

definite, probable and possible cause of stillbirth. The most common groups being chromosomal abnormalities, infections, transfusion abnormalities, hypoxia, placental insufficiency, placental abruption, pre-eclampsia and umbilical cord complications. The Stockholm classification does not mention multiple gestations as a cause of stillbirth and reports placental abruption individually – under representing obstetric complications in comparison to the work by Bukowski et al. [9,19].

More recent work by Bring et al. encompassing not just Stockholm but all of Sweden reported on the causes of stillbirth in 2013 [20]. The group's findings mirrored their previous data, showing that placental insufficiency and infection were the two major causes in Sweden. Parast et al. in 2007 reviewed placental slides from 62 stillbirth cases, with 25 of these going unexplained. However, 13 of the 25 had significant cord compression [21]. Due to a lack of autopsies and placental pathology in developing nations, there is little data covering the possible cause of the majority of stillbirths [22]. It is believed that the majority of these could be prevented through folate supplementation, malarial prevention and generally improved healthcare for pregnant mothers [6].

These studies by Bukowski et al., Varli et al. and Bring et al. whilst informative also highlight the relative lack of published data into the causes of stillbirth based upon post-mortem analysis [9,20,22]. There is no unified definition of stillbirth, and little consensus in classifying its causes, making definitive epidemiological work difficult in the developed world and impossible elsewhere [6,9,14,19,23]. While many stillbirths go unexplained, significant research has been carried out to identify factors that increase risk. This has provided some evidence as to the possible mechanisms that cause it [11,24].

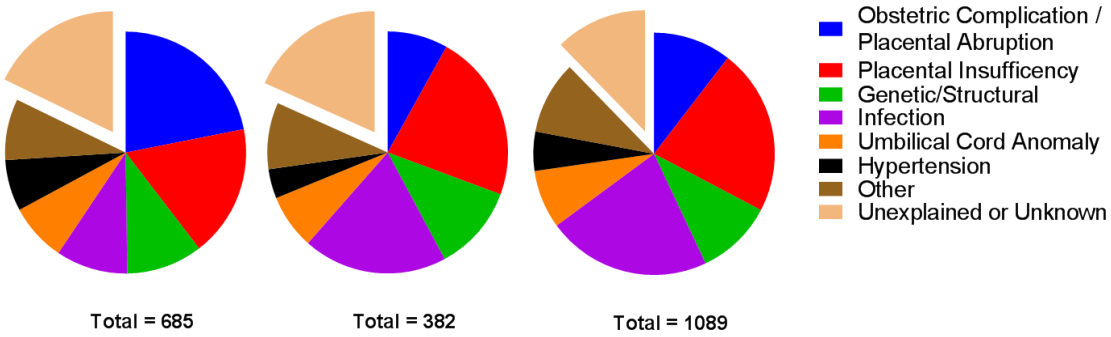


*Figure 1.1.* **Causes of stillbirth following post-mortem**. Charts from three separate studies tallying the possible cause of premature foetal death. Figures are adapted from data published by Bukowski et al., Varli et al. and Bring et al. [9,19,20].

| Cause of Stillbirth | Bukowski 2011 [9] N = 512 (%) | Varli 2008 [19] N = 382 (%) | Bring 2013 [20] N = 1089 (%) |
|---|---|---|---|
| Obstetric Complication / Placental Abruption | 150 (29.3) | 31 (8.1) | 114 (10.5) |
| Placental Insufficiency | 121 (23.6) | 86 (22.5) | 242 (22.2) |
| Genetic/Structural | 70 (13.7) | 44 (11.5) | 112 (10.3) |
| Infection | 66 (12.9) | 74 (19.4) | 239 (21.9) |
| Umbilical Cord Anomaly | 53 (10.3) | 28 (7.3) | 85 (7.8) |
| Hypertension | 47 (9.2) | 15 (3.9) | 57 (5.2) |
| Other | 56 (10.9) | 34 (8.9) | 106 (9.8) |
| *Unexplained or Unknown* | *122 (23.8)* | *70 (18.3)* | *134 (12.3)* |

*Table 1.1.* ***Statistics of stillbirth following post-mortem analysis.*** *Statistics adapted from Bukowski et al., Varli et al. and Bring et al. [9,19,20]. Total occurrence and (percentages) of the total are given. Bukowski et al identified multiple causes of death for some cases resulting in more causes of death than total stillbirths.*

### 1.1.3 Risk Factors of Stillbirth

As noted, few studies have attempted to tackle the pathological causes of stillbirth using in-depth post-mortem analysis [9,20,22]. Observing lifestyle choices and maternal factors associated with foetal death rates can give mechanistic insight into what causes a healthy pregnancy to become stillborn.

*Gestational Age*

Bukowski et al. found a marked difference in the proportion of placental and obstetric disorders thought to be the probable cause of stillbirth when their study population was split into early (<24 weeks) and late (>24 weeks) stillbirths [9]. In 52.4% of early stillbirths, obstetric complication was the most likely cause, compared to only 17.8% in stillbirths after 24 weeks. Conversely placental disorders were found to account for 28.4% of late stillbirths, compared to 14.1% in early stillbirths. Bring et al. found that 18.7% of stillbirths were due to infection between the 22$^{nd}$ and 36$^{th}$ week of gestation compared to 26.3% at ages over 37 weeks.

A much larger scale study, conducted from 1987 to 1989 by George Feldman studied the links between gestational age, ethnicity and maternal age on the likelihood of pregnancy ending in stillbirth [12]. Studying a huge cohort of 367,597 live births and 2,454 stillbirths after 25 weeks gestation, Feldman showed how multiple risk factors interact to potentially precipitate stillbirth. Of 822 births at 26 weeks of gestation, 151 were stillborn, 18.4% of the total births (Figure 1.2). However, by 36 weeks only 0.1% of the 12,717 births were stillborn, and this rate remained low with 0.2% of births at 40 weeks being stillbirths. Interestingly, after this point and up to 43 weeks of gestation, the rate of stillbirth appeared to increase marginally to 0.3% of live births. A key observation is that although the risk of stillbirth halves from 26 weeks onward every 2.9 weeks (95% CI, 3.2 – 2.7), the number of stillbirths each gestational week remains remarkably constant despite over 92% of births occurring after 35 weeks (Figure 1.2B).

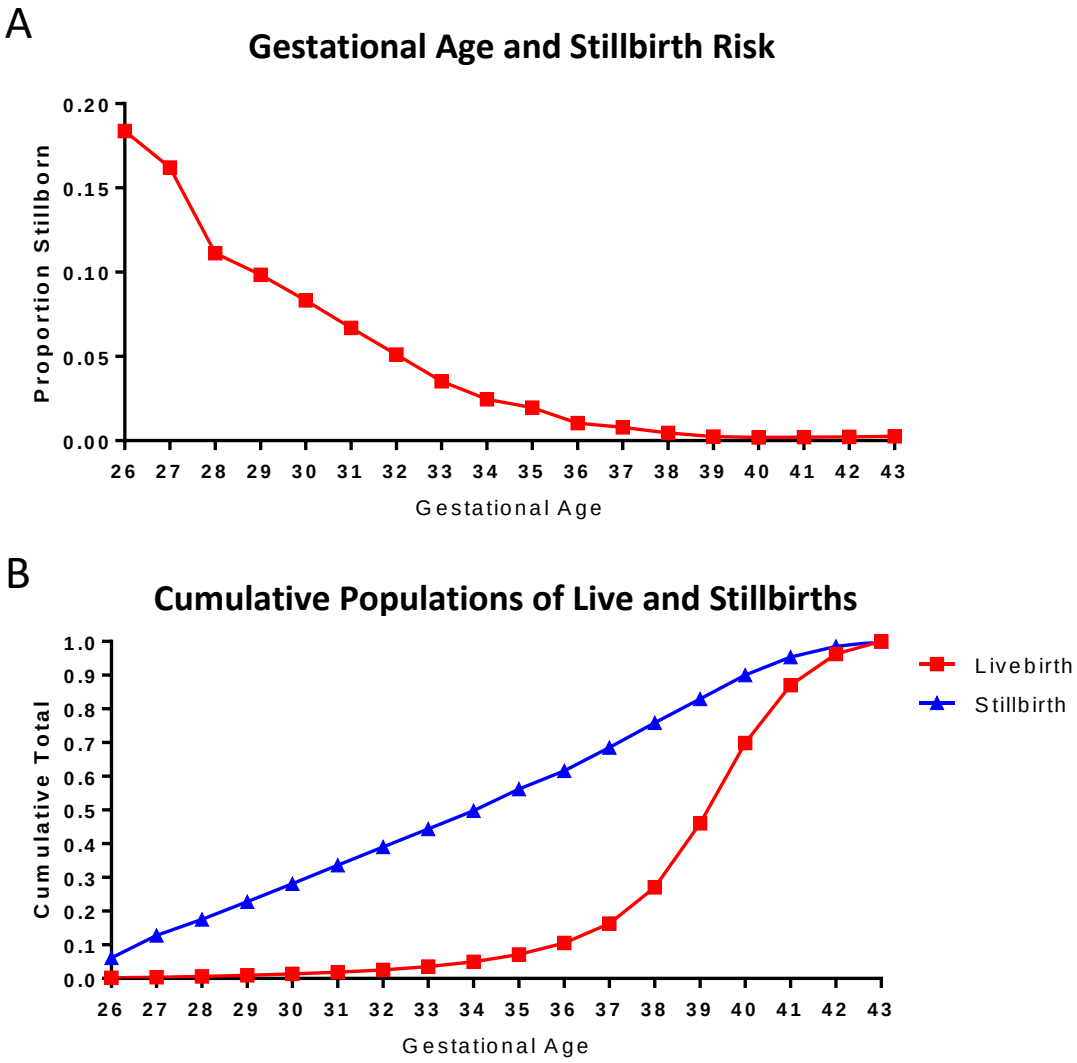


*Figure 1.2.* ***Link between gestational age and stillbirth.*** **A** *The proportion of pregnancies ending in stillbirth at gestational ages from 26 weeks.* **B** *Cumulative proportions of total stillborn (blue) and live births (red) in New York between 1987-1989. Created from data published by Feldman et al.* [8].

*Maternal Factors*

A meta-analysis of 96 separate studies published in 2011 highlighted a large number of lifestyle related risk factors that can adversely affect pregnancy outcome [11]. Maternal obesity had the largest effect on stillbirth occurrence, contributing to roughly 8000 stillbirths annually across a range of high income countries. Flenady et al. showed that having a BMI between 25-30 kg/m$^2$ increased risk of stillbirth by 23%, while being over 30 kg/m$^2$ increased it by 63% [11]. Maternal age over 35 years significantly increased the likelihood of stillbirth by 65%, while primiparity (a first pregnancy) was associated with a 42% increase. This study noted maternal smoking in disadvantaged populations could account for up to 20% of stillbirths. Data from Mohsin et al. from Australia also showed smoking during pregnancy increased risk of stillbirth by between 5-17% depending on whether gestational age was taken into account [25]. Maternal diabetes and hypertension also increased stillbirth rates by 82% and 20% respectively. Mothers of low and medium economic status also had a significantly higher risk of stillbirth compared to those who had a higher economic status [25]. This effect is mirrored in Sweden, where population-based data from 702 stillbirths and 702 controls showed 'blue-collar' skilled or unskilled workers are more than twice as likely to have a stillborn child compared to high level 'white-collar' workers [26].

*Antenatal Care*

The provision of care for pregnant mothers has a huge statistical effect on stillbirth rate. Mohsin et al. found those that received no antenatal care were twice as likely to have a stillborn child, while reports in 2016 from China show mothers with no antenatal visits are 14.97 times as likely to have a stillbirth compared to those with more than 10 visits [8,25]. The quality of care mothers receive in hospitals also appears to influence stillbirth rates. Mothers who attended poorer hospitals (those that had fewer beds) were 54% more likely to have a stillbirth compared to those in large, well-funded hospitals.

### 1.1.4 Unexplained Stillbirth

Despite extensive post-mortem investigation of cases in the study by Bukowski, 30% could not be given a 'probable' cause of death and therefore were completely unexplained [9]. In a smaller study of 310 stillbirths, Horn et al. found that in 15.2% of cases, despite 'systematic examination of all major cranial, thoracic and abdominal organs', the cause of death could not be found [10]. Data from Sweden found over 18% (Figure 1.1) of stillbirths were unexplained or the cause of death was unknown [19,20]. Many other studies have noted the alarmingly high rate of unexplained stillbirths [13,27,28]. These unexplained stillbirths appear to also follow a similar trend to explainable stillbirths in terms of risk factors. A study of single pregnancies in Oslo between 1986 and 1995 showed that sudden unexplained stillbirth risk increased when mothers were older, smoked or were overweight and obese [24].

Unexplained intrauterine death or stillbirth is a disease of exclusion. Only after detailed post mortem analysis and genetic karyotyping can a stillborn baby be classified as unexplained. This is unusual for many diseases, where specific symptoms and autopsy findings are hallmarks of certain pathologies, for example chest pain and coronary artery occlusion in myocardial infarction (MI). However, a specific area of cardiac pathology draws similar parallels to unexplained stillbirth - cases of sudden cardiac death (SCD). Initially, like unexplained stillbirth, SCD was a disease of exclusion. For a death to be classified as a SCD, post mortem analysis must show a complete lack of underlying disease in any other organ. Now, increased knowledge of cardiac biology and genetic variants that cause disease can provide explanations for these sudden deaths.

## 1.2 Sudden Cardiac Death

Sudden cardiac death is one of the most common causes of death worldwide, and is commonly attributable to cardiovascular disease or myocarditis [29]. Common causes of stillbirth normally involve congenital abnormalities or placental problems. Apart from pre-eclampsia, few if any are related to a cardiovascular specific defect. However, like unexplained stillbirth, SCDs go completely unexplained despite post-mortem analysis and are also known as sudden unexplained deaths (SUDs) [30,31]. In contrast to unexplained stillbirth, genetic and molecular autopsy of key genes associated with SCD can provide a likely mechanism of death [32].

### 1.2.1 Incidence

Reporting of SCD varies greatly, but most studies refer to a sudden collapse followed rapidly by death, or an unexpected death known to have been acute [33]. The incidence of SCD across the globe is estimated to be between 180,000 and 450,000 cases a year [34]. Prospective studies in Ireland report that 51.2 SCDs per 100,000 people occur annually. A similar study from the Netherlands also reported that in 1000 people from the general population, one will have a cardiac arrest every year [35,36] .

Coronary artery disease (CAD) is one of the biggest causes of morbidity and mortality in the world, and SCD accounts for more than 50% of deaths in patients with CAD [37]. A study on out of hospital cardiac arrests showed how devastating this condition can be, in 44% of males and 53% of women this was the first manifestation of any heart disease [36]. Alarmingly 18.5% of people who have a sudden cardiac arrest (SCA) died suddenly and only 6% of patients who received resuscitation were discharged alive from hospital. Secondly, the survival rate from SCAs witnessed at home was only 8%, compared to 18% outside of the home.

### 1.2.2 Causes of SCD

The very nature of SCD makes it difficult to dissect mechanistically as it is sudden, with very few chronic symptoms to suggest a likely acute episode leading to death. It is hypothesised that a transient event and underlying electrical instability of the myocardium precipitates lethal ventricular arrhythmia – producing a complete loss of synchronous contraction and rapid hemodynamic collapse [29,37]. There are several possible arrhythmogenic substrates that precipitate lethal SUDs, but these can be grouped into coronary disease, cardiomyopathies and channelopathies.

Coronary disease is believed to be responsible for the vast majority of SCDs [38]. Compared to 2.4% of sudden deaths attributable to cerebral haemorrhage in a study of 584 acute sudden deaths, 91% of white males and 48% of white females were reported to have suffered from CAD [38]. Narrowing of coronary vasculature is very common in survivors of cardiac arrest, and patients resuscitated from ventricular fibrillation often show evidence of MI [37]. Coronary thrombi and vulnerable plaques have been found in men who have died suddenly, showing a clear role for vascular inflammation in some SCDs [39].

The mechanism by which CAD produces a fatal arrhythmia is assumed to be triggered by ischemic areas of the heart, however because of the acute nature of the disease it is impossible to be certain [40]. Although these findings suggest a clear link between heart disease and SCD, 48% of people who arrest will have a functionally normal heart, with a left ventricular ejection fraction (LVEF) over 55% [41]. The heart acts as a pump that is controlled synchronously by electrical excitation of cardiac myocytes. These electrical signals can be measured and relate to the activity of different compartments in the heart. Many electrophysiological studies have shown a clear link between the perturbation of synchronous electrical activity of the heart, the altered activity of ion channels that underlie this, and sudden cardiac death.

### 1.2.3 Risk Factors for SCD

Like stillbirth, age noticeably affects the incidence of SCD independent of ethnicity and gender, with men aged 80 eight times more likely to have a SCA than 50 year old males [42]. The female gender also appears to play a protective role against SCD independent of age [43]. However 64% of SCD in women will occur with no prior CAD compared to only 50% of men, denoting a more 'unexplained' phenotype in women despite a reduced incidence on the whole. Furthering this idea, 10% of women who survive SCAs have structurally normal hearts compared to only 3% of men [29].

Ethnicity influences not only the probability of suffering a SCA but also the chance of surviving [42]. In Seattle the age-adjusted incidence of cardiac arrest was more than twice as likely in people of African American ancestry compared to Caucasians (3.4 vs 1.6 per 1000, respectively) [44]. Initial resuscitation success (17.1% vs 40.7%) and hospital survival (9.4% vs 17.1%) are both roughly halved. The effect ethnicity has on SCD has been replicated in Chicago, with survival rates 67.5% lower than those recorded in Caucasians.

Alongside this, many other risk factors have been shown to influence rates of SCD in patients. In 7,735 middle aged British males, ischemic heart disease, arrhythmia, systolic blood pressure, cholesterol level, elevated heart rate and lack of physical activity all increased the risk of SCD [45]. The Framingham Study is a cross-generational study established in 1948 to identify the causes of CVD by following 5,209 participants throughout their lives. This study suggested CAD increases SCD risk, while congestive heart failure (CHF) also increases the chances of SCD [46].

### 1.2.4 Electrophysiology and SCD

A powerful predictor of cardiac arrest is analysis of a patient's electrocardiogram (ECG). Twelve lead ECGs record the heart's electrical activity from electrodes placed on the skin and give an insight into the electrical activity of different sections of the myocardial tissue. As well as heart rate, ECGs reveal a vast amount of information about the activity of the heart (Figure 1.3), including: atrial depolarisation (P wave), ventricular depolarisation (QRS complex), ventricular repolarisation (QT interval) and the time between atrial and ventricular depolarisation (PR interval). Anomalous ECG readings have been associated with SCD incidence; elevated resting heart rate is a clear risk factor for sudden death in middle-aged men [47].

Prolongation of ventricular depolarisation, seen as a QRS longer than 120ms on an ECG trace, is significantly associated with both mortality and sudden death in patients with heart failure [48]. A larger prospective study of 2,049 men aged between 42 and 60 provided data to suggest QRS duration over 110ms had a 2.5 fold risk of SCD compared to those whose QRS duration was less than 96ms [49]. Specific case studies also provide evidence to suggest an abnormal ECG can lead to sudden death. In an 18-year old male who suffered a near death SCA, abnormal morphology of the QRS complex was observed [50]. Polymorphic ventricular tachycardia was visible during examination which could be normalised by quinidine prescription. After drug treatment, no further arrhythmias were observed until the patient discontinued their medication and died shortly afterwards.

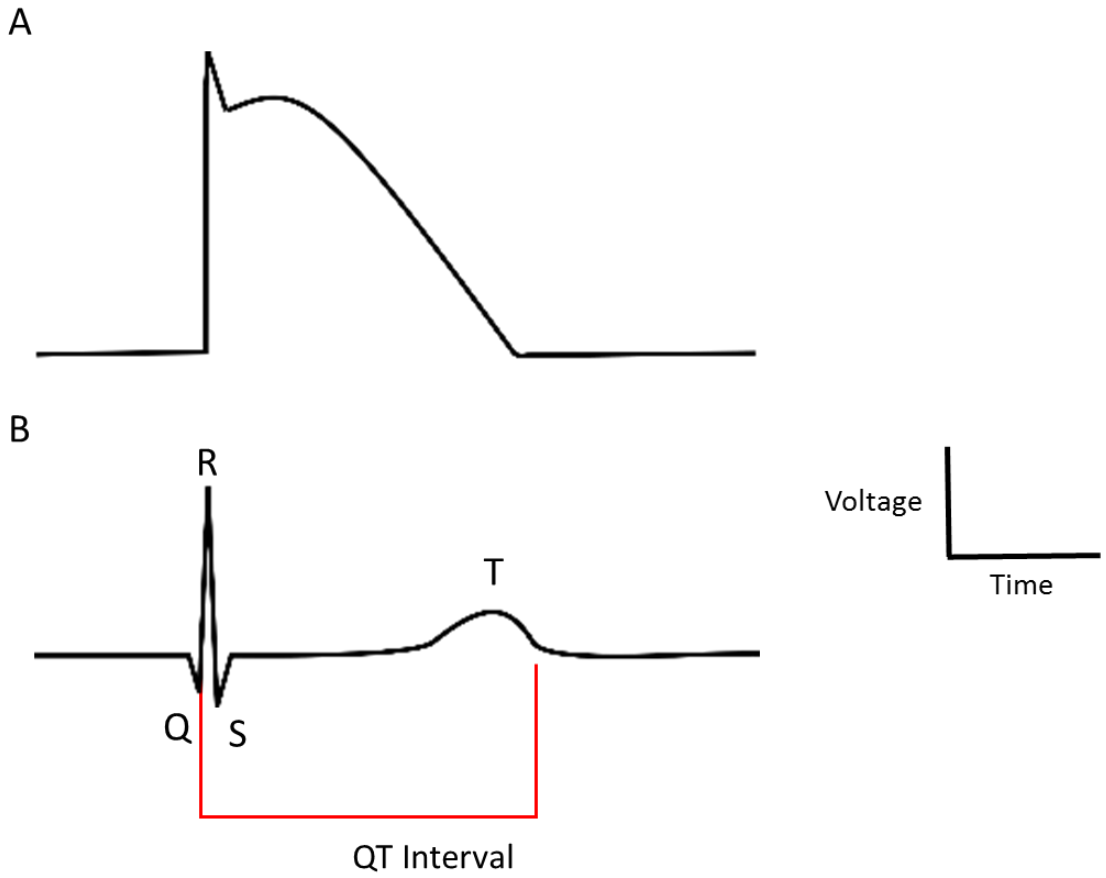


*Figure 1.3.* ***Ventricular action potentials shape the ECG. A*** *Archetypal shape of the ventricular action potential above a temporally matched ECG.* ***B*** *Surface ECG depicting the corresponding electrical activity that can be measured in A. Ventricular depolarisation occurs during the QRS complex, while the T wave indicates repolarisation.*

To accurately compare the QT interval scientifically between individuals involves the base QT value being corrected for differences in the patient's heart rate – which will naturally influence the shape and length of each cycle. The physiologist Henry Cuthbert Bazett formulated a basic correction in 1920: QTc = QT/√RR interval. Although commonly used, this correction overcorrects QT length at fast heart rates and undercorrects at low rates. In 1992, analysis of baseline electrocardiogram data from 5,018 subjects from the Framingham Heart Study yielded a more reliable formula: QTc = QT + 0.15(1-RR) [51]. Prolongation of ventricular repolarisation, seen as a long QTc interval, is an independent risk factor for sudden death in the general population [52].

Long QT syndrome (LQTS) is a disorder characterised by a prolonged QT interval due to a specific mutation in one of 15 genes [53-57]. A large number of well characterised mutations lie within the 15 LQTS genes, many of which encode for ion channels involved in the depolarisation and repolarisation of the myocardium [58]. There are two 'classical' monogenic forms of LQTS – the autosomal dominant Romano-Ward (RW) syndrome and autosomal recessive Jervell and Lange-Nielsen syndrome (JLNS) [59,60]. At the population level, the QT interval has a clear heritable component and genome-wide association studies (GWAS) have found single nucleotide polymorphisms (SNPs) at 35 genetic loci that clearly demonstrate an effect on the duration of the QT interval [61-63]. A prolonged QT interval infers a slowly and spatially dispersed repolarising ventricular myocardium, which is highly susceptible to early afterdepolarisations, producing fatal ventricular arrhythmias and ultimately SCA [64]. Collectively, these data confirm that the electrical activity of cardiomyocytes is intrinsically linked to SCD, as perturbed cellular electrophysiology can clearly provoke arrhythmia and ultimately SCD.

## 1.3 Sudden Infant Death Syndrome

### 1.3.1 Introduction

Despite SUD in adults being a diagnosis of exclusion, there is growing evidence to explain causes and risk factors in this previously unexplainable pathology [37]. An emerging area of medical research is now devoted to elucidating the biological cause of sudden infant death syndrome (SIDS) [65]. SIDS is the leading cause of mortality in the first year of human life and the third most common cause of infant mortality in the USA [66].

Defined in 1991 by Willinger et al. a death is classified as SIDS when it is sudden, and despite complete autopsy and clinical review remains unexplained [67]. Alarmingly, in a study of all SUDs in children aged between 1 week and 18 months, 80% are diagnosed as SIDS after autopsy [68]. Negative autopsy findings have not prevented researchers from developing multiple models to predict the causes of SIDS. Since 1972 the accepted paradigm of a 'triple risk hypothesis' to explain sudden deaths has been used [69-71]. These models state that SIDS is a combination of a vulnerable infant, in a critical developmental period which undergoes an exogenous stress such as respiratory infection. Guntheroth & Spiers proposed in 2002 that these triple risk models do not necessarily conform to the actual situation in SIDS [72]. Firstly, the reliance of 'exogenous stress' such as a viral infection causing SIDS is tenuous due to the large number of healthy infants who survive these events every year. Secondly, a small proportion of SIDS occur in the first month of life, this distribution of deaths according to age does not match other congenital abnormalities, where the vast majority of deaths occur in the first month of life. This casts doubt the likelihood of vulnerability in early development being a vital part of SIDS. Lastly, there is little consensus on what constitutes a 'vulnerable infant'. Triple risk models mention central nervous system (CNS) abnormalities, neonatal neurologic abnormalities, post-natal abnormalities and pregnancy-related factors. Despite continuing debate over the requirement of these abnormalities in causing sudden infant death, these factors have shown epidemiologically that there are risks associated with increased SIDS occurrence [72].

### 1.3.2 Risk Factors for SIDS

Many factors are associated with increasing the chance of sudden death in infants, these include: ethnicity, age of mother, alcohol use, gender of foetus, low birth weight and sleeping position [73]. This portrays a complex disease, of which the two most common risk factors are cigarette smoking during pregnancy and sleeping position. Cigarette smoking has been demonstrated to have a clear link to SIDS occurrence and is of course, easily preventable. Of infants who survived the first week of life, Haglund & Cnattingius found 0.49 sudden deaths in 1,000 from non-smoking mothers [74]. However, in mothers who smoked 1-9 cigarettes a day there were 0.93 SIDs per 1,000. In those who smoked more than 10 cigarettes per day, this increased to 1.47 sudden deaths per 1,000 births [74].

Analysis of sleeping position in SIDS has revealed a relative risk of 2.02 in infants asleep on their sides compared to those placed on their backs [75]. Following a number of prospective and interventional studies aimed at avoiding prone sleeping, multiple health services worldwide addressed this common association, with the USA launching it's 'Back to Sleep' campaign in 1994 [76-78]. Although seemingly simple, this intervention led to a 50% reduction in SIDS, from 1.2 in 1,000 to 0.55 in 1,000. Maternal alcohol consumption initially appeared to promote sudden death in infants. However, this consumption is strongly correlated to smoking and following multivariate analysis appeared to have no independent effect on SIDS [79]. Further work in 1999 by Alm et al. found postnatal alcohol consumption, but not prenatal intake predisposed children to SIDS [80]. Alm also showed there is little interaction between caffeine consumption >800mg/day and SIDS risk after adjustment for maternal smoking, maternal age and education. In contrast Ford et al. showed >400mg/day of caffeine increased risk of SIDS by 65% [81].

While sleeping position and maternal smoking are environmental factors that have been targeted by multiple healthcare campaigns, SIDS rates vary greatly between different ethnic groups even when corrected for these aforementioned risk factors. Reportedly, SIDS is twice as likely in African American or American Indian mothers compared to Caucasians in the USA,

despite both groups co-existing in the developed world [78]. Initial post-mortem cell culture studies of SIDS cases in 1970 also revealed genetic abnormalities in 10 of 11 karyotyped leukocytes [82]. These initial findings propose the paradigm of genetic variation coupled with environmental stimulation acting together on precipitating SIDS in infants.

### 1.3.3 Genetic Risk Factors

Common polymorphisms and rare genetic variation have, over many years, been linked to promoting or causing SIDS through a wide range of possible mechanisms. Genetic variability in interleukin genes such as *IL-1β* and *IL-6* have been associated, in experimental models and children with SIDS [83,84]. These inflammatory responses affect several physiological responses and have been postulated as possible causes of sudden death. The c.C-511T polymorphism within the *IL-1β* promoter is associated with a higher cytokine response in people of Bangladeshi and Australian Aboriginal descent but with an intermediate or low profile in Caucasians [85]. These findings tie in with observations that Bangladeshi and Aboriginal infants are at much greater risk for SIDS than Caucasians. Similarly, in Australian populations a homozygous *IL-6* c.G-174C promotor polymorphism was observed in 38% of controls compared to 58% of SIDS infants [86].

SNPs in the autonomic nervous system also associate with increased SIDS risk. Polymorphisms in the 5' regulatory region of the serotonin transporter (5-HTT) were shown in 2001 by Narita et al. who found that 13.9% of age-matched control participants possessed a long or extra-long promoter region compared to 27.8% of SIDS victims [87]. The study linked this elongated promoter to increased transportation of serotonin outside of the cell and the lower excitatory function in the respiratory centre of the brain. Further studies of 92 SIDS cases and 92 gender/ethnic-matched controls investigated the frequency of genetic polymorphisms linked to SIDS. Weese-Mayer et al. identified nonsynonymous variation in five genes associated with the autonomic nervous system: *PHOX2a, RET, ECE1, TLX3,* and EN1 [88].

Perturbation of metabolic homeostasis has also been explored as a possible route to SIDS. Of 38 SIDS victims in 1989, Burchell et al. found 10 with raised hepatic glycogen, 8 of which had glucose-6-phosphatase deficiency while 2 had transport protein T2 deficiency – indicating that disrupted glycogen storage mechanisms may be involved in SIDS [89]. More recently in 2005, Forsyth et al. presented corroborating data showing three novel polymorphisms in the glucokinase gene in infants who died suddenly [90].

### 1.3.4 Channelopathies and SIDS

Interest in linking inflammatory, neuronal and metabolic pathways to SIDS have produced promising results that may explain sudden deaths in infants, however it is in the area of cardiovascular disease that the most progress has been made in identifying and potentially treating children at risk of SIDS. Evidence to suggest a link between sudden infant death and cardiac conduction was put forward first by Keeton et al. who reported six infants delivered at term and of average birth weight who were found either collapsed in their cots or found cyanosed in their hospital ward [91]. The illness occurred unexpectedly and without immediate treatment it is likely that all six infants would have died. Keeton found ECG abnormalities in all six infants, one had altered sinus rhythm, two had sinoatrial block whilst three showed ventricular tachycardia. Keeton et al. proposed that in five of these infants, cardiac arrhythmia caused their acute illness, while in the sixth an arrhythmia associated with Wolff-Parkinson-White syndrome likely produced the near fatal cerebral hypoxia she suffered from. Treatment by digoxin or atropine after diagnosis by ECG was successful at removing symptoms, however one infant suffered ischaemic brain damage which produced severe psychomotor retardation. These near-miss cases highlighted the importance of neonatal ECG screening, as aberrant ECG recordings could have highlighted the benefits of a prophylactic treatment, circumventing these life-threatening attacks.

Peter Schwartz proposed one year prior to the study by Keeton et al. that sympathetic imbalance may underlie SIDS by increasing the likelihood of ventricular fibrillation [92]. Prolongation of the QT interval in infants, as previously described in adults, is measurable clinically and is pathologically important in producing arrhythmia, in particular in infants with a higher heart rate than adults [92,93]. In 1976 Maron et al. obtained ECG data from 42 parental sets with one infant who had died suddenly, 15 of which showed a prolonged QT interval [94]. The ECGs from the siblings of SIDS infants also suggested inheritance of the long QT phenotype, with 39% having a prolonged QT interval. One infant with "near-miss" SIDS also showed prolonged QT in the Maron et al. study. Interestingly siblings of SIDS infants whose parents had normal QT intervals showed no sign of a prolonged QT.

In contrast to the findings by Keeton et al. and Maron et al., several studies have also reported findings that failed to find a link between abnormal ECG recordings and SIDS [95-97]. These include 21 near-miss SIDS infants whose QT intervals were no different to age and sex matched controls, and a prospective study of 15 SIDS infants from a cohort of 7,254 newly born infants where no significant difference in QTc could be found. In 1982 Schwartz et al. published the findings of their prospective study measuring the QT interval in 4,205 newborns [98]. Alongside the finding that QT interval lengthens significantly during the first months of life, at 1 year three infants had suffered an unexpected sudden death. All three had a prolonged QTc intervals four days after birth, with one whose QTc was more than 9 standard deviations above the mean (563ms). Sadeh et al. in 1987 published data that appeared to validate this hypothesis that a proportion of SIDS victims are due to dysrhythmia brought on by impaired handling of cardiac repolarisation [99]. Sadeh's data showed that of 10 SIDS infants, five were unable to shorten their QT interval in response to an increase in heart rate, and this prolonged repolarisation predisposed them to fatal ventricular arrhythmia.

Although evidence suggested a strong positive link between long QT and SIDS, in 1989 eminent paediatric cardiologist Warren Guntheroth published a review repudiating the

hypothesis of Schwartz et al. [100]. Guntheroth highlighted a number of prospective studies that found no prolongation of QTc intervals in SIDS cases compared to control infants [101]. He also argued that Sadeh et al. in not finding one arrhythmia in any 6 hour ECG tapes and finding a shorter QTc interval in SIDS cases before altering the Bazett's exponent to give an apparent prolonged QT interval compared to controls – failed to provide sufficient evidence to equate QT interval in causing SIDS [100].

In 1998 Schwartz et al. published their ECG study containing data from 34,442 infants, 33,034 of which had follow-up data collected at one year of life [98,102]. This study cohort contained 24 SIDS cases, whose QTc interval was significantly longer than that of infants who had died of known causes. Of these, 50% showed a QTc interval that would be reported clinically as prolonged (>440ms). This was in comparison to infants with a known cause of death, where their QTc was shorter than 440ms. Using this data, the risk of SIDS in infants showing a normal QTc is 0.037%, compared to those with prolonged QTc who are 41.3 times as likely to suffer a sudden death. A follow-up study in 44,596 infants published later in 2009 investigated the prevalence of genetic variants associated with LQTS in 29 infants with a QTc >450ms [103]. Screening 7 genes thought to cause prolonged QT, 12 neonates possessed mutations thought to have a deleterious effect on ion channel function – causing LQTS. 28 of the 29 infants were treated successfully with β-blockers. Genetic variants that alter the function of cardiac ion channels are also linked to SCD in adults. These diseases are a form of heritable electrical cardiac diseases known as "channelopathies".

This evidence was supported by further data from a clinical case study where a 44 day old infant presented with ventricular fibrillation and would surely have died if not for defibrillation at a hospital [65]. A *de novo SCN5A* mutation was identified in the infant and he showed a prolonged QT interval. Further molecular proof of a link between channelopathies and SIDS was shown a year later, when Wedekind et al. identified another *de novo SCN5A* mutation, p.A1330P, in a 9 week old infant who had died suddenly [104]. Functional testing of the variant

showed a LQT3-like mechanism of slowed channel inactivation which would lead to a prolonged QT interval.

## 1.4 Ion Channels and the Heart

### 1.4.1 Introduction

Ion channels are a key protein family responsible for the synchronous contraction of cardiac myocytes throughout the heart. It is the opening and closing of these channels which allows ions to enter and exit the cell in an organised fashion. Ionic fluxes produce the action potential, allowing contraction and relaxation of cardiomyocytes. In inherited disorders such as LQTS, genetic variants occur that adversely affect protein function. These alterations can produce asynchrony in the heart - which can lead to death. This disruption of the shape of the action potential produces arrhythmias, it can be caused by multiple factors but is chiefly due to dysregulated ion channel function.

### 1.4.2 Ion Channels In Cardiomyocytes

The cardiac action potential is the key determinant of cellular contraction and consists of five key phases (Figure 1.4). Myocardial cells at rest are hyperpolarised (known as phase 4), with a negative membrane potential of -90mV. During depolarisation the membrane potential increases rapidly to over +40mV (phase 0). Phase 1 consists of a short period of repolarisation followed immediately by phase 2, a plateau of membrane potential during which calcium enters the cell. Phase 3 entails rapid repolarisation back to the initial resting membrane potential. Sodium, potassium and calcium are the three key ions whose electro-chemical gradient cardiomyocytes exploit to control their excitatory state. Ion channels allow the movement of these ions across the lipophilic cell membrane, while ion transporters and exchangers maintain specific concentrations of ions in the cytoplasm and extracellular milieu.

Due to high concentrations of intracellular potassium (>140mM), before depolarisation two currents (IK1 and IKAch) allow the efflux of potassium ions to maintain the resting membrane potential. The IK1 current consists of two potassium channel subunits, Kir2.1 and Kir2.2, transcribed by the *KCNJ2* and *KCNJ12* genes respectively [105,106]. The acetylcholine-activated $K^+$ channel responsible for the IKAch current is coupled to a G protein and is highly expressed in atrial and nodal cells, but is expressed less in the ventricle.

Rapid depolarisation is conducted by the opening of the cardiac sodium channel $Na_v1.5$. The gene *SCN5A* encodes the key pore-forming α-subunit, which in the heart forms functional channels in complex with multiple $\beta_1$-subunits [107]. $Na_v1.5$ exists in a closed state at resting membrane potential, however they open extremely rapidly (<2ms) when the membrane potential depolarises [108]. This allows the influx of $Na^+$ ions to raise the membrane voltage from -90mV to over +40mV. These channels then inactivate rapidly, to limit the length of depolarisation and to allow repolarisation, although there are reports of delayed and slow currents through the $Na_v1.5$ channel [108].

Early depolarisation or phase 1 of the action potential is shaped by the opening of transient outward potassium currents Ito,f [109]. This current is voltage-gated and activates and inactivates rapidly in response to depolarisation. Ito,f outwardly rectifies to allow potassium ions to leave the cell, producing a short reduction in membrane voltage.

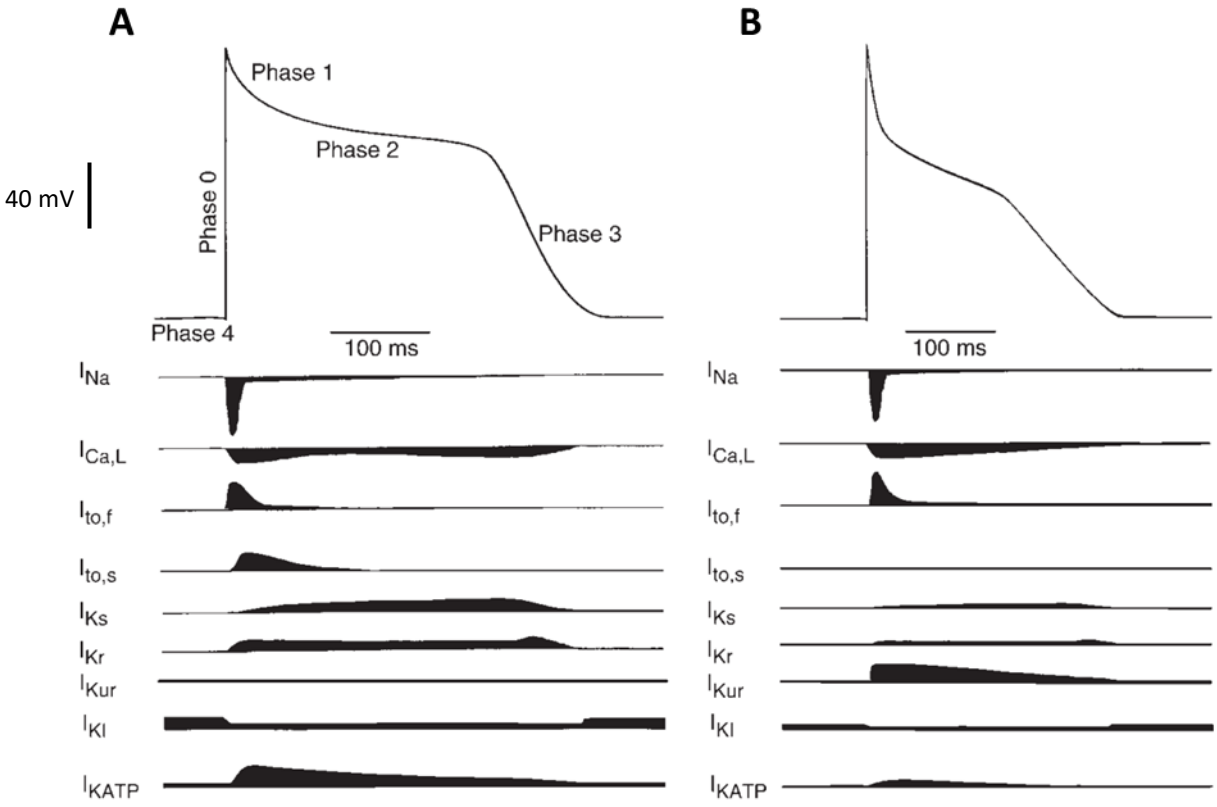


*Figure 1.4.* ***Comparison of action potential morphology in adult ventricular and atrial myocytes. A*** *Ventricular and* ***B*** *Atrial cell types share similarities in voltage gated sodium and calcium channel expression. The distinction in action potential shape is primarily dictated by their distinct expression of potassium channels. Figure is adapted from [110].*

After early repolarisation, the plateau phase of the action potential is determined by two competing currents, the delayed outward rectifying potassium currents and the inward calcium currents. Distinctly in the ventricle, Ito,s opens rapidly alongside Ito,f after depolarisation. This current inactivates slower than Ito,f. By comparison, in the atria the delayed potassium current (IKur) activates rapidly while inactivating slowly - it is responsible for their shorter atrial action potential duration (APD) compared to that in the ventricles [111]. The influx of calcium during this plateau is split between L- and T- type calcium channels (low threshold and transient) respectively. The L-type calcium channel can be found in all cardiac cells while T-type channels mainly reside in pacemaker, atrial and Purkinje fibre cells. Both calcium channels are voltage-gated, with the T-type opening at -60mV while L-type channels open later at -50mV. Calcium entry during phase 2 of the cardiac action potential is vital in coupling membrane excitation to contraction [112]. In the heart, the L-type calcium channel α-subunit is encoded by the *CACNA1C* gene, while *CACNA1G* produces the T-type calcium current α-subunit [113].

Following calcium entry and during subsequent myocardial contraction, two separate outward potassium currents are responsible for restoring the cell's membrane voltage back to its resting state. These two components are IKr and IKs, the rapid and slow potassium currents, respectively. The *KCNH2* gene encodes the HERG potassium channel α-subunit, and is responsible for the rapidly activating current [114]. HERG channels are found in abundance in the left atrium and ventricular endocardium. β-subunits such as KCNE1 and KCNE2, encoded by the *KCNE1* and *KCNE2* genes respectively, confer changes in gating and response to adrenergic stimulation [115]. The *KCNQ1* gene encodes the α-subunit (protein also called KCNQ1) of the slowly rectifying potassium current. This potassium channel is expressed in all cardiomyocytes but is markedly reduced in sub-endocardial cells [116]. *KCNE1* encodes the key β-subunit of IKs, by interacting with the pore region to reduce channel conductance but increase open channel probability – ultimately increasing cellular current [117]. Both IKr and IKs activate during the plateau phase to bring about delayed repolarisation back to the resting membrane potential.

### 1.4.3 Electrical Cardiac Diseases

*Long QT Syndrome*

A long QT interval is a strong predictive factor for SCD and SIDS. As ECG peaks and troughs mirror electrical changes in the states of specific heart regions, identification of the ion channels and genes that shape it can elucidate the causes of pathological ECG changes such as LQTS. It is through studying genetic mutations in patients with LQTS and other electrical disorders of the heart that permit an explanation of SCD and create an opportunity for novel therapies.

There are over 15 genes linked to LQTS (Table 1.2) by deleterious genetic mutations. The most common lie within the three key genes that determine the APD: the sodium channel gene *SCN5A*, and the two delayed rectifying potassium channels KCNQ1 and KCNH2. In 1957 the first family with LQTS was reported, and in 1997 they were shown to possess a dominant homozygous mutation in the *KCNQ1* gene [118,119]. Mutations in *KCNQ1* cause LQTS1 and are due to a loss-of-function in the channel, this can be due to altered trafficking inside the cardiomyocyte, directly affecting the pore domain or interrupting its interaction with KCNE1 or other proteins [120,121]. Reducing outward potassium current and therefore prolonging the repolarisation phase of the action potential can lead to fatal arrhythmia [64].

The second LQTS gene identified was *KCNH2*, the gene encoding the HERG protein [55]. Loss of function in this gene leads to LQT2, where reduced IKr perturbs correct cardiomyocyte repolarisation. The majority of LQT2 mutations appear to reduce potassium current by altering trafficking of the channel to the membrane where it can effectively efflux $K^+$ ions [122]. In contrast to LQT1 & LQT2, it is gain-of-function mutations in *SCN5A* that are responsible for prolonging APD in LQT3 patients [57]. Responsible for the inward sodium current, LQT3 mutations can produce persistent currents that depolarise the cell, prolonging action potential duration.

Although there are now 15 genes (Table 1.2) associated with congenital LQTS, of patients who suffer a SCA and possess a known LQT mutation, it will lie within *KCNQ1, KCNH2* or *SCN5A* in 90% of cases [58,103]. Of note is the severity of LQT3 compared to LQT1 & LQT2, with patients suffering more severe events and having a higher chance of SCD [123].

Variants in many genes can delay cardiac repolarisation and cause LQTS, but there is marked variation between what can precipitate SCD. Work by Schwartz et al. dissecting genotype-phenotype interaction in LQT1-3 showed that of 392 cardiac events in LQT1 mutation carrying patients, 62% occurred during exercise, while only 3% occurred during sleep or rest [54]. Contrast this to the LQT2 mutation carrier group where only 13% of events occurred during exercise and 43% occurred during heighted periods of emotion (stress, shock and or arousal). Lastly, LQT3 patients had similar cardiac arrest rates during periods of exercise, but only 19% had cardiac events due to emotional stress. In these 39% of patients with damaging sodium channel mutations, the trigger for cardiac events usually occurred during sleep or periods of rest – the polar opposite of LQT1 patients. This is an interesting paradigm, where clinically all patients present with long QT on an ECG due to delayed onset of repolarisation, but the substrate for arrhythmia appears to differ greatly.

| LQTS | Gene | Protein | Current | Functional Effect |
|---|---|---|---|---|
| LQT1 | *KCNQ1* | KCNQ1 or Kv7.1 | IKs | Loss of Function[124] |
| LQT2 | *KCNH2* | HERG | IKr | Loss of Function[55] |
| LQT3 | *SCN5A* | Nav1.5 | INa | Gain of Function[57] |
| LQT4 | *ANK2* | Ankyrin-B | - | Loss of Function[56] |
| LQT5 | *KCNE2* | KCNE2 (Originally MiRP1) | IKr | Loss of Function[125] |
| LQT6 | *KCNE1* | KCNE1 (Originally Mink) | IKs | Loss of Function[126] |
| LQT7 | *KCNJ2* | Kir2.1 | IK1 | Loss of Function[127] |
| LQT8 | *CACNA1C* | Cav1.2 | ICa,L | Gain of Function[128] |
| LQT9 | *CAV3* | Caveolin 3 | INa | Gain of Function[129] |
| LQT10 | *SCN4B* | Navβ | INa | Gain of Function[130] |
| LQT11 | *AKAP9* | Yotiao/AKAP9 | IKs - Adrenergic | Loss of Function[131] |
| LQT12 | *SNTA1* | A-Syntrophin | INa | Gain of Function[132] |
| LQT13 | *KCNJ5* | Kir3.4 | IKAch | Loss of Function[133] |
| LQT14 | *CALM1* | Calmodulin 1 | ICa,L | Gain of Function[134,135] |
| LQT15 | *CALM2* | Calmodulin 2 | ICa,L | Gain of Function[134,135] |

*Table 1.2.* ***Summary of genes associated with LQTS and the proteins they encode.*** *Currently there are 15 genes that harbour genetic variants which are attributed to prolonging the QT interval. Listed are the gene and protein names, and the subsequent ion currents they conduct, modify or contribute to. Also listed are the published effects that disease causing variants have on the protein's function.*

The list of genes associated with LQTS represent a deeper understanding of the disease compared to other channelopathies, with studies finding non-ion channel genetic variants plausibly prolonging repolarisation [56,62,131,136]. The fourth gene causally linked to LQTS in 2003 was the Ankyrin-B gene [56]. Prior to the work by Mohler et al. the accepted paradigm of channelopathies relied upon mutations purely affecting ion channels. Ankyrin-B is a 200kDa adaptor protein which interacts with numerous proteins including the voltage-gated sodium channel, $Na^+/Ca^{2+}$ exchanger, $Na^+/K^+$ ATPase and the inositol triphosphate receptor found in the sarcoplasmic reticulum (SR). A presumed loss-of-function dominant mutation p.E1425G was found in a large French family which appeared to segregate with a prolonged QT phenotype. Further work on *ANKB* heterozygous knockout mice demonstrated a clear role in heart rate variability and sudden cardiac death. Two years later Mohler et al. showed numerous nonsynonymous variants within the N-terminal regulatory domain of Ankyrin B that severely perturbed calcium handling and contractility in cardiomyocytes [137].

Long QT types 5 and 6 relate to LQT 1 & 2, with variants in the *KCNE1 and KCNE2* genes leading to reductions in IKs and IKr respectively [125,126]. Up to four KCNE1 β-subunits complex with four KCNQ1 α-subunits, with relative densities controlling the voltage-dependence and gating kinetics of the potassium channel [138].

### *Brugada Syndrome*

Brugada syndrome (BrS) is an inherited channelopathy but in comparison to LQTS, is characterised by an elevated ST segment on the ECG [139]. Most cases are identified during adulthood, with the youngest patient diagnosed at the age of 2 days, while the oldest being 84 years [140]. Prevalence of BrS has proven difficult to calculate with Pedro, Josep and Ramon Brugada estimating that it is responsible for 4-12% of sudden deaths and >20% of deaths with structurally normal hearts [140]. Other estimates of BrS have reported a 1 in 2,000 prevalence, but this brings it in line with LQTS, which is generally believed to be more widespread [141]. Brugada

syndrome positive patients are at high risk of SCD and recent work has identified genetic variants thought to cause the disease [142].

Seven years after Brugada and Brugada characterised their eponymous syndrome, Dumaine et al. published patch-clamp data involving an *SCN5A* missense mutation (p.T1620M) previously linked to BrS [143,144]. At 32˚C the p.T1620M variant recovered from inactivation slower and right shifted steady-state activation compared to wild-type sodium currents. Unlike many potassium channel mutations, the arrhythmogenic potential of this mutation only revealed itself closer to physiological temperatures. When examined at room temperature, wild-type (WT) and p.T1620M channels showed similar normalised current and rate of recovery from fast inactivation. Bezzina et al. presented another *SCN5A* mutation p.1795insD, which when expressed in Xenopus oocytes produced a positive shift of steady-state activation compared to wild-type channels [145]. These findings were interpreted initially as reducing outward sodium current, accentuating the action potential notch in phase 1, consequently losing the epicardial action potential dome and shortening repolarisation [145,146]. Since the initial findings in *SCN5A*, several other genes have been linked to BrS: *GPD1L* a sodium channel trafficking protein, *SCN1B* and *SCN3B* the β-subunits of sodium channels, and several calcium channel subunit genes [147-151]. Larger scale genetic testing of 12 BrS-linked genes in unrelated patients with possible BrS identified putative pathogenic mutations in 20% of the cohort [152]. These results depict BrS as a complex channelopathy involving sodium, calcium and potassium ion channel gene variability.

### *Cathecholaminergic Polymorphic Ventricular Tachycardia*

Cathecholaminergic polymorphic ventricular tachycardia (CPVT) is a rare but lethal condition first described in a single case study in 1975 [153]. Arrhythmias induced by catecholamines are usually lethal, but treatment with β-blockers is very effective at preventing these SCDs. Without treatment, mortality of CPVT is >30% by the age of 30. The initiation of tachycardia is linked to physical exercise or emotional stress, therefore blockage of adrenergic

drive has proven an effective, if not ideal therapy [154]. A hall mark of CPVT is syncope or near-SCD without structural heart disease alongside normal ECG traces at rest. However, significant ventricular ectopy is observed during patient exercise or infusion of isoproterenol, which if prolonged can lead to sudden cardiac death.

Current molecular analysis points to rare variants in three genes causing CPVT: *RYR2*, encoding the cardiac ryanodine receptor (RyR2), *CASQ2* a major SR calcium binding protein and *TRDN* which transcribes triadin, a protein involved in regulating RyR2 in the heart [155]. RyR2 is found in the SR, the major $Ca^{2+}$ store in the cell, and is critical in calcium-induced calcium release after the cardiomyocyte is flooded with calcium from the L-type calcium channel. Following calcium entry the channel opens, allowing calcium to leave the SR and bind Troponin C, which enables sliding of myofilaments and cellular contraction. This is followed by calcium reuptake back into the SR [156]. Unsurprisingly dysregulation of this calcium release cycle can significantly affect the heart. The first *RYR2* mutations were found in CPVT patients with no structural cardiac abnormalities in 2001 [157]. Deleterious *RYR2* variants are thought to increase open probability during diastole – resulting in delayed afterdepolarisations or sudden depolarisations triggering arrhythmia [158]. Mouse models have highlighted Purkinje cells as being particularly vulnerable to generating these delayed afterdepolarisations (DADs) in response to adrenergic stimulation [159].

### *Short QT Syndrome*

In contrast to LQTS, short QT syndrome (SQTS) is characterised by a short QT interval and a shortened action potential duration in cardiomyocytes. Expectedly, genetic variants thought to cause the disease are found in LQTS genes but produce an opposite effect. SQTS patients are characterised by having a rate-corrected QT-interval <320ms and there have been reported cases of familial SCD, representing an inheritable trait [160]. The first two genes identified as harbouring SQTS-causing mutations were *KCNH2* and *KCNQ1*, incidentally the first two genes found to cause LQTS [161,162]. Gain-of-function mutations in these repolarising potassium channel

currents will increase potassium efflux during phase 3 of the action potential. Most commonly this short QT manifests as atrial fibrillation. From the initial patient cohort of 13, nine had a form of atrial fibrillation [163]. Harmful genetic variation in channels conducting the outward depolarising currents, specifically the L-type calcium channel are also associated with SQTS [164,165].

| Channelopathy | Genes involved | Cellular Processes |
|---|---|---|
| Brugada | ***SCN5A*** [145]<br>*SCN1B*<br>*SCN3B* [149] | Sodium Current |
| CPVT | *RYR2* [158]<br>*CASQ2*<br>*TRDN* | Calcium Uptake into SR<br>Calcium Storage |
| SQTS | ***KCNH2*** [161]<br>***KCNQ1*** [162]<br>***KCNJ2***<br>***CACNB2b1*** [165]<br>***CACNA1C*** | Potassium Current<br>Calcium Influx |

*Table 1.3.* ***Summary of other ion channelopathies and the genes thought to cause them.*** *Genetic variants in some genes have been identified in patients with distinct clinical conditions, these are highlighted in bold. Cellular processes are listed as those pathways perturbed by deleterious variants in the preceding genes. SR – Sarcoplasmic Reticulum.*

### *Other Conduction Disorders*

LQTS, BrS, CPVT and SQTS are genetically well characterised channelopathies, however there are many other intermediate phenotypes and conditions implicated in SCD without underlying heart complications. Sick sinus syndrome (SSS) is a disorder stemming from failure of sinoatrial node action potential firing which can lead to arrest or dysrhythmia [166]. In 2003, Bensonet al. provided familial hereditary and whole-cell patch-clamp data implicating recessive mutations in *SCN5A* as being a likely culprit in SSS in some cases [167]. Transfection of the $Na^+$

channel into tsA201 embryonal kidney cells showed a wide spectrum of delayed channel inactivation compared to wild-type current. Two variants, p.R1623X and p.G1408R, produced a non-functional sodium channel, highlighting the variable expressivity of sodium channelopathies – a non-functional channel can lead to SSS, reduced or increased current can lead to LQTS or BrS, even the same variant can produce BrS, SSS or a cardiac conduction-like defect [53,168].

The J point of the ECG covers the interface between depolarisation (QRS complex) and repolarisation in the ventricle (T wave). As previously noted for LQTS and other channelopathies, it is these abnormal ECG features that implicate detrimental ionic handling in cardiac cells [169]. First observed in hypothermic dogs in the early 50s, elevated J waves have been extensively studied in hypothermic humans [170,171]. Raised J waves are a spectrum of diseases named early repolarisation syndromes (ERS), they have been difficult to define with separate data reporting contrasting results. Ventricular fibrillation (VF) has clearly been linked to prominent J waves on a case study basis, contrasting to early work showing a notched QRS and ST-segment elevation in healthy young males [172-174]. More recent, large population association studies comparing J-point elevation to survival free of cardiac related death and arrhythmia showed clear trends suggesting J-point elevation increased risk of SCD [175].

While LQTS and BrS have genetic association with variants within ion channels, the genetic basis of J wave syndromes is less clear [176]. The Framingham Heart Study showed that siblings of an ERS patient were at least twice as likely to have ERS, alongside work by Reinhard et al. who found parents with an ERS positive child had a 2.5-fold increased chance of having ERS themselves [177]. As of 2013, genetic variation in six genes had been linked to causing ERS, with the first rare variant found within the *KCNJ8* gene [176,178]. *KCNJ8* transcribes the Kir6.1 α-subunit of an ATP-sensitive potassium channel found in cardiomyocytes [179]. This inwardly rectifying $K^+$ channel, in comparison to voltage-gated channels, is gated directly by cytoplasmic ATP and ADP. The p.S422L *KCNJ8* variant found in both a BrS and an ERS patient showed marked

gain-of-function in heterologous expression systems, it was hypothesised that a significant inward potassium current in the epicardial myocytes could shorten APD – a sure substrate for arrhythmogenesis [178]. Interestingly, work by Antzelevitch has also highlighted loss-of-function mutations in L-type calcium channel subunits [180]. Two of these genes, *CACNA1C* and *CACNB2*, are also known to cause short QT syndrome when harbouring loss of function mutations. By now unsurprisingly, *SCN5A* mutations (this time loss-of-function) have been found in patients with VT due to early repolarisation [181].

The final channelopathy covered will be isolated cardiac conduction defects (ICCD) or Lenègre disease. ICCD is characterised by slow conduction between the atria and ventricles, and widening of the QRS complex on an ECG. Between 1999 and 2001, three papers showed how *SCN5A* mutations associated strongly with ICCD, and in heterologous cell expression systems a p.G514C variant increased channel inactivation kinetics [168,182,183]. Interestingly, in the report by Kyndt et al. the group showed both BrS and ICCD patients possessed a complete loss of current p.G1406R mutation [168]. The other gene implicated in ICCD, *SCN1B* also codes for a subunit of the inward sodium channel – the β1 subunit. *SCN1B* mutations have been implicated not only in cardiac conduction defects but BrS as well, highlighting the pleiotropic nature of inward sodium channel variation.

### 1.4.4 Ion Channelopathies and Age of Event

The INTERHEART case-control study across 52 countries and with over 30,000 participants reported that only 6% of myocardial infarctions occurred before the age of 40 [184]. This is not the case for channelopathies however, which appear to show an inverse association with age and the likelihood of a cardiac event. Large scale studies by Schwartz et al. following 479 probands with a long QT interval found 74% of males and 51% of females had a cardiac event before the age of 15 [185]. Of these 479, 162 patients carried a known pathological variant in long QT genes 1-3.

Similarly, the mean age of a cardiac event in 200 BrS patients was 33 years [186]. Giustetto et al. reported that in 29 SQTS patients the median age of diagnosis was 30 years with two having a cardiac arrest in the first 8 months of life [187]. Sub-group analysis by Zareba et al. in 243 genotype positive LQTS patients has shown that the age and severity of cardiac events is genotype dependant [188]. Males with LQT1, 2 or 3 had a median age of a first cardiac event at 8, 11 and 16 respectively, with the female median age at event as 12, 16 and 19 respectively. Before the age of 15, males had cardiac events significantly earlier only if they were LQT1 positive (P = 0.030), while over the age of 15 both LQT1 & 2 positive females were much more likely to have a cardiac event (P = 0.035 & P = 0.001, respectively). While LQT3 positive patients had less cardiac events and at an older age, they were markedly more severe, as 19% of events in males and 18% in females resulted in death, compared to 5% and 2% in LQT1, or 6% and 2% in LQT2 positive males and females respectively.

### 1.4.5 Dominant Negative Mutations

Harmful hereditary mutations that alter ion channel activity often show a pathophysiological effect despite only occurring on one allele, the other allele inherited from the other parent being functionally normal. This effect is known as a dominant negative mutation, whereby the detrimental effect of a variant on one allele is able to harmfully compensate for the otherwise normally functioning allele [189].

Examples of this have been characterised in calcium, potassium and sodium channels in a range of clinical settings. A dominant negative form of LQT2, p.A561V was characterised in 2000 by Kagan et al. [190]. Co-expression with WT channel resulted in rapid proteolysis of functional HERG channels formed by WT and p.A561V subunits. Proteasome inhibition rescued the resulting loss of current usually observed when mutant and wild-type current were expressed in equal proportions by heterologous cell lines. Harmful mutations in *KCNA5*, a

voltage gated potassium channel expressed in the atria have also shown significant dominant negative effects [191]. While WT channels showed outward current density of >0.3nA/pF when cells were patch-clamped at +80mV, cells co-transfected with both WT and p.E375X showed significant reduction to <0.15nA/pF.

Sodium channel dominant negative mutations have also been documented, one being an *SCN3B* variant p.A130V linked to atrial fibrillation in the Chinese population [192]. This gene codes for a β-subunit of $Na_v1.5$. Wang et al. provided data to show p.A130V, when transfected into cells expressing $Na_v1.5$, significantly reduced sodium current. Transfection of these cells with WT and p.A130V *SCN3B* also inhibited sodium currents but to a lesser extent, whereas transfection with the WT subunit alone did little to affect current-voltage relationships. This effect did little to alter trafficking or expression, and therefore formation of WT-mutant proteins were directly altering or blocking the sodium channel's ability to conduct sodium ions.

Harmful mutations in the calcium channel gene, *CACNA1A,* which encodes a pore-forming subunit of $Ca_v2.1$ have been associated with a dominant negative form of episodic ataxia, a neuronal channelopathy [193]. Expression of p.R1279X $Ca_v2.1$ alongside WT $Ca_v2.1$ results in significant inhibition of calcium currents compared to cells transfected purely with the WT calcium channel. Interestingly, surface expression was markedly reduced in fluorescently tagged cells, representing competition for cell trafficking machinery by non-functional channels – reducing observable current at the membrane.

Mutations have been observed in multiple ion channels that alter cell trafficking, expression and conductance in sodium, potassium, calcium and other ion channels that result in pathology through a dominant negative mechanism [191-194]. This way, heterozygotic mutations that adversely alter ion channel function can potentially lead to harmful pathology despite the presence of a functioning wild-type protein.

## 1.5 Cardiac Ion Channelopathies and Intrauterine Foetal Death

### 1.5.1 Evidence for Cardiac Causes of Foetal Death

Due to the criteria of exclusion in diagnosing a sudden death, it has been proposed that many SIDS and SCD cases are the result of ion channelopathies in the heart leading to arrhythmia. Patients carrying a harmful LQTS variant may appear asymptomatic, while the onset of significant cardiac events is age-dependant, with over 50% of LQT1-3 carriers experiencing syncope or cardiac arrest before they are 16 [54]. Many deaths thought to be caused by ion channelopathies occur at a very early age independent of which ion channel may be affected [102,187,188].

There have been two anecdotal studies which attempted to link recurrent foetal loss and long QT syndrome. In 2004 Miller et al. reported on a male infant diagnosed with ventricular arrhythmias *in utero* at 28 weeks post gestation, who had LQTS after birth and ultimately required a heart transplantation [195]. The mother showed no symptoms of LQTS but genetic analysis revealed mosaicism for an *SCN5A* variant, p.R1623Q. A subsequent pregnancy ended with stillbirth at 7 months. The surviving infant, following their heart transplantation, was also found to be heterozygous for the p.R1623Q variant.

Four years later Bhuiyan et al. described a family with recurring early miscarriages and two intrauterine foetal losses [196]. ECG recordings of the father and mother showed no symptoms, but low heart rate (~90bpm) in the first foetus was detected at 22 weeks. Later echocardiography of the foetus showed ventricular tachycardia. At 28 weeks gestation labour was induced and resulted in a stillborn child, who showed a fully formed sinus node and no structural abnormalities. A second pregnancy also developed ventricular tachycardia at 29 weeks. By 30 weeks there was a diagnosis of LQT syndrome and 2 weeks later the child was born through caesarean. After 12 hours the child underwent surgery for the insertion of a pacemaker. After one month the child was discharged, but will be on β-blocker treatment for the remainder

of their life. Sequencing the *HERG* gene identified a homozygous nonsense mutation p.Q1070X which leads to the translation of a truncated protein ~10kDA smaller than the wild-type. Interestingly the p.Q1070X-HERG current inactivated faster and at -50 to -30mV recovered significantly faster from inactivation compared to WT channels. As other parameters were not significantly different (peak currents, activation rates and fast/slow deactivation), biophysically there is little difference compared to WT channels. However by investigating nonsense-mediated mRNA decay (NMD) Bhuiyan et al. found 88% less p.Q1070X mRNA compared to WT HERG [196].

### 1.5.2 Population-based Studies

Due to the unexplained nature of stillbirth, and the high prevalence of channelopathies in the general population, Crotti et al. evaluated the prevalence of LQT1-3 variants in 91 unexplained intrauterine foetal deaths [197]. Through the use of high-performance liquid chromatography and Sanger sequencing they identified 14 genetic variants in 18 individuals not observed in a large panel of ethnically similar controls from the Helmholtz Zentrum exome database and 3 publicly available databases: 1000 (1,094 individuals) Genomes Project, NHLBI GO Exome Sequencing Project (5,379 individuals) and the Exome Chip Design (12,000 individuals) [198-200]. Three variants (*KCNQ1*, p.A283T and p.R397W and *KCNH2*, p.R25W) found in the LQT 1 & 2 genes were considered putative pathogenic variants due to absence in the aforementioned databases and adverse biophysical findings compared to WT channels. Both *KCNQ1* p.A283T and p.R397W significantly reduced peak and tail current density by 70% when compared to WT when transfected into CHO cells. The *KCNH2* p.R25W similarly produced a ~40% reduction in current density compared to WT.

Six nonsynonymous *SCN5A* variants were identified, three (p.T220I, p.R1193Q, and p.P2006A) of which had been previously reported as affecting ion channel function. Two of the

*SCN5A* variants were categorized as variants of uncertain clinical significance as two (p.D772N and p.R1116Q) showed no functional difference compared to WT. Crotti et al. reported the minor allele frequency of p.R1116Q in African Americans was 0.07, unexpectedly high for a variant linked to stillbirth [197]. While the ClinVar database reports the *SCN5A* p.R1116Q variant as a likely benign allele, the ExAC database with coverage in 31,272 individuals reports allele frequency of 0.0012 in African Americans – significantly lower than stated by Crotti et al. three years ago.

Crotti's work in 2013 showed that a proportion of unexplained intrauterine foetal deaths could be attributed to LQTS, as 8.8% of sequenced cases possessed a dysfunctional ion channel mutation. These data may have underestimated the true prevalence of channelopathies associated with intrauterine foetal death. The differences, specifically in the age of event between different LQT genes may play a significant role in how potentially arrhythmic variants precipitate lethal arrhythmias in the developing foetus [185]. Phenotypically the population contained not only stillbirths but also late abortions and miscarriages. This represented a wide range of foetal ages, ranging from 14 to 41 weeks of gestation. Interestingly both *KCNQ1* putative pathogenic mutations reported in the paper were found in cases whose estimated gestational age was less than 17 weeks.

Crotti et al. only interrogated the three most common LQTS genes found in adults, compared to the 15 currently known LQTS genes, notwithstanding genes associated with BrS, CPVT, SQTS and other conduction disorders [103,141,154,201]. Pathogenic mutations in *KCNQ1* and *KCNH2*, although relatively common in the general LQT adult patient population precipitate less severe cardiac events than those reported in patients with sodium channel related LQT [188]. Patients with JLNS have complete IKs loss and are born, representing a possible redundancy during development or requirement of secondary variants to trigger events. Indeed, even in a mouse model of JLNS (*KCNQ1* knockout*),* homozygotes appear at normal Mendelian frequencies [202].

Conversely, variants in genes known to regulate cardiac electrophysiology in the adult may play a more pronounced, detrimental role during cardiogenesis. Work by Pfeufer et al. in 2010 studied the role of common genetic variation in determining PR interval variability [62]. Interestingly, alongside an association with voltage gated sodium channel genes, a number of genetic loci were found near genes involved in cardiac development (*NKX2-5, SOX5, WNT11, MEIS1 and TBX5/3*). In 2014 Arking et al. identified several genetic loci that explain ~9% of QT variation [63]. This study also identified 11 nonsynonymous variants in symptomatic LQTS patients without a known causative mutation. These variants were absent in controls from online exome sequencing databases (Esp6500 [203]) and resided within genes not previously associated with LQTS. These tools provide a powerful way of identifying genes involved in cardiomyocyte electrophysiological control, without the need to identify adult patients with symptomatic cardiac disease. Genetic variants that cause or predispose pregnancies to stillbirth may not reside in genes commonly attributed to adult ion channelopathies. Therefore it is important to study not just the most commonly associated channelopathy genes, but any genes thought to contribute to cardiac development and electrophysiology in the setting of sudden death – particularly foetal.

## 1.6 Cardiac Ion Channelopathies in Unexplained Stillbirth

### 1.6.1 CICUS Study

To investigate whether deleterious genetic variation in ion channel genes were associated with unexplained stillbirth, our group established the Cardiac Ion Channelopathies in Unexplained Stillbirth (CICUS) study. Crotti et al. had recently shown that 8.8% of unexplainable stillbirths possess harmful variants in LQTS ion channel genes.

Initially the study intended to prospectively collect samples, allowing access to parental DNA. However due to difficulties in acquiring a sufficient number of samples, retrospective case DNA was also collected. Retrospective samples were fresh frozen tissue samples from Sheffield Children's Hospital. As these samples were taken before the CICUS study began – no access to parental DNA was possible. DNA from 70 unexplained stillbirth cases was available, this was obtained from muscle, liver, spleen or heart tissue and processed for sequence analysis. An experienced perinatal pathologist classified these cases as completely unexplained, unexplained but with placental abnormalities and partly explained. In contrast to previous work with stillbirth and LQT, an expanded sequence panel was used to assess variation in 35 genes. This included known genes associated with LQTS, BrS, SQTS and SCD alongside 21 genes linked to a prolonged QT interval through GWAS (Table 1.4) [61-63,204].

The aim of this study was to investigate the link between reported and suspected LQT genes and unexplained stillbirth. CICUS recruited 70 unexplained stillbirth cases where DNA was readily available. The gene panel included the known long QT genes and 23 new genes associated with SCD and LQTS by recent genome-wide association studies [63].

| Gene Sequenced | Exon Count | Link to Channelopathy | Gene Sequenced | Exon Count | Link to Channelopathy |
|---|---|---|---|---|---|
| *AKAP9* | 50 | LQTS9 [131] | *NDRG4* | 16 | GWAS |
| *ANK2* | 47 | LQTS4 [56] | *NKX2-5* | 2 | GWAS |
| *ATP1B1* | 6 | GWAS | *NOS1AP* | 10 | GWAS |
| *ATP2A2* | 21 | GWAS | *PLN* | 2 | GWAS |
| *BAZ2B* | 37 | SCD | *PRKCA* | 17 | GWAS |
| *CACNA1C* | 50 | LQTS8/SQTS/BrS [164,180] | *RYR2* | 105 | BrS/CPVT [157] |
| *CASQ1* | 11 | Calcium Handling [205] | *SCN10A* | 27 | BrS |
| *CAV1* | 3 | GWAS | *SCN4B* | 5 | LQTS10 [130] |
| *CAV2* | 3 | GWAS | *SCN5A* | 28 | LQT3/BrS [57,145] |
| *CAV3* | 3 | LQTS9 [129] | *SLC8A1* | 10 | GWAS |
| *CREBBP* | 31 | GWAS | *SMARCAD1* | 24 | GWAS |
| *KCNAB2* | 16 | GWAS | *SNTA1* | 8 | LQTS12 [132] |
| *KCNE1* | 3 | LQTS5 [125] | *SP3* | 7 | GWAS |
| *KCNE2* | 2 | LQTS [126] | *SRL* | 6 | GWAS |
| *KCNH2* | 15 | LQTS2/SQTS [55] | *TCEA3* | 11 | GWAS |
| *KCNJ2* | 2 | LQTS7/SQTS [127] | *TRPM7* | 39 | GWAS |
| *KCNQ1* | 16 | LQTS1/SQTS [124] | *TTN* | 363 | GWAS |
| *MKL2* | 17 | GWAS | | | |

*Table 1.4.* ***List of 35 genes selected for the custom CICUS sequencing panel.*** *Gene name and exon counts are listed alongside which channelopathies are caused by variants within that gene, or how the gene has been linked to causing channelopathies.*

### 1.6.2 Predicted Damaging Variants Found in the CICUS Study

A miSeq Multiplexed Sequencing Platform was used to sequence a custom panel of 35 genes (Table 1.4). After sequencing quality checks, 311 nonsynonymous, exonic single nucleotide variants (SNVs) were identified in the cases that differed to the reference genome (hg 19). Variants more likely to have a functional effect on the protein of interest were sorted from these 311 variants using a variety of computational tools. These tools rank nonsynonymous variants using base pair conservation, amino acid chemistry and protein secondary structure (detailed in Methods Section 2.2).

We found 18 variants predicted to be damaging in established LQT genes: one novel in *CACNA1C* and 17 rare (*AKAP9, ANK2, CACNA1C, KCNE1, KCNE2, KCNJ2* and *SCN5A*)[206]. In the two most commonly associated genes with LQTS (*KCNQ1* and *KCNH2*) we did not identify any predicted damaging variants. Twenty-five predicted damaging variants in non-LQT (GWAS candidate) genes were discovered, six were novel while 19 were rare [206].

Of the rare LQT gene variants found in the CICUS population, three had deleterious functional data previously associated with them. One case was heterozygous for variants in both *KCNE1* (p.D85A) and *KCNE2* (p.T8A) genes, these variants lead to susceptibility to drug-induced arrhythmia [207,208].

### 1.6.3 Functional Testing of Variant Associated with Stillbirth in CICUS Study – *KCNJ2*

The first genetic variant to be functionally tested from the CICUS project was a novel (at the time) nonsynonymous mutation in *KCNJ2*, p.R40Q [206]. This variant was located in a highly conserved amino acid residue within the N-terminal domain of the inward rectifying potassium channel, Kir2.1 (Figure 1.5). Loss-of-function mutations in *KCNJ2* are associated with LQT7 and many of them act in a dominant negative manor [127,209]. Gain-of-function variants have also been reported, p.D172N and p.V93I, which cause SQT3 and atrial fibrillation, respectively [210,211]. These

loss-of-function mutations are associated with ~60% of Andersen-Tawil syndrome (Type 1) cases and LQT can occur alongside micrognathia, widely spaced eyes and clinodactyly. Some patients have short stature or abnormal spine curvature – clearly indicating a developmental facet to the disease.

When this variant was transfected into CHO-K1 cells, inward potassium current density below -100mV was significantly reduced compared to wild-type *KCNJ2* transfected cells (Figure 1.5E). Many of the published *KCNJ2* variants that cause loss-of-function result in a dominant negative phenotype that is thought to significantly prolong the QT interval. This variant could predispose developing foetal hearts to arrhythmia, if this occurred during a vulnerable stage in development and may have precipitated the stillbirth.

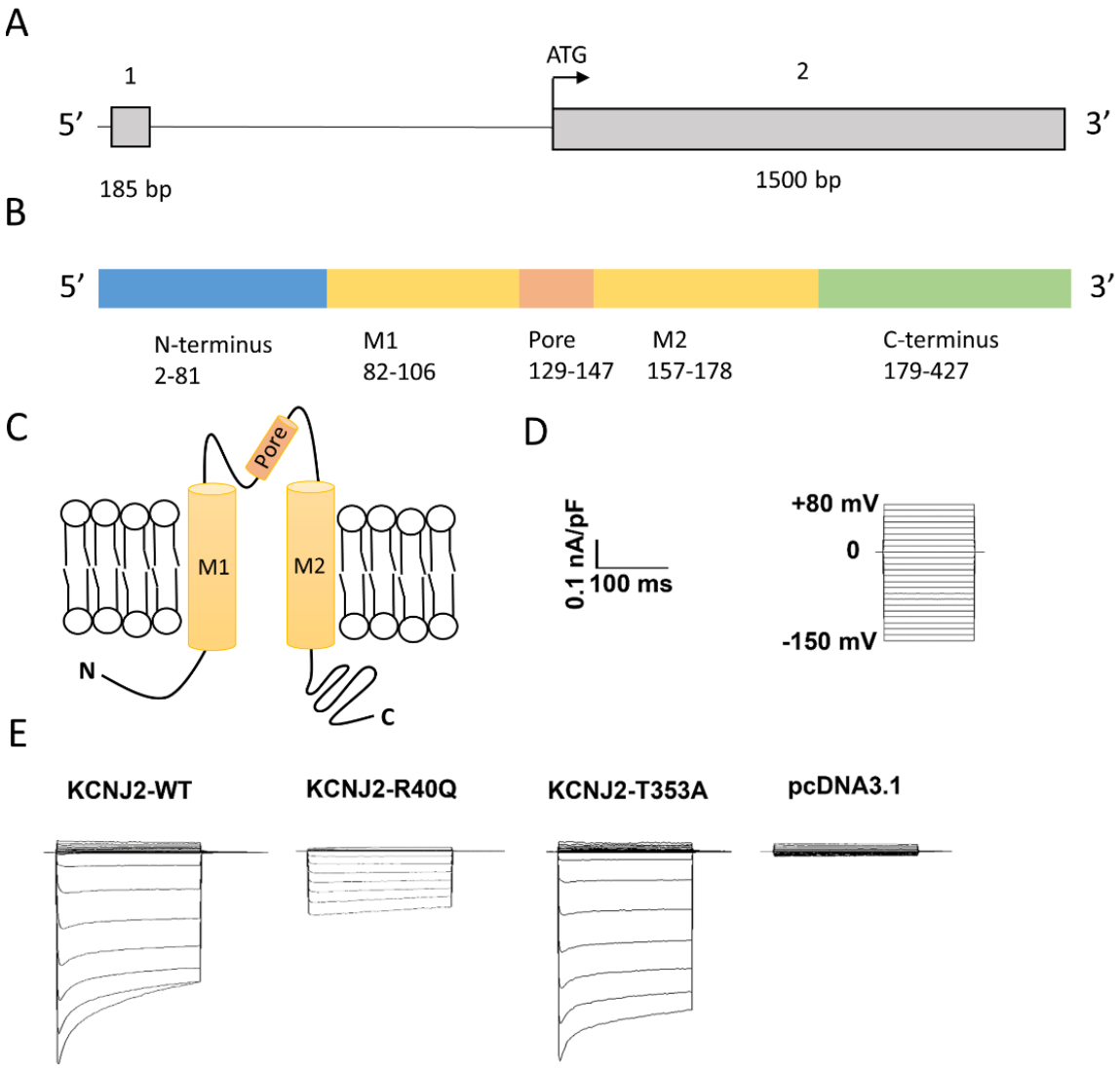


*Figure 1.5.* ***The KCNJ2 CICUS variant p.R40Q leads to significantly reduced current density when expressed in heterologous cells. A*** *Genomic map of KCNJ2's two exons denoting base pair length and start ATG codon.* ***B*** *Protein domain map of KCNJ2, numbers listing amino acid length of specific domains.* ***C*** *Graphical representation of KCNJ2 inside the plasma membrane, both N and C termini are cytoplasmic.* ***D*** *Scale of current/time used in E and voltage protocol for whole-cell patch-clamp of transfected cells.* ***E*** *Representative traces of cells expressing WT, putative pathogenic p.R40Q and p.T353A KCNJ2 plasmids. For comparison, pcDNA3.1 transfected cells were also analysed. Figure taken from* [206].

### 1.6.4 Selection of Variants in *AKAP9* and *TRPM7* for Functional Testing

Sequencing of *AKAP9* and *TRPM7* in 70 unexplained stillbirth cases resulted in 25 distinct nonsynonymous SNVs in the exons of these genes. The genes *TRPM7* and *AKAP9* were included in the sequencing panel based on the following factors.

*TRPM7* has been demonstrated through GWAS findings to be a gene involved in regulating adult myocardial repolarisation [63]. This included the identification of multiple nonsynonymous variants in symptomatic LQT patients, who were genotype negative for classic LQTS variants. Alongside these human data, several studies in mice have demonstrated that *TRPM7* is indispensable to mouse development – in particular cardiogenesis [212-214].

*AKAP9* has an established role in associating with KCNQ1/KCNE1 in cardiomyocytes to couple adrenergic stimulation with increased IKs current [131]. Prolongation of the QT interval by variants located in the *AKAP9* gene are designated as LQT11. LQTS patients have a lower median age of first cardiac event if they are LQT1 genotype-positive compared to LQT2 or LQT3 (mentioned in 1.5.2) [123]. Interestingly, cardiac events in LQT1 patients are primarily precipitated during exercise or stress (covered in 1.4.3). Clearly this indicates a key role for proteins whose function lies in regulating adrenergic control of IKs. However no predicted damaging variants were sequenced in *KCNQ1* or *KCNE1* in any CICUS cases. A genetic study by Villiers et al. has shown that in a founder LQT1 population (168 mutation carriers & 181 non-carriers), divergent *AKAP9* genotypes were able to double or halve the risk of cardiac events [215].

### 1.6.5 Prioritising *AKAP9* and *TRPM7* Variants for Functional Analysis

In total 17 missense SNVS were sequenced in the *AKAP9* gene in the CICUS study (Table 1.5). Only those variants which were highly conserved and predicted to be damaging by at least one of the following predictive software was prioritised for functional studies: SIFT, Polyphen and Mutation Taster. After excluding all variants not predicted to affect protein function, five of the 17 initial *AKAP9* variants remained to be taken forward for functional analyses (Table 1.6). Of these five, p.T155N was predicted to be damaging only by PolyPhen, whilst p.D1507H was listed as 'possibly' damaging by PolyPhen and Mutation Taster.

In the CICUS study population we identified six heterozygous nonsynonymous SNVs (Table 1.7) in *TRPM7*. These variants were sorted to prioritise those most likely to functionally effect the TRPM7 protein as previously mentioned for *AKAP9* variants. Two variants, p.E1205G and p.T860M were novel variants not found in either of the 1000G or Esp6500 databases. The remaining two, p.R494Q and p.G179V had not been found in the 1000g database and were reported at very low frequency in the Esp6500 data set. Interestingly, all *TRPM7* variants that lay within constrained nucleotides and were novel/rare were predicted to be damaging by at least two predictive tools.

There was an apparent bias towards favouring pathogenicity in *TRPM7* variants over those in *AKAP9.* Annotation tools take into account known functional/structural domains and studied functional epitopes. Therefore *TRPM7*'s polypeptide sequence has been annotated with a number of functional protein domains and predictive tools are more likely to interpret variants within or near them as damaging.

In comparison, *AKAP9* is annotated with a single putative PKA subunit binding domain and there is a single variant thought to cause pathological disease [131]. All CICUS *TRPM7* variants were novel in the 1000g database, and in the case of esp6500 either extremely rare (p.G179V and p.R494Q) or novel.

| AKAP9 Variant DNA : Protein | GERP++ Score | Esp6500 Frequency | 1000g Frequency | CICUS Frequency |
|---|---|---|---|---|
| C464A : T155N | 5.37 | 0.0003 | 0.0002 | 1 |
| G6037A : E2013K | 5.72 | 0.003 | 0.0004 | 1 |
| G4127C : S1376T | -1.51 | 0.001 | 0.0002 | 1 |
| A6176G : E2059G | 5.62 | 0.0005 | 0.0002 | 1 |
| G4519C : D1507H | 4.36 | 0.004 | 0.003 | 1 |
| A10672G : I3558V | 0.64 | 0.001 | 0.001 | 1 |
| G4841A : R1614Q | 1.43 | 0.0085 | 0.01 | 1 |
| G9929A : R3310Q | -3.44 | 0.007 | 0.008 | 1 |
| T6556C : S2186P | 3.2 | 0.002 | 0.002 | 1 |
| T4199C : M1400T | 0.25 | 0.037 | 0.05 | 1 |
| G9127A : A3043T | 4.89 | 0.0009 | 0.0004 | 2 |
| C139T : H47Y | 0.48 | 0.01 | 0.002 | 3 |
| A10840G : M3614V | 1.11 | 0.01 | 0.007 | 3 |
| A7451G : K2484R | -8.74 | 0.0945 | 0.066 | 15 |
| A8375G : N2792S | -2.13 | 0.36 | 0.3 | 46 |
| G1389T : M463I | -3.46 | 0.44 | 0.37 | 48 |
| C8935T : P2979S | 2.47 | 0.99 | 0.99 | 70 |

*Table 1.5.* ***List of all 17*** **AKAP9** ***nonsynonymous SNVs found In CICUS cases.*** *Variants are listed as both genomic DNA alteration and protein substitution compared to hg 19. GERP++ Score is a scale of conservation. Esp6500 and 1000g frequency represent the incidence of that specific variant in the Exome Sequencing Project and 1000 Genome Project databases respectively. CICUS Frequency reports the amount of cases which carried the variant listed.*

| AKAP9 Variant DNA : Protein | SIFT | Polyphen | Mutation Taster | Predicted Damaging |
|---|---|---|---|---|
| G4519C : D1507H | 0.31 | 0.874 | 1 | 0-2/3 |
| C464A : T155N | 0.06 | 0.967 | 0.566 | 1/3 |
| G9127A : A3043T | 0.34 | 0.999 | 1 | 2/3 |
| A6176G : E2059G | 0 | 1 | 1 | 3/3 |
| G6037A : E2013K | 0 | 0.998 | 1 | 3/3 |

*Table 1.6.* ***Five*** **AKAP9** ***variants to be carried forward for functional testing.*** *Variants are listed as both genomic DNA alteration and protein substitution. Mutational analysis scores rating the likelihood of a variant being damaging from the three mutational software are listed. Entries in red are considered damaging using the algorithm indicated, those in blue are possibly damaging. Each tool reports a variant as deleterious on different score parameters: SIFT < 0.05 and Polyphen > 0.85, while Mutation Taster scores are not wholly indicative of its predictive output.*

| TRPM7 Variant DNA : Protein | GERP++ Score | Esp6500 Freq | 1000g Freq | CICUS Freq |
|---|---|---|---|---|
| A3614G : E1205G | 5.3 | - | - | 1 |
| C2579T : T860M | 5.59 | - | - | 1 |
| G1481A : R494Q | 4.11 | 0.000086 | - | 1 |
| G536T : G179V | 4.65 | 0.000084 | - | 1 |
| A223G : I75V | -2 | 0.0013 | - | 1 |
| C4445T : T1482I | 2.19 | 0.0797 | 0.075879 | 15 |

*Table 1.7.* ***List of* TRPM7 *nonsynonymous SNVs found In CICUS cases.*** *GERP++ Score is a scale of conservation. Esp6500 and 1000g frequency represent the incidence of that specific variant in the Exome Sequencing Project and 1000 Genome Project databases respectively. CICUS Frequency reports the amount of cases which possess the variant listed. A "-" shows that variant has not been sequenced in this population.*

| TRPM7 Variant DNA : Protein | SIFT | Polyphen | Mutation Taster | Predicted Damaging |
|---|---|---|---|---|
| G536T : G179V | 0 | 1 | 1 | 3/3 |
| G1481A : R494Q | 0.21 | 1 | 1 | 2/3 |
| C2579T : T860M | 0 | 1 | 1 | 3/3 |
| A3614G : E1205G | 0 | 0.561 | 1 | 2-3/3 |

*Table 1.8. T****he four* TRPM7 *variants prioritised for further functional testing.*** *Variants are listed as both genomic DNA alteration and protein substitution. Mutational analysis scores rating the likelihood of a variant being damaging from the three mutational software are listed. Entries in red are considered damaging using the algorithm indicated, those in blue are possibly damaging. Each tool reports a variant as deleterious on different score parameters: SIFT < 0.05 and Polyphen > 0.85, while Mutation Taster scores are not wholly indicative of its predictive output.*

## 1.7 Transient Receptor Potential Melastatin 7

### 1.7.1 Introduction

Transient receptor potential channels (TRP) are classically characterised as a primordial family of ion channels that act as cellular sensors [216]. First described in *Drosophila* as calcium channels responsive to light, it is now understood that TRP channels play a role in many areas of tissue and cellular biology [217]. These range from allowing mice to discriminate between genders to the regulation of macrophage polarisation [218,219]. There are currently 28 TRP channels divided into 6 families, Vanilloid, Canonical, Mucolipin, Polycystin, Ankyrin and Melastatin, the majority being ubiquitously expressed. Although there is little similarity in terms of biological function between the families, all channels are non-selective.

The TRP melastatin family (TRPM) are named as a consequence of conserved sequence homology of the N-terminal region. TRPM6 and 7 are unique in that they are cation channels fused to functional serine/threonine kinases [220]. The channel consists of six transmembrane domains, and it is assembled as a tetramer to form the active pore in the plasma membrane (Figure 1.6). Human TRPM7 is 1865 amino acids long, with a mass of 212 kDa. This channel is non-selective and predominantly conducts divalent cations under physiological conditions. Although all cell types constitutively express TRPM7, the highest levels of protein are found in the heart, liver, bone and adipose tissues [221]. TRPM7's C-terminal domain is a functioning α-kinase domain capable of phosphorylating a number of specific targets such as annexin-1A [222,223].

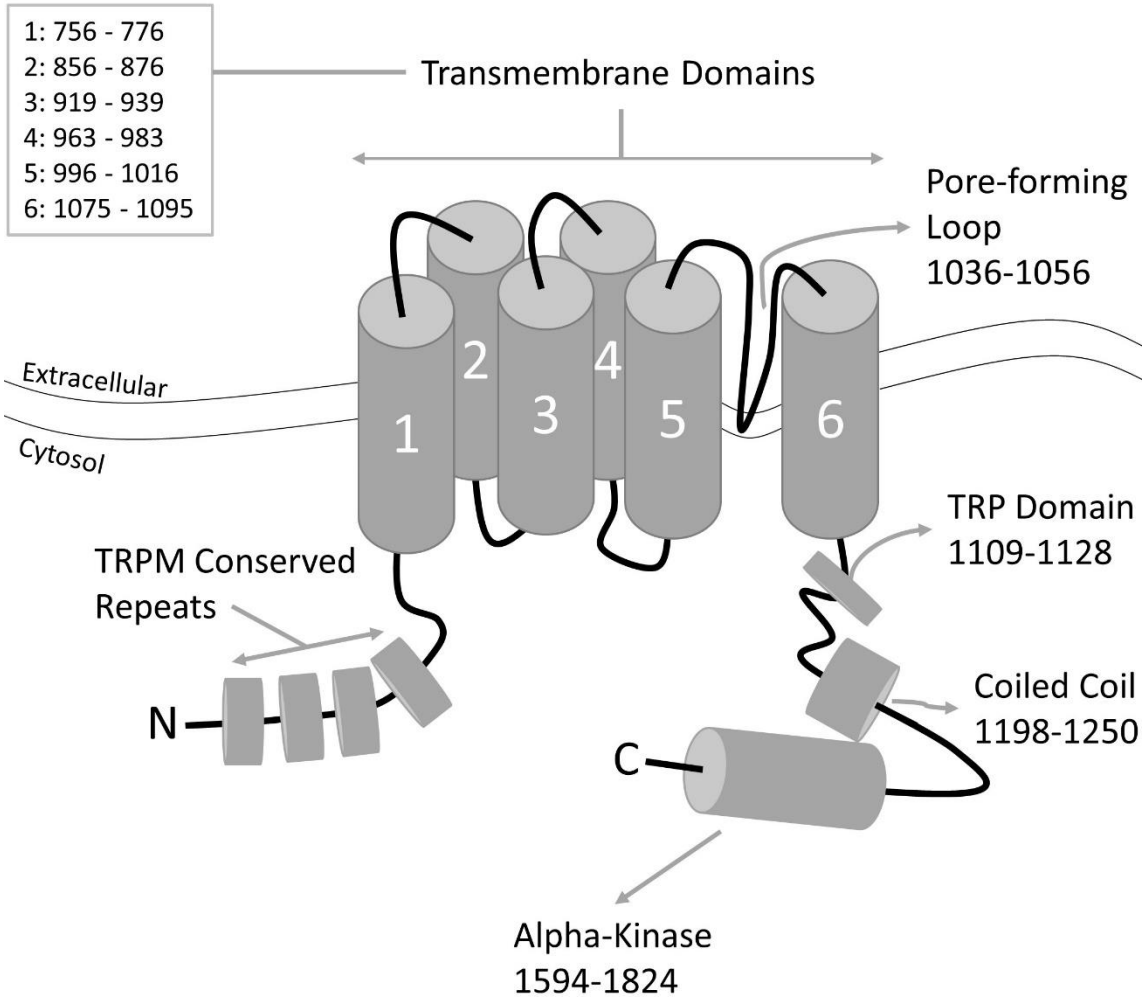


*Figure 1.6.* ***Schematic of TRPM7 and annotated domains.*** *Amino acid positions for each domain are listed, figure based upon a previously published figure* [224].

### 1.7.2 Conduction and Gating

As a non-selective ion channel, under normal physiologically relevant conditions TRPM7 conducts divalent cations such as $Ca^{2+}$ and $Mg^{2+}$ [225]. However, it also allows $Zn^{2+}$, $Mn^{2+}$ and $Co^{2+}$ to enter and leave the cell alongside the toxic divalent cations $Ni^{2+}$, $Cd^{2+}$, $Ba^{2+}$ and $Sr^{2+}$ [226]. The channel is constitutively open, but sensitive to inhibition by intracellular (millimolar) concentrations of $Mg^{2+}$ and $Mg^{2+}$-nucleotides [227]. Depletion of intracellular $Mg^{2+}$ leads to activation of TRPM7 currents showing a nonlinear current-voltage (I-V) relationship: negative voltage resulting in inward divalent current and positive voltage producing an outward monovalent flux.

Mutation of residues in the TRPM7 C-terminus have produced evidence for regulatory $Mg^{2+}$ binding sites [227]. In addition to $Mg^{2+}$, TRPM7 current is regulated by several secondary signals including $PIP_2$, fluid flow and lipids [228-230]. While the mechanisms behind this regulation are not fully understood, increased fluid flow speed across the surface of a patch-clamped cell appeared to upregulate vesicular transport of ion channels into the plasma membrane. While there is no known small molecule inhibitor specific to TRPM7, the compound 2-aminoethyldiphenylborinate (2-APB) inhibits TRPM7 currents in the micromolar range, but potentiates them at millimolar concentrations. Interestingly 2-APB increases TRPM6 currents at micromolar concentrations and is a key method in differentiating between TRPM6 and TRPM7 currents [231].

### 1.7.3 TRPM7 and Magnesium Biology

Initial reports of TRPM7 knock-out in mice revealed the ion channel as vital to embryonic development, and the key regulator of $Mg^{2+}$ homeostasis alongside its close homolog TRPM6 [232,233]. Schmitz et al. showed cells deficient in TRPM7 become $Mg^{2+}$ deficient, affecting viability and proliferation which is rescued by supplementation of extracellular magnesium [232].

Ryazanova et al. more recently created TRPM7-kinase domain specific knock-out mice [233]. Homozygous deletion resulted in embryonic lethality, but heterozygous mice were viable, showing symptoms of hypomagnesaemia and lacking intestinal $Mg^{2+}$ absorption. Homozygous TRPM7 knock-out embryonic stem cells were unable to grow unless growth media was supplemented with 10mM $Mg^{2+}$.

Data from the Clapham laboratory also demonstrated that *TRPM7* deletion prevents embryonic development [214]. However, tissue specific *TRPM7* knockout in T cells disrupted thymopoiesis in a non-$Mg^{2+}$ dependant mechanism. Total cellular and acute uptake of $Mg^{2+}$ was similar between knock-out and WT T cells despite dysregulated mRNA transcription in 12 growth factors known to regulate tissue growth. There remains conflicting opinion surrounding the importance of TRPM7 in regulating cellular magnesium levels. While it is clear TRPM7 allows $Mg^{2+}$ entry into cells and is itself inhibited by intracellular magnesium, the channel is also permeable to a number of other divalent cations to a greater extent [226].

### 1.7.4 Regulating Cell Death

In 2003 Aarts et al. showed TRPM7 channels have a key role in regulating anoxic neuronal death [234]. Following prolonged oxygen glucose deprivation, a non-selective cation channel caused neuronal calcium overload and exacerbated reactive oxygen species production. By supressing TRPM7 expression or blocking the nonselective cation channel, Aarts et al. were able to reduce calcium uptake of cells and significantly improve neuronal survival during oxygen glucose deprivation.

Recently, cleavage of the TRPM7 channel-kinase has been implicated in regulating Fas-induced apoptosis [235]. Fas-induced apoptosis is a vital pathway to cell death, and is mediated in response to cell damage, particularly DNA-damaging agents but also when induced by Fas-ligand released by cytotoxic T cells [236]. Desai et al. reported that cleavage between the TRPM7 channel

and its kinase releases the C-terminus, leaving the pro-apoptotic channel peptide which regulates internalisation of the Fas Receptor, a key step in initiating the caspase cascade.

### 1.7.5 Cardiac Biology

A key study demonstrated TRPM7's central role in heart function and development through the elegant generation of three cardiac-targeted *TRPM7* knock-out mice [213]. By using three separate cre promotors which activate at embryonic days 7, 9 and 12.5 Sah et al. demonstrated the exquisite temporal importance of the TRPM7 ion channel in cardiac growth and conduction. Cardiac deletion of *TRPM7* at E7 or E9 led to fatal congestive heart failure due to a lack of myocardial compaction at E11.5. Deletion of *TRPM7* at E13.5 led to viable mice with normal ventricular morphology and function. However, knockout of *TRPM7* at E12.5 in mice possessing only one *TRPM7* allele leads to a markedly different cardiac phenotype [213]. Half of these mice developed cardiomyopathy and heart block, showed impaired repolarisation and ventricular arrhythmia. In these cardiomyopathic mice, there was evidence of transcriptional changes, in particular reduced *Kcnd2* expression - a component of the transient outward potassium current.

In the same year Sah et al. also reported on the effect of *TRPM7* knockout on cardiac automaticity [212]. *In vitro* knock-down of TRPM7 in embryonic cardiomyocytes reduced $Ca^{2+}$ transient firing rates and reduced expression of the pacemaker current *Hcn4,* T-type calcium current *Cav3.1* and SR calcium transport ATPase isoform *SERCA2a*. Adult mice lacking TRPM7 showed atrioventricular (AV) block and sinus pauses (SP), while zebrafish treated with a morpholino targeted to *TRPM7* showed a significant reduction in heart rate. Interestingly, postnatal targeting of *TRPM7* deletion in the sinoatrial and AV node recapitulated these phenotypes of SP and AV block. This demonstrates that not only does TRPM7 regulate cardiac conduction throughout the heart but this occurs throughout adult life.

Prior to the work by Sah et al. in 2010, Du et al. linked TRPM7-mediated $Ca^{2+}$ entry in cardiac fibroblasts to atrial fibrillation [237]. Atrial fibroblasts from patients with atrial fibrillation (AF) showed significantly higher TRPM7 currents compared to those found in patients without AF. These fibroblasts were also more prone to myofibroblast differentiation, cells thought of as central regulators in fibrogenesis [238]. *TRPM7* knockdown by shRNA reduced the rate of differentiation and inhibited transforming growth factor-β1 induced proliferation, another key driver of atrial fibrosis.

### 1.7.6 TRPM7 C-terminal Kinase

Recently the Clapham laboratory published the observation that *TRPM7* is cleaved in a cell-specific manner to allow the C-terminal kinase to translocate to the nucleus where it binds transcription factors [223]. The process of cleaved kinase binding to these chromatin modifying proteins appeared to rely on the cytosolic free $[Zn^{2+}]$. As TRPM7's conductance of zinc is significantly higher than that of magnesium, it could be reasoned that this mechanism is central to how the channel-kinase exerts its control of cation homeostasis and gene regulation across an abundance of tissues and cell types [212-214,232-234].

The TRPM7 ion channel is therefore vital in cardiac heart development and the creation of a functioning conduction system [213]. However, the channel is also required for atrial and ventricular myocardial function, with its deletion in early embryonic development fatally impacting cardiogenesis. It also clearly plays a role in adult pathophysiology, with increased TRPM7 current correlated to AF while knock-out in adult mice leads to a conduction disorder-like phenotype [212,238]. TRPM7's central role in the cardiac system occurs alongside significant contribution to cellular divalent cation homeostasis and apoptosis, and it is therefore clear that predicted damaging DNA variants in *TRPM7* are of interest not only as a possible cause of unexplained stillbirth but to scientific interest in these areas as a whole [224].

## 1.8 A-kinase Anchoring Protein 9

### 1.8.1 Adrenergic Stimulation

During periods of exercise or stress, there is increased sympathetic tone in the heart resulting in raised heart rate, conduction velocity, stroke volume and increased lusitropy – the rate of relaxation. The raised level of catecholamines, primarily adrenaline and noradrenaline are ligands for β-adrenoceptors. Activation of these G-protein coupled receptors (GPCRs) is required to increase the outward potassium current that repolarise the cardiomyocyte during high heart rates. In particular the IKs current significantly increases following β-adrenergic receptor stimulation, as shown by Volders et al. in using canine ventricular myocytes [239]. This effect has also been seen in frog atrial cells, rabbit SA node cells and guinea-pig ventricular myocytes [240,241].

Following GPCR activation, the $G\alpha_s$ effector protein activates adenylyl cyclase - producing raised cAMP levels. Cytosolic cAMP binds to the regulatory subunit of Protein Kinase A (PKA), releasing a catalytic subunit capable of phosphorylation – and activating a vast array of target proteins throughout the cell. Despite the ubiquitous nature of increased cAMP levels throughout the cell, cardiomyocytes respond by targeted phosphorylation of the KCNQ1 membrane-bound protein. Until 2002, the precise molecular mechanism of coupling β-adrenergic stimulation to increased IKs current was unknown.

### 1.8.2 Yotiao and Adrenergic Coupling

It is clear that patients who possess a prolonged QT interval and are positive for a pathological variant in *KCNQ1* (LQT1) are more likely to have a cardiac event during exercise or, more broadly, sympathetic nervous stimulation [123]. In 2002, Robert Kass's group published that the β-adrenergic response of the IKs current required an accessory protein - Yotiao [109]. Yotiao co-transfected cell's IKs tail current doubled when treated with cAMP, mimicking activation of

PKA through the binding of the β-receptor by adrenaline, in comparison to untransfected CHO cells which did not respond. Marx et al. postulated that Yotiao was required to coordinate phosphorylation of the KCNQ1/KCNE1 channel complex by PKA in response to β-adrenergic stimulation. Yotiao is classified as an A-Kinase Anchoring Protein (AKAP), a family of proteins that compartmentalise enzymes regulated by secondary messengers [242].

Importantly, the protein described by Kass et al. ("Yotiao" in their paper) as required for β-adrenergic coupling, is an isoform produced by the larger *AKAP9* gene [243]. Full length AKAP9 (NM_005751) is 3,907 amino acids in length and approximately 450kDa in size. The protein identified in Kass's paper likely refers to the 1637 amino acid isoform, which shows sequence homology to the N-terminus of the full-length protein.

### 1.8.3 Discovery of LQTS11

Five years later the same group identified a putative LQTS-causing variant p.S1570L in *AKAP9*, believed to lie within the KCNQ1 binding domain of the channel [131]. The mutation reduced KCNQ1-Yotiao binding affinity and eliminated the response of IKs to cAMP stimulation. Mathematical modelling of this effect during maximal adrenergic stimulation predicted an APD increase of 121ms in homozygote p.S1570L cardiomyocytes. Interestingly, while the p.S1570L mutation lies expectedly within the short and long isoform, the single putative PKA binding domain is at amino acid residues 2554 - 2567, a site not contained in the smaller isoform.

While mechanistically it is believed that activation of KCNQ1/KCNE1 by β-adrenergic stimulation is required for meaningful $K^+$ influx by IKs to contribute to APD, only one case of definitive LQT11 has been found. However, investigation of *AKAP9* variation in LQTS1 populations has revealed interesting associations with cardiac event risk. De Villiers et al. reported that in a South African LQTS1 founder population, certain *AKAP9* haplotypes were associated with a doubling of cardiac event chances [215].

These population-based approaches have called into question the validity of *AKAP9* variants being the sole contributing factor to LQTS11 and subsequent cardiac events. Interestingly, Imredy et al. showed HEK293 cells transfected with IKs alone respond to adrenergic stimulation with forskolin [244]. They found a PKA-dependent response similar to that observed in native cardiomyocytes. This data suggests an intact signalling pathway that couples PKA activation to the targeted phosphorylation of KCNQ1 in HEK293 cells. Whilst the group did not discover the key protein responsible for this interaction, analysis of mRNA from HEK293 cells in the ENCODE database reveals significant *AKAP9* exon expression across the full length of the gene (Figure 1.7A). Evidence for the presence of AKAP9 protein can be found in the Human Proteome Atlas, with peptides identified by mass spectrometry residing across the whole length of the protein (Figure 1.7B).

With only one reported case of LQTS due to genetic variation in *AKAP9*, the discovery of five predicted damaging variants in this gene in the CICUS population make it an interesting target for follow-up functional studies to ascertain pathological significance.

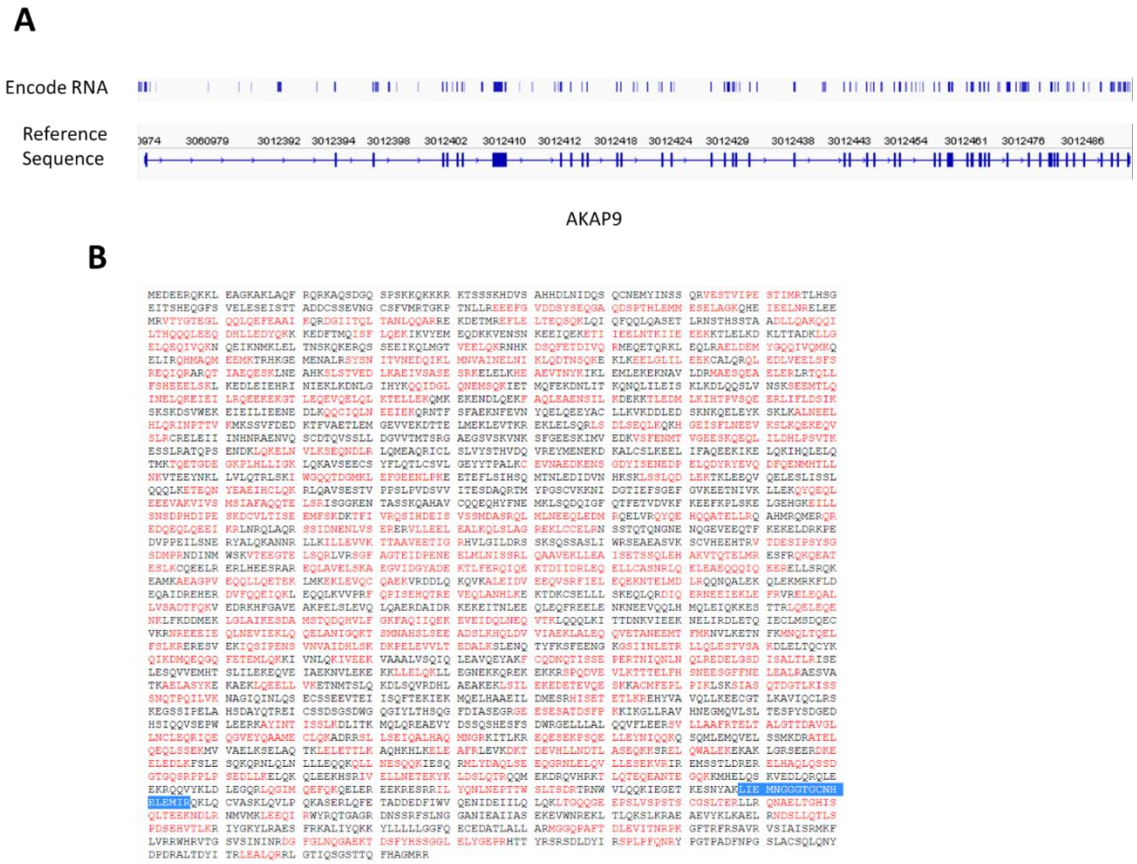


*Figure 1.7.* ***HEK293 mRNA and proteome found in online databases. A*** *Exon sequencing data from HEK293 cells sequenced for the ENCODE project (top) compared to* AKAP9 *genome map (below)* [245]*. Large blue blocks denote exons, the arrow depicts the direction of transcription. Total RNA was harvested from 5 x* $10^6$ *cells.* ***B*** *AKAP9 full length amino acid sequence with peptides present in human foetal heart tissue in red from the Human Proteome Map* [246]*. Proteins were quantified using high resolution mass spectrometry. The highlighted blue section shows the most abundant peptide found in the tissue.*

## 1.9 Modelling Cardiovascular Disease with Pluripotent Stem Cells

### 1.9.1 Generating Pluripotent Stem Cells

Modelling the effect of deleterious ion channelopathy variants on the cardiovascular system can be difficult in comparison to other diseases due to the difficulty in obtaining and culturing adult cardiomyocytes. These cells do not proliferate readily and rapidly commit to anoikis when left unattached to a surface for long periods of time [247,248]. Using small animals to model cardiovascular diseases has provided numerous insights into human physiology [249], but substantial differences exist on the cellular level between the cardiomyocytes of large mammals and small rodents [250]. For example, the repolarising $K^+$ currents expressed in mammal cardiomyocytes varies greatly across species and accounts for major electrophysiological differences in action potential duration. While slowly activating $K^+$ currents such as IKs are thought to be key in repolarising human cardiomyocytes, it is unlikely to contribute to repolarisation in mice whose rapid heart rate (>500bpm) means ion channels opening after 50ms will have no meaningful effect. Mouse models where the *KCNQ1* gene has been deleted show few abnormal AP characteristics under normal conditions (+8ms QTc); prolonged QT was exacerbated by only adrenergic challenge [251]. However, these slight differences are not comparable to Jervell and Lange-Nielsen Syndrome in humans, where patients present with significantly prolonged QT at rest (557ms QTC) and have a severe history of cardiac arrest and sudden death [252].

Breakthroughs in developmental biology yielded a viable alternative to relying on mice to model cardiomyocyte biology, generating contractile heart cells from human pluripotent embryonic stem cells [253]. This was limited initially to the generation of contractile aggregates, these spontaneously contracting bodies that stain positive for human cardiac structural proteins and expressed genes associated with early human cardiomyocytes. These cells had calcium transients lasting ~130ms and showed delayed relaxation, which were sensitive to isoproterenol

and carbamylcholine treatment. However, efficiency of this process was low, with spontaneously contracting sections only occurring in 8.1% of stem cell embryoid bodies.

The recent advances of human induced pluripotent stem cell (iPSC) technology in 2007 by Shinya Yamanaka now allows pluripotent stem cells to be derived from human somatic cells instead of human embryos [254]. By transducing skin fibroblasts with four reprogramming factors (Oct3/4, sox2, Klf4 and c-Myc), Yamanaka et al. transformed fibroblasts into pluripotent stem cells capable of differentiating into cell types of all three germ layers. This has given laboratories the ability to generate iPSC cell lines from any cell line, and therefore a possible supply of human cardiomyocytes to assay and model human cardiovascular disease. Progress in stem cell biology has been coupled with improved protocols to differentiate cells into cardiomyocytes, from simple monolayers to 3-dimensional printed cardiac muscle patches [255,256]. These cells have been used to repair damaged myocardium in animals, study early cardiac development, investigate cell metabolism and screen drugs for arrhythmia-related side effects [257]. Characterisation of these cells from the Burridge et al. protocol shows that stem cell-derived cardiomyocytes express cardiac structural proteins, express cardiac specific genes and appear to be a heterogenous population of nodal, atrial and ventricular-like cells. However, these cells do not reach the structural and electrophysiological maturity of adult human cardiomyocytes, and transcriptionally they are less mature than foetal human cardiomyocytes [258,259].

### 1.9.2 Modelling Channelopathies with iPSC-CMs

Despite these drawbacks, several groups have studied a multitude of different ion currents in iPSC-CMs. In a seminal paper in 2010, Moretti et al. published patch-clamp recordings from cardiomyocytes derived from iPSCs reprogrammed from healthy and a LQTS1 patient [260]. The iPSCs were heterozygous for a p.R190Q variant in the *KCNQ1* gene. Action potential recordings from ventricular and atrial-like cells showed significantly prolonged APD compared

to control cells. Whole-cell recording of IKs showed significantly decreased current density recordings from LQTS patient iPSC-CMs. This recapitulated the expected phenotype seen in patients, albeit observed KCNQ1/KCNE1 current densities even in control patients were extremely low (<3 pA/pF).

One year later, Itzhaki et al. published whole-cell patch-clamp recordings of CMs differentiated from iPSC cells derived from a patient with p.A614V LQTS2 [261]. Action potential duration in LQTS2 iPSC-CMs (atrial and nodal) was strikingly prolonged compared to control cells. There was also evidence of EADs and triggered arrhythmias recorded in cells possessing the mutant allele, but not in controls. These two studies showed that iPSC-derived cardiomyocytes can be used to model cardiac ion channelopathies. Cells derived from mutant cells did have prolonged APDs and reduced potassium currents, but these results only recapitulated data previously seen from heterologous cell work and predicted computational modelling, although in a more physiologically relevant system [262,263].

In 2012 Davis et al. used mouse- and patient-derived iPSC cells with a heterozygous p.1798insD *SCN5A* mutation to recapitulate LQTS3 [264]. Action potentials had reduced upstroke velocity and prolonged duration, similar to primary cells isolated from mice with the same mutation. In iPSC-CMs heterozygotic for p.1798insD, inward sodium currents were reduced and $APD_{90}$ was significantly reduced compared to WT cells. The rare autosomal dominant LQTS8, or Timothy syndrome has also been modelled with iPSC-CMs [265]. Cardiomyocytes derived from iPSCs with a p.G406R variant in *CACNA1C* showed reduced calcium currents, prolonged APD and increased putative DAD rate compared to WT cells. These results were consistent with the properties of mutant channels observed in heterologous cells [128].

## 1.10 Hypothesis and Aims

Unexplained stillbirth is common across the world, with diagnosis made by exclusion of any known causes. It would be a significant step to identify pathological genetic variants that increase risk, or cause stillbirth.

*Hypothesis: nonsynonymous variants discovered from unexplained stillbirth cases in AKAP9 and TRPM7 may functionally affect protein function, potentially causing stillbirth.*

The aim of my PhD project was to carry out functional analysis on the effect of nine nonsynonymous variants, four in *TRPM7* and five in *AKAP9* by:

1. Procurement of plasmids expressing *TRPM7* and *AKAP9*, followed by site-directed mutagenesis to insert the nonsynonymous variants into the genes
2. Establish protocols to assay normal function of wild-type TRPM7 ion channel and the anchoring protein AKAP9
3. Compare the effect of CICUS variants in *TRPM7* and *AKAP9* against their wild-type proteins to investigate possible functional effects
4. Investigate the expression and importance of *TRPM7* in human cardiogenesis using *in vitro* cardiomyocyte differentiation from iPSCs

# 2 Methods & Materials

## 2.1 Ethical Approval

We prospectively collected fresh tissue (heart, muscle, kidney) from unexplained stillbirths (>22 weeks) where no definite cause of death could be identified after a full autopsy, from four National Health Service (NHS) hospitals (University College London Hospital, Great Ormond Street Hospital, Southampton University Hospital and Sheffield Children's Hospital) between 2007 and 2013, after informed parental consent. In addition, we included previously archived fresh frozen tissue from a stillbirth cohort from Sheffield Children's Hospital.

The Central London Research Ethics Committee 2 approved the study (code - 10/H0713/26). Patient samples for stem cell work were used with informed consent (code - 13/LO/0224) and approved by the UK's National Research Ethics Service.

## 2.2 Variant Prioritisation

In total, 311 nonsynonymous SNVs were present in the CICUS population of unexplained stillbirths. Therefore it was important to prioritise variants to allow for the functional testing of those most likely to be deleterious [266]. 563 samples from the 1000 Genomes project were selected as a "control" sample for burden testing [267]. The samples were randomly selected to reflect the same ethnic super code profile as the stillbirth samples; 69.6% European, 3.3% East Asian, and 1.4% African with the remaining 25.7% being randomly selected from the remaining samples in the 1000 Genomes project.

We first filtered variants based upon nucleotide constraint using the GERP++ scoring tool [268]. A higher GERP++ score reflects base pairs across species that have fewer substitutions than would occur during natural selection. Nucleotides within exons that resist evolutionary pressure across multiple species (said to be conserved or constrained) are more likely to be

important to the function of the protein. We used a GERP++ score of ≥2 as a cut-off to discern variant substitutions that occurred in conserved regions. Although an arbitrary value, it has been used in prior work investigating genetic variants and infant sudden cardiac death [269]. This value selects for variants that occur in nucleotides above the average level of constraint in coding regions (GERP++ ~2).

Constrained variants were removed if they occurred at a frequency above 0.1 in either the 1000g or Esp6500 project databases [270]. For a severe pathological phenotype like stillbirth, it can be assumed that genetic variants that predispose for the condition will be completely novel or very rare in the general population. As no studies have conclusively linked channelopathies to stillbirth, it is not known whether it is a Mendelian or complex genetic disorder. Studies into LQTS have shown a complex trait-like phenotype – a highly variable QT interval has been found in an LQTS population with an identical *KCNQ1* variant (p.A341V) but diverse *AKAP9* genotype [215]. Lastly we excluded any variants deemed not likely to be damaging by three separate mutation analysis tools – SIFT, PolyPhen and Mutation Taster [271,272].

## 2.3 Plasmid Preparation

### 2.3.1 Expression Vectors

To functionally test the effect nonsynonymous variants have on protein function it is vital to have an effective measure of a protein's basal function. The first stage in interrogating the effect of *TRPM7* and *AKAP9* CICUS variants is to establish a cellular system that measures ion channel activity or β-adrenergic coupling respectively. The first step in this aim is to heterologously express the relevant components in cell lines. This was accomplished through the use of DNA expression vectors that upon entry into a cell translocate into the nucleus where transcription of the gene of interest can occur. Following mRNA translation in homologous mammalian cells, the resultant protein is modified and transported to its intended subcellular location due to transport motifs inside the protein.

The TRPM7 cDNA cloned into a pcDNA4/TO plasmid was gifted to our lab by Professor Schmitz [222]. The tetracycline repressor plasmid, pcDNA6/TR was also supplied by Professor Schmitz. An eGFP plasmid from (Clontech) was used to identify successfully transfected cells.

Due to its large size (11,724bp mRNA) and there being no reports of an available plasmid from other research groups, the *AKAP9* expression plasmid was constructed by Genscript (Clone ID: OHu26045, USA).

### 2.3.2 Bacterial Transformation

The use of expression vectors on an experimental scale requires a large quantity of DNA that will require constant replenishment. To scale up quantities of DNA, the vector is commonly transformed into a recipient bacteria that copies the invasive DNA using their own replication machinery. This process occurs alongside rapid bacterial growth – allowing micrograms of DNA to be harvested over the course of a few days. Plasmids contain a number of specific elements that allow targeted replication of vector DNA (Figure 2.1). For example, a pUC plasmid will be readily replicated in *E.coli* at a high copy number. Antibiotic resistant genes give transformants antibiotic resistance while others allow for selection of stable mammalian transfectants.

Bacteria are grown in agar or nutrient broth containing an antibiotic specifically matched to the gene product found within the experimental vector. This targeted selective pressure ensures that only transformant bacteria carrying the plasmid are able to replicate.

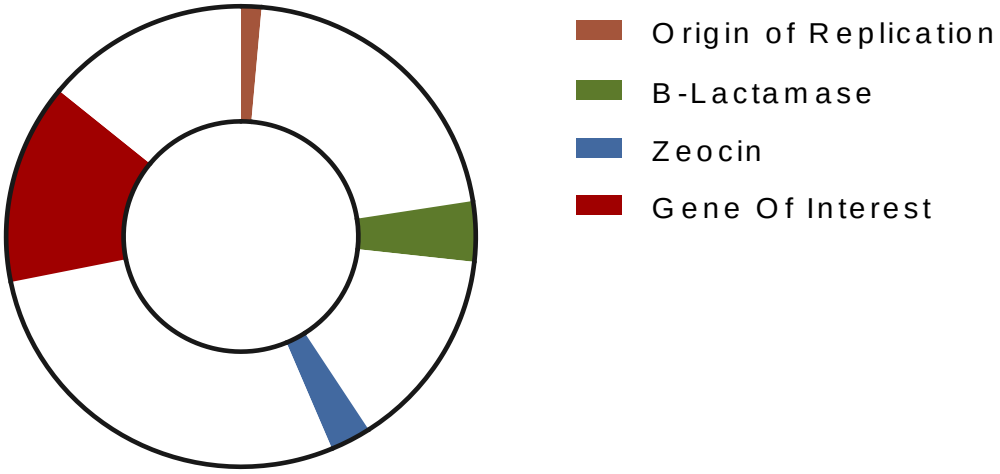


*Figure 2.1.* ***Simplified bacterial plasmid map depicting key DNA elements.*** *An origin of replication allows DNA replication inside transformed bacteria. Resistant genes β-lactamase and zeocin (also called Sh ble) confer resistance to media containing ampicillin (or carbenicillin) and zeocin, respectively. This allows selection for transformed bacteria and transfected mammalian cells, respectively. Transcription of a gene of interest is usually controlled through a combination of CMV/T7 enhancer/promoter. Without a gene of interest insertion standard expression plasmids are usually 5000 to 6000bp in circumference.*

Six tablets of LB were added to 300ml of double distilled water (dd$H_2O$) to make LB broth, and four LB tablets and 3g agar was added to 200ml dd$H_2O$. 200µl of carbenicillin (100mg/ml) was added to the agar before it was allowed to set in plastic petri dishes. Competent top ten (TT) E coli (Invitrogen, USA) cells were thawed from -80˚C on ice for 30 minutes. 100µg of expression vector DNA was added to 50µl of TT. These underwent a 90 second heat shock at 42˚C on a heated block. Then, TTs were placed back on ice for 2 minutes before mixing with 800µl of LB broth. Following incubation at 37˚C for 45 minutes cells were centrifuged at 13,200rpm for 1 minute and resuspended in 100µl LB. This LB/cell mixture was then plated overnight on cooled agar plates containing the expression vector specific antibiotic.

The following day single colonies were picked from the agar plates and incubated in 5ml of LB plus 5µl antibiotic (100mg/ml) at 37˚C. Following this initial growth phase, this starter culture was mixed with 45ml LB and 5µl antibiotic (100mg/ml) and left overnight at 37˚C to grow to confluency. The resulting 50ml cultures were centrifuged at 4000rpm for 30 minutes, chilled

at 4˚C to give a large bacterial pellet. The supernatant was removed and the pellets frozen at -20˚C until harvesting.

DNA vectors were isolated from bacterial pellets using the Qiagen Midi kit. Pellets were frozen before sequential re-suspension in 4ml of buffer P1 and buffer P2. The solution was inverted 6 times and incubated at room temperature for 5 minutes to ensure complete lysis of bacteria. 4ml of chilled buffer P3 was added, the solution was then inverted 6 times and incubated on ice for 15 minutes to allow precipitation of bacterial genomic DNA, proteins and cellular debris. This precipitate was filtered out using 150mm Whatman filter paper. A qiagen-tip-100 was equilibrated by the addition of 4ml Buffer QBT and the filtered supernatant poured through. The column was washed twice with 10ml Buffer QC before elution of DNA with 5ml Buffer QF. 3.5ml 2-propanol was then added to precipitate out the DNA and the solution was then centrifuged for 90 minutes at 4000rpm, 4˚C. The supernatant was removed and the DNA pellet washed with 1ml 70% ethanol, this solution was then centrifuged at 14,000rpm for 10 minutes. The ethanol wash was repeated following removal of the supernatant and the DNA pellet was air-dried for 10 minutes. Nuclease free water was then added to dissolve the DNA before its concentration determined by Nanodrop (ThermoScientific, USA).

### 2.3.3 Sanger Sequencing

Prior to the use of expression vectors it was important to ascertain their sequence identity, this was done using the Sanger method. Although pioneered in 1977 by Fred Sanger, the chain-termination technique is still considered the 'gold-standard' in reporting sequencing data [273]. Sanger sequencing involves DNA polymerase copying single-stranded DNA through the extension of a growing chain of nucleotides. When dideoxynucleotides (ddNTPs) are incorporated by DNA polymerase, subsequent chain extension is impossible. When specific ddNTPs are added in sequence to these reactions, DNA chains are terminated at specific lengths

corresponding to the final ddNTP. By incorporating fluorescent dye-conjugated terminator ddNTPs, automated sequencing can detect fluorescent signals at specific wavelengths in sequential order during sequencing.

10µl of plasmid DNA at 100ng/µl was submitted to the William Harvey Research Institute Genome Centre per sequencing reaction alongside 5µl of sequence specific primers at 10pmol/µl. After Sanger sequencing the resulting chromatogram was analysed using GenomeCompiler (USA). All sequencing primers used in this thesis are listed in Table 2.1. To ascertain sequence identity, the received DNA vectors were aligned to their reference genes using EMBOSS Needle (www.ebi.ac.uk/Tools/psa/emboss_needle/nucleotide.html).

| Primer Target | Nucleotide Sequence 5' – 3' | Primer Target | Nucleotide Sequence 5' – 3' |
|---|---|---|---|
| CMV | CGCAAATGGGCGGTAGGCGTG | TRPM7 Reverse Sequencing Primers | GCCTGTTCCTTCACACACAA |
| TRPM7 Forward Sequencing Primers | GTCCCTGTGGTGGCACTTAT | | AAGGAAAGCGCTTGGTTTCT |
| | AGCCCTACCGACCAAAGATT | | TGGTTTACTTTCCCAGCTTCA |
| | CCTTCAGTTCAAGAATGGATTG | | TTGACACGATCTCCAACTTCTTT |
| | GATGACAAATTTCATTCTGGGA | | CAATCCGGTATTAAAGCTGC |
| | TGTCACAGAACTTCCATTCCTG | | GAATTACAGTGATGTTTTGCTCTGA |
| | GCAGAAGAAAAGAGATCCTGTGA | | |
| AKAP9 Forward Sequencing Primers | CAAGCAAGAAGAGAAAAGGATGA | AKAP9 Reverse Sequencing Primers | TCACTAGCCTGTAATTGCTGAAA |
| | AGACAACACATGGCACAGATG | | ATTTGAATATGACCTTAAAGCATTC |
| | GCAGTTTGAAAAGGACAATTTGA | | TGACTTTGAATTTACAAGAGACTGC |
| | TCTGTCTTTGATGAAGACAAAACTT | | TTCTCTCGCTTGGTTACCTCA |
| | GCTCAAGAGGAAAAGATCAAGG | | AGGCTTTCCTTCATCACCTG |
| | CAAGCTTACCTGTTGATTCGG | | CCAGAAAACTCTATTGTACCATCAAT |
| | AGACAGCGAGAAGACCAGGA | | CCAGGTTTTCATTATCTATGGAGG |
| | CGACTACAAGCAGCAGTTGA | | CTCACGCATCAACTCTGTCTG |
| | TGTATTCCAACAGGAAATACAGAAA | | TGATTTGCTAACTGTTCAACCTC |
| | AAATGAACTGATAAGGGATCTTGAA | | TGAGCTGCTCTATTTCTTCTTCTC |
| | AAAGTGGCTGCTGCTCTTGT | | CAGGTTCTGATGAAATTGTTTGA |
| | CAGATGGGACTCTGAAGATCA | | TCTGAGGAACATTCACTCTGTAAA |
| | AGAGCTTCTCAGACTGGCGA | | CGTCCGAAATGCTGCTAGTAA |
| | TCAGAAACAAAGGAATCTTCAGC | | AGCATTCTCTGTGATTCTATTTTT |
| | GAAGGAGAAACAAAAGAATCAAA | | TTTCTAATTCATGATTACAGCCG |
| | ATACCTGCTGCTGTTACTGGG | | CTAGATCCGTGAAAGCTGGC |

*Table 2.1.* ***List of all sequencing primers used during this thesis.*** *All primers are listed in their 5' to 3' direction.*

### 2.3.4 Site-directed Mutagenesis

To investigate the effect of amino acid substitution on protein function, targeted specific nucleotide changes are required in the expression construct. The QuikChange II Site-Directed Mutagenesis Kit was used to insert nonsynonymous mutations into the *TRPM7* gene. Primers that anneal to the mutation site ~10-15bp both up- and down-stream of a single mismatch variant were synthesised by IDT (Iowa, USA) according to Table 2.2.

Denaturing wild-type DNA allows binding of mutagenic primers, this is followed by DNA extension of the oligonucleotides by the provided *PfuUltra* DNA polymerase. Followed by thermal cycling, both strands of the vector will be replicated incorporating the new primer, and will hopefully generate a mutated plasmid. Treatment of the sample by *Dpn* 1 digests any methylated DNA, as all *E. coli* strains methylate their DNA after replication this removes any DNA strands not arising from both primers. The mutagenesis reaction mixture reagents are listed in Table 2.4.

The mutagenesis reaction mixture was made and tubes inserted into a thermal cycler, which upon heating to 95˚C cycled through a 30 second step at 95˚C, one minute at 55˚C and 11 minutes at 68˚C. The protocol lasted for 12 cycles. Tubes were then placed on ice for 2 minutes to cool before addition of 1µl of *Dpn* I. The reaction was mixed by pipetting before incubation at 37˚C for 1 hour to allow parental DNA to be digested. This product was transformed into competent bacterial cells as previously described in 2.3.2.

| Target Mutation<br>TRPM7 | Forward Primer Nucleotide Sequence (5’ – 3’)<br>Reverse Primer Nucleotide Sequence (5’ – 3’) |
|---|---|
| c.G536T:p.G179V | CTGGAGGAGTAAACACAG**T**TGTGGCAAAACATGTTG<br>CAACATGTTTTGCCACA**A**CTGAGTTTATTCTTCAAG |
| c.G1481A:p.R494Q | CTGTTTCATCTTGTTC**A**AGACTGTCAAACAGG<br>CCTGTTTGACAGTCT**T**GAACAAGATGAAACAG |
| c.C2579T:p.T860M | GTAAAATTCTGGTTTAACA**T**GTTGGCATATTTAGGATTTC’<br>GAAATCCTAAATATGCCAAC**A**TGTTAAACCAGAATTTTAC |
| c.A3614G:p.E1205G | CTTTTGAAAGAGTGG**G**ACAGATGTGCATTCAG<br>CTGAATGCACATCTGT**C**CCACTCTTTCAAAAG |

*Table 2.2.* ***Site-directed mutagenesis primers targeting TRPM7 CICUS variants.*** *Both forward and reverse primers are listed with the altered nucleotide labelled in bold. All primers are shown 5’ to 3’.*

| AKAP9 | Forward Primer Nucleotide Sequence (5’ – 3’)<br>Reverse Primer Nucleotide Sequence (5’ – 3’) |
|---|---|
| c.C464A:p.T155N | GGAGCACAAGACAGTCCGA**A**TCATCTAGAGATGATG<br>CATCATCTCTAGATGA**T**TCGGACTGTCTTGTGCTCC |
| c.G4519Cp.D1507H | GGTTTTCAGACTTTTGAGACAGTG**C**ATGTGAAATTTAAAGAAGAATTTAA<br>TTAAATTCTTCTTTAAATTTCACAT**G**CACTGTCTCAAAAGTCTGAAAACC |
| c.A6176G:p.E2059G | GACAGCAAAACCAAGCATTGG**G**AAAGCAGTTAGAAAAAATGAG<br>CTCATTTTTTCTAACTGCTTT**C**CCAATGCTTGGTTTTGCTGTC |
| c.T6556C:p.S2186P | TAGAAGCTAAACCAGAATTG**C**CCCTAGAAGTACAATTGCAG<br>CTGCAATTGTACTTCTAGGG**G**CAATTCTGGTTTAGCTTCTA |
| c.G9127A:p.A3043T | GAAGAGCGTAGTGTTTTACTA**A**CAGCATTTCGGACGGAGC<br>GCTCCGTCCGAAATGCGG**T**TAGTAAAACACTACGCTCTTC |

*Table 2.3.* ***Site-directed mutagenesis primers targeting AKAP9 CICUS variants.***

| Component | Volume |
|---|---|
| 10X RT Buffer | 5µL |
| *TRPM7*/*AKAP9* expression vector | 2µL |
| Forward Mutagenesis Primer | 125ng |
| Reverse Mutagenesis Primer | 125ng |
| dNTP mix 10mM | 1µL |
| Nuclease-Free $H_2O$ | Up to 50µL |
| *Pfu* DNA polymerase 2.5 U/µL | 1µL |

*Table 2.4.* ***Recipe for a single QuikChange II Mutagenesis reaction.***

## 2.4 Cell Culture

### 2.4.1 Cell Selection

To investigate the effect of predicted harmful nonsynonymous variants on protein function, a cellular system is required to transcribe and translate the expression plasmid DNA into a recombinant protein. Two cell lines, human embryonic kidney 293 (HEK293) and Chinese hamster ovary – K1 (CHO-K1) were used for all cellular experiments. Due to TRPM7's ubiquitous expression in mammalian cells, it is impossible to select a cell system that does not express TRPM7. Therefore HEK293 and CHO-K1 were selected due to their low background ion channel expression, and due to their well characterised nature in patch-clamp experiments [223,226,227,274,275].

To examine the effect that *AKAP9* CICUS variants had on wild-type protein, we required a cell line responsive to adrenergic stimulation but initially lacking the capacity to couple PKA activation to KCNQ1 phosphorylation. This would ensure we could measure a robust effect of wild-type *AKAP9* transfection before comparison between mutants. Initially IKs was measured in a stable HEK293 cell line expressing *KCNQ1/KCNE1*, however this current responded to adrenergic stimulation without *AKAP9* transfection. Therefore we used CHO-K1 cells to measure

adrenergic-coupling to IKs as this response was only found following co-transfection of *KCNQ1/KCNE1* and *AKAP9.*

### 2.4.2 Cell Culture

Mammalian cell transfection is most efficient when cells are growing in an approximately physiological environment with sufficient surface area to proliferate unimpeded. To ensure this, cells are cultured in heated incubators injected with gaseous 5% $CO_2$. HEK293 cells were grown in MEM supplemented with FBS (10%) and penicillin-streptomycin (1,000 units/ml). CHO-K1 cells were cultured in HAM F-12 also supplemented with FBS and penicillin-streptomycin (10% & 1,000 units/ml respectively). All cells were cultured in T75 flasks in ~12ml of media at 37˚C with 5% $CO_2$ before growth to >95% confluency. When cells reached confluency they were passaged to ensure cells were kept in growth phase – required for efficient transfection.

The T75 flask media was removed before a single 7ml PBS wash to remove any remaining media. Trypsin (3ml) was added to the flasks before incubation at 37˚C for five minutes. Using a light microscope, cell detachment was monitored and after 5-10 minutes 7ml of media was added to inactivate the trypsin and ensure cell viability. From the resulting 10ml, 1ml of HEK293 cells (1:10) was added to 12ml MEM media in fresh T75 flasks. Due to their rapid proliferation, 0.3ml of CHO-K1 cells (1:30) were added to 12ml HAM F-12. These new flasks were incubated at 37˚C for 4-5 days before growth to confluency. The remaining cells were reseeded in 6-well dishes at 70% confluency for transfection experiments.

### 2.4.3 Transfection

A number of transfection reagents were employed in a cell specific manner to facilitate the entry of plasmid DNA into the cells. There are biological, chemical and physical methods

available to facilitate the uptake of foreign DNA by mammalian cells [276]. FuGENE® Transfection Reagent is a nonliposomal formulation that has been documented to successfully transfect both HEK293 and CHO-K1 cells, it was used to transfect HEK293 cells. NovaCHOice Transfection reagent (Merck, USA) was specifically designed for efficient CHO cell transfection and was used to transfect CHO-K1 cells. Vector DNA was co-transfected alongside an eGFP expression plasmid to identify successful transfected cells. All transfections were incubated for 15 minutes in 37˚C Opti-MEM (ThermoFisher, USA) media prior to pipetting into 6-well dishes. The proportions of vector DNA, eGFP and transfection reagent are given in Table 2.5.

| **Transfection Component** | **Amount** | **Concentration** |
|---|---|---|
| TRPM7 plasmid construct | 500 ng | 5ng/µl |
| Tetracycline Repressor | 1800 ng | 18ng/µl |
| eGFP plasmid | 50 ng | 0.5 ng/µl |
| FuGENE | 6 µl | |
| NovaCHOice / Booster Reagent | 2 µl / 1µl | |
| Opti-MEM | 100 µl | |

*Table 2.5.* ***Standard transfection reaction in 6-well dish using FuGENE or NovaCHOice.***

### 2.4.4 Cell Harvesting

Following transfection, cells were either harvested for analysis or dissociated into single cells to allow for patch-clamp experiments. To harvest cell pellets, the media was removed and adherent cells washed with 2ml of PBS. After the wash step 100µl of ice cold PBS was added to cells before scraping the bottom of the dish with cell scrapers. The resulting 100µl cell suspension was centrifuged at 10,600 *g* at 4˚C for 10 minutes and the supernatant removed. All pellets were stored at -20˚C before further experimentation.

Native proteins, particularly ion channels may not present an epitope to allow antibody binding unless the cell lysates have been properly prepared. Cell pellets were mixed with 100µl NP40 lysis buffer (0.15nM NaCl, 1% NP40 and 0.05mM Tris) diluted in dd$H_2O$. The solution was kept on ice for 20 minutes followed by centrifugation at 10,600 g for 20 minutes to pellet any remaining cellular debris. NP40 is a mild non-ionic detergent and removes plasma membrane attached to proteins. The supernatant was removed and its protein concentration determined using the bicinchoninic acid (BCA) assay.

### 2.4.5 BCA Assay

The BCA assay relies upon colorimetric detection to quantify the concentration of protein in a cell lysate sample. The reduction relies upon the reduction of $Cu^{2+}$ to $Cu^{+}$ by protein in alkaline solutions. The product of this reaction, produces a purple product which absorbs light at 562nm. A linear relationship between increased protein concentration and absorbance at 562nm allows known protein concentrations to generate a standard curve, and allow interpolation of unknown protein concentrations by comparing them to this plot.

Standards were prepared using Bovine Serum Albumin (BSA) ranging in concentration from 25µg/ml to 2mg/ml, diluted in NP40 lysis buffer. A working reagent containing $Cu^{2+}$ and bicinchoninic acid was prepared, which was used to dilute 10µl of standards and unknown

lysates (in duplicate) in a ratio of 1:20. These were then pipetted into 96-well plates and incubated at 37˚C for 30 minutes. The plate was then cooled and absorbance measured at 562nm using a Victor Multilabel Plate Reader (PerkinElmer, USA).

## 2.5 Western Blotting

### 2.5.1 Introduction

Developed in 1979 by Harry Towbin, the western blot is a laboratory technique that enables the detection of denatured proteins from tissue or cellular lysates [277]. Quantifiable expression of a protein is vital if it is to function on a cellular basis. Detectable protein levels will ensure not only that transfection is occurring successfully, but quantification of expression may show significant differences between wild-type transfected cells and those expressing harmful variant DNA.

### 2.5.2 Protein Lysate Preparation

Before protein can be analysed by western blot, first lysates were mixed with a 6X loading buffer containing: 4% sodium dodecyl sulfate (SDS), 20% glycerol, 0.004% bromophenol blue and either 100mM β-mercaptoethanol or dithiothreitol (DTT) at pH 6.8. This solution was heated at 95˚C for 5 minutes to denature any higher order peptide structures. Polyacrylamide gels (Precast 4-20% gradient gels or 4% stacking – 8% running polyacrylamide gels) were cast and inserted into gel tanks filled with running buffer (25mM Tris base, 190mM glycine and 0.1% SDS). To allow bands that appear in the sample lanes to be quantified by size, 10µl of pre-stained protein ladder (Spectra Multicolour High Range Protein Ladder) was loaded into the first well. In subsequent lanes 100µg of sample (concentration measured by BCA assay) was loaded into each well.

Due to proteins negative charge, passing electrical voltage across the gel will cause denatured proteins to run towards the cathode in the gel tank. Gels were ran at 60V for 10 minutes to allow the gels to stack before increasing the voltage to 100V. After gel separation by size, to visualize protein bands, lysates are transferred to PVDF to allow antibody blotting. PVDF membranes were primed in methanol for 30 seconds, washed in dd$H_2O$ before equilibrating in transfer buffer (25mM Tris base, 190mM glycine) for at least 5 minutes.

### 2.5.3 Gel Separation and Membrane Transfer

The polyacrylamide gel, with PVDF membrane on top was sandwiched between blotting paper and placed inside a transfer tank filled with 1L of transfer buffer (25mM Tris and 192mM glycine) and placed in the cold room at 4˚C. Transfers were run at 90mA overnight. Membranes were then removed, and non-specific binding blocked by agitating with 10ml PBS-T (0.1% Tween 20) and 5% non-fat milk for one hour at room temperature. The membrane was then incubated with a primary antibody (Table 2.6) at room temperature for a further hour. Membranes were then washed to remove any non-bound primary antibody, with 10ml PBS, 10ml PBS-T and finally 10ml PBS, each for 5 minutes.

### 2.5.4 Developing using Chemiluminescence

To visualize protein bands on X-ray film, secondary antibodies conjugated to horse radish peroxidase (HRP) were used. 2µl of IgG HRP mouse or rabbit targeting secondary antibodies were added to 10ml PBS-T 5% non-fat milk and incubated with membranes at room temperature for one hour. PVDF membranes were washed with PBS/PBS-T as previously mentioned and dried briefly before addition of Amersham ECL Prime detection reagent for two minutes. In the presence of HRP hydrogen peroxide is oxidised alongside luminol, producing light. This is absorbed by X-ray film and appears as a band corresponding to the secondary

antibody's position. Polyvinylidene fluoride (PVDF) membranes were gently rinsed in dd$H_2O$ and imaged in a dark room using Amersham Hyperfilm and a Konica SRX-101A processor.

| **Primary Antibody (product code)** | **Clonality** | **Origin** | **Supplier** |
|---|---|---|---|
| TRPM7 (N74/25) | Monoclonal | Mouse | Neuromab |
| TRPM7 (ACC 047) | Polyclonal | Rabbit | Alomone |
| TRPM7 (sc271099) | Monoclonal | Mouse | Santa Cruz |
| FLAG (F3165) | Monoclonal | Mouse | Sigma-Aldrich |
| β-Actin (ab8226) | Monoclonal | Mouse | Abcam |
| Calnexin (sc11397) | Monoclonal | Mouse | Santa Cruz |
| AKAP9 (ab32679) | Monoclonal | Mouse | Abcam |

*Table 2.6.* ***List of primary antibodies used for western blot.***

## 2.6 Patch-clamp

### 2.6.1 Introduction

The ionic current passing through ion channels, or the fluctuating membrane potential of a cardiomyocyte are governed by Ohm's Law. The movement of ionic charge is called current and is measured in amps (I). The potential difference between two charged solutions is measured in volts (V), and the ease at which the current flows between these two solutions is known as conductance (g, measured in siemens). Ohm's law states:

$$I = gE$$

The reciprocal of conductance is called resistance (R, measured in ohms or Ω), and Ohm's law can be rewritten as:

$$V = IR$$

The cell's plasma membrane has a very high resistance due to a low conductance - the hydrophobic core strongly inhibits ionic movement. When ion channels open, the membranes resistance is dramatically reduced by pores that allow ions to pass through the membrane, this resulting movement of ions can be measured using the patch-clamp technique. Hodgkin and Huxley won the Nobel prize in 1963 for their work on the giant squid axon, these experiments went on to lay the groundwork for the modern method [278]. Their findings provided a mathematical model with clear rules to govern the passage of ions in a nerve cell during action potentials. Three years previously Ling and Gerard, using glass microelectrodes, had measured the membrane voltages of frog Sartorius fibres [279]. In 1981, Neher and Sakmann investigated ionic currents through single acetylcholine-activated channels, once again in frog muscle fibres [280]. Patch-clamp requires glass microelectrodes filled with specific ionic solutions (usually mimicking intracellular concentrations) being pressed against single cell membranes. Following light suction an electrical seal, usually >1GΩ, will form between the cell membrane and the glass,

this allows the measurement of currents between the inside of a cell and the patch pipette (Figure 2.2).

Through the use of a piezo-electric manipulator, polished micropipettes are attached onto the cell membrane and suction applied to form a seal between glass and membrane. Small bursts of suction can burst the attached area of membrane but leave the adjacent annealing membrane attached – this allows electrical access of the internal pipette electrode into the 'whole-cell' and permits control of a cell's membrane voltage or current.

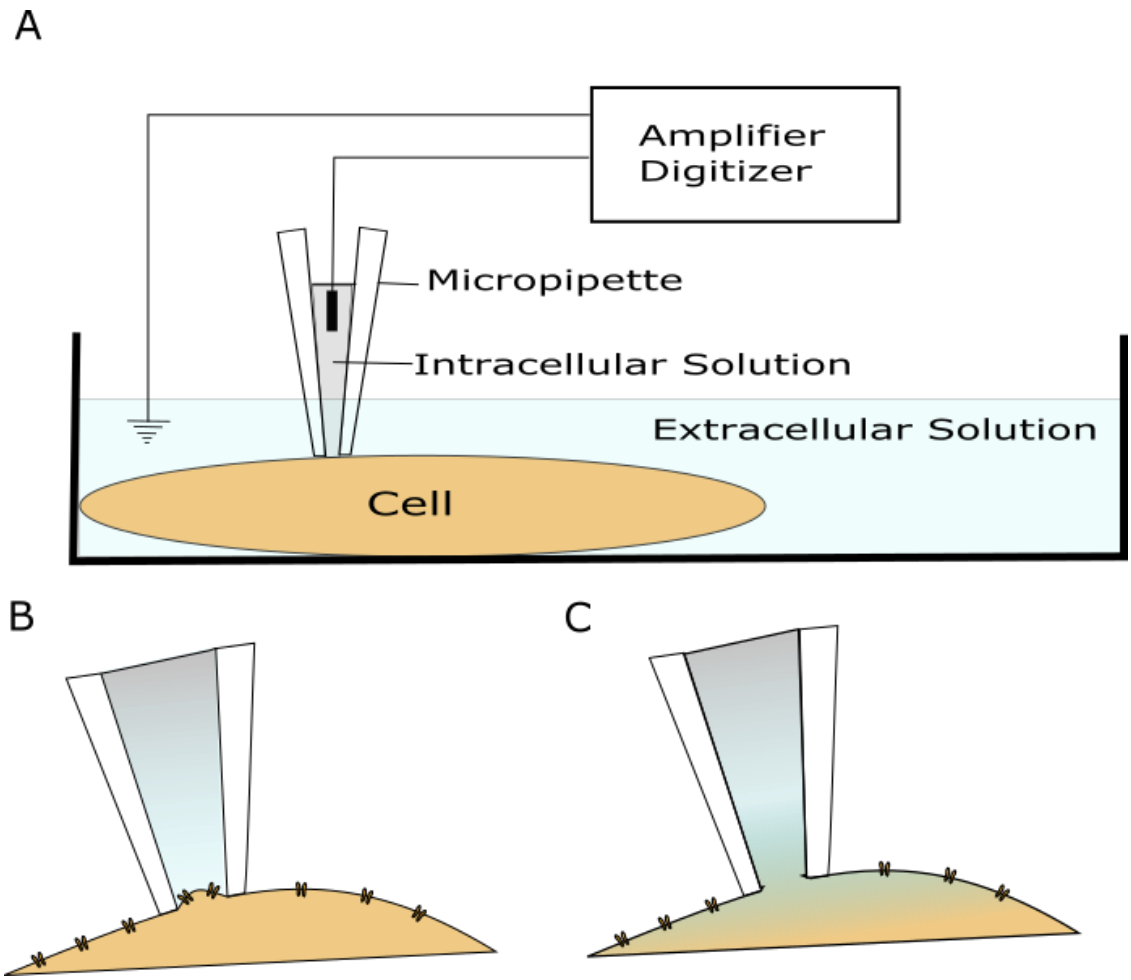


*Figure 2.2.* ***Schematic of Patch-Clamp Experiments. A*** *Cells adhering to glass coverslips are submerged in extracellular solution before a borosilicate glass pipette is gently pushed onto the cell membrane using a manipulator. Current is measured through two electrodes, one inside the bath, and the other inside the micropipette.* ***B*** *Pipette attachment to the plasma membrane followed by slight suction results in a seal, ensuring currents are measured through plasma membrane.* ***C*** *Following light suction the membrane is broken to allow dialysis this is called the whole-cell configuration.*

### 2.6.2 Modelling Cells using Basic Electrical Circuits

The purpose of the patch-clamp technique is to measure either current or voltage changes across a cell's membrane when voltage or current is altered. These measurements are made by the patch-clamp amplifier through a simple electrical circuit (Figure 2.3). Current measurements are initially recorded between the pipette and bath electrodes after the pipette tip enters the bath solution (Figure 2.3A). Rapid +10mV voltage steps at this stage confirm electrical access through the bath solution – normally a low resistance <3MΩ. The pipette also acts as a capacitor because it separates the two conducting solutions.

After pipette-cell attachment, a high resistance seal is formed between the cell's membrane and the pipette tip. Ideally this seal is greater than 1GΩ, significantly reducing current between both electrodes via the bath. After membrane breakthrough, the pipette-bath electrode circuit is reformed – but passes through two new resistors (Figure 2.3B). Firstly 'access' through the cell's cytoplasm acts as a resistor, while the membrane ideally acts as a high ohmic resistor. Ideal whole-cell conditions rely upon low access resistance while seal and membrane resistance remain high. Current flow across the membrane can now be measured in response to voltage changes by the amplifier.

A cell's membrane also acts as a capacitor, whose surface area can be measured. Voltage pulses build charge across the plasma membrane, whose decay can be measured to approximate cell surface area. Recorded whole-cell currents can then be normalised to cell surface area – giving standardised current readings between cells.

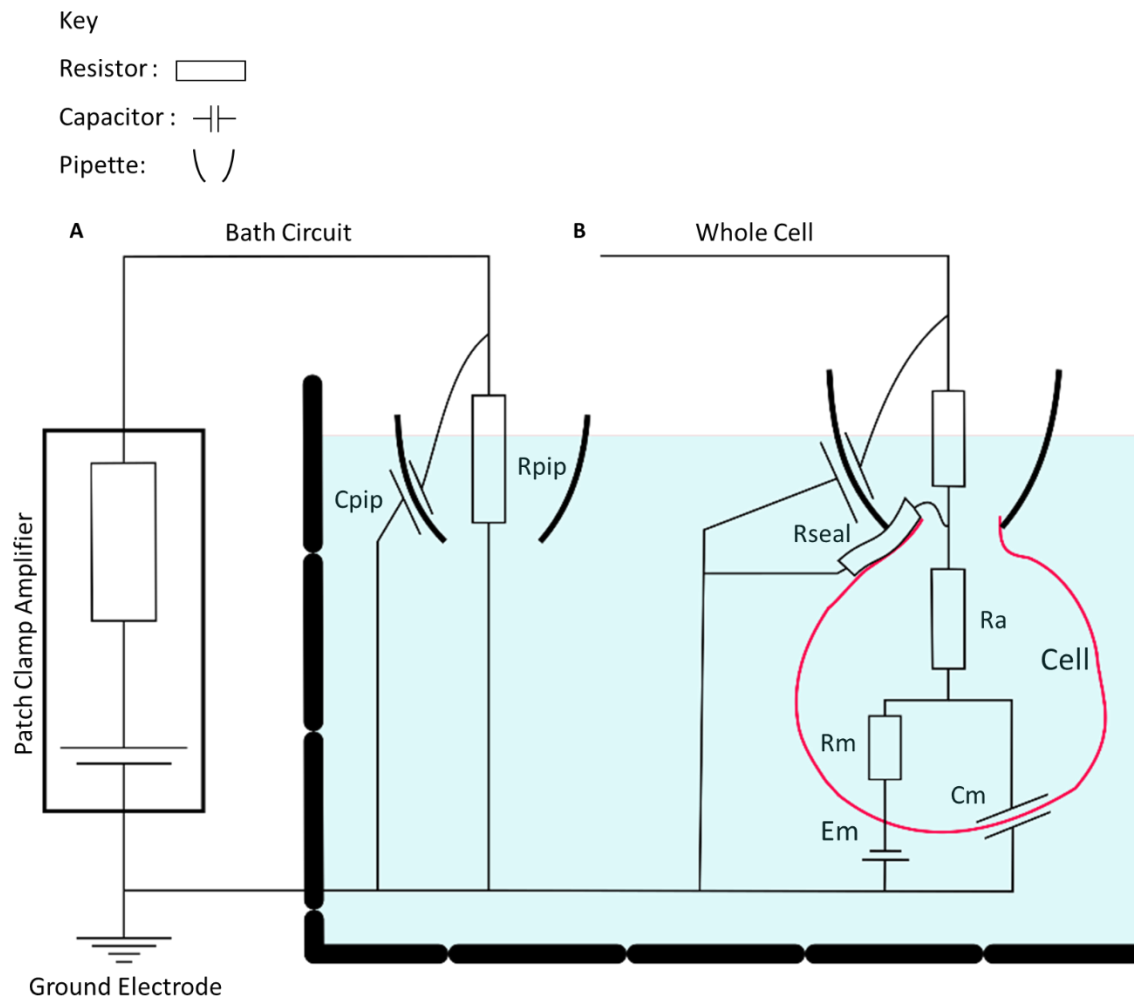


*Figure 2.3.* ***Whole-cell patch-clamp schematic represented as an electric circuit. A*** *Upon entering the bath, a low resistance circuit between the pipette and recording device is formed. Some charge build-up is observed between the pipette and bath. Rpip – Pipette Resistance, Cpip – Pipette Capacitance.* ***B*** *Whole-cell after membrane breakthrough circuitry. The strength of the seal between the membrane and pipette can adversely affect the amplifier's ability to clamp a cell's voltage. Complete membrane breakthrough ensures low electrical resistance into the cell, while membrane resistance is usually high. A cell's membrane acts as a capacitor, holding charge. When the amplifier clamps specific current or voltage across the cell's membrane, the resulting voltage or current change is measured. Rseal – seal resistance, Ra – access resistance, Rm – membrane resistance, Cm – membrane capacitance, Em – membrane voltage.*

During whole-cell patch-clamp, it is assumed that the voltage applied to the pipette is equal to the voltage applied across the cell membrane. For this to be true, the theoretical voltages applied across the membrane must be compensated for cell capacitance and series resistance – chiefly arising from the pipette and access resistance. Whole-cell compensation removes the large current transients observed when the cell's membrane accumulates charge in response to artificial voltage steps.

The effect of resistance in 'series' between the patch-clamp amplifier and membrane results in a temporal voltage difference between the pipette electrode and cell membrane. Membrane voltage changes slowly, leading to slow changes in observed currents. The amplifier can correct for this resistance by artificially increasing the initial voltage applied to the pipette, this results in membrane voltage changing at a greater rate. As membrane voltage more closely limits the voltage set by the patch-clamp rig, the current measured corresponds to the voltage protocol more accurately. However, series resistance compensation increases noise due to large artificial voltage changes, and can cause current oscillations.

### 2.6.3 Perforated Patch-Clamp

Whole-cell patch-clamp recording is a convenient method to measure ion channel current density especially if buffering intracellular ions, as in the case of TRPM7, is required to record conductivity. This is due to the small volume of cellular cytosol in comparison to the pipette. There can be specific drawbacks to this method, which are a direct result of dialysis by the intracellular pipette solution [281]. After initial membrane break-in, the concentration of endogenous intracellular signalling molecules such as cAMP, drastically reduces as they are dialysed out of the cell. β-adrenergic stimulation initiates accumulation of cAMP due to activation of adenylyl cyclase at the plasma membrane drastically raising cAMP levels. This cAMP accumulation binds the regulatory subunit of PKA, freeing the catalytic subunit which goes on

to phosphorylate a huge number of downstream targets. These targets include the slow delayed rectifier potassium current and the L-type voltage-gated calcium channel.

To test the effect of adrenergic drive in heterologous cells, the perforated patch-clamp technique was used to limit the disruption of cytosolic signalling molecules, maintain endogenous calcium, reduce the rundown of IKs and allow for stable, long term recordings. Disadvantages of using the perforated patch technique include the higher access resistance encountered compared to whole-cell and the significantly prolonged time required to gain electrical access to the cell (>15 minutes).

The first example of perforated patch recordings used nyastatin in the intracellular solution to slowly perforate the plasma membrane after forming a gigaohm electrical seal between the cell and pipette [282]. Three years later Rae et al. showed that another antibiotic, amphotericin B could also be used to create pores in the membrane and due to its faster perforation rate will be used in perforated patch-clamp experiments in this thesis [283]. Amphotericin B forms pores (0.8nm radius) over time in cell membranes, these pores conduct small monovalent cations and anions while excluding larger signalling molecules [284]. Another pore forming reagent, β-escin, has also been used to gain electrical access to cells without membrane rupture in neurons to study voltage-gated calcium currents without rundown [285].

### 2.6.4 Recording Current

Currents were recorded using a Multiclamp 700B Amplifier (Molecular Devices) and digitised with a Digidata 1550B (Molecular Devices). Micropipettes were pulled from thin walled filament borosilicate glass and fire polished at 2-4MΩ resistance when backfilled with intracellular solution. Internal solution for TRPM7 consisted of: 145mM Cs-methanesulfonate ($CsSO_3CH_3$), 8mM NaCl, 10mM EGTA and 10mM HEPES, adjusted to pH 7.2 with CsOH. The contents of these solutions allow the measured ionic currents to be attributed to TRPM7 at the

plasma membrane. Caesium methanesulfonate at a high concentration is a substitute for intracellular potassium, whilst also acting as an endogenous potassium channel blocker. This solution also contains physiologically low levels of sodium. Intracellular EGTA chelates magnesium, as TRPM7 is inhibited by cytosolic $Mg^{2+}$, only after removal of divalent cations will current be seen. Therefore any immediate current recorded following cell break-in is not TRPM7. The organic buffer HEPES maintains cell viability by maintaining constant pH values during recording.

The extracellular solution for TRPM7 patch-clamp recordings consisted of: 145mM NaCl, 5mM KCl, 2mM $CaCl_2$, 10mM glucose and 10mM HEPES at pH 7.4 adjusted with NaOH as seen in work by Qin et al. [230]. The external bath solution aims to mimic extracellular physiological salt concentrations; with high sodium and calcium combined with low potassium. Glucose in the bath ensures cells remain healthy during recordings whilst HEPES buffers extracellular pH. All patch-clamp experiments were done over the course of at least three individual transfections.

The voltage ramp protocol to record TRPM7 was delivered every 5 seconds and lasted a total of 250ms. Holding potential was at 0mV while the voltage ramp initiated at -100mV and reached +100mV before returning to 0mV (Figure 2.4). Recordings were corrected for whole-cell capacitance and were compensated at 70% to account for series resistance. Only cells with membrane resistance >800 MΩ and access resistance <12 MΩ were used for data analysis. All recordings except action potentials were carried out at room temperature, sampled at 10kHz and filtered at 1kHz.

To record potassium current through KCNQ1/KCNE1 channels and how they respond to β-adrenergic stimulation, a step protocol was used (Figure 2.5). Resting membrane potential at -80mV was raised, according to sweep number for two seconds, before returning to -40mV to record tail current for two seconds before returning back to -80mV. This occurred nine times, with each sweep increasing the peak voltage by 20mV up to +80mV. The protocol was repeated every minute, to allow for five similar recordings to have been taken before addition of

isoprenaline or forskolin in the case of perforated patch or halted in the case of whole-cell. Alongside whole-trace analysis, current measurements are made 200ms into the voltage step to discern rapid current, at the end of the voltage step to measure peak current and at the start of the 'tail' step to calculate currents that would occur following cell repolarisation (Figure 2.5).

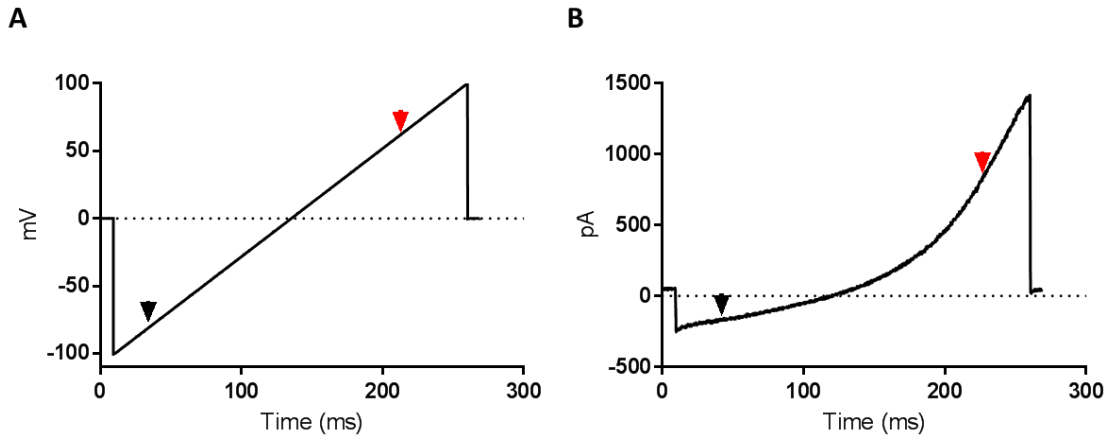


*Figure 2.4.* ***TRPM7 voltage ramp profile and representative trace.*** ***A*** *Voltage protocol as seen in Clampfit, from initial -100mV depolarisation to +100mV peak is 250ms, this ramp occurs every 5 seconds following whole-cell current break-in.* ***B*** *Typical TRPM7 recording, showing small initial current at negative potentials before increasing to a large current at +100mV.*

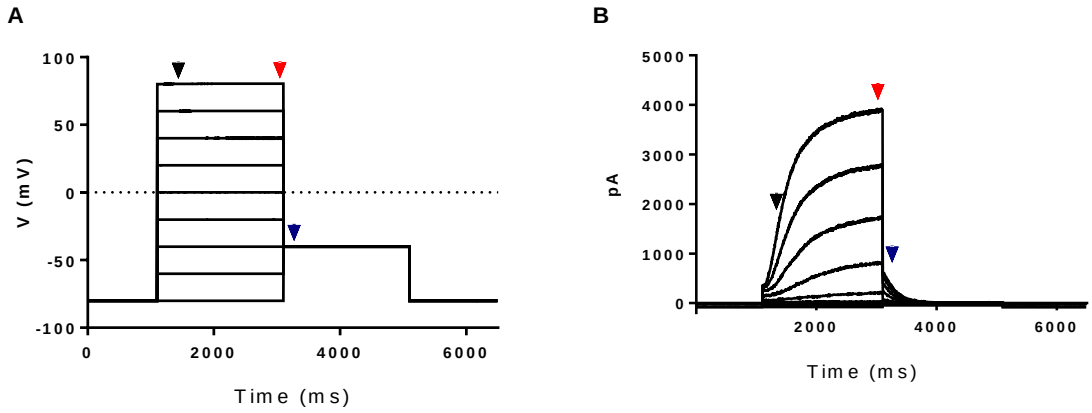


*Figure 2.5.* ***Voltage protocol and representative recording of the KCNQ1/KCNE1 potassium channel.*** ***A*** *Typical recording of IKs current, showing slow activation of the channel up to a plateau, over 2 seconds followed by a slowly inactivating 'tail' current at -40mV.* ***B*** *Voltage protocol depicting +20mV steps from -80mV to +80mV followed by -40mV tail current. Measurements are made at three points, initial current 200ms into the voltage step (black arrow), peak current (red) and tail current following the -40mV step immediately (blue).*

For perforated patch recordings the intracellular solution consisted of (mM): 70 $K_2SO_4$, 10 HEPES, 1 $MgCl_2$, 1 $CaCl_2$ and 10 NaCl at pH 7.2 with KOH. Intracellular whole-well patch-clamp solution contained (mM): 150 KCl, 5 EGTA, 10 HEPES, 2 $MgCl_2$, 1 $CaCl_2$ and 5 $(Na)_2ATP$ at pH 7.2 with KOH. Extracellular solution for all IKs recordings was made up of (mM): 150 NaCl, 5 KCl, 10 HEPES, 2 $MgCl_2$ and 1 $CaCl_2$ at pH 7.4 with NaOH. When filled with intracellular solution pipette resistance was between 1.6MΩ and 2.2MΩ. Successfully transfected cells were identified by expression of fluorescently tagged KCNQ1 protein.

## 2.7 RNA Harvesting and qPCR

### 2.7.1 Total RNA Isolation from Cells

To measure transcribed mRNA message of specific genes, total RNA was harvested from adherent cell cultures using an RNeasy mini kit (QIAGEN, USA). Cells were initially homogenized in the presence of guanidine-thiocyanate containing buffer – minimizing the activity of RNases before being centrifuged through a spin column capable of binding RNA molecules. After several washes to remove impurities, RNA is eluted using water.

All reagents used to isolate RNA were provided in the RNeasy mini kit unless otherwise stated. All centrifugation steps were carried out at 10,600 g for 15 seconds using a 5424 eppendorf centrifuge. Monolayer cultures of cells were lysed by addition of 350µL RLT before mechanical homogenisation with a pipette and then mixed with 350µL of 70% ethanol. The sample was added to an RNeasy spin column and centrifuged. After flow-through was discarded, RNA was washed by addition of 350µL Buffer RW1, before 80µL of DNase I incubation mix (DNase I, diluted 1:7 with Buffer RDD) was directly pipetted onto RNeasy spin column membrane. DNase digestion was carried out using an RNase-Free DNase Set (QIAGEN, USA) to ensure only RNA was present for qPCR experiments.

After a 15 minute incubation at room temperature, DNase I was removed by washing the spin column with 350µL Buffer RW1, followed by another 500µL wash with Buffer RPE. A final wash of 500µL Buffer RPE was added and centrifuged for 2 minutes to dry the column membrane. RNA was eluted using 30µL of RNase-free water and the concentration was measured using a nanodrop. Only RNA samples with concentrations >50ng/µL and 260/280 absorbance >1.9 were used for further reverse transcription reactions. All RNA samples were immediately stored at -80˚C to prevent sample digestion or degradation.

### 2.7.2 cDNA Synthesis

To quantify relative mRNA signals from lysed cells, RNA was converted to cDNA using the High-Capacity cDNA Reverse Transcription Kit (Thermofisher, USA). This process involves the conversion of up to 2µg of input RNA (harvested as stated in 2.7.1) into single-strand cDNA, allowing quantification of specific mRNA messages using Taqman probes (outlined in 2.7.3). All reactions were carried out in 20µL volumes, processing up to 2µg of RNA if possible, depending on input RNA concentrations. The RNA-cDNA conversion reaction was made as noted in Table 2.7.

PCR tubes were sealed and placed in a thermal cycler, the conditions for the cDNA synthesis reaction are listed in Table 2.8. Following cDNA synthesis, all samples were stored at -20˚C to preserve DNA stability.

### 2.7.3 Quantitative PCR

Quantitative reverse transcription polymerase chain reaction (qPCR) allows the precise quantification of RNA in samples between each cycle of a PCR reaction using fluorescent quantification. All gene expression assays (Applied Biosystems, USA) were carried out using the TaqMan® system with the probes shown in Table 2.5.

Each qPCR expression assay was carried out in triplicate inside a 96-well plates (Thermofisher, USA) at a total volume of 20µL. The components of each reaction are listed in Table 2.7. Plates were sealed and centrifuged at 2400 g for 3 minutes at room temperature. Thermal cycling was conducted using the protocol listed in Table 2.11 and carried out using a CFX Real-Time PCR Detection System (Bio-rad, USA).

Quantification is achieved through the measurement of the fluorescence levels between every cycling stage. Unbound TaqMan® probes consist of a gene-specific target DNA sequence that allows homologous binding to complementary ssDNA, bookended by a fluorophore and quenching molecule (Figure 2.6). Under normal conditions, probes do not fluoresce due to the close proximity of quencher to fluorophore. During qPCR reactions, probes that bind to complementary target sequences are cleaved by DNA polymerisation during the amplification step of the reaction. The intensity of fluorescence measured in each reaction well is representative of cleaved qPCR probes and is correlated to the abundance of that target.

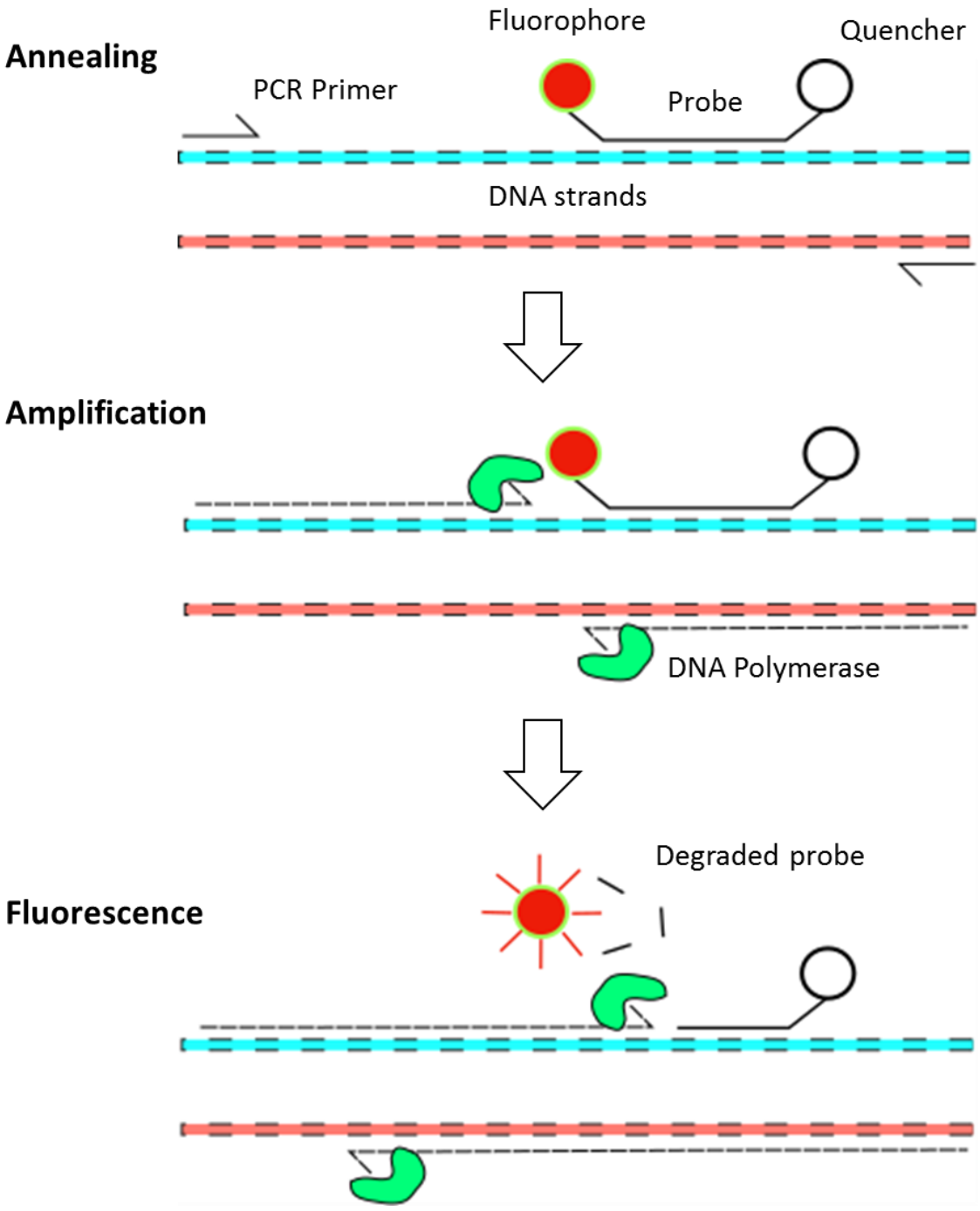


*Figure 2.6.* ***Taqman qPCR fluorescent measurement occurs in three distinct phases.*** *Initially denatured cDNA strands are bound by sequence specific probes when the mix is cooled. These probes are fluorescently inert due to the close proximity of fluorophore and quencher molecule. The reaction mixture is heated to activate DNA polymerase, which amplifies DNA using non-specific PCR primers. During chain extension, attached probes are degraded by extending DNA polymerase, releasing the fluorophore into the reaction mixture where intensity can be measured. This reaction is repeated 40 times, with fluorescence measured between each cycle.*

The cycle threshold (Ct) value defines the number of PCR cycles required to cross a set fluorescence value. When comparing relative amounts of mRNA in samples, the comparative Ct method was used [286]. Ct values were normalised to that of endogenous housekeeping genes (GAPDH or 18S) and then to that of control samples, with control sample expression normalised to 1. For these comparative experiments expression was listed as relative units based on $2^{-\Delta\Delta Ct}$. Experiments where there is no control sample, relative RNA amounts are expressed as target/control ratios.

For the majority of qPCR experiments measuring mRNA in heterologous cell lines, GAPDH was chosen as a housekeeping gene. However, for all qPCR experiments performed using stem cell-derived cardiomyocytes, a probe measuring the expression of 18S ribosomal RNA was used. 18S rRNA expression has been reported as a reliable housekeeping marker in a number of publications. This includes the paper documenting the differentiation protocol used in this thesis, as well as recent work investigating the transcriptomic profile of differentiating cardiomyocytes [255,287].

| Component | Volume |
|---|---|
| 10X RT Buffer | 2µL |
| 25X dNTP Mix | 0.8µL |
| 10X RT Random Primers | 2µL |
| Multiscribe™ Reverse Transcriptase | 1µL |
| RNA | RNA sample concentration / 2µg |
| Nuclease-Free $H_2O$ | 3.2 + (10 – RNA volume) µL |
| Total Reaction Volume | 20µL |

*Table 2.7.* ***Recipe for single cDNA synthesis reaction.***

| Step | Temperature (˚C) | Time (mm:ss) |
|---|---|---|
| **1** Primer Binding | 25 | 10:00 |
| **2** cDNA Synthesis | 37 | 120:00 |
| **3** Stop Reaction | 85 | 05:00 |
| **4** Storage | 4 | - |

*Table 2.8.* ***Thermal cycling reaction program for cDNA synthesis.***

| Target Gene | Assay ID | Target Exons | Amplicon Length (bp) |
|---|---|---|---|
| *TRPM7* | Hs00559080_m1 | 5-6 | 69 |
| *18S rRNA* | Hs99999901_s1 | 1 | 187 |
| *GAPDH* | Hs02786624_g1 | 7 | 157 |
| *AKAP9* (Short isoform) | Hs01091035_m1 | 5-6 | 92 |
| *AKAP9* (Long isoform) | Hs00323978_m1 | 39-40 | 107 |
| *OCT4* (POU5F1) | Hs04260367_gH | 5 | 77 |
| *NANOG* | Hs02387400_g1 | 1-2 | 109 |
| *SOX2* | Hs01053049_s1 | 1 | 91 |

*Table 2.9.* ***List of all TaqMan Expression Probe sets used in this thesis.***

| qPCR Component | Volume per reaction (µL) |
|---|---|
| 20X TaqMan Expression Probe | 1 |
| 2X Taqman Gene Expression Master Mix | 10 |
| cDNA Template (50ng) diluted in RNase-free Water | 9 |

*Table 2.10.* ***Reagents used to make a single 20µL qPCR reaction.***

| Step | Temperature (˚C) | Time (mm:ss) |
|---|---|---|
| **1** Hold | 50 | 02:00 |
| **2** Hold | 95 | 10:00 |
| **3** Cycle (x40) | 95 | 00:15 |
| | 60 | 01:00 |

*Table 2.*11. ***Thermal cycling conditions for qPCR experiments.***

## 2.8 Cell Staining

### 2.8.1 Immunocytochemistry

Fluorescent staining techniques were used to visualise protein location in cells transfected with fluorescently tagged proteins or washed with conjugated antibodies. 48 hours after transfection (if required) adherent cells were first washed with PBS three times to remove media and serum. Cells were fixed with 4% formaldehyde solution (Sigma-Aldrich, USA) at room temperature for 15 minutes to preserve DNA and protein structural integrity. To allow antibody access to intracellular epitopes, samples were permeabilised with PBS containing 0.1% Triton X-100 (Sigma-Aldrich, USA) for 10 minutes. After three PBS washes, slides were incubated for 30 minutes in 1% BSA PBS-T to block any possible unspecific binding of antibodies. Following removal of blocking solution, primary antibodies with 1% BSA PBS-T were added to cell samples at a concentration, time and temperature noted below (Table 2.12).

Primary antibody solution was decanted before cells were washed with PBS, then incubated with fluorescent secondary antibody for 1 hour at room temperature. The secondary antibody was diluted with PBS-T with 1% BSA. After three PBS washes, nuclei were counterstained with 0.5µg/ml 4',6-diamidino-2-Phenylindole, dihydrochloride (DAPI, ThermoFisher, USA) before a final rinse with PBS. Cells were stored at 4˚C before imaging fluorescently with either an EVOS FL Auto microscope (ThermoFisher, USA) or LSM710 confocal scanning microscope (Zeiss, Germany).

| Primary Antibody Target (reference) | Raised In | Epitope Amino Acids | Dilution in 1% BSA PBS-T | Incubation Time | Incubation Temperature |
|---|---|---|---|---|---|
| TRPM7 (sc-271099) | Mouse | 1251-1550 | 1:100 | Overnight (>12hrs) | 4 ˚C |
| Cardiac Troponin T (ab8295) | Mouse | 171-190 | 1:200 | 1 Hour | 20-25˚C |
| Tra-1-60 (ab16288) | Mouse | Not Listed | 1:200 | 1 Hour | 20-25˚C |

*Table 2.12.* ***List of primary antibodies used to for immunocytochemistry.***

### 2.8.2 Live Cell Imaging

CHO-K1 cells were seeded at a density of 1:5 onto 6 well plates. The following day adherent cells were transfected with 250ng KCNQ1-GFP and 250ng KCNE1 expression plasmids in 250ul Opti-MEM. The transfection reagent NovaCHOice (0.5µL) and NovaCHOice booster reagent (0.25µL) were added to the mixture and incubated at room temperature for between 10 and 30 minutes as per manufacturer's instructions, before addition to cells. Six hours later, cells were trypsinised and seeded into Nunc glass bottom dishes (ThermoFisher, USA) at a density of 1:10. After 36 hours live adherent cells were imaged using an LSM710 confocal scanning microscope.

### 2.8.3 Fluorescent Microscopy

Visualisation of tagged/antibody bound proteins is achieved through illumination of samples with filtered light of a specific wavelength. For example, DAPI-stained DNA absorbs 358nm light strongly, this absorption leads to electron excitation to a higher energy level. Excited

electrons will subsequently lower their energy state, emitting light at a higher wavelength (461nm in DAPI's case) that is filtered into a detector. The relative excitation and emission wavelengths of fluorophores used in this thesis are listed below in Table 2.13. The relevant information of the lasers used to excite the corresponding fluorophore in confocal microscopy are listed in Table 2.14.

| **Fluorophore** | **Excitation (nm)** | **Dichroic beamsplitter (nm)** | **Emission (nm)** |
|---|---|---|---|
| DAPI | 365/60 Peak/FWHM | 395 | 420-470 BP |
| GFP | 450-490 BP | 495 | 500-550 BP |
| DsRed | 545/25 Peak/FWHM | 570 | 570-640 BP |

*Table 2.13.* ***List of fluorescent filters used, with their corresponding excitation and emission wavelengths.*** *Peak – Peak of excitation wavelength. FWHM (Full Width at Half Maximum) – wavelength width equal to half maximal excitation. BP (Bandpass) – wavelength of transmitted light range.*

| **Laser** | **Used to excite** | **Excitation (nm)** |
|---|---|---|
| Diode | DAPI | 405 |
| Argon | GFP | 488 |
| Helium/Neon | DsRed | 543 |

*Table 2.14.* ***Lasers used for confocal microscopy in this thesis.*** *All lasers were used simultaneously, with switching time <5µs.*

### 2.8.4 TUNEL Assay

Since 1993, a widely used method to detect cell death has been the labelling and detection of 3'-OH fragmented DNA in apoptotic cells [288]. This assay uses terminal deoxynucleotidyl transferase to bind exposed 3'OH DNA bases generated during the apoptotic cascade and add biotinylated nucleotides. These are detected using a HRP conjugate, which reacts with diaminobenzidine (DAB) to generate an insoluble brown substrate visible with a light microscope.

To recognize apoptotic nuclei, cells fixed to tissue culture dishes or slides were treated using an *in situ* Apoptosis Detection Kit (Abcam, 206386). All reagents mentioned are supplied with the *In Situ* Apoptosis kit unless otherwise stated. Following cell treatment, samples were fixed with 4% paraformaldehyde as previously noted. Proteinase K was diluted 1:100 in 10mM Tris buffer and specimens were covered for 5 minutes at room temperature before three Tris-buffered saline (TBS) washes. Endogenous peroxidases that could interfere with staining were quenched using 3% $H_2O_2$ (Sigma-Aldrich, USA) for 5 minutes at room temperature. After a single TBS wash, samples were treated with TdT Equilibration Buffer for 30 minutes at room temperature. This buffer was carefully blotted before application of 40µL of TdT Labeling Reaction Mixture (1µL TdT Enzyme to 39µL TdT Labeling Reaction Mix). Samples were incubated in a humidified cell culture incubator at 37˚C for 90 minutes. The labelling reaction was terminated by an initial TBS wash before addition of 100µL of Stop Buffer for five minutes. To prevent non-specific binding of the HRP-conjugate antibody, samples were treated with 100µL of Blocking Buffer for 10 minutes. Conjugate antibody solution diluted in Blocking Buffer (1:25) was added to cell samples before being placed in a humidified chamber for 30 minutes. Slides were then rinsed with TBS and treated with development solution: 4µL DAB Solution 1 mixed with 116µL DAB solution 2 per slide/well. Cells were covered with DAB solution and incubated at room temperature for 15 minutes before being rinsed with $dH_2O$. To counterstain cell morphology, slides were covered with Methyl Green Counterstain for 3 minutes before

repeated rinsing in 100% ethanol. Finally slides were dipped into 100% xylene before coverslip mounting. Live and apoptotic cells were counted using a light microscope.

## 2.9 Collection of Human Heart RNA

### 2.9.1 Introduction

The published literature regarding full length-*AKAP9* and *TRPM7* rarely references their relative abundance in human heart tissue. For *AKAP9*, publications focus solely on the small *Yotiao* isoform which lacks any putative PKA binding domain [131,215]. Conversely, the abundance of *TRPM7* and its temporal importance in development and function has been thoroughly investigated in the mouse [212-214,233]. Our laboratory has access to human heart RNA samples from three separate donors obtained from the four heart chambers. This provided a novel opportunity to confirm the expression of *AKAP9* and *TRPM7* in the adult human heart, as well as explore any differences in chamber specific expression.

### 2.9.2 Sample Information

Twelve samples of total human RNA was acquired from Amsbio (UK) consisting of four heart chamber samples from three male donors, additional information can be found in Table 2.15. Each 50µg sample was DNase I treated before shipment, and transported using dry ice. Samples were thawed upon arrival and stored as 10µL aliquots at -80˚C.

| Donor ID (Sex) | Age | Chamber | | RNA Concentration (µg/µL) |
|---|---|---|---|---|
| C711147 (M) | 49 | Right | Atrium | 2.82 |
| | | | Ventricle | 1.96 |
| | | Left | Atrium | 2.09 |
| | | | Ventricle | 1.76 |
| C709084 (M) | 69 | Right | Atrium | 0.72 |
| | | | Ventricle | 1.69 |
| | | Left | Atrium | 1.22 |
| | | | Ventricle | 1.87 |
| C109121 (M) | 65 | Right | Atrium | 1.75 |
| | | | Ventricle | 1.89 |
| | | Left | Atrium | 1.72 |
| | | | Ventricle | 1.91 |

*Table 2.15.* ***Human heart chamber RNA information.***

### 2.9.3 Preparation of cDNA and qPCR Analysis

Human heart RNA samples were converted to cDNA libraries as mentioned previously in section 2.6.2 using a High-Capacity cDNA Reverse Transcription Kit. Briefly, 1µg of RNA was added to a reaction mixture containing dNTPs and reverse transcriptase to make a 20µL reaction (Table 2.7). The thermal cycling conditions for cDNA synthesis are described in Table 2.8. From these reactions, 20µL qPCR reactions were made using 50ng of cDNA per well (Table 2.10). *GAPDH* expression was used as an endogenous housekeeping control. The Taqman qPCR probes used to measure *GAPDH, AKAP9* and *TRPM7* expression are listed in Table 2.9. Gene expression was calculated using the comparative Ct method – firstly between target housekeeping genes within samples, and then between samples (explained in 2.7.3).

## 2.10 Induced Pluripotent Stem Cell Culture

### 2.10.1 Introduction

There is significant evidence to suggest that most cardiomyocytes are mitotically locked, and those that are capable of cell division do so at a drastically lower rate compared to most other cell types [247,289]. Therefore the ability to generate and analyse significant numbers of human cardiomyocytes has relied upon expensive post-mortem tissue biopsies. The discovery of human iPSC technology in 2007 revolutionised the capacity of generating human stem cells in laboratories [254]. If cultured properly these cells provide a ready source of pluripotent cells that can be differentiated towards a cardiac phenotype. As these cells differentiate from a pluripotent to cardiac phenotype, they can be used as a model of cardiovascular development to investigate the expression and importance of genes during cardiogenesis.

### 2.10.2 Pluripotent Cell Generation

A healthy human pluripotent stem cell line (named - HS1M) was generated in our laboratory by Duncan Miller. Human dermal fibroblast (HDF) cultures were derived from 4mm skin punch biopsies from a healthy 'control' individual following overnight digestion with collagenase I (Sigma, USA). After two to five passages, HDFs were reprogrammed by lentiviral transduction of a polycistronic vector hSTEMCCA or nucleofection of three plasmids containing reprogramming factors [290,291]. Colonies were isolated and expanded clonally in DMEM:F12 medium containing 20% knock-out serum replacement and 20 ng/ml FGF2 (Peprotech, USA) on mitotically inactivated mouse embryonic fibroblasts (MEFs), and characterised for pluripotency. hPSC lines were generally maintained and expanded on MEFs, and transitioned onto Matrigel (Corning, Netherlands) in mTeSR1 for several passages prior to differentiation [292].

### 2.10.3 Maintaining Induced Pluripotent Stem Cells

Cell stocks (~1million cells) frozen in liquid nitrogen were warmed rapidly in a 37˚C water bath before being added dropwise to 9ml of mTeSR1 with 5µM Y27632 (Merck, USA) to inhibit the Rho-associated, coiled-coil containing protein kinase (ROCK). The ROCK protein is a key driver of anoikis-induced cell death in dissociated stem cells [293]. This suspension was centrifuged for 5 minutes at 100 *g*, 37˚C and the supernatant removed. The cell pellet was resuspended with 5ml mTeSR1 plus 5µM Y27632 and added to a T25 flask, the media was changed every day until approaching confluency. To store cell stocks following expansion, cells from three confluent T25 flasks were washed and dissociated with Accutase before being centrifuged at 100 *g* for 5 minutes. When the supernatant was removed, cell pellets were resuspended in 3ml freezing medium composed of 60% Hyclone FBS (GE Healthcare, USA), 30% mTesR1, 10% DMSO Hybrimax and 5µM Y27632. This suspension was aliquoted into 3 cryo-vials and frozen at -80˚C inside a Nalgene® Mr. Frosty container overnight. The next day vials were stored in liquid nitrogen.

Prior to differentiation into cardiomyocytes, iPSCs were expanded as feeder-free cultures with mTeSR1 media. Cells were grown on growth factor reduced Matrigel T25 coated flasks (Sarstedt, Germany)[294]. Matrigel was initially thawed on ice before dilution to 9µg/cm$^2$ in DMEM/PenStrep and pipetted into 24-well plates or T25 flasks. At room temperature Matrigel sets within one hour, and the remaining liquid media removed by PBS washes. Adherent stem cells were dissociated by treatment of Accutase (Bd Biosciences, USA) at 37˚C for 7 minutes. Detached stem cells were centrifuged at 100 *g* for 5 minutes and resuspended in 5ml of mTeSR1 supplemented with 5µM Y27632 (Merck, USA). If cells counted were >14 million, cells were reseeded in T25 flasks, otherwise cells were seeded 300,000 per well into Matrigel coated 24-well plates for differentiation. Media was changed daily after cells were seeded, but without Y27632, 5ml for T25 flasks and 0.5ml per well in a 24-well plate.

### 2.10.4 Cardiomyocyte Differentiation

Cardiomyocytes were differentiated by a protocol based upon previous work published by Burridge et al [255]. Pluripotent stem cells were seeded at 300,000 cells per well in a 24-well plate with 0.5ml of mTeSR1 with 5μM Y27632. Media was changed daily until cells reached >80% confluency, usually 1-2 days. Differentiation was initiated by changing the cell medium to 'CDM3', a basic media consisting of three components plus penicillin/streptomycin. CDM3 consists of RPMI1640 (Thermofisher, USA), 500μg/ml *O.sativa*-derived recombinant human albumin (Sigma Aldrich, USA) and 213μg/ml L-ascorbic acid 2-phosphate (Sigma Aldrich, USA). When stem cell density approached confluency (>80%) CDM3 supplemented with 6μM CHIR99021 was added to the cells in place of mTeSR1 – this is noted as day 0. CHIR99021 is a small molecule that inhibits GSK3B and activates the Wnt signalling pathway [295]. This is critical in inducing cardiac differentiation by creating an initial mesodermal phenotype in stem cells [296]. At day 2, the cell culture media is replaced with CDM3 supplemented with C59, a Wnt signalling inhibitor – to induce cardiac differentiation. From day 4 onwards, media was changed every two days with CDM3 alone. Individual beating cells can be observed by 7 days, with increased beating observed until day 12.

To re-plate human stem cell-derived cardiomyocytes for further experiments, cells were washed with PBS to remove residual media before the addition of 500μL of Accutase or TrypLE Express Enzyme (ThermoFisher, USA). Cells were incubated for ~15 minutes at 37˚C to allow for detachment, then centrifuged at 130 *g* for 4 minutes. The cell pellet was resuspended in CDM3 plus penicillin/streptomycin and supplemented with 10% FBS to aid in cell survival and attachment. Cells were seeded onto 0.1% gelatin coated wells with 10mm coverslips (60,000 cells per well) or without them (300,000 cells). This procedure was carried out at either day 10 or day 15 of differentiation depending on the appearance of large beating clusters. One day later media was changed to CDM3 and changed every 48 hours afterwards.

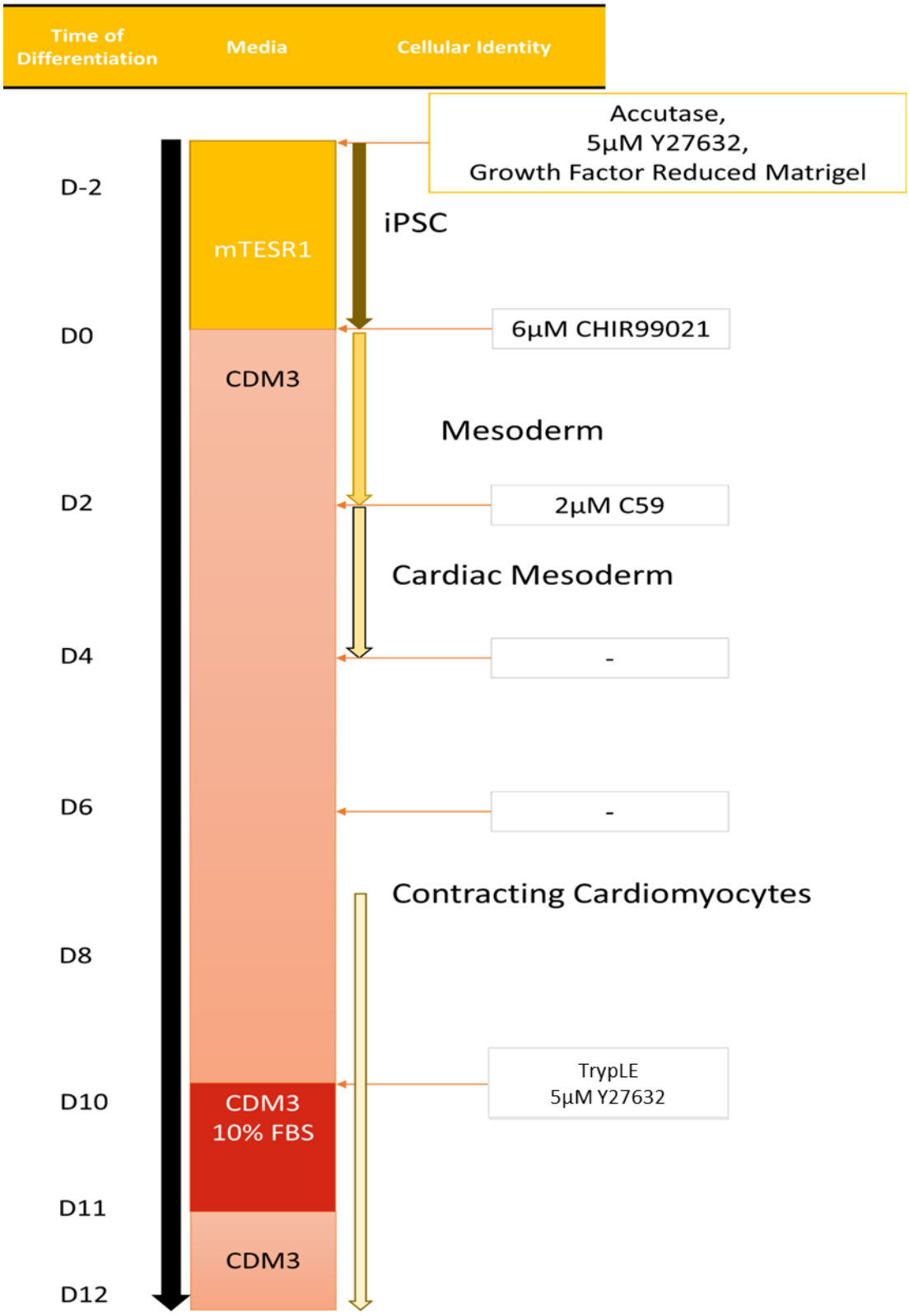


*Figure 2.7.* ***Induced pluripotent stem cell-derived cardiomyocyte differentiation.***

### 2.10.5 siRNA Transfection of Stem Cell-derived Cardiomyocytes

RNA silencing in eukaryotic organisms was serendipitously discovered by Guo and Kemphues in 1995 while investigating *C. elegans* embryonic polarity [297]. A sense par-1 RNA was able to target endogenous par-1 transcript for degradation. Three years later Andrew Fire and Craig Mello provided evidence to show that contaminating dsRNA (which could be formed by hybridisation of sense and antisense ssRNA) was responsible for the observed gene silencing [298]. It was shown that dsRNA was cleaved into 21-23nt small interfering RNA (siRNA) molecules, which targeted homologous sequences when bound *in vivo* [299]. Using this system, it is therefore possible to transfect siRNA into recipient cells, transiently reducing mRNA expression levels due to homology-directed cleavage of RNA molecules.

To knockdown mRNA levels of TRPM7 in iPSC derived cardiomyocytes, siRNA transfection was used. 5nmol of SMARTpool: ON-TARGETplus siRNA targeted to either TRPM7 or a scrambled control was used (Dharmacon, USA). Upon receipt siRNA, was resuspended in RNase-free water at 20µM. Transfection was carried out 72 hours before cardiomyocytes were due to undergo patch-clamp analysis.

Stocks of 2µM siRNA solution were prepared in RNase-free water and diluted in 45µL serum-free Opti-MEM, 2.5µL of siRNA per well. To confirm successful transfection for patch-clamp experiments, 2.5µL of 2µM siGLO (Dharmacon, USA) was also added to transfection mixture. DharmaFECT transfection reagent 1 was also diluted 2.5:47.5µL Opti-MEM per well. Following five minute incubation at room temperature both tubes were mixed and incubated for a further 20 minutes. CDM3 was removed from cells and antibiotic-free CDM3 (400µL per well) was added to the siRNA transfection mixture before being aliquoted between wells. To reduce cytotoxicity and prevent infection, CDM3 supplemented with 1% pencillin/streptomycin was added 24 hours later.

### 2.10.6 Whole-Cell Patch-Clamp of Stem Cell-derived Cardiomyocytes

Cardiomyocytes plated onto coverslips underwent patch-clamp analysis between differentiation days 21-23. Whole-cell current measurements of TRPM7 in cardiomyocytes were carried out as stated in section 2.6, however different extracellular and intracellular solutions were used to better mimic the physiological make-up of these distinct cells compared to the heterologous systems previously described. Internal TRPM7-CM solution consisted of (mM): 120 L-aspartic acid, 20 CsCl, 2.5 EGTA, 2.5 EDTA, 10 HEPES, 120 CsOH, 5 $Na_2ATP$, 0.5 $Na_2GTP$ at pH 7.2 with CsOH. Extracellular solution: 135 NaCl, 5.4 CsCl, 10 HEPES, 10 Glucose, 0.1 $CdCl_2$ and 1 $CaCl_2$ at pH 7.4 adjusted with NaOH as done by Sah et al. [213]. The ramp protocol previously used to measure TRPM7 current in CHO-K1 and HEK293 cells was used in these experiments.

Action potential recordings were taken from cardiomyocytes plated onto coverslips as mentioned above. Internal pipette 'AP-lowEGTA solution' consisted of (mM): 110 K-Gluconate, 20 KCl, 10 HEPES, 0.05 EGTA, 0.5 $MgCl_2$, 5 MgATP, 0.3 $Na_2$-GTP and 5 $Na_2$phosphocreatine at pH 7.4 with KOH. Extracellular solution for action potential recordings (mM): 140 NaCL, 2.7 KCl, 1 $MgCl_2$, 2 $CaCl_2$, 0.5 $Na_2HPO_4$ and 5 glucose at pH 7.4 with NaOH. Recordings were done in current-clamp mode – measuring changes in membrane voltage, only cells with membrane resistance >800MΩ and access resistance <10MΩ were used in action potential analysis.

When measuring action potential membrane voltage, it is important to correct results for the natural voltage imbalance that occurs between bath and intracellular solutions – known as the liquid junction potential (LJP) after results are recorded. In all previously mentioned voltage-clamp recordings, LJP is corrected by the amplifier automatically. The LJP arises due to the contact of two solutions with different ionic mobility and concentrations. The bath solution has a high concentration of NaCl, whereas inside the pipette K-gluconate is abundant. Although equal in charge, $Cl^-$ ions are more mobile than gluconate whereas $K^+$ is more mobile than $Na^+$. The net effect of this (alongside the movement of less abundant ions) leads to the bath being more positive than the pipette.

The LJP was calculated as +16.3mV using pCLAMP 10.6 software supplied with the patch-clamp amplifier and all voltage recordings altered accordingly. Following whole-cell access and two minute dialysis, possible spontaneous activity was recorded for one minute before one minute of triggered action potentials using current injections of 400-900pA depending on cell capacitance with a frequency of 1Hz. Action potential duration and voltage measurements were made, when possible, on the average of the final 10 triggered beats. A schematic of these measurements on a representative action potential trace is shown in Figure 2.8.

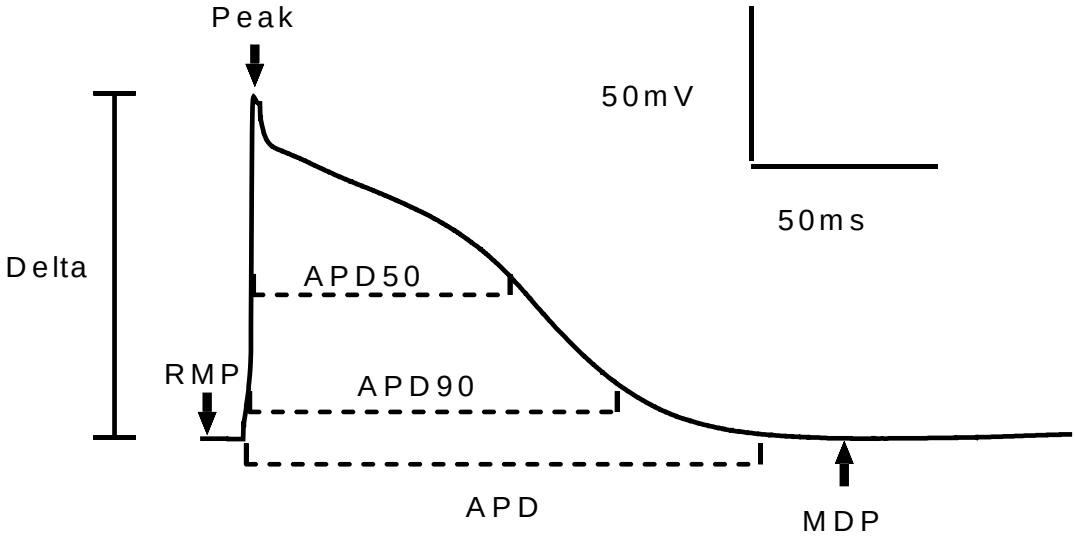


*Figure 2.8.* ***Diagram of measurements taken from action potential recordings of iPSC-CMs.*** *RMP: Resting Membrane Potential, MDP: Maximum Diastolic Potential, Peak: Maximum recorded voltage, Delta: Voltage difference between RMP and peak, APD50/90: Action potential duration at 50%/90%/maximum of delta voltage.*

## 2.11 Statistics and Data Analysis

All quantitative data was analysed with GraphPad Prism 6. Grouped data were tested with one-way ANOVA, using Dunnett's multiple comparison to test variants vs wild-type unless otherwise stated. For individual analysis of two groups, unpaired t-testing was used to calculate statistical differences. When comparing two independent variables, two-way ANOVA with Sidak's multiple comparison test was used. Significance was denoted by an adjusted P value $<0.05$. All group data is presented as mean ± S.E.M. Electrophysiological recordings were made with pCLAMP v10.5 software (Axon Instruments, USA), and were analysed with Clampfit v10.5 (Molecular Devices, USA). Data is presented as mean ± S.E.M. Significant genetic variant enrichment between cases and controls was calculated using a two-tailed Fisher's exact test.

## 2.12 Materials used in this Thesis

| Material | Reference Code | Supplier | Country of Origin |
|---|---|---|---|
| 13mm Glass Cover Slips | 631-0149 | VWR | USA |
| 2-Propanol | 190764 | Sigma-Aldrich | USA |
| 30% Hydrogen peroxide Solution | H1009-100ML | Sigma-Aldrich | USA |
| 4-20% Mini-PROTEAN TGX Precast Protein Gels | 4561094 | Bio-Rad | USA |
| Absolute qPCR Plate Seals | AB1170 | ThermoFisher Scientific | USA |
| Accutase Cell Detachment Solution | 561527 | BD Biosciences | USA |
| Agar | 05038 | Sigma Aldrich | USA |
| Amersham ECL Prime Detection Reagent | RPN2232 | GElifesciences | UK |
| Amersham Hyperfilm | 28-9068 | GElifesciences | UK |
| Bovine Serum Albumin | A2934-25G | Sigma-Aldrich | USA |
| Carbenicillin disodium salt | C3416 | Sigma Aldrich | USA |
| Cell Scrapers | 15621-005 | VWR | USA |
| Corning Matrigel (Growth Factor Reduced) | 356230 | Corning | Netherlands |
| DAPI (4',6-Diamidino-2-Phenylindole, Dihydrochloride) | D1306 | ThermoFisher Scientific | USA |

| Material | Reference Code | Supplier | Country of Origin |
|---|---|---|---|
| DharmaFECT 1 Transfection Reagent | T-2001-03 | Dharmacon | USA |
| Dithiothreitol | D0632 | Sigma-Aldrich | USA |
| DMSO Hybri-Max™ | D2650-5X5ML | Sigma-Aldrich | USA |
| Dulbecco's Phosphate Buffered Saline | D8537 | Sigma Aldrich | USA |
| Falcon 6-well clear flat bottom culture dishes | 10110151 | ThermoFisher Scientific | USA |
| Fetal Bovine Serum | 10500064 | ThermoFisher Scientific | USA |
| Formaldehyde solution 37 wt. % in $H_20$ | 25249-100ML | Sigma-Aldrich | USA |
| FuGENE HD Transfection Reagent | E2311 | Promega | USA |
| Glycine | G8898 | Sigma-Aldrich | USA |
| HAM-F12 Media | 11765-054 | Gibco | USA |
| High-Capacity cDNA Reverse Transcription Kit | 4368814 | ThermoFisher Scientific | USA |
| Human Heart RNA | R1234126-50-D03<br>R1234138-50-D03<br>R1234139-50-D03 | Amsbio | UK |
| HyClone™ Fetal Bovine Serum | SH30088.02 | GE Healthcare | USA |
| IgG HRP-linked Antibodies Mouse/Rabbit | NA931/ NA934 | GElifesciences | UK |
| Immobilon-P PVDF membrane | IPFL00010 | Merck Millipore | USA |
| *In situ* Apoptosis Detection Kit | Ab206386 | Abcam | UK |
| InSolution™ Y-27632 in DMSO | 688002 | Merck | USA |
| L-ascorbic acid 2-phosphate | A8960-5G | Sigma-Aldrich | USA |
| Luria Bertani | L3022 | Sigma Aldrich | USA |
| MEM | 11095-080 | Gibco | USA |
| mTeSR™1 | #85850 | STEMCELL Technologies Canada Inc | Canada |
| Nanodrop | | ThermoFisher Scientific | USA |
| NovaCHOice Transfection Kit | 72622 | Merck Millipore | USA |
| Nunc™ Glass Bottom Dishes | 150680 | ThermoFisher Scientific | USA |
| Opti-MEM Reduced Serum Medium | 11058021 | ThermoFisher | USA |
| pcDNA4/TO | V1020-20 | AddGene | USA |
| PCR Plate, 96-well, semi-skirted, flat deck | AB1400 | ThermoFisher Scientific | USA |
| Penicillin and Streptomycin | 15140122 | Gibco | USA |

| Material | Reference Code | Supplier | Country of Origin |
|---|---|---|---|
| Pierce BCA Protein Assay Kit | 23227 | ThermoFisher Scientific | USA |
| QIAGEN Plasmid Midi Kit | 12145 | Qiagen | USA |
| QuickChange II Site-Directed Mutagenesis Kit | 200523 | Agilent | USA |
| Recombinant Human Albumin | A9731-5G | Sigma-Aldrich | USA |
| RNase-Free DNase Set | 79254 | QIAGEN | USA |
| RNeasy Mini Kit | 74104 | Qiagen | USA |
| RNeasy Mini Kit | 74104 | QIAGEN | USA |
| RPMI 1640 | 11875-093 | ThermoFisher Scientific | USA |
| siGLO Green Transfection Indicator | D-001630-01-05 | Dharmacon | USA |
| SMARTpool: ON-TARGETplus TRPM7/ctrl | L-005393-00-0005 5nmol / L-006233-00-0005 | Dharmacon | USA |
| Spectra Multicolour High Range Protein Ladder | 26625 | ThermoFisher Scientific | USA |
| T25 Flasks | 83.3910.002 | Sarstedt | Germany |
| T75 Flasks | 83.3911.002 | Sarstedt | Germany |
| Top Ten Competent E. Coli | C404006 | ThermoFisher Scientific | USA |
| Tris Base | T1503 | Sigma-Aldrich | USA |
| Triton X-100 | T8787-100ML | Sigma-Aldrich | USA |
| TrypLE™ Express Enzyme (1X), no phenol red | 12604013 | ThermoFisher Scientific | USA |
| Trypsin | 15090046 | ThermoFisher Scientific | USA |
| Tween 20 | P2287 | Sigma Aldrich | USA |
| Whatman Quantitative Filter Paper | Z241407 | Sigma-Aldrich | USA |

# 3 Results – Functional studies of TRPM7 CICUS Genetic Variants in Heterologous Cell Systems

## 3.1 Sequencing of *TRPM7* Vector

Upon receipt of the *TRPM7* vector, sequencing and alignment against the reference mRNA sequence (NM_017672.5) was performed. Sequence homology showed 99.98% (5597/5598) similarity between the reference sequence and the gene cloned into the pcDNA4/TO plasmid. The single DNA nucleotide difference (c.C4986T: p.Y1662Y) was a synonymous mutation (Figure 3.). This variant did not alter the primary amino acid sequence and was >1200bp from the nearest point mutations for testing, therefore it was unlikely to affect the following mutagenesis or experimental work.

## 3.2 *TRPM7* Variant Mutagenesis

Sanger sequencing following site-directed mutagenesis of the *TRPM7* expression vector revealed successful insertion of a nonsynonymous variant into four separate plasmids (Figure 3.1B). The first variant, p.G179V, showed that in contrast to the reference glycine, following mutagenesis a valine will be translated. This represents a large structural change, from the hydrogen side chain of glycine to the hydrophobic valine. Secondly, p.R494Q altered the reading of an arginine codon to a glutamine. This meant substituting the positively charged polar amino acid for an uncharged amino acid. At c.2579, a cytosine was replaced by a thymine, producing the nonsynonymous variant c.C2579T:p.T860M. The threonine codon was replaced by a hydrophobic amino acid side chain that is capable of binding to metals. Finally, a guanine was sequenced at position c.3614 instead of an adenine, resulting in a glycine replacing a glutamic acid – p.E1205G. The large, negatively charged side chain was replaced by a hydrogen, representing a significant structural change.

A

```
Reference TRPM7 Sequence    4971 ATGGTCAAGTATTTACAAAGAAGATACAGT 5000
                                 |||||||||||||||*|||||||||||||||
TRPM7 from Schmitz          4971 ATGGTCAAGTATTTATAAAGAAGATACAGT 5000
```

B

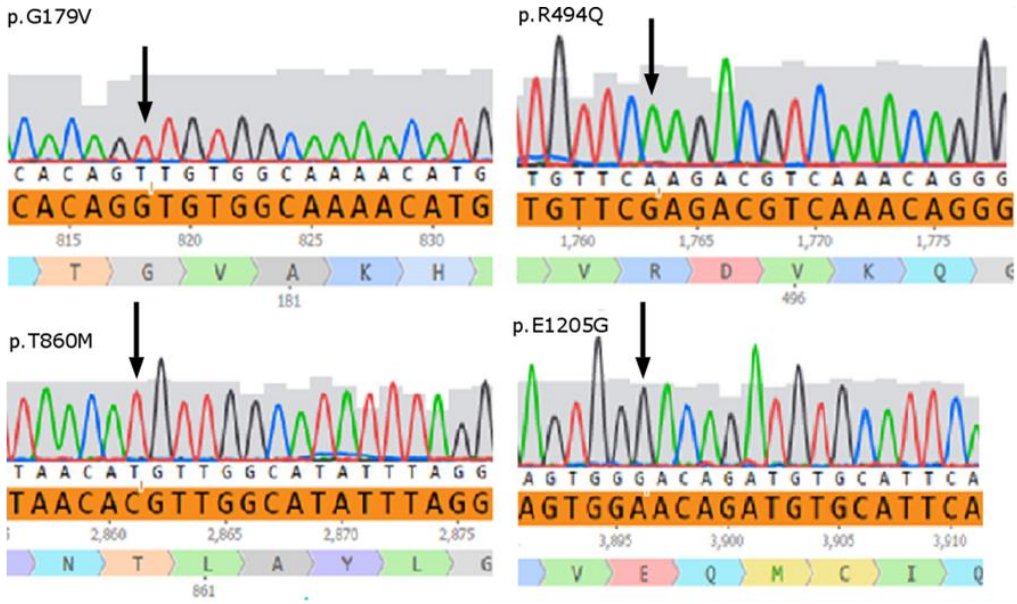


*Figure 3.1.* ***Sanger sequencing of TRPM7 expression vector. A*** *Sanger sequencing of the received DNA plasmid revealed a single synonymous variant at c.C4971T. All other nucleotides showed sequence homology to the reference mRNA sequence of human TRPM7.* ***B*** *Chromatograms depict dye signal strength and the equivalent nucleotide sequence below. In orange is the reference mRNA transcript NM_017672 and below corresponding amino acid sequence depicted in codons.*

## 3.3 Measuring TRPM7-like Ion Channel Current in Heterologous Cells

CHO-K1 cells were transfected with 500ng of *TRPM7* wild-type plasmid, 1800ng of the tetracycline repressor plasmid and 50ng of eGFP. 24 hours later, cells were incubated in tetracycline to induce expression of TRPM7, allowing for patch-clamp experiments. Whole-cell patch-clamp recordings from eGFP-positive cells 48 hours after transfection showed significantly increased TRPM7 current following current run-up compared to untransfected cells.

Due to its ubiquitous expression, TRPM7 current was observed in untransfected CHO-K1 cells (Figure 3.2). Following whole-cell break-in current density measured at +80mV and -80mV peaked at 49.70 ± 6.34pA/pF and -7.42 ± 1.33pA/pF, respectively. Transfection of CHO-K1 cells with wild-type TRPM7 current increased outward current, at 110.0 ± 13.24 pA/pF while inward current (-80mV) showed no significant increase, measured at -5.77 ± 0.86.

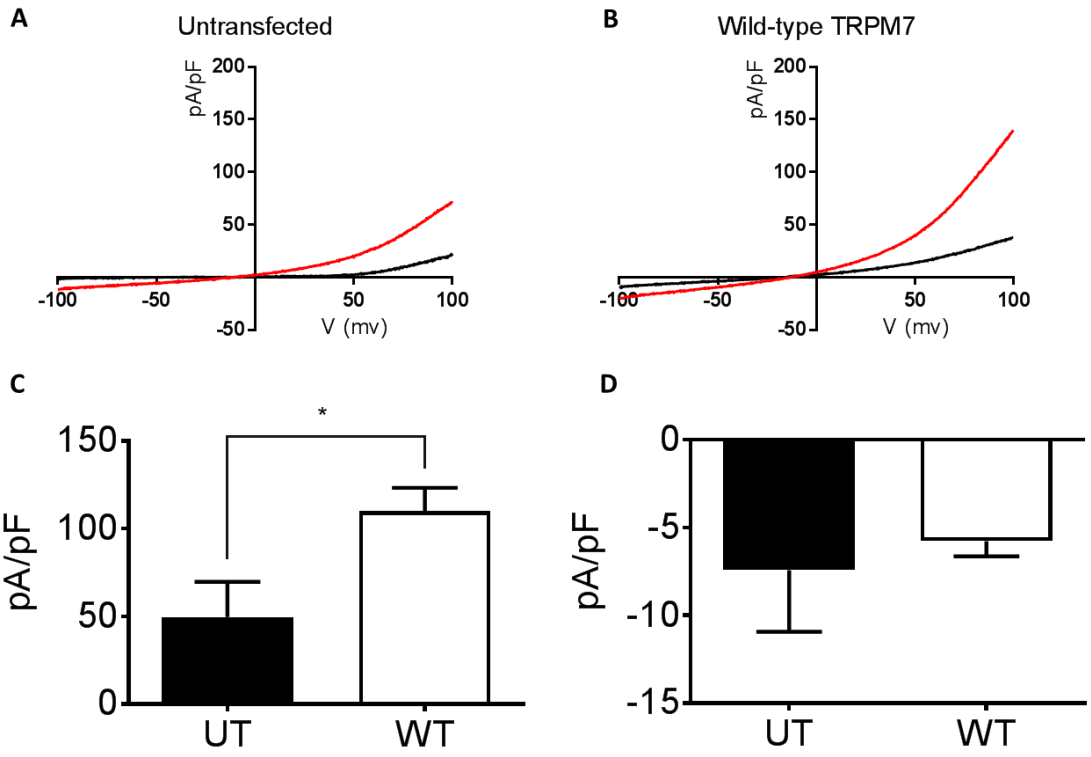


*Figure 3.2.* ***TRPM7 current in untransfected and transiently transfected CHO-K1 cells 24 hours post tetracycline induction. A*** *TRPM7 current from untransfected CHO-K1 cell at initial whole-cell break-in (black) and after 5 minutes (red)****. B*** *TRPM7 current from wild-type transfected CHO-K1 cell at initial whole-cell break-in (black) and after 5 minutes (red).* ***C*** *Mean data of current density at +80mV in untransfected cells (n=10) and WT transfected cells (n=30).* ***D*** *Group data of current density at -80mV in untransfected (n=7) and WT transfected (n=28) CHO-K1 cells. * - P<0.05.*

## 3.4 Validating the Identity of TRPM7 Ionic Currents using Specific Inhibitors

To confirm that TRPM7 was being specifically recorded, two known inhibitors of the ion channel were used in further patch-clamp experiments. Millimolar concentrations of magnesium have been reported to block TRPM7 channel current, and micromolar concentrations of extracellular 2-APB have been reported to inhibit TRPM7 but potentiate TRPM6 current [226,231]. Addition of 10mM magnesium to TRPM7 extracellular solution reduced currents significantly in both untransfected and cells transfected with *TRPM7* (Figure 3.3A & B). Mean TRPM7 current at +80mV decreased from 129.9 pA/pF to 7.764 pA/pF after 10mM magnesium was added to the bath ($P<0.0001$, Figure 3.3C). Magnesium also significantly inhibited a presumed endogenous TRPM7 current in untransfected cells ($P<0.0001$, Figure 3.3C). Analysis of the inward TRPM7 current at -80mV showed similar inhibition of current density in both WT transfected and untransfected cells ($P<0.0001$, Figure 3.3D). This current was also inhibited by application of 50µM 2-APB (Figure 3.3E & F).

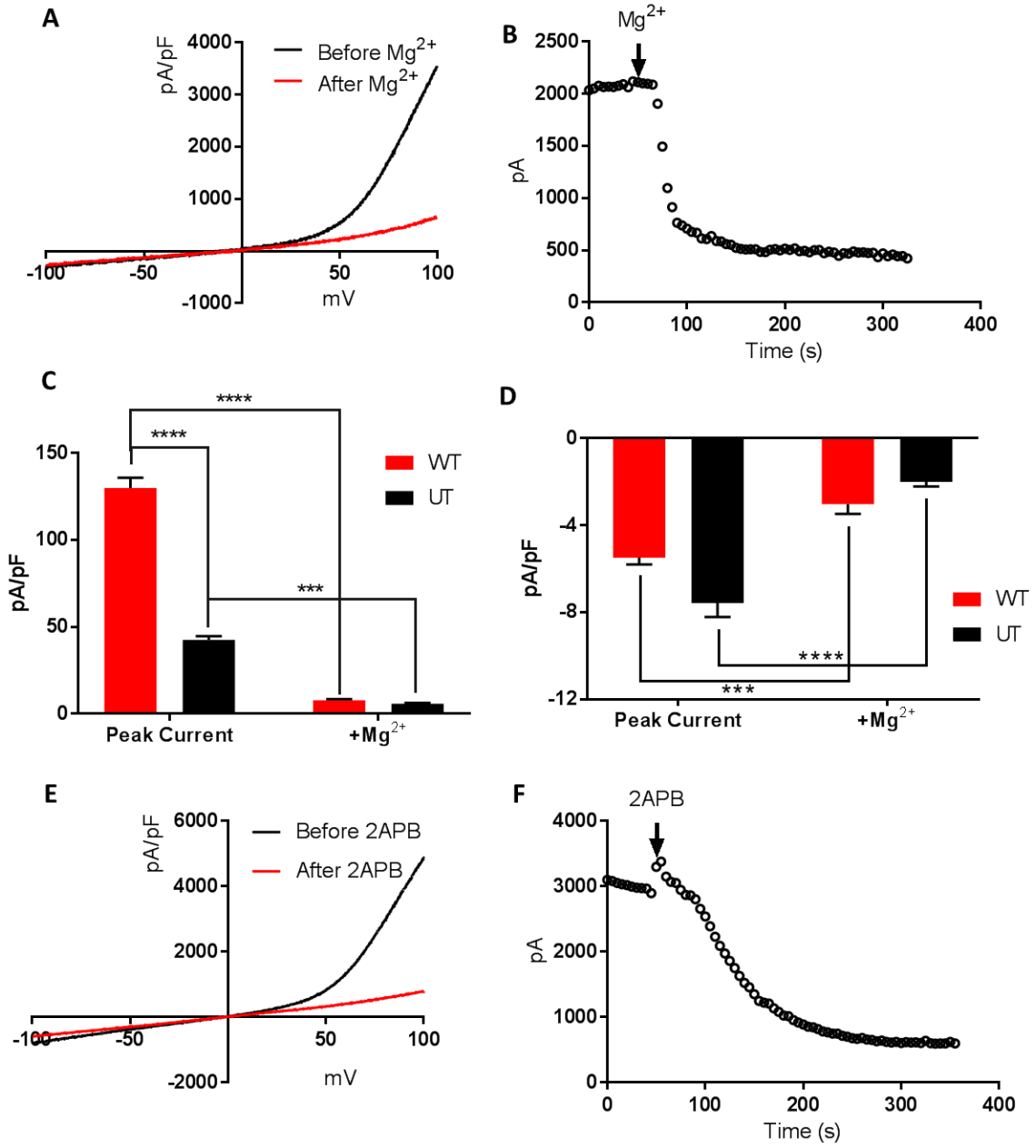


*Figure 3.3.* ***Characteristic inhibition of TRPM7 by $Mg^{2+}$ and 2-APB. A*** *Current traces before (black) and after (red) addition of 10mM magnesium to extracellular solution during whole-cell recording of WT TRPM7 transfected CHO-K1 cell.* ***B*** *Time course of cell from A showing immediate reduction in current at +80mV following 10mM magnesium treatment.* ***C*** *Mean current density at +80mV comparison between wild-type transfected (n=13) and untransfected (n=6) CHO-K1 cells before and after treatment with 10mM $Mg^{2+}$.* ***D*** *Corresponding current density at -80mV from cells analysed in C.* ***E*** *Current traces before (black) and after (red) addition of 50μM 2-APB to extracellular solution during patch-clamp recording of CHO-K1 transiently transfected with TRPM7 WT.* ***F*** *Time course of current at +80mV from cell shown in (E), showing current reduction over 300seconds following 2-APB addition. *** - P<0.0005, **** - P<0.0001.*

## 3.5 Investigating the Effect of CICUS Variants on TRPM7 Current Density in CHO-K1 Cells

Transient transfection of TRPM7 ion channels into CHO-K1 cells yielded measurable TRPM7 current from all four transfected variants (Figure 3.4). Mean current density of mutant TRPM7 channels was as follows: p.G179V at +80mV was 34.03 ± 3.02 pA/pF, p.R494Q 273.6 ± 51.88 pA/pF, p.T860M 44.5 ± 9.91 pA/pF and p.E1205G 60.74 ± 4.27 pA/pF (Figure 3.5A). Corresponding current density at -80mV was as follows: p.G179V -4.29 ± 0.79 pA/pF, p.R494Q transfected 14.40 ± 2.15 pA/pF, p.T860M -8.24.69 ± 1.91 pA/pF and cells transfected with p.E1205G was -6.29 ± 1.01 pA/pF (Figure 3.5B).

Analysis of the mean data using one-way ANOVA with Dunnett's multiple comparisons test reported that compared to wild-type, p.R494Q resulted in a statistically significant increase in outward current (110.0 vs 273.6 ± 31.96 pA/pF, P<0.0001). This was mirrored by a significant increase in inward current at -80mV as well (-5.77 vs -14.40 ± 1.752 pA/pF, P<0.0001). There was a significant decrease in outward current at +80mV in cells transfected with p.G179V *TRPM7* (Figure 3.5A).

The other two variants, p.T860M and p.E1205G were not statistically significant compared to wild-type transfected cells. This warranted further investigation, as changes in current density due to genetic variation have been reported previously in the setting of neurodegenerative disease [300].

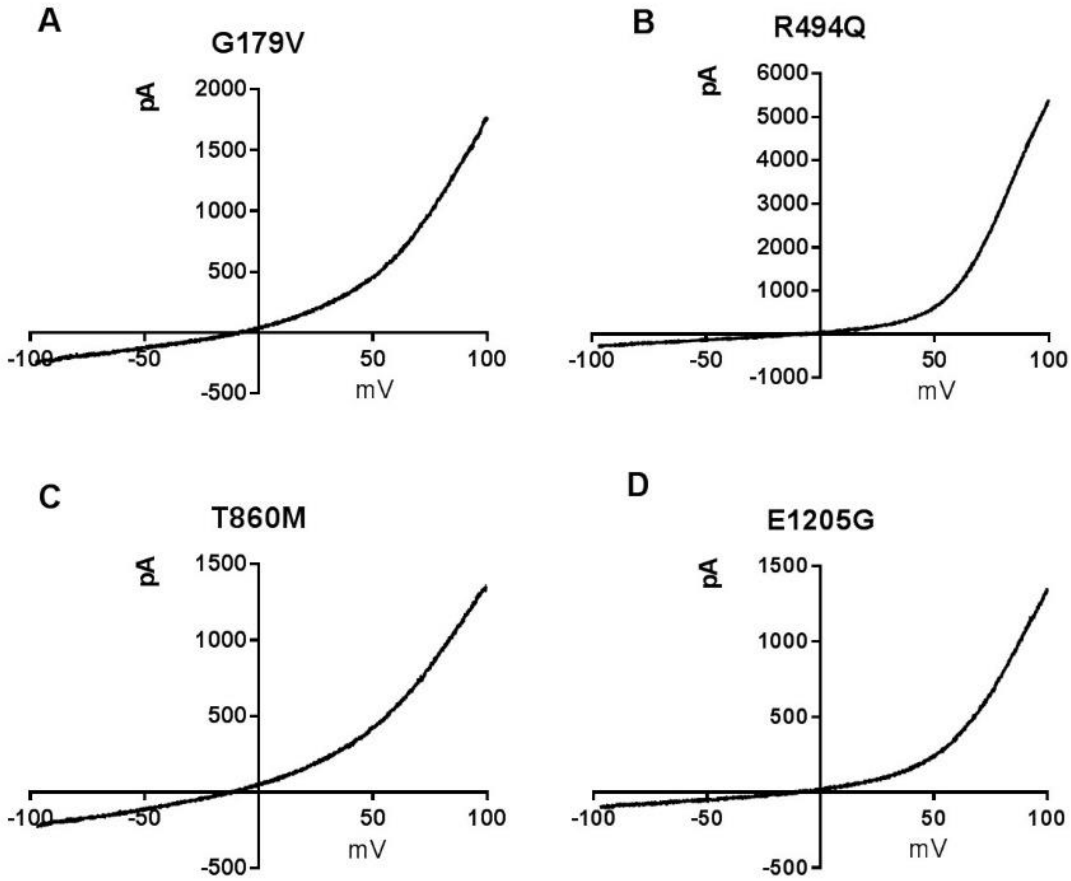


*Figure 3.4.* ***Traces of whole-cell recordings from CHO-K1 cells transiently transfected with four different CICUS variants for TRPM7. A-D*** *Whole-cell patch-clamp recordings from cells transfected with G179V (A), R494Q (B), T860M (C) and E1205G (D) mutant TRPM7 channels.*

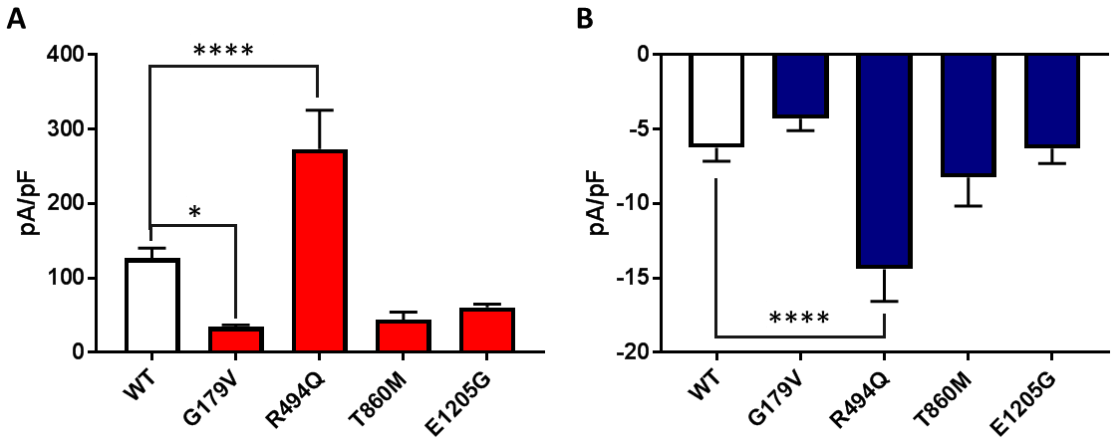


*Figure 3.5.* ***Transiently transfected CHO-K1 TRPM7 current is increased by the p.R494Q variant. A*** *Whole-cell patch-clamp data from CHO-K1 cells transiently transfected with wild-type (n=30) and four different TRPM7 variants (n=9-13) measured at +80mV.* ***B*** *Patch-clamp data from CHO-K1 cells transfected with wild-type and four CICUS TRPM7 variants measured at -80mV. * - P<0.05, **** - P<0.0001.*

## 3.6 Investigation of how TRPM7 CICUS Variants Respond to Magnesium Inhibition

To assess how TRPM7 channels responded to $Mg^{2+}$ inhibition, transfected cells were patch-clamped in extracellular solutions containing a range (0mM – 6mM) of magnesium concentrations (Figure 3.6). At 0mM $Mg^{2+}$, WT TRPM7 current was measured as 129.95 pA/pF at +80mV, and -5.49 pA/pF at -80mV. The p.G179V variant significantly decreased +80mV current density at 0mM magnesium to 36.49 pA/pF ($P<0.005$, Figure 3.6A). In concordance to Figure 3.5, p.R494Q significantly increased current density at 0mM magnesium to 297.71 pA/pF for outward (+80mV) and by -17.56 pA/pF inward (-80mV) currents ($P<0.0001$, Figure 3.6C & D). This variant also increased outward current when compared to wild-type when treated with 0.5mM $Mg^{2+}$, ($P<0.001$). p.R494Q increased inward current density significantly compared to wild-type at 0.5mM $Mg^{2+}$ to -14.18 pA/pF and at 1.0mM $Mg^{2+}$ to -10.44 pA/pF (Figure 3.6D, $P<0.0001$ and $P<0.05$, respectively). The p.T860M variant decreased outward current when compared to wild-type at 0mM $Mg^{2+}$ to 53.34 pA/pF ($P<0.05$, Figure 3.6E).

To assess whether these changes in current density were due to an altered dose-response to magnesium, the data were normalised to show how magnesium concentrations reduced TRPM7 outward current in relation to initial peak current (Figure 3.7). Normalised outward currents compared to peak current before magnesium treatment were not significantly different from wild-type TRPM7 transfected cells at any magnesium concentration when transfected with p.G179V, p.R494Q, p.T860M and p.E1205G TRPM7 variants (Figure 3.7).

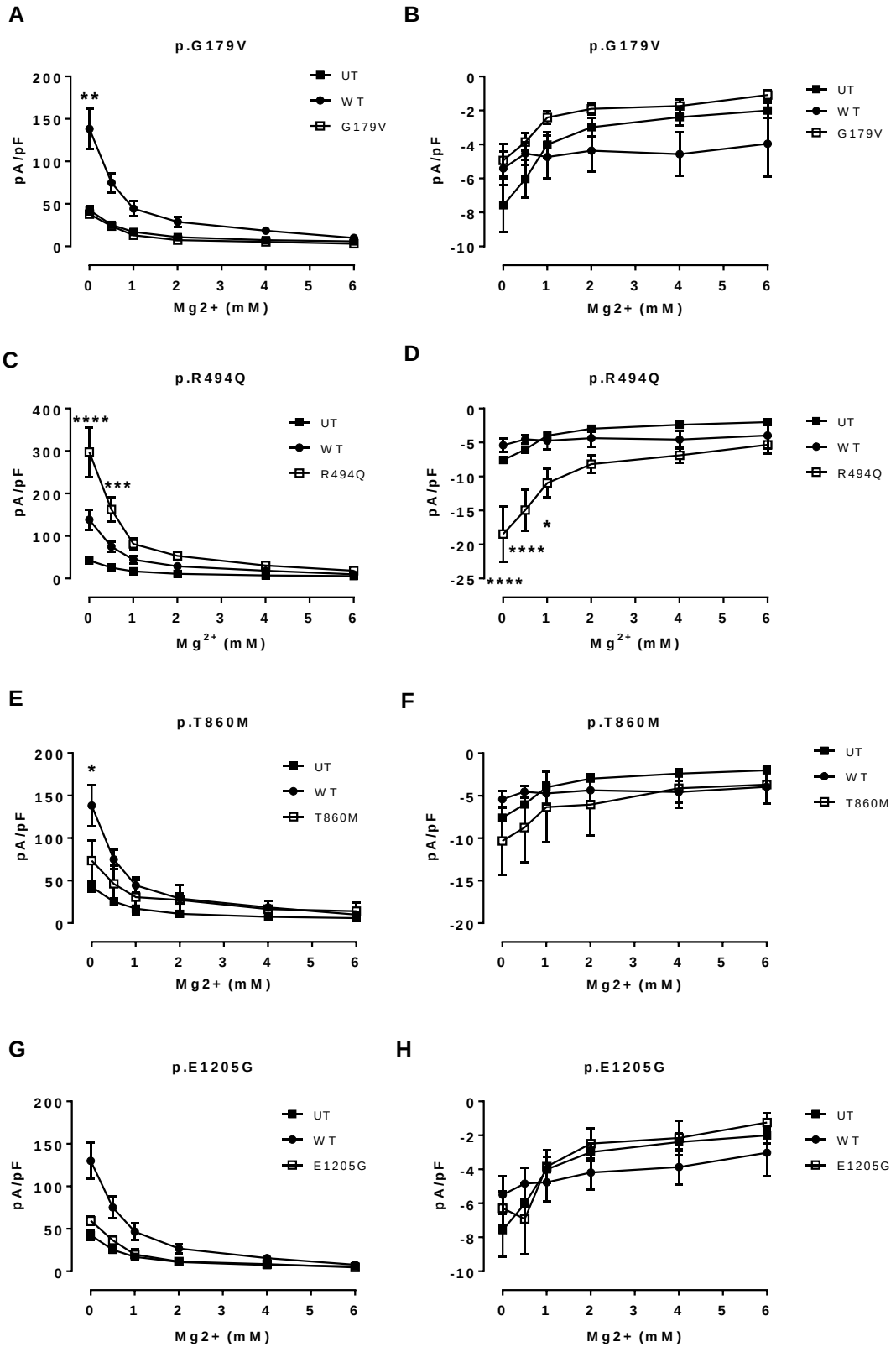


*Figure 3.6.* ***Magnesium inhibition curves of CHO-K1 cells transfected with wild-type or CICUS variant TRPM7. A, C, E, G*** *Current recorded at +80mV from cells transfected with p.G179V, p.R494Q, p.T860M and p.E1205G at +80mV compared to untransfected and wild-type TRPM7 transfected CHO-K1 cells.* ***B, D, F, H*** *Inward current recorded at -80mV from the same cells as in A, C, E and G. * = P<0.05, ** = P<0.005, *** = P<0.0005, **** = P<0.0001 vs WT, n = 7-8.*

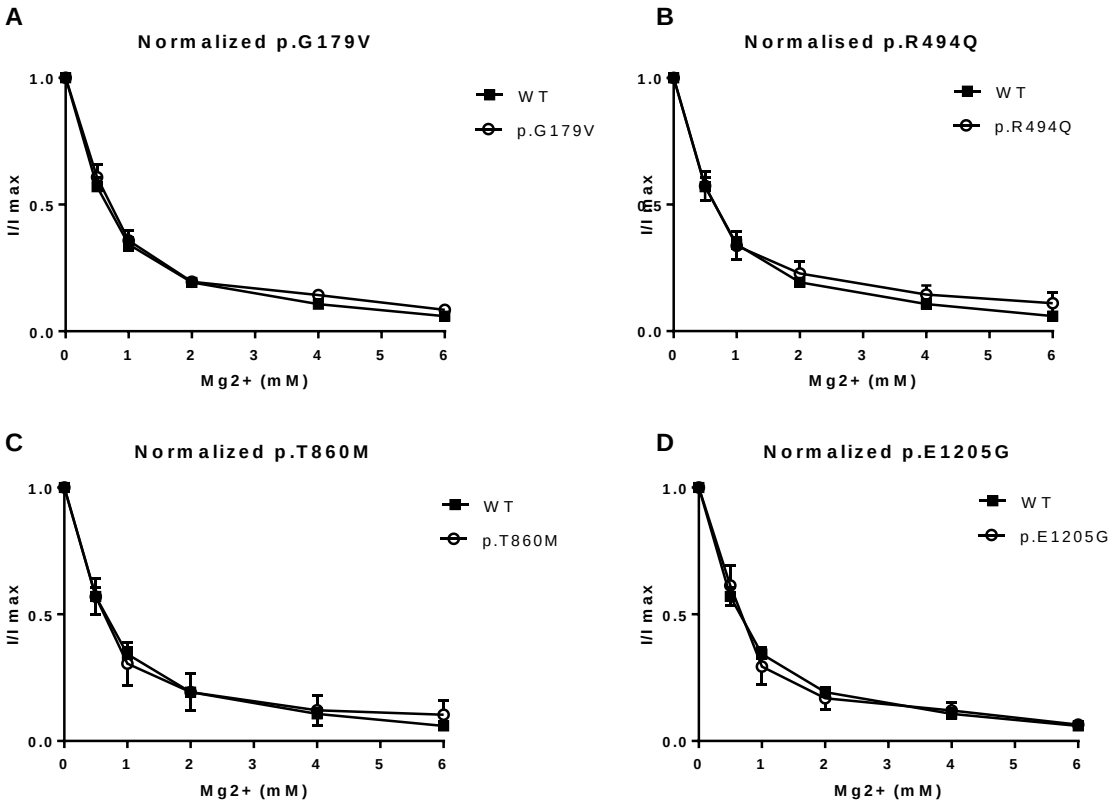


*Figure 3.7.* ***Normalised outward current recordings from CHO-K1 cells transfected with TRPM7*** **and CICUS mutants.** ***A-D*** *Whole-cell patch-clamp current data from Figure 3.6, WT and p.G179V (A), p.R494Q (B), p.T860M (C) and p.E1205G (D). TRPM7 transfected CHO-K1 cells exposed to a range of extracellular magnesium concentrations (0 – 6 mM) n = 7-8.*

## 3.7 Investigating the Effect of CICUS Variants on TRPM7 Current Density in HEK293 Cells

We sought to verify these findings in an alternative cellular system to ensure the observed current density differences were not due to artefacts of using purely a CHO-K1 heterologous expression system. HEK293 cells transfected with TRPM7 showed similar recordings to those seen in CHO-K1 cells (Figure 3.8). Compared to CHO-K1 cells transfected with TRPM7 (n=30), HEK293 cells (n=15) had larger peak currents at +80mV (163.2 ± 27.87 pA/pF vs 110.0 ± 13.24 pA/pF). HEK293 cells showed greater inward current at -80mV (-9.78 ± 2.22 pA/pF vs -5.77 ± 0.86 pA/pF). Although an apparent increase in both inward and outward current was observed when transfected with wild-type TRPM7 channel, this was not statistically significant (P=0.56 for +80mV and P=0.051 for -80mV)(Figure 3.8B).

HEK293 cells transfected with wild-type, p.G179V, p.R494Q, p.T860M and p.E1205G TRPM7 were patch-clamped and whole-cell currents recorded (Figure 3.9). Strikingly, HEK293 mean data showed in p.R494Q transfected cells, TRPM7 current recorded at +80mV and -80mV was not statistically different to wild-type transfected cells (P=0.95 and P=0.91 respectively).

In contrast to data recorded from transfected CHO-K1 cells, patch-clamp recordings from HEK293 cells showed that both p.G179V and p.T860M, significantly reduced outward ion channel current compared to wild-type channel. Outward current density of WT TRPM7 at +80mV was 133.20 pA/pF , while p.G179V was significantly reduced, at 39.26 pA/pF (P=0.005). HEK293 cells transfected with p.T860M recorded 36.32 pA/pF at +80mV (P=0.007). Current density measured at -80mV however was no different in p.G179V or p.T860M cells compared to wild-type (P>0.99 and P=0.99 respectively).

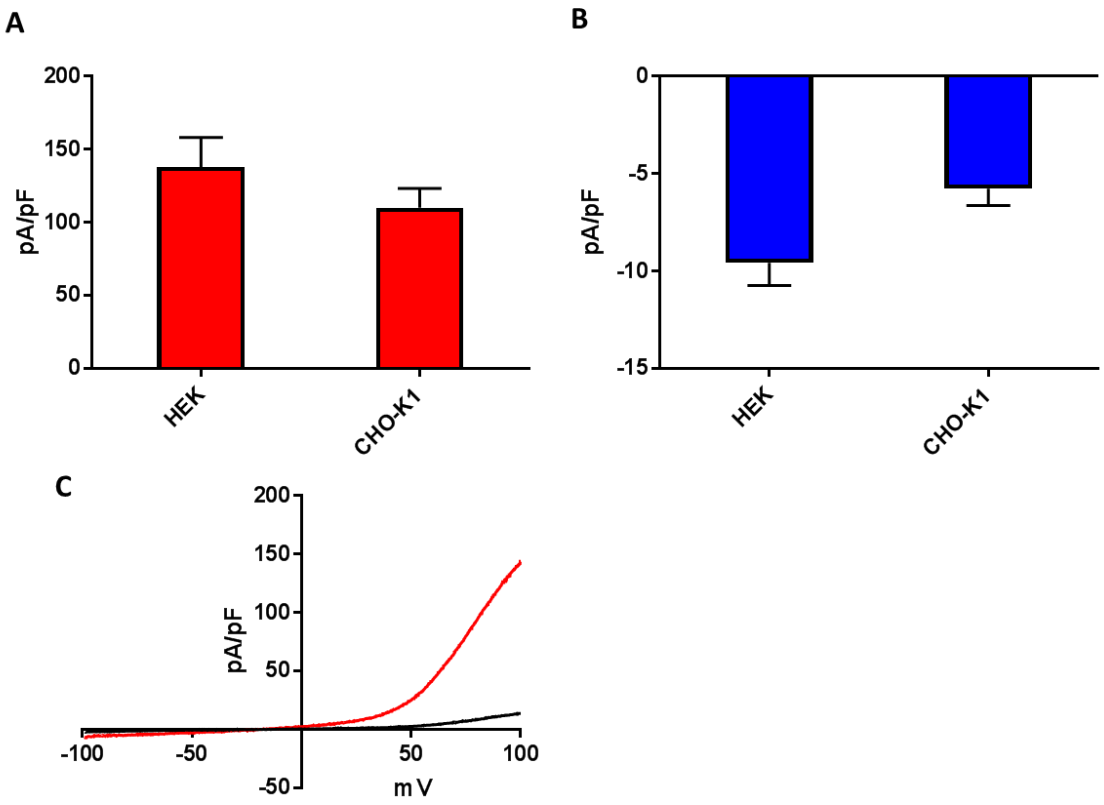


*Figure 3.8.* ***TRPM7 current recorded from HEK293 and CHO-K1 cells 24-48 hours after transfection. A*** *Comparison of current density recorded at +80mV between HEK293 and CHO-K1 cells.* ***B*** *Current density at -80mV recorded from transfected HEK293 and CHO-K1 cells.* **C** *Representative traces from a HEK293 cell transiently transfected with wild-type TRPM7 at whole-cell break-in (black) and after magnesium chelation (red).*

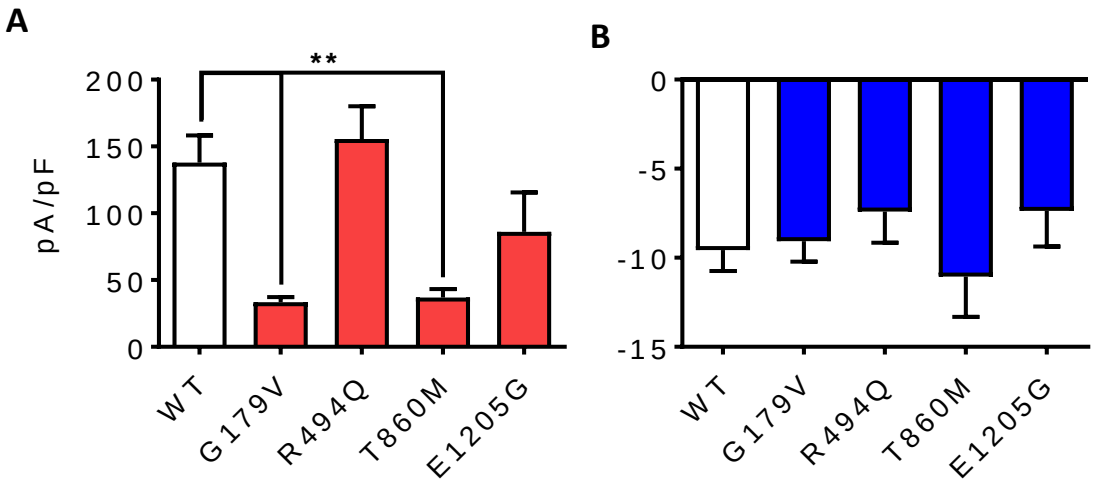


*Figure 3.9.* ***CICUS variant HEK293 mean current density data. A*** *Whole-cell patch-clamp data from HEK293 cells transiently transfected with wild-type (n=28) and four different TRPM7 variants (n=8-12) measured at +80mV.* ***B*** *Patch-clamp data from HEK293 cells transfected with wild-type and four CICUS TRPM7 variants measured at -80mV. ** = P<0.001.*

## 3.8 Investigating TRPM7 Wild-type and CICUS Variant Protein Expression

In parallel to patch-clamp experiments, the lysates of cells transfected with TRPM7 were analysed using the western blot technique to look at cellular expression. Initially, CHO-K1 cells were transfected with 500ng of WT TRPM7, 500ng of each of the CICUS variant vectors or left untransfected. Lysates from these cells were collected and blotted using calnexin as a loading control. The Neuromab N74/25 antibody initially did not produce any discernible bands from any lysates from multiple experiments (n=3; Figure 3.10). Recordable current from WT transfected cells was significantly greater than untransfected cells (Figure 3.2), supporting the presence of the TRPM7 channel albeit at low protein concentrations following cell harvest. Therefore CHO-K1 cells were transfected with increasing amounts of TRPM7 DNA prior to tetracycline induction and lysate harvesting. Increasing amounts up to 2.0µg of DNA produced no discernible TRPM7 ion channel band (~230kDa) even following long film exposure times of >35minutes (Figure 3.11). Of note, calnexin gene expression was highly variable (Figure 3.10A) despite protein concentration calculation using the BCA assay and therefore β-actin was used for further loading controls.

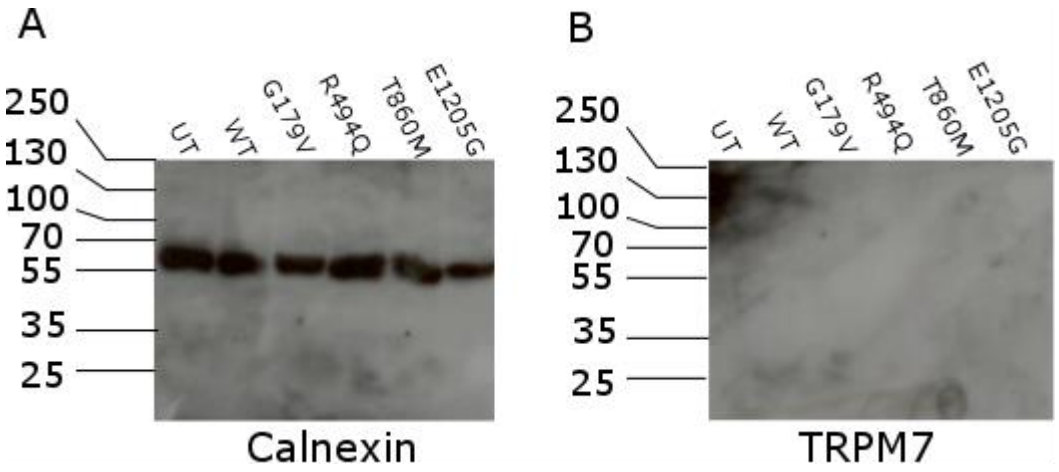


*Figure 3.10.* ***Initial western blot of CHO-K1 lysates for calnexin and TRPM7 antibody N74/25.*** *Lysates were run into 8% polyacrylamide gels.* ***A*** *Calnexin antibody staining of CHO-K1 cell lysates either untransfected or transfected with 500ng of WT TRPM7 or one of the CICUS variants.* ***B*** *Western blot of the same lysates in A showing lack of TRPM7 staining in all lysates after probing using the N74/25 Neuromab antibody.*

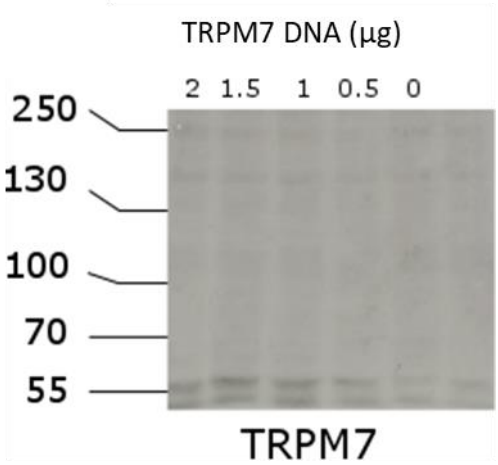


*Figure 3.*11. ***Increasing amount of TRPM7 DNA does not produce visible protein staining in CHO-K1 cells.*** *Lysates of CHO-K1 cells run into 8% polyacrylamide gels. CHO-K1 cells were transfected with between 2 and 0 µg of vector DNA as noted above each column. TRPM7 antibody, N74/25 from Neuromab with 40 minutes of exposure showing background noise.*

The use of different reducing agents may adversely affect protein unfolding and therefore which epitopes are available for antibody binding. An alternative to β-mercaptoethanol, DTT, was used to provide alternative protein reducing conditions to attempt to see if ineffective unfolding was masking the TRPM7-antibody epitope. However, despite visible β-actin staining, no visible TRPM7 bands were identifiable in either the β-mercaptoethanol treated lysates or those treated with DTT (Figure 3.12). Another facet of the reduction process is heating, multi-pass membrane proteins can aggregate when lysates are boiled at 95˚C. Reducing the reaction temperature to 55˚C or 70˚C and prolonging the time to 10 minutes did not produce visible bands after lysate western blotting (Figure 3.13). Due to repeated failure at identifying quantifiable amounts of TRPM7 protein using the western blot technique despite patch-clamp analysis of the current, two different lysate buffers were used to harvest cellular proteins alongside using an alternative Alomone (ACC-047) antibody (Figure 3.14). When using NP40 lysis buffer and the Alomone antibody, a <250kDa signal was visible, albeit very faint despite >30minute film exposure. Blotting of CHO-K1 cell lysates using Neuromab antibody N74/25 showed only aggregate signal at the top of the wells in both NP40 and RIPA harvested samples.

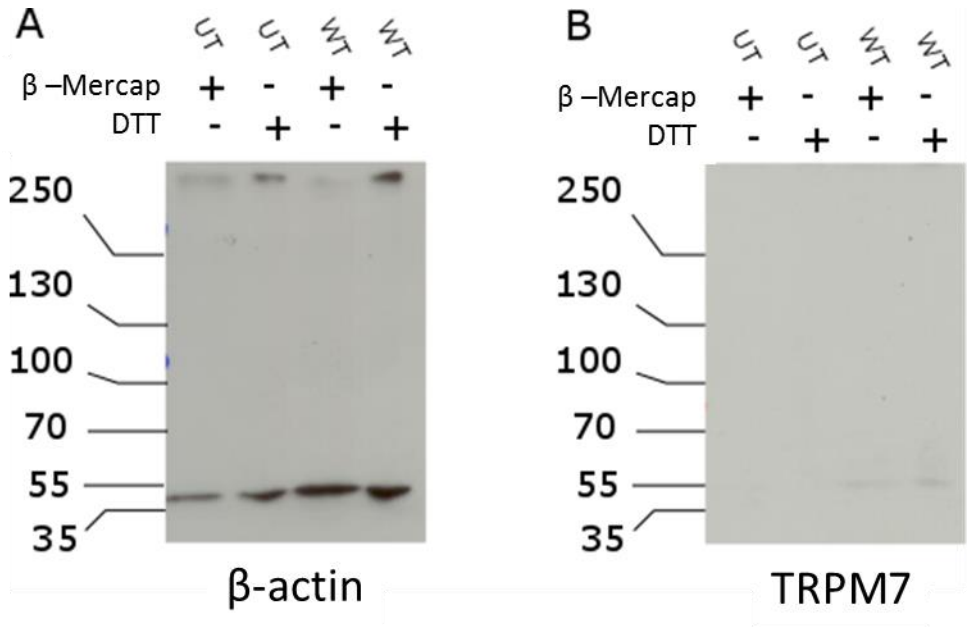


*Figure 3.12.* ***Optimisation of reducing agents β-mercaptoethanol and dithiothreitol with new loading control β-actin. A*** *HEK 293 cell lysates transfected with 500ng of WT TRPM7 DNA were run on a 4-20% gradient gel. B-actin staining of protein lysates reduced in either B-mercaptoethanol or DTT as noted above.* ***B*** *TRPM7 antibody N74/25 staining of the same lysates as in A*

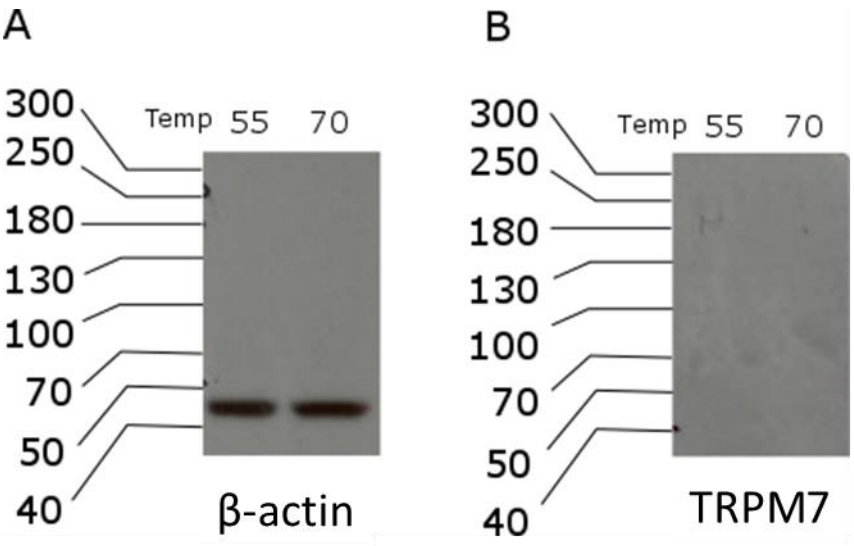


*Figure 3.13.* ***Denaturing temperature does not affect TRPM7 blotting.*** *Protein lysates were reduced with two different temperatures as noted, 55˚C or 70˚C for 10minutes. Lysates were run through a 4-20% polyacrylamide gradient gel.* ***A*** *B-actin staining showing clear bands.* ***B*** *TRPM7 blotting of corresponding lysates seen in A using Neuromab TRPM7 antibody.*

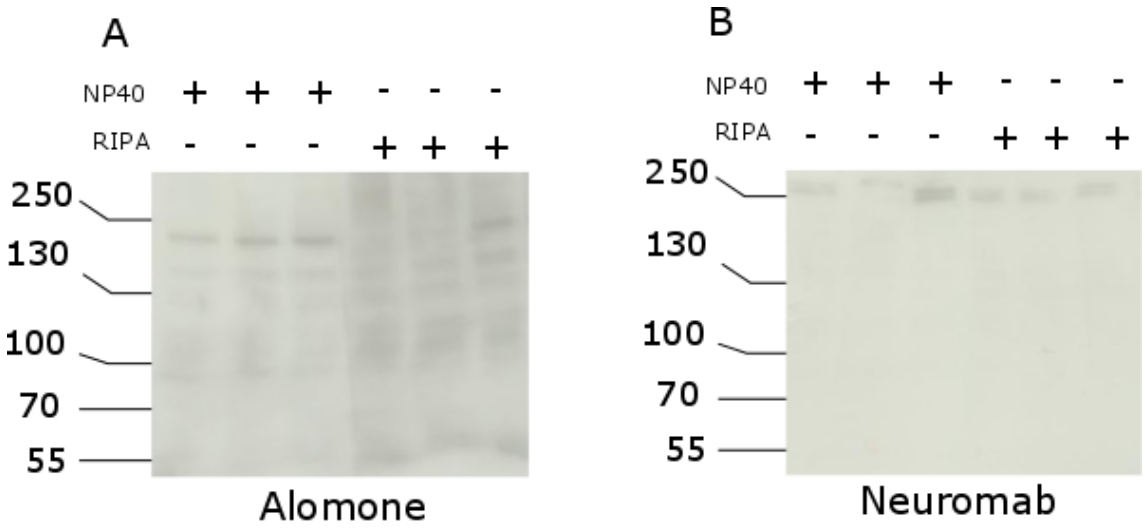


*Figure 3.14.* ***Alomone and Neuromab antibody staining of TRPM7 transfected CHO-K1 cell lysates.*** *Protein lysates were harvested in either 100µL of NP40 or 100µL RIPA buffer as shown. Lysates were run into polyacrylamide 4-20% gradient gel.* ***A*** *Alomone antibody (ACC-047) TRPM7 staining.* ***B*** *Neuromab N74/25 antibody staining for TRPM7 of the same protein lysates used in A.*

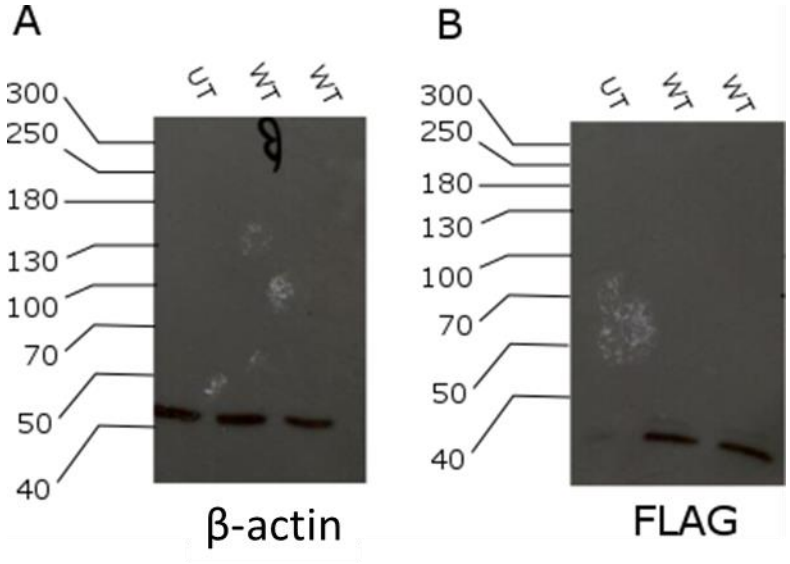


*Figure 3.15.* ***FLAG-epitope targeting antibody identifies cleaved N-terminal protein in TRPM7 transfected HEK293 cells.*** *Lysates were harvested from HEK293 transfected cells and ran into 4-20% gradient polyacrylamide gels.* ***A*** *β-actin loading control.* ***B*** *Cleaved FLAG-tagged N-terminal domain <40kDa in size visible only in TRPM7 transfected cells.*

The TRPM7 expression plasmid received from Schmitz et al. contains an N-terminal FLAG tag. Using a well-characterised antibody in our lab (F3165), TRPM7 transfected CHO-K1 cell lysates were blotted. The only visible bands using a FLAG targeting antibody were small cleavage products of the N-terminus <30kDa - not full length ion channels (Figure 3.15). Although both TRPM7 antibodies produced by Alomone and Neuromab were unable to successfully identify TRPM7 proteins in a variety of conditions, a mouse monoclonal antibody produced by Santa-Cruz showed TRPM7 to be present in CHO-K1 cells transfected with 500ng of TRPM7 compared to untransfected cells which showed a complete lack of staining. Interestingly, small C-terminally cleaved kinases were also visible in these lysates ~40kDa and 100kDa (Figure 3.16). While untransfected cells showed no protein present, wild-type transfected cells showed a clear ~250kDa band and either a glycosylated product or dimerised form of the ion channel (Figure 3.17).

In contrast, p.G179V and p.T860M TRPM7 cells showed expression profiles similar to untransfected cells, in-line with the significantly reduced current observed in single-cell patch-clamp experiments of these cells (Figure 3.9). The p.R494Q and p.E1205G transfected cells had expression profiles similar to WT cells, although showing less un-aggregated TRPM7 ion channel. Interestingly, in comparison to the CHO-K1 system, no visible cleaved C-terminal kinases were observed, in keeping with published observations of the cell-specific manner of this process [223].

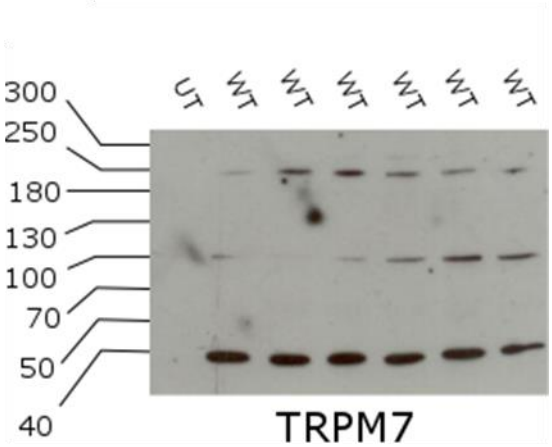


*Figure 3.16.* ***TRPM7 and its cleaved products are detectable following HEK293 cell transfection when using Santa Cruz sc271099 antibody.*** *Cell lysates were run into 8% polyacrylamide gel. The lysates show TRPM7 ion channel ~ 250kDa as well as small cleaved C-terminal kinases.*

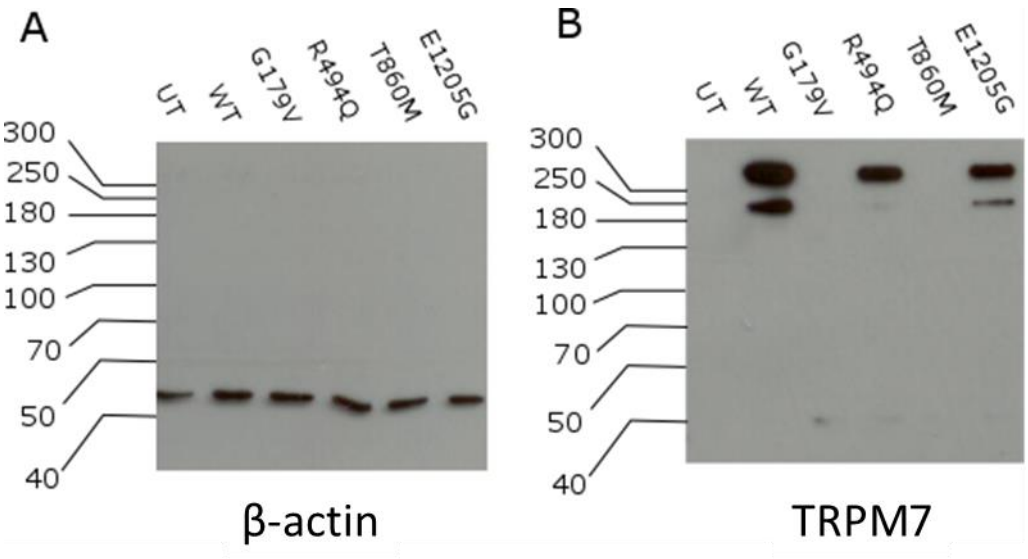


*Figure 3.17.* ***CICUS variants p.G179V and p.T860M produce no quantifiable protein when transfected into HEK293 cells.*** *Western blot of cell lysates* ***A*** *β-actin blotting showing equal loading control expression when 30µg of protein loaded into gel.* ***B*** *Protein lysates probed with Santa Cruz TRPM7 antibody on 8% polyacrylamide gel showing full length TRPM7 protein.*

## 3.9 Analysis of TRPM7 mRNA following WT and CICUS Variant Transfection

To ascertain whether this observed lack of protein expression in p.G179V or p.T860M transfected cells was caused by transcriptional or translational perturbation we performed qPCR analysis to measure TRPM7 mRNA expression following cell transfection. Total RNA isolation was performed as in Methods and Materials (2.7.1).

Briefly, HEK293 cells were seeded onto 6-well dishes for 24 hours before transfection with 500ng of TRPM7 WT or CICUS variant and 1800ng of tetracycline repressor plasmids. The following morning, media was changed to contain 1µg/ml tetracycline. At 24 hours post tetracycline treatment cells were harvested using an RNeasy mini kit (QIAGEN, USA).

Following reverse transcription, qPCR was carried out using cDNA samples from five independent experiments and TRPM7 expression normalised to housekeeping gene GAPDH (Figure 3.18). Compared to untransfected cells, TRPM7 mRNA increased ~20 fold 48 hours after transfection with WT expressing plasmid (Figure 3.18B; 0.06± vs 1, $P < 0.0001$). When each individual experiment was normalised to WT TRPM7 experiments, no significant difference was observed between HEK293 cells transfected with WT or any of the four CICUS variants (G179V, $P = 0.76$, R494Q, $P = 0.68$, T860M, $P = 0.89$, E1205G, $P = 0.85$).

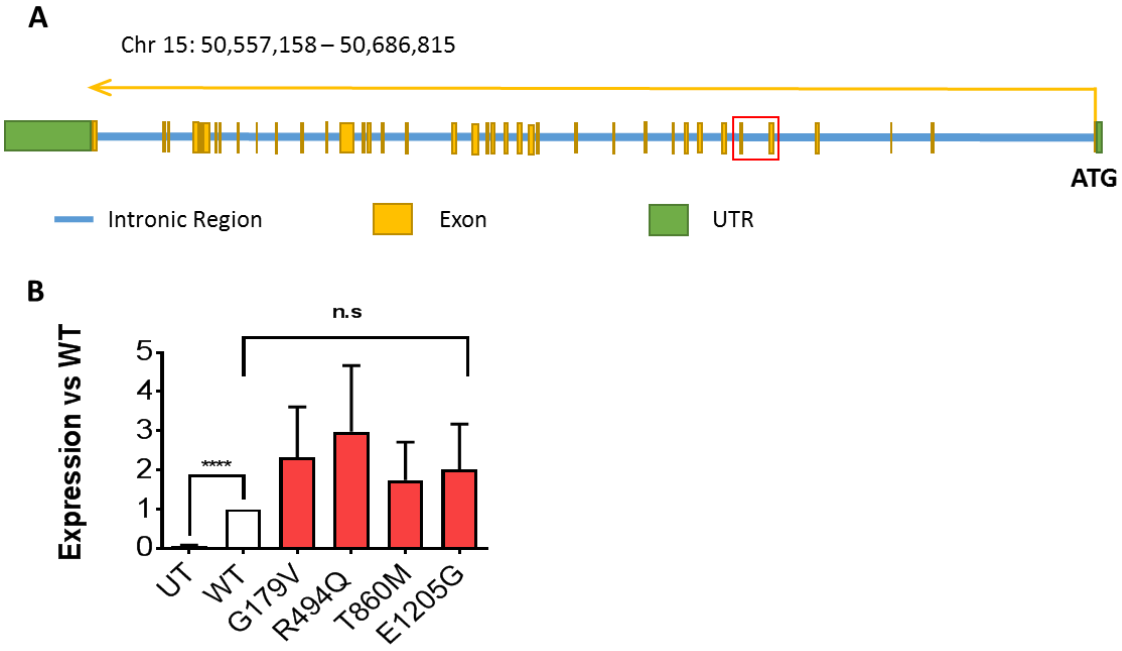


*Figure 3.18.* ***qPCR analysis of TRPM7 mRNA 48 hours after transfection. A*** *Schematic of TRPM7 gene located on chromosome 15. The coding sequence of TRPM7 consists of 39 exon, shown in yellow of representative sizes. Intronic regions are shown in blue while both 5' and 3' areas are illustrated green. The exons 5 and 6, targeted by the probe are boxed in red.* ***B*** *Comparison of TRPM7 mRNA between untransfected (black), wild-type (white) and four CICUS variant (red) transfected HEK293 cells. Untransfected cells show reduced expression compared to WT while all four variants do not. Data was analysed using repeated measures one-way ANOVA using Dunnett's multiple comparison test vs WT value. ****- P < 0.0001.*

## 3.10 Analysis of MG132 Proteasomal Inhibitor Following TRPM7 Variant Transfection

Cell transfection with p.G179V or p.T860M TRPM7 showed a lack of protein expression but similar mRNA levels to wild-type transfected cells. To investigate whether this was due to degradation we inhibited protein degradation following transfection. Cells were transfected with 500ng of WT TRPM7 or 500ng of CICUS variant DNA alongside 1800ng of tetracycline repressor plasmid (Figure 3.19). After transfection (5 hours) media was changed and the following day substituted with 1µg/ml tetracycline, at 5pm media was supplemented with MG132 (5µM final concentration) to inhibit degradation of proteins through the 26S proteasomal pathway.

Following MG132 treatment, even in untransfected cells smaller fragments of TRPM7 were detected in whole-cell lysates. In wild-type and p.E1205G transfected cells there were similar amounts of full length TRPM7 ion channel protein visible (~250kDa, Figure 3.19C). Interestingly in cells transfected with p.R494Q TRPM7 a much greater proportion of full length protein was visible following MG132 treatment compared to WT (Figure 3.17B, Figure 3.19C). MG132 treatment did not rescue TRPM7 ion channel expression, however a faint visible band >250kDa was seen when cells were transfected with p.T860M.

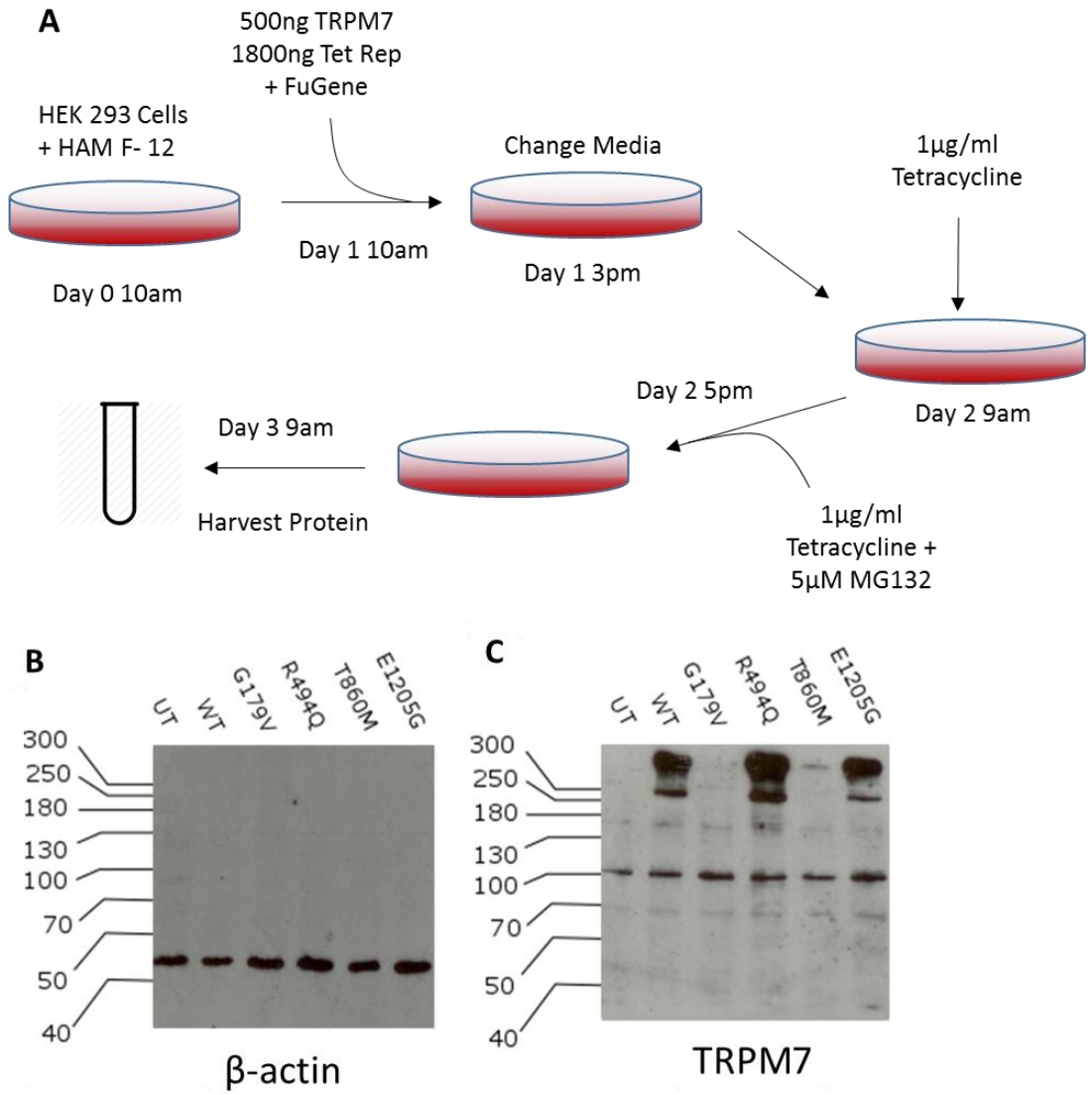


*Figure 3.19.* ***MG132 rescues the protein expression of p.T860M TRPM7 in transfected HEK293 cells. A*** *Methodology for TRPM7 transfection and induction of transcription followed by proteosomal inhibition with MG132. Cells were plated in HAM F-12 before transfection with TRPM7 and tetracycline for 5 hours. Following overnight media change tetracycline was added to media to induce transcription before overnight MG132 treatment and subsequent protein harvest.* ***B*** *Western blot of β-actin loading control on 6% polyacrylamide gel.* ***C*** *Primary antibody (sc271099) targeting TRPM7 from same lysates used in B.*

## 3.11 Investigating Dominant Negative Effects of Functionally Harmful TRPM7 Variants

To establish whether transfection of p.G179V or p.T860M TRPM7 could influence transcription or translation of WT protein in heterologous cells, HEK293 cells were transfected with a mixture of WT and CICUS plasmid. Briefly, cells were plated in 6-well dishes and transfected at ~70% confluency for 4-6 hours with 500ng or 250ng of WT vector, or a 500ng mix of WT and variant plasmid (plus 1800ng tetracycline repressor plasmid and 50ng eGFP). Cells were then split onto glass coverslips overnight and incubated with 1µg/ml tetracycline to induce transcription. Adherent cells underwent whole-cell patch-clamp analysis as previously mentioned for TRPM7 transfected cells. Positively transfected cells were identified using green fluorescence.

Although there was a marked current density increase in HEK293 cells transfected with 500ng WT TRPM7 vector compared to 250ng WT vector, this did not reach statistical significance (Figure 3.20; 334.4±119.8 pA/pF vs 169.2±56.38 pA/pF, P = 0.3941). At both +80mV and -80mV, there was no significant difference between any combination of TRPM7 transfections containing either WT or CICUS variant TRPM7 vectors (one-way ANOVA Tukey's multiple comparison, P > 0.2066).

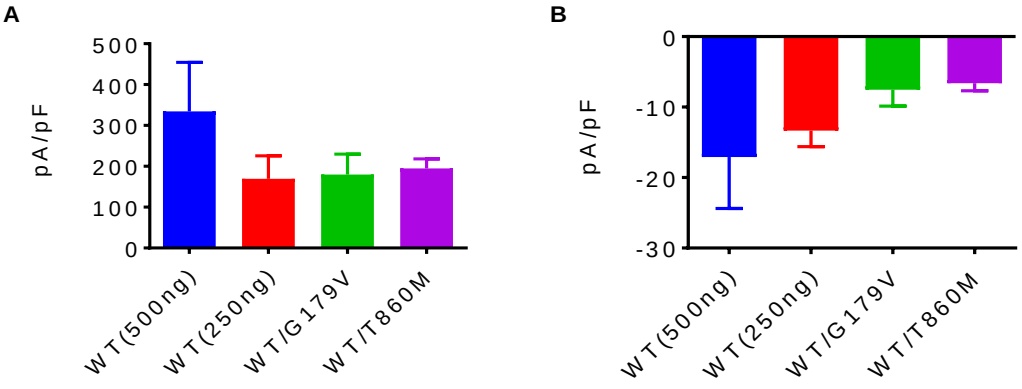


*Figure 3.20.* ***G179V and T860M TRPM7 variants do not influence wild-type TRPM7 current. A*** *TRPM7 ion channel current measured in HEK293 cells at +80mV following chelation of $Mg^{2+}$ removal.* ***B*** *Corresponding current density at -80mV from cells measured in A. n = 7-12.*

## 3.12 Investigation of Apoptosis following Transfection of TRPM7 and CICUS Variants

The TRPM7 ion channel has been shown to participate in Fas-induced apoptosis. We wanted to investigate whether any of the CICUS variants may affect this signalling pathway. To do this we transfected cells with TRPM7 wild-type and CICUS variants for 48 hours, before using light microscopy to count apoptotic cell bodies. Visualising apoptotic cells following TRPM7 transfection was carried out as described in Methods and Materials (2.8.4). Briefly, HEK293 cells were transfected with WT TRPM7 or CICUS variant expressing vector at ~70% confluency alongside 1800ng of tetracycline repressor plasmid. The following day 1µg/ml tetracycline was added to the media and cells fixed after 24 hours with 3.7% formaldehyde. Identification of apoptotic bodies (dark brown) was performed using light microscopy following staining of cells using an *In Situ* Apoptosis detection assay (Figure 3.21A). Pictures were taken from two separate experiments in 12-well dishes. Random images of each well were taken for analysis using an EVOS FL Auto Cell Imaging microscope.

In total 2,527 cells were counted, on average 13.9±1.46% were apoptotic across 9 groups. The average number of cells counted in each group was 361±42.96 cells. There was no significant difference between cells transfected with WT TRPM7 vector and any CICUS variant ($P > 0.99$), cells transfected but without TRPM7 ($P = 0.6$) or untransfected cells ($P = 0.17$, One-way ANOVA using Dunnett's multiple comparisons, all values compared to wild-type TRPM7 transfection). A detailed break-down of cell count, apoptotic cells and statistical significance vs wild-type transfected cells is listed in (Figure 3.21C).

A

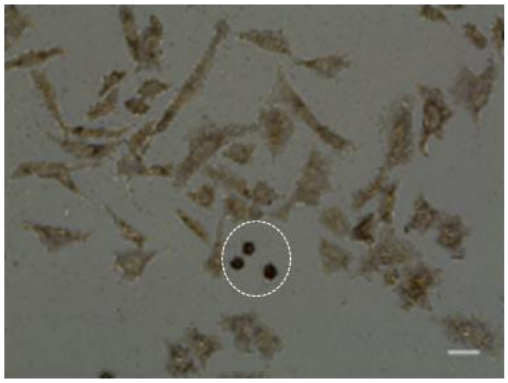

B

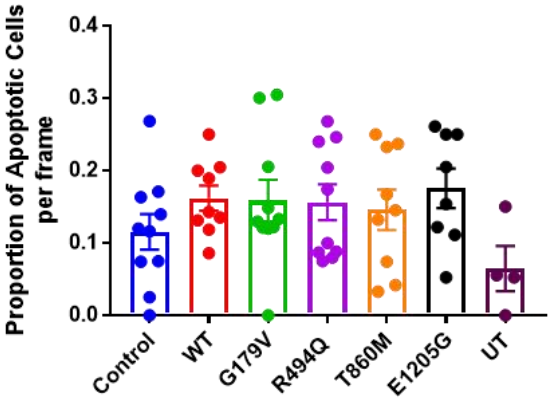


C

| Variant | Control | WT | G179V | R494Q | T860M | E1205G | UT |
|---|---|---|---|---|---|---|---|
| Cells Counted | 383 | 409 | 474 | 418 | 344 | 379 | 120 |
| n | 10 | 10 | 10 | 10 | 9 | 8 | 4 |
| Apoptotic cells (%) | 1.1 | 1.62 | 1.58 | 1.56 | 1.46 | 1.76 | 0.65 |
| P value vs WT | 0.62 | - | 0.99 | 0.99 | 0.99 | 0.99 | 0.16 |

*Figure 3.21.* ***CICUS variants do not influence apoptosis in transfected HEK293 cells. A*** *Representative image of 3 apoptotic cell bodies (white circle) identified following In Situ labelling of fragmented DNA. Live cells are depicted by light brown colour and flattened morphology.* ***B*** *CICUS variants do not alter the prevalence of apoptotic HEK293 cells following TRPM7 transfection. One-way ANOVA using Dunnett's multiple comparisons, from two separate transfections.* ***C*** *Summary of data presented in B. All images were taken at random by microscope software prior to analysis.*

## 3.12 Fluorescent Analysis of TRPM7 Transfected Cells

To confirm lack of expression in cells transfected with p.G179V and p.T860 TRPM7, we used immunocytochemistry to fluorescently label transfected cells. Initially we did this using an epifluorescent microscope to confirm we could successfully image TRPM7 *in vitro*. CHO-K1 cells were transfected with TRPM7 as previously mentioned in Methods and Materials. Briefly, cells were transfected in 6-well dishes at ~70-80% confluency with 250ng WT TRPM7 expressing plasmid alongside 1800ng tetracycline repressor. Four to six hours later cells were split using trypsin onto glass coverslips for imaging. The following morning TRPM7 transfection was induced by supplementing media with 1µg/ml tetracycline. 24 hours later cells were fixed with 3.7% formaldehyde. Cells were permeabilised with Triton-x 100 and either incubated with PBS-T and 1% BSA alone or with primary anti-TRPM7 antibody overnight. After removal of any remaining primary antibody all cells were stained with an Alexa-488 anti-mouse antibody for one hour.

CHO-K1 cells transfected with TRPM7 but not incubated with anti-TRPM7 antibody stained positive for DAPI but were negative for TRPM7 staining (Figure 3.22A-D). Conversely, cells positive for TRPM7 were found in transfected CHO-K1 cells after incubation with an anti-TRPM7 primary antibody (Figure 3.22E-L). Quantification of fluorescence was analysed from a cross-section of positively stained cells (Figure 3.23A). TRPM7 green fluorescent intensity was distributed throughout the cell, but was reduced in the area occupied by the nucleus.

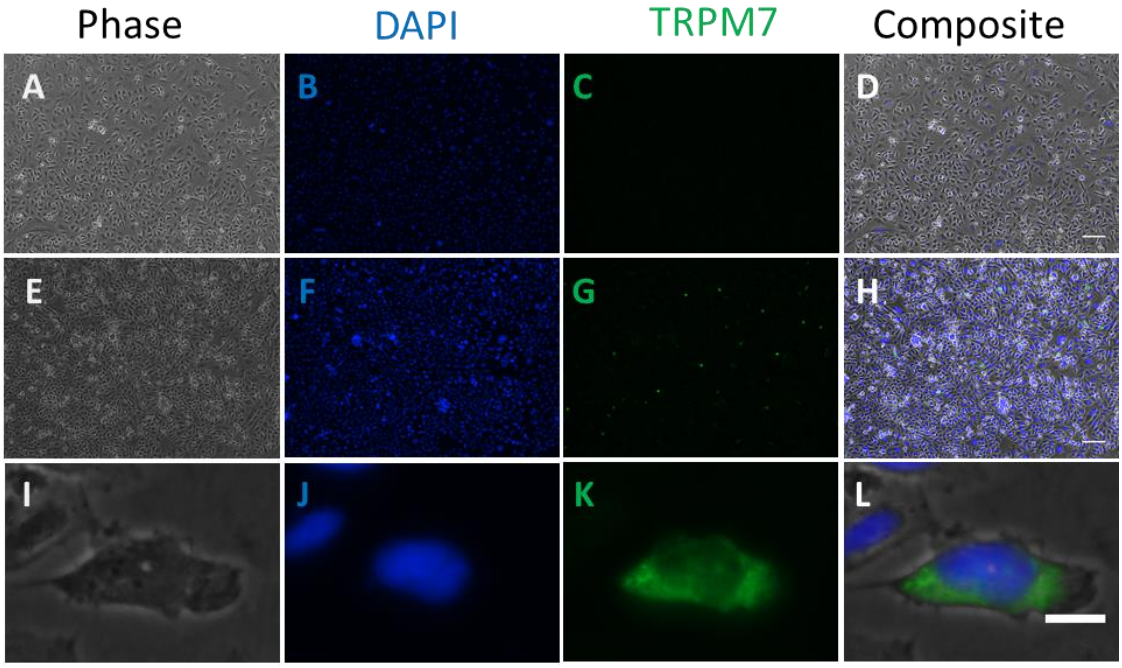


*Figure 3.22.* ***Immunocytochemical analysis of transfected CHO-K1 cells following TRPM7 transfection using sc271099. A – D*** *CHO-K1 cells transfected with TRPM7 but treated without primary antibody to TRPM-7 adhere to glass coverslips (A, phase), show nuclei positive for DAPI staining (B) and lack non-specific off-target secondary antibody signal (C).* ***E-H*** *Positive TRPM7 staining in cells following treatment with primary antibody showing positive cells throughout the glass coverslip.* ***I – L*** *Cropped image from H showing lack of nuclear localisation in TRPM7 +ve cell. Magnification A – H: x10, I – L x40. Scale bar D & H: 40µm, L: 5µm.*

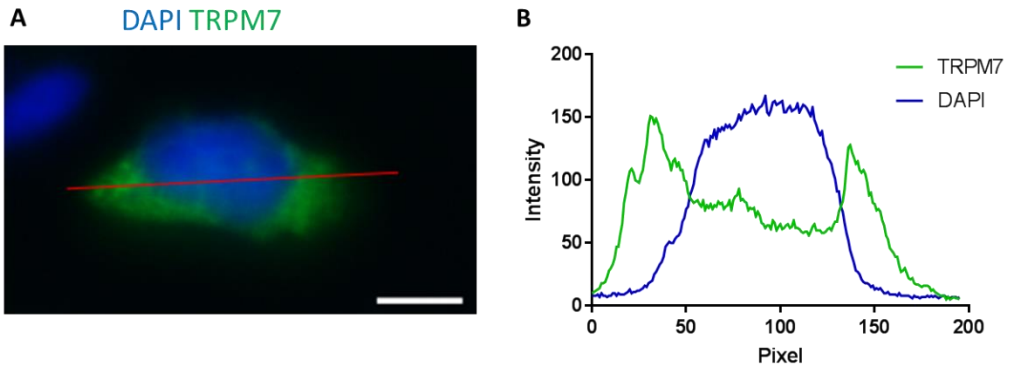


*Figure 3.23.* ***Distribution of TRM7 48hours after transfection in CHO-K1 cells using fluorescent microscopy. A*** *Fluorescent image of cell taken from Figure 3.22K & J. DAPI is stained in blue, green represents TRPM7 antibody. Red line indicates where pixel intensity measurements were taken. Scale bar: 5µm* ***B*** *Relative intensity of each pixel from panel A (red line) from left to right.*

## 3.13 Confocal Analysis of TRPM7 Transfected CHO-K1 Cells

After confirming successful fluorescent staining, we wanted to use confocal microscopy to analyse in more detail the cellular localisation of TRPM7, and any effect CICUS variants may have on it. Alongside this, we transfected cells with DsRed, a red fluorescent tag that localises to the endoplasmic reticulum. Co-transfection alongside TRPM7 will allow us to confirm transfection in experiments where we see a lack of expression, and to look at co-localisation between TRPM7 and the ER. CHO-K1 cells were transfected with TRPM7 as mentioned in Methods and Materials and section 3.12. Briefly, cells were grown to ~70% confluency before TRPM7 transfection before expression was induced the following day with 1µg/ml tetracycline for 24 hours. In addition to TRPM7 vector transfection, cells were also transfected with 250ng of a fluorescently tagged DsRed-endoplasmic reticular (DsRed-ER) targeting plasmid. After fixation with 3.7% formaldehyde cells were stained with 1:200 diluted anti-TRPM7 antibody overnight at 4˚C followed by treatment with secondary Alexa-488 anti-mouse antibody for one hour. Confocal image analysis was performed using a Zeiss 710 Confocal Laser Scanning Microscope. DAPI fluorescence was excited at 405nm, emission measured at 454nm. Alexa-488 excited at 488nm, emission measured at 528nm while DsRed fluorescence was excited at 543nm and emitted at 620nm.

Fluorescently tagged DsRed and TRPM7 staining was seen at x63 magnification outside of the nucleus (Figure 3.24). Quantification of this fluorescence in CHO-K1 cells showed cytoplasmic TRPM7 staining around the cell's nucleus (Figure 3.25). Cells transfected solely with DsRed showed strong intracellular fluorescent signal throughout CHO-K1 cell bodies, mostly distinct from DAPI emission (Figure 3.26).

In all slides transfected with DsRed-ER, there were multiple cells positive for red fluorescence distinct from the nucleus, indicating successful transfection (Figure 3.27 C, G, K & O). There were several cells in wells transfected with p.R494Q and p.E1205G that stained double positive for both TRPM7 and DsRed-ER (Figure 3.27 E-H & M-P). However in wells transfected

with p.G179V or p.T860M, only cells single positive for DsRed-ER were seen (Figure 3.27 A-D & I-L). When cells were transfected with WT TRPM7 and stained with secondary Alex Fluor 488 but without the primary mouse antibody to TRPM7, no cells were fluorescent after staining.

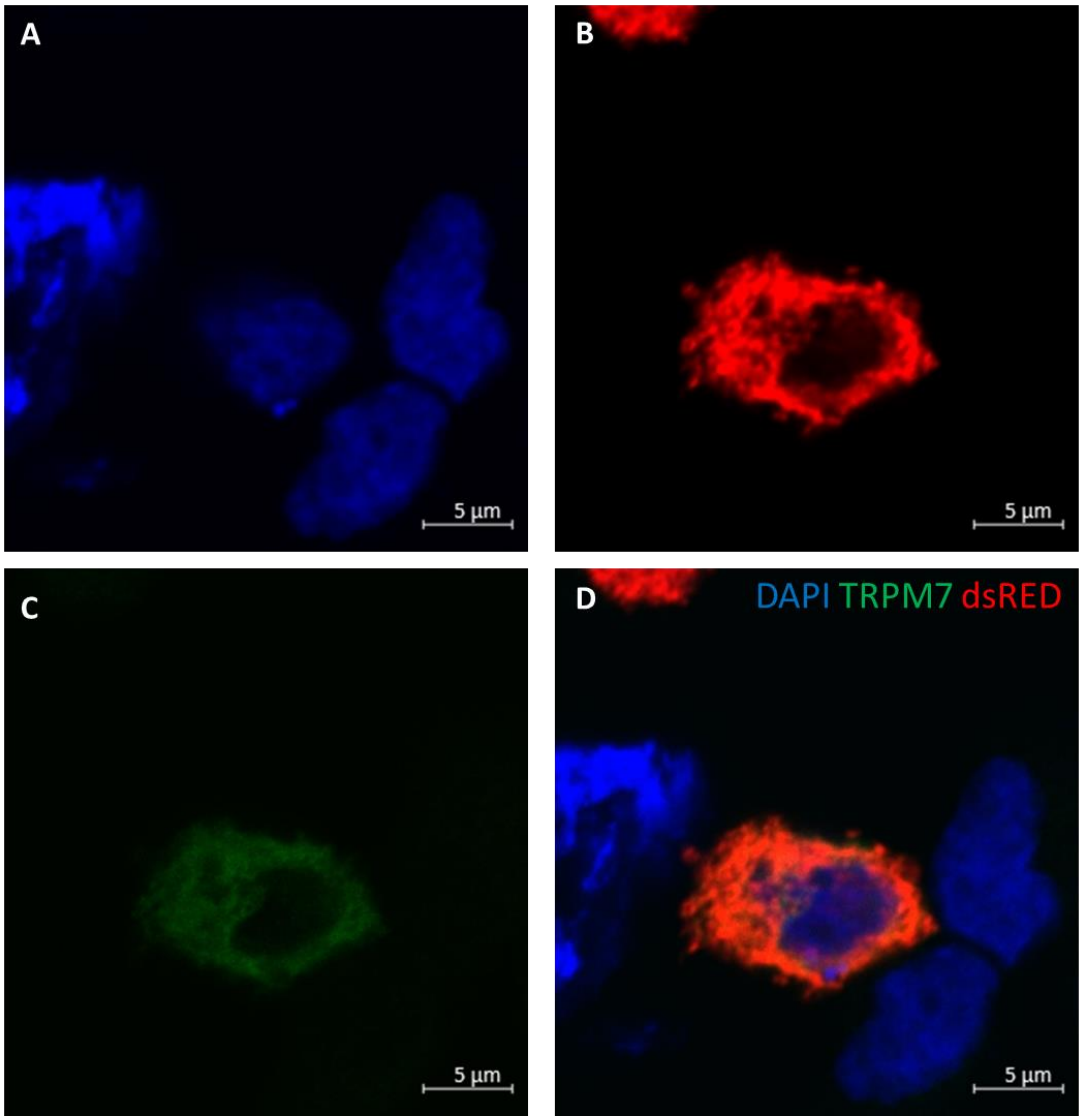


*Figure 3.24.* ***TRPM7 localises to the cell cytoplasm in transfected CHO-K1 cells. A*** *DAPI staining of CHO-K1 cell nuclei.* ***B*** *DsRed fluorescence is reduced in the nuclear area and occupies the ER of the cell.* ***C*** *TRPM7 resides in the cell cytoplasm but avoids the nucleus.* ***D*** *All fluorescent channels merged together.*

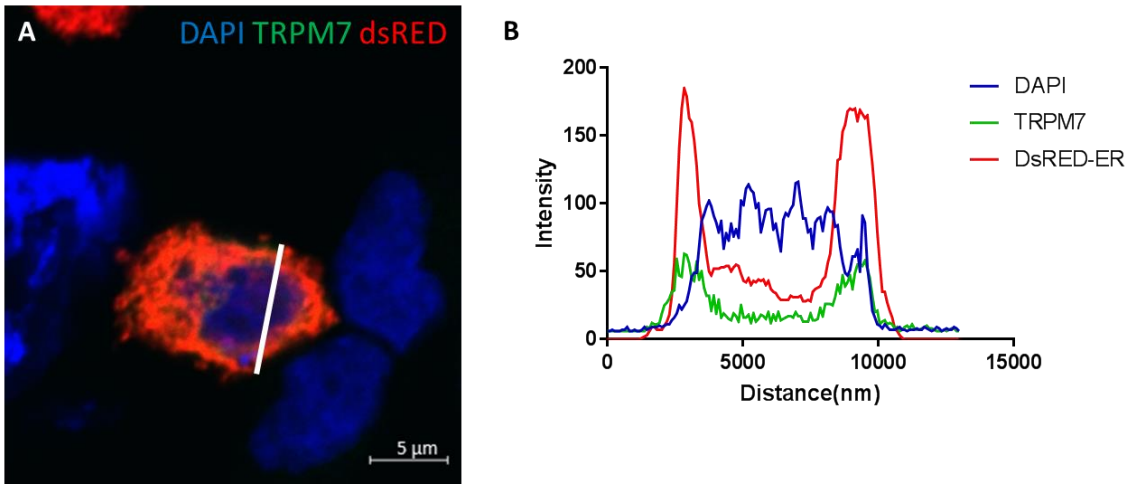


*Figure 3.25.* ***Fluorescent signal quantification of transfected CHO-K1 cell. A*** *Cell from Figure 3.24 where fluorescence was measured, indicating where measurements were taken (white line).* ***B*** *Quantification of fluorescence from cell in A.*

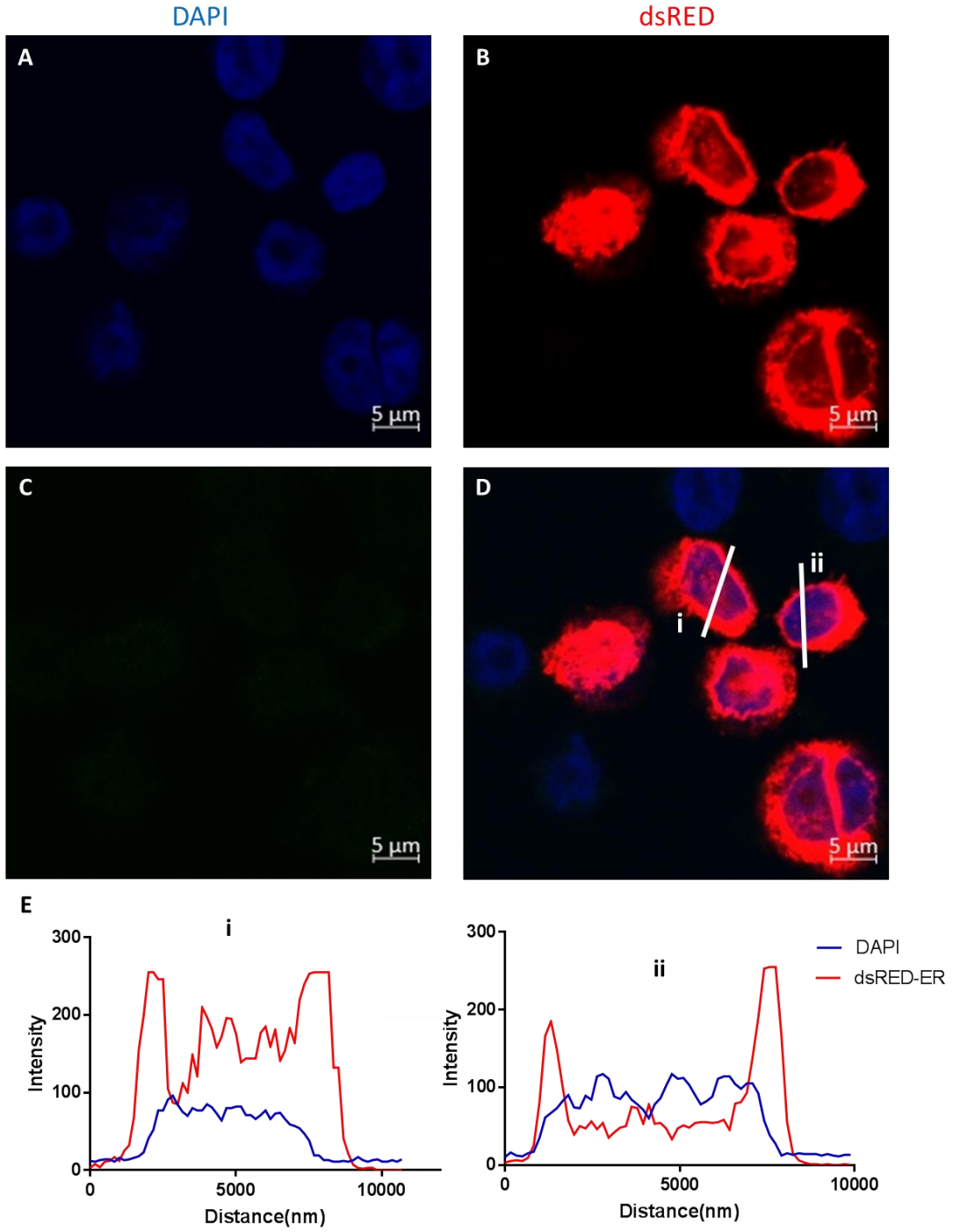


*Figure 3.26.* ***CHO-K1 cells transiently transfected with DsRed-ER. A*** *DAPI nuclear staining of CHO-K1 cells.* ***B*** *DsRed fluorescence observed in a transfected cluster of five cells.* ***C*** *Fluorescence measured at wavelengths used to excite Alexa-488, showing a lack of signal.* ***D*** *Overlay of three merged channels indicating successfully transfected CHO-K1 cells and three of which whose fluorescence was quantified.* ***E*** *Quantified fluorescent measurements of three cells from D.*

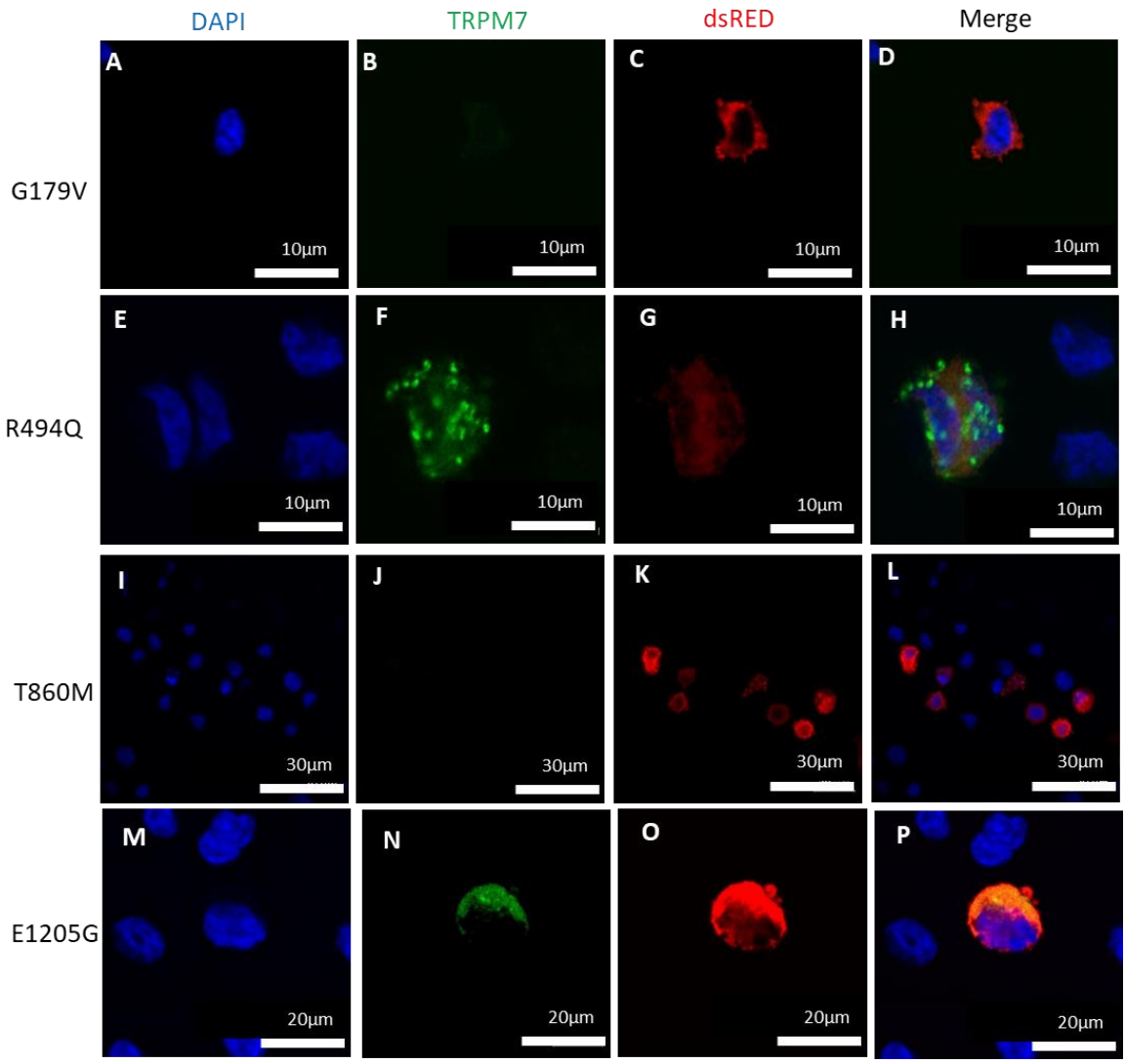


*Figure 3.27.* ***The two CICUS variants P.G179V and p.T860M produce no protein following transfection.*** *CHO-K1 cells transfected with 500ng p.G179V (**A-D**), p.R494Q (**E-H**), p.T860M (**I-L**) and p.E1205G (**M-P**) TRPM7 alongside 250ng DsRed-ER. DAPI cell staining A, E, I, M. Alexa Fluor 488 B, F, J, N. DsRed fluorescence C, G, J, O. Merged image of three channels D, H, L, P. Scale bars have length listed above them and range from 5 - 20 µm.*

## 3.14 Discussion

The role that predicted damaging genetic variants may play in perturbing the function of the TRPM7 ion channel was examined. Four nonsynonymous variants were sequenced from four unexplained stillbirth cases: p.G179V, p.R494Q, p.T860M, p.E1205G. Using heterologous cell systems, the effects of the variants on channel function, magnesium response, expression, cellular distribution and apoptosis were scrutinised.

Firstly, the WT *TRPM7* construct was sequenced to ascertain sequence homology to online published databases. We found a single synonymous nucleotide difference at c.C4986T, amino acid tyrosine 1662 in the C-terminal domain. A previously published *TRPM7* variant (p.T1482I) shown to alter magnesium sensitivity is located within the cytoplasmic domain, illustrating the role this region plays in controlling channel function [300]. However, this was unlikely to alter the TRPM7 channel activity, being outside of published ATP/metal binding domains and not altering protein sequence. This mutation is also over four hundred amino acids away from the nearest CICUS mutant so had no influence on possible mutagenesis reactions.

The four CICUS *TRPM7* variants sequenced in unexplained stillbirth cases represent a variety of structural changes. Two variants, p.G179V and p.R494Q lie within the N-terminal domain, whose structure and function is still currently unknown. The p.G179V variant would represent a large amino side chain size change. While the p.R494Q mutation substitutes a positively charged arginine for an uncharged glutamine – which may disturb protein-protein interactions. The p.T860M variant may be a small structural change, this takes place inside the second transmembrane domain which may be critical in controlling tetramer folding. Lastly, p.E1205G resides within the coiled-coil domain of TRPM7, while our data show this variant had no effect on TRPM7 function here, the loss of this charged amino acid in this dub-domain may have other deleterious effects.

The cell lines used in this study, HEK293 and CHO-K1, were chosen for numerous reasons. Due to the ubiquitous nature (in mammals) of the TRPM7 ion channel it was not

possible to find a cell line that lacks channel expression completely. HEK293 and CHO-K1 cells are extensively used throughout cell biology due to their rapid proliferation and the relative ease at which they can be transfected [274,275]. Alongside this there are numerous studies regarding successful characterisation of TRPM7 expression in HEK293 [230,301] and CHO-K1 [228,302] cells following transient transfection. Although TRPM7 is known to play a vital role in mouse cardiac development [213], the basic function of the channel in human cells is still widely debated. To test whether variants sequenced from unexplained stillbirth cases lead to perturbed channel function, heterologous cell lines were chosen to provide a relatively noise-free system to isolate TRPM7 channel expression and function.

Firstly CHO-K1 cells were transiently transfected with TRPM7 and current density at ±80mV measured. Current ramps were recorded between ±100mV and typical TRPM7 conductance observed in line with published literature [228,302]. Initial currents measured shortly after whole-cell membrane break-in were low across all voltages, however over time (~5minutes) large outward currents were measured in all transfected cells. This was likely due to chelation of intracellular magnesium by EDTA and EGTA inside the pipette solution. Current traces in CHO-K1 cells showed characteristically low inward current at -80mV, but large outward current when the ramp voltage increased past +50mV. Reintroducing high (10mM) $Mg^{2+}$ to the bath resulted in rapid inhibition of the observed current, reinforcing the likelihood of TRPM7 being responsible for the measured conductance. Furthermore, current density was significantly reduced by addition of micromolar concentrations of 2-APB, thought to inhibit conductance through cytoplasmic acidification [303]. Taken together these data indicates that using heterologous cells we can successfully transfect and measure WT TRPM7 in a cellular system. Being able to measure ion channel conductance equates to successful transfection, transcription of the TRPM7 cDNA, translation and trafficking to the cell surface. Due to its ubiquitous expression, even in untransfected CHO-K1 cells, outward current could be measured after allowing time for cytoplasmic magnesium to be chelated.

The four CICUS variants were successfully generated in the pcDNA4/TO vector using site-directed mutagenesis and this was confirmed using Sanger sequencing. The first two, p.G179V and p.R494Q reside in the N-terminal cytoplasmic domain. The third, p.T860M results in a mutation inside the second transmembrane domain. Lastly, p.E1205G is a nonsynonymous mutation in the C-terminal domain. These CICUS variant TRPM7 expressing constructs were transfected into CHO-K1 cells and current ran-up over time following whole-cell access. After current run-up CHO-K1 cells transfected with p.R494Q had significantly increased current densities at ±80mV compared to wild-type channels. Both inward and outward current densities were at least twice that of WT channels, indicating increased open probability of channels or abundance of ion channels at the cell surface. The current density of p.G179V was significantly reduced, with outward currents less than a third of WT values. Outward currents for p.T860M and p.E1205G were lower than WT but greater than untransfected cells. As a previous disease associated variant in TRPM7 was thought to alter magnesium sensitivity, it was important to measure how CICUS variants responded to varying concentrations of magnesium.

Whole-cell patch-clamp experiments have shown that although intracellular magnesium can be removed by chelation using EDTA/EGTA, application of 10mM external magnesium reverses this potentiation. CHO-K1 cells were transfected with WT TRPM7 and the four CICUS variants and the subsequent current density recorded after current run-up. The bath extracellular solution was then changed with 5 serial dilutions of magnesium (0.5, 1, 2, 4, 6mM) until full inhibition was reached. Interestingly, at low concentrations of magnesium (0.5mM for +80mV, 0.5 & 1mM for -80mV) transfecting CHO-K1 cells with p.R494Q TRPM7 increased current density compared to WT. Cytosolic free magnesium is thought to vary between 0.5 and 1mM, indicating that under physiological conditions p.R494Q would be functioning differently to WT TRPM7 in cells [304]. The resting membrane potential of a cardiomyocyte can be as low as -80 to -90mV, and therefore able to conduct inward current of divalent cations if TRPM7 is expressed in human cells. During time-course experiments, both p.G179V and p.T860M showed reduced outward conductance compared to cells expressing WT channel at 0mM $Mg^{2+}$. This indicates a

significant lack of functional TRPM7 at low concentrations of intracellular magnesium when p.G179V and p.T860M are present, similar to that observed later in transfected HEK293 cells.

When magnesium concentration was increased to 0.5mM this effect was abrogated, although p.G179V's response to increased magnesium at +80mV closely mimicked that of untransfected cells. Apart from p.R494Q expressing cells, no differences were observed between any CICUS TRPM7 variants and WT channels at -80mV. This was due to inward conductance being very low (<-10pA/pF), making it hard to identify differences between WT channels, loss of function CICUS variants and recording noise. When outward current data was normalised to maximum current before magnesium, there was no difference between any CICUS variants and WT TRPM7 channel. All groups showed ~50% inhibition of outward current at 0.5mM magnesium and total inhibition by 6mM.

Studies into how TRPM7 responds to various inhibitors, genetic modification and how it plays a role in cell biology are often carried out in multiple cell systems to eliminate possible cell type differences in expression, post translational modification and trafficking [223,232,234,305]. Therefore, HEK293 cells were used to confirm whether observed current density changes in CHO-K1 cells were replicated in another cellular system. Following transient transfection, TRPM7 current was detected in HEK293 cells. This current built up over 5-10minutes, as previously observed in CHO-K1 cells, with a similar voltage-current profile. Interestingly, larger currents at ±80mV were seen in HEK293, cells despite CHO-K1 cells being widely used in industry to produce large amounts of protein [275]. This may be due to HEK293 cell's ability to modify and transport native human protein to the cell surface in comparison to CHO-K1 cells response to transfection with a non-native protein.

Strikingly, in HEK293 cells transfected with p.R494Q there was no difference in current density compared to the WT ion channel. This contrasts with that observed in CHO-K1 cells where current density at +80mV was more than doubled. Conversely, both p.G179V and p.T860M significantly reduced outward current density compared to WT channels. Whereas in

CHO-K1 mean data this difference was not significant, perhaps due to lower WT current therefore reducing the difference seen in loss of function variants. In HEK293 cells p.G179V and p.T860M outward current was at least 100pA/pF below that observed in WT transfected cells indicating a marked difference in current. Once again at -80mV, there was little difference in the current between WT and any of the CICUS variants. As there was no significant difference in current density measured at -80mV between untransfected and WT transfected CHO-K1 cells, and no difference at -80mV between HEK293 cells expressing WT, p.G179V or p.T860M, there is likely small but significant endogenous currents present in both cellular systems that mask small changes in inward current. Larger inward currents were observed in CHO-K1 cells transfected with p.R494Q, this could be inhibited by millimolar concentrations of magnesium so is likely to be TRPM7 current. While p.E1205G did not alter TRPM7 currents at ±80mV, in CHO-K1 cells p.R494Q current significantly increased. In both HEK293 and CHO-K1 cells, p.G179V and p.T860M in low magnesium conditions showed stark reductions in current density at +80mV. To explore whether this was due to altered protein channel expression, western blotting was performed on cell lysates from transfected cells.

Due to their nature as multi-pass membrane proteins, commercially available TRP channel antibodies have caused frustration amongst the scientific field and have led to controversial research results being published [306,307]. It was therefore of little surprise that lysates from transfected CHO-K1 cells did not show any bands when probing for TRPM7, but showed calnexin staining around ~65kDa size in all lanes. Increasing the amount of DNA transfected into CHO-K1 cells also did not result in visible TRPM7 bands. Faint bands were observed at the 55kDa mark, corresponding to some observed cleaved C-terminal fragments previously reported [223]. No full length ion channel (~250kDa) was blotted in any CHO-K1 lysates despite observing ion channel current in transfected cells. We therefore decided to use HEK293 cells to measure TRPM7 protein expression as even in untransfected cells there will be human TRPM7 present, with more detectable WT in transfected cells. Despite using both DTT or β-mercaptoethanol as reducing agents, no visible TRPM7 band could be seen despite a strong

loading control signal even in HEK293 cells. Subsequent protein harvesting involving lower reduction temperatures and using both RIPA and NP40 lysis buffers gave no visible signal. An alternative polyclonal antibody (Alomone, Israel) was also unsuccessful in blotting full length TRPM7 protein. Interestingly, using a FLAG-epitope targeting monoclonal antibody resulted in seeing a small <40kDa fragment in western blot gels. This was likely a small cleavage product present in cells transfected with TRPM7, but is below the expected and published size of the full length channel (+200kDa) [223,305,308]. Although TRPM7 is predicted to be 213kDa in size, publications always show smeared signal and/or smaller cleavage products, indicating either autophosphorylation and/or C-terminal kinase cleavage when using antibodies specific for TRPM7 epitopes[223,308,309].

Using an alternative mouse monoclonal antibody (sc271099) targeting the area immediately after the final transmembrane domain, full length TRPM7 ion channel alongside cleaved downstream products could be seen in whole-cell lysates. This allowed analysis of protein expression in cells transfected with CICUS variant TRPM7.

HEK293 cells were transfected with CICUS variant TRPM7 and subsequent protein lysate harvesting. Western blot analysis of these lysates showed full length TRPM7 ion channel (>210kDa) present in large quantities in cells transfected with WT, p.R494Q and p.E1205G TRPM7. There was no discernible ion channel present in untransfected cells or cells transfected with p.G179V or p.T860M despite equal loading of protein between all wells. These data corroborated whole-cell patch-clamp data, indicating that cells transfected with p.G179V or p.T860M TRPM7 do not express full length functional ion channels or are degraded rapidly. This lack of expression could arise due to a lack of mRNA transcription in the nucleus or perturbed protein translation by the ribosome. Therefore it was important to analyse cells upstream of the TRPM7 protein and investigate the levels of TRPM7 mRNA in transfected cells.

To ascertain whether p.G179V and p.T860M TRPM7 variants were successfully expressing mRNA, HEK293 total cell RNA was isolated from transfected cells. To ensure genomic

DNA was not processed, a probe that spans exons 5-6 was used to ensure that elongation of PCR products would only occur across exons. During harvesting, any residual plasmid DNA was digested by treating samples with a DpnI restriction enzyme. This enzyme recognizes the DNA sequence Gm6ATC and cleaves it, this ensured only mRNA could be analysed by downstream qPCR. All TRPM7 measurements were normalised to an internal GAPDH control before being normalised to the WT transfected cells in that qPCR plate. Due to its ubiquitous nature, TRPM7 mRNA could be quantified by qPCR in untransfected HEK293 cells. Although present, this was significantly lower (at least >20x) than cells transfected with WT TRPM7. When comparing the four CICUS TRPM7 to WT transfected cells, there was no significant difference between any of the four variants and WT. These experiments were relatively variable, despite five repeats, probably due to the stochastic nature of cell transfection efficiency. However, all CICUS variants were of an equal order of magnitude to WT transfected cells and quite distinct from untransfected HEK293 TRPM7 levels. This suggested that the respective mRNA was present in cells transfected with p.G179V or p.T860M TRPM7. Interestingly this meant that TRPM7 mRNA for these variants was not being translated into protein or that protein levels were undetectable by western blot and whole-cell patch-clamp.

There is evidence that the variant p.Q141K in ABCG2 influences proteasomal degradation [310]. *TRPM4* variant p.E7K attenuates deSUMOylation of the channel, increasing its density at the cell surface and is associated with familial heart block [311]. Because of these previous reports implicating membrane proteins (especially TRPM4) with degradation and genetic variation, the effect of proteosomal blockage following transfection was investigated.

The proteasomal inhibitor MG132 has been extensively characterised in a number of systems to block the degradation of protein, as it acts by inhibiting the assembly of the 26S proteasome [310,312,313]. When cells were transfected with TRPM7 CICUS variants alongside overnight treatment with MG132, even in untransfected cells small C-terminal cleavage products were seen in western blots. These cleaved kinases are known to be present in all cells

at cell-type specific levels [223]. Proteosomal blockade overnight appeared to be sufficient to allow an accumulation of C-terminal fragments but insufficient to visualize significant amounts of full length protein in p.G179V cells. Interestingly, faint bands >210kDa were visible in cells transfected with p.T860M, indicating that the full length TRPM7 ion channel is present. This appears to suggest that the p.T860M nonsynonymous variant predisposes TRPM7 for proteolytic degradation by the 26S proteasome. Conversely, while all transfected cells received 500ng of TRPM7, there was a significant amount of full length TRPM7 in p.R494Q lysates compared to both WT and p.E1205G. Although protein expression experiments were carried out in HEK293 cells, this appears to support a potential gain-of-function phenotype consistent with increased current density observed in transfected CHO-K1 cells. A plausible hypothesis is that excess TRPM7 protein transcribed in HEK293 cells overloads transport to the plasma membrane. This would explain why no increase in current density was observed in HEK293 cells despite there being a large increase in abundant protein following MG132 treatment compared to wild-type.

In cells transfected with p.G179V no bands were present above the 100kDa fragments as also seen in the untransfected lane. All CICUS TRPM7 variants were heterozygotes, therefore whether loss-of-function variants p.G179V and p.T860M can influence co-expressed WT TRPM7 was worthy of exploration. Dominant negative effects are well documented in ion channelopathies, whereby wild-type channel is adversely affected by the presence of the loss-of-function allele [189]. This is thought to be a key mechanism in the pathophysiology of certain LQT1 and LQT2 variants that are symptomatic despite the presence of one fully functioning copy of the gene [190,262]. Due to their multimeric nature, a single point mutation in one allele can adversely affect the formation of purely wild-type ion channel multimers. Other dominant negative mechanisms can include competition for accessory proteins at the cell membrane, rapid degradation when forming complexes with wild-type channel and retention in the endoplasmic reticulum [192,314]. Cells were transfected with 500 or 250ng TRPM7 plasmid or 250ng TRPM7 plasmid and either p.G179V or p.T860M. There was a discernible difference in current density in cells that received 500ng or TRPM7 over the other groups at ±80mV but this was not

significant. There was no difference in current density in cells transfected with 250ng WT TRPM7 alone or those with WT and either CICUS variant – indicating that these two loss-of-function variants did not appear to influence the expression, translation or trafficking of WT TRPM7.

TRPM7 has been shown to regulate a variety of cellular functions, notably apoptosis [235]. This TRPM7-mediated process is thought to be independent of the C-terminal kinase and therefore of interest due to the fact that all four CICUS variants lie upstream of this domain. We decided to investigate whether there was a discernible difference in the prevalence of apoptotic cells following transfection of wild-type TRPM7 or those harbouring CICUS variants. While there was an increase in apoptotic cells that underwent transfection (even without TRPM7 vector), it appeared that no CICUS variants had an effect on the prevalence of apoptosis in cultured HEK293 cells.

Recent studies have highlighted the importance of TRPM7's subcellular location in distinct vesicles that may contain the majority of TRPM7 protein [305]. It was therefore important to analyse any possible consequence that CICUS TRPM7 variants may have on the localisation of the ion channel in cells. Immunocytochemistry analysis of Alexa Fluor 488 positive, transfected cells indicated disperse localisation throughout the cytoplasm (Figure 3.22). Following on from this, transfected CHO-K1 cells were analysed with confocal microscopy to more closely examine the distribution of TRPM7. For these confocal experiments, DsRed-ER, a fluorescently tagged construct that is trafficked into the endoplasmic reticulum was co-transfected alongside TRPM7. Firstly, this allows confirmation of successfully transfected cells without any antibody treatment, and is a useful means to compare the location of transfected TRPM7. Analysis of transfected CHO-K1 cells with TRPM7 and DsRed-ER showed a similar pattern of cell distribution, surrounding the cell's nucleus. Quantification of the DAPI, DsRed-ER and Alexa 488 signals showed TRPM7 to be distinct from the nucleus and strongest at the edge of the cell, but not distinctly membrane bound. This was in agreement to other published data, either highlighting TRPM7's role outside of the cell membrane or showing distinct retention inside the ER. Analysis

of multiple DsRed-ER positive cells confirmed a lack of nuclear staining and distinct cytoplasmic distribution. This all provided a methodology to confirm successful transfection of cells and analyse the location of TRPM7 staining in CHO-K1 cells.

Unsurprisingly, in cells transfected with p.G179V or p.T860M TRPM7, a strong TRPM7 positive signal was lacking. There was however a number of DsRed-ER positive cells, indicating that transfection of dsDNA was occurring in these cells. Double positive cells were found in wells transfected with both p.R494Q and p.E1205G. Notably, in some cells transfected with p. clearly visible clusters of protein appeared, indicating possible aggregates or large vesicles. The previously published data on TRPM7 by Clapham et al. used super-resolution microscopy to identify minute (<400nm) TRPM7 vesicles. At this resolving power it is not clear whether these are aggregated vesicles or simply clusters of channel at the membrane, but it does confirm that p.R494Q transfection results in significant amounts of TRPM7 protein created in CHO-K1 cells.

Taken together with the patch-clamp data, two TRPM7 CICUS variants p.G179V and p.T860M adversely affect the creation of TRPM7 despite successful transfection into HEK293 and CHO-K1 cell systems. This results in a lack of TRPM7 current measured at the cell surface, but does not appear to affect cell apoptosis. Interestingly, HEK293 cells transfected with p.T860M TRPM7 incubated overnight with the proteosomal inhibitor MG132 appeared to result in a small amount of full length TRPM7 protein, indicating that this variant may predispose the protein to rapid degradation by the 26S proteasome. The p.R494Q variant significantly increased current density recordings in CHO-K1 cells and confocal microscopy analysis showed strong vesicular-like aggregates. However, TRPM7 current did not increase when transfected into HEK293 cells, implicating possible cell-type specific effects.

| Variant | G179V | R494Q | T860M | E1205G |
|---|---|---|---|---|
| Current Density | Reduced | Increased (In CHO-K1) | Reduced | - |
| mRNA | - | - | - | - |
| Protein | Reduced | Increased | Reduced | - |
| Apoptosis | - | - | - | - |

*Table 3.1.* ***Summary of functional differences found between CICUS TRPM7 variants compared to wild-type.*** *"–" indicates difference to wild-type*

# 4 Results – Investigating the Functional Effect of CICUS AKAP9 Variants

## 4.1 Sequencing the AKAP9 Expression Vector

Due to its large size (>9kbp) and lack of availability, a custom *AKAP9* expression vector was synthesised commercially for our group (by Genscript Biotech, USA). Following receipt of the vector, it underwent Sanger sequencing of both reverse and forward strands using 16 pairs of sequencing primers (Table 2.1). Following amalgamation of 17 pairs of forward and reverse reads, the sequence was aligned alongside the reference sequence (NM_005751). Sequence homology was 100% identical to the online reference sequence. Including the N-terminal FLAG tag epitope, homology between the *AKAP9* plasmid and NM_005751 was 11720/11724 (0.99966).

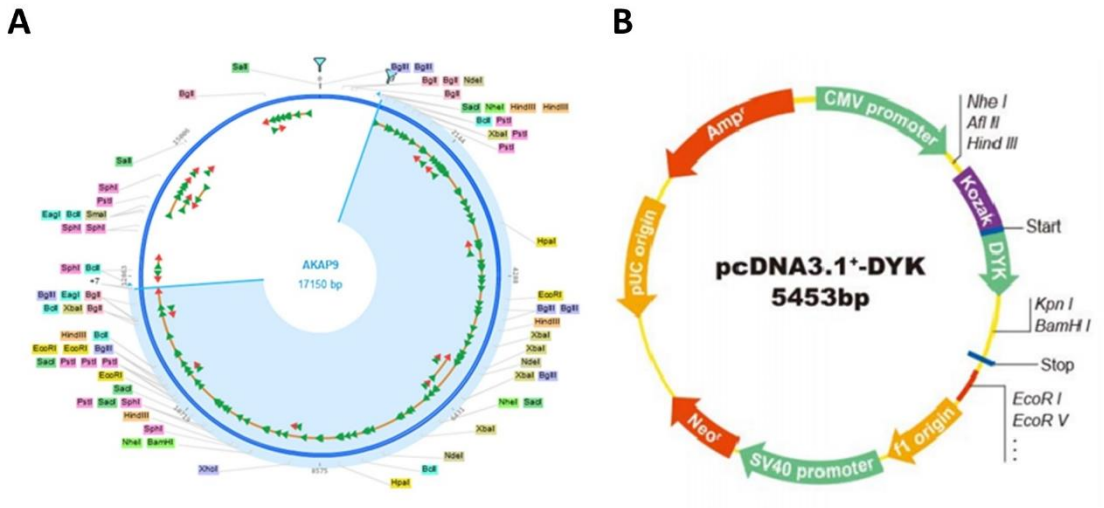


*Figure 4.1.* ***AKAP9 gene in the pcDNA3.1 expression vector. A*** *Shows the sequenced AKAP9 gene (11724bp) inserted into the FLAG-tagged expression vector pcDNA3.1(+) containing a neomycin resistance cassette (795bp). The AKAP9 mRNA is highlighted in blue, green arrows depict the putative reading frames.* ***B*** *Shows the vector map of the pcDNA3.1 plasmid without an insert, highlighting neomycin resistance, DYK tag and ampicillin resistance.*

## 4.2 AKAP9 CICUS Mutagenesis

To test whether CICUS variants had an effect on the function of AKAP9, *in vitro* mutagenesis was carried out using the Qiagen XL Site-Directed Mutagenesis Kit. Mutagenesis primers were synthesised (Table 2.3) and incubated with the wild-type *AKAP9* plasmid and mutagenesis reagents as per kit instructions before PCR cycling (outlined in 2.3.4). After digesting non-mutated parental DNA with the *Dpn* I restriction enzyme, mutated dsDNA was transformed into XL10-Gold ultracompetent cells and grown on carbenicillin-containing agar plates overnight. After several attempts at mutagenesis and transformation, only cells incubated with p.D1507H and p.A3043T DNA grew colonies that could be prepared for Qiagen Midi plasmid kit growth.

## 4.3 Measuring IKs Current in a HEK293 Cell Line Stably KCNQ1/KCNE1

To establish whether *AKAP9* variants found in CICUS cases had an affect on the coupling of IKs to β-adrenergic drive, a suitable model system had to be created to measure potassium channel currents and then analyse their response to PKA activation. The first studies on IKs current and adrenergic stimulation were conducted on CHO-K1 cells either untransfected or transfected with the small AKAP9 isoform Yotiao [131,243].

We selected a HEK293 cell line to model the IKs current and its response to adrenergic stimulation, as it is widely used as an *in vitro* model of KCNQ1/KCNE1 by our group. These cells (known as s5.3 cells) stably express both KCNQ1-GFP and KCNE1, providing an ideal platform to analyse changes in IKs current. These cells were cultured in media containing both G418 and zeocin, which allowed for selection of only double-positive cells. Cells were subjected to whole-cell patch-clamp, using a voltage protocol that measured current between -80mV and +80mV in 10mV increments. After each voltage ramp of two seconds, voltage was reduced to -40mV for two seconds before reverting to the holding potential of -80mV (Figure 4.2A).

Characteristic IKs recordings were observed in all cells analysed, with slowly activating peak currents and signature deactivating tail current morphology of KCNQ1/KCNE1 (Figure 4.2C-D) [111]. This stable cell line showed consistent IKs recordings when using the whole-cell patch-clamp methodology and thus would be a suitable system for studying the response to adrenergic stimulation.

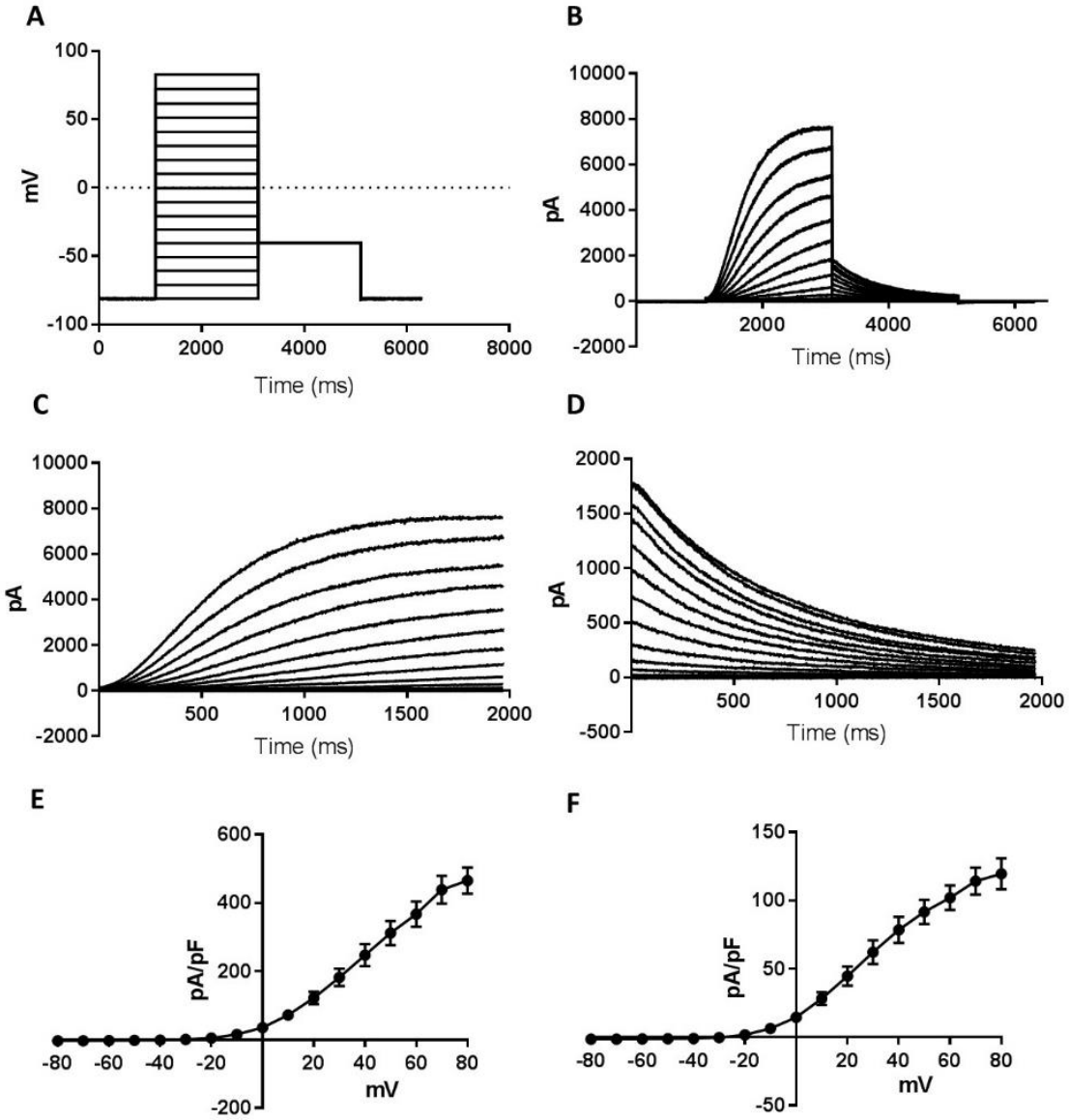


*Figure 4.2.* ***Voltage protocol and recorded currents from a HEK293 cell line stably expressing KCNQ1-GFP and KCNE1.*** ***A*** *Voltage-clamp protocol used to measure IKs current from cells. All currents were measured after 2minutes of dialysis.* ***B*** *Representative current recording from HEK293 cells showing characteristic slow sloping activation and expected slow deactivation.* ***C*** *Close-up of trace showing characteristic slow activation over 2s.* ***D*** *Slowly deactivating 'tail' current typical of IKs current.* ***E*** *Mean current recorded at peak activation.* ***F*** *Mean peak tail current before deactivation. n = 8 cells.*

## 4.4 Identifying a Native Adrenergic Response in HEK293 Cell

In contrast to HEK293 cells, published data from CHO-K1 cells transiently expressing KCNQ1/KCNE1 show lack of any robust response to raised cellular cAMP [131,243]. To investigate how IKs current in HEK293 is affected during β-adrenergic stimulation we used a short voltage protocol of one step at +30mV, which repeated every 10 seconds during continuous patch-clamp recording. HEK293 cells were seeded onto coverslips before patch-clamp analysis 48-72 hours later, only fluorescent cells were chosen.

Due to the prolonged nature of these experiments (>10 minutes), the perforated patch-clamp technique was used to measure IKs current during β-adrenergic stimulation. Briefly, intracellular solution was mixed with amphotericin-B before insertion into the glass pipette. When electrical sealing occurred between the cell plasma membrane and pipette, the seal was left for ~15-30minutes to allow electrical access to develop through membrane pores. Access resistance was allowed to stabilise before recording occurred, the five current sweeps preceding isoprenaline treatment were analysed as the baseline. Isoprenaline was added after current was stable for ~5 minutes and final current was measured as an average of five sweeps after current plateau.

Surprisingly, Iks in HEK293 cells was exquisitely sensitive to even 1nM of isoprenaline treatment (Figure 4.3). IKs current rapidly increased following isoprenaline treatment, at concentrations ranging from 1nM-100nM, at 1μM current density plateaued and then returned to baseline after extracellular solution (EC) wash-off (Figure 4.3B). Current-voltage relationships from subsequent cells showed a large increase in current density following 100nm isoprenaline treatment (Figure 4.3C-D). Whole-cell patch-clamp analysis of current density at peak and tail currents showed a significant increase in current compared to untreated cells above +20mV and +30mV respectively (Figure 4.3E-F). At +80mV, peak current density was increased by 335.6pA/pF ($P<0.001$, two-way ANOVA, Sidak's multiple comparison). Peak tail current at

+80mV was significantly increased by 214.8pA/pF ($P<0.001$, two-way ANOVA, Sidak's multiple comparison).

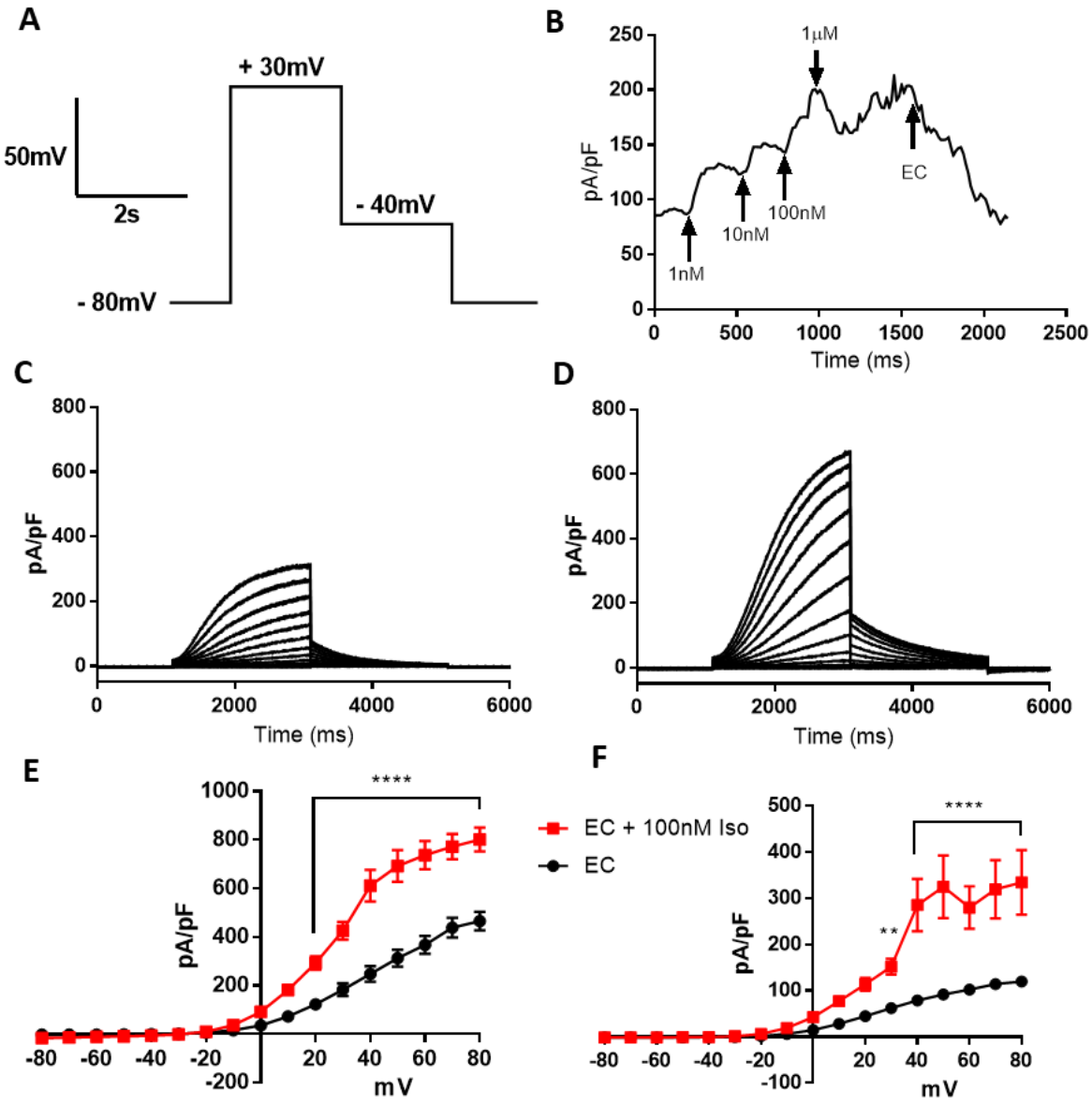


*Figure 4.3.* ***Iks in HEK293 cells responds to treatment with isoprenaline. A*** *Voltage step protocol used to measure IKs current in the perforated patch-clamp configuration.* ***B*** *Measuring IKs current in HEK293 cells stably expressing KCNQ1 and KCNE1 following addition of increasing concentrations of isoprenaline to the extracellular solution.* ***C*** *Current-voltage profile before addition of 100nM isoprenaline.* ***D*** *Current density after addition of 100nM isoprenaline for 5 minutes.* ***E-F*** *Whole-cell current density at peak (E) and tail (F) following two minutes of dialysis with (red) or without (black) pre-treatment with 100nM isoprenaline. Two-way ANOVA with Sidak's multiple comparison, n = 6-8, ** - P<0.01, **** - P<0.0001. EC – Extracellular solution. Iso – Isoprenaline.*

## 4.5 Perforated Patch-clamp Analysis of HEK293 Adrenergic Response Using Forskolin

To validate that this was a robust response to adrenergic stimulation, we substituted isoprenaline with an adenylate cyclase activator, forskolin [315]. Perforated patch-clamp recordings were carried out on HEK293 cells stably expressing KCNQ1-GFP/KCNE1. After cytoplasmic electrical access was stabilised, a current-voltage step protocol was repeated every minute, measuring current between -80mV and +80mV in 20mV steps (Figure 4.4A). As seen during isoprenaline treatment, 10μM forskolin, when added to extracellular solution transiently increased IKs current (Figure 4.4B). Alongside large increases in peak and tail current density, peak current activation was visibly steeper following forskolin treatment (Figure 4.4C-F). Mean current density at +40mV in 7 cells showed stable IKs current recordings indicative of the perforated patch-clamp technique. Following forskolin treatment currents rapidly increased to plateau after ~5minutes of exposure (Figure 4.4G).

Further detailed analysis of the KCNQ1/KCNE1 current-voltage profiles showed that following 10μM forskolin treatment, peak current density at +40mV was almost equal (93%) to peak current density at +80mV before β-adrenergic stimulation (Figure 4.5A). There was a significant difference in normalised current at +40, +60 and +80mV after forskolin treatment (two-way ANOVA, Sidaks Multiple comparison, P=0.001, P<0.0001, P<0.0001 respectively). Significant forskolin-dependent increases in peak tail current were also observed at +40, +60 and +80mV (two-way ANOVA, Sidaks Multiple comparison, P=0.01, P<0.01, P<0.01 respectively, Figure 4.5B).

Averaged deactivation voltages were fitted with a Boltzmann equation before and after treatment with forskolin (Figure 4.5C). Before treatment, $V_{50}$ was +29.22 ± 4 .968 mV compared to 16.75 ± 2.242mV after forskolin. Analysis of steady-state inactivation with two-way ANOVA reveals significant divergence of relative peak tail currents at 0, +20, +40mV during deactivation (two-way ANOVA, Sidaks Multiple comparison, P=0.01, P<0.01, P<0.01 respectively). There was

no statistical difference in deactivation time constants observed before or after forskolin treatment (Figure 4.5D). Time to half activation however, was significantly reduced by forskolin treatment at voltage steps higher than -40mV (two-way ANOVA, Sidaks Multiple comparison, $P<0.0001$, Figure 4.5E). Forskolin was used for all further β-adrenergic experiments. These data show the effect adrenergic stimulation has on IKs current, however this model system is unsuitable to investigate how specific *AKAP9* genetic variants influence this coupling due to the unknown endogenous elements clearly already present in HEK293 cells.

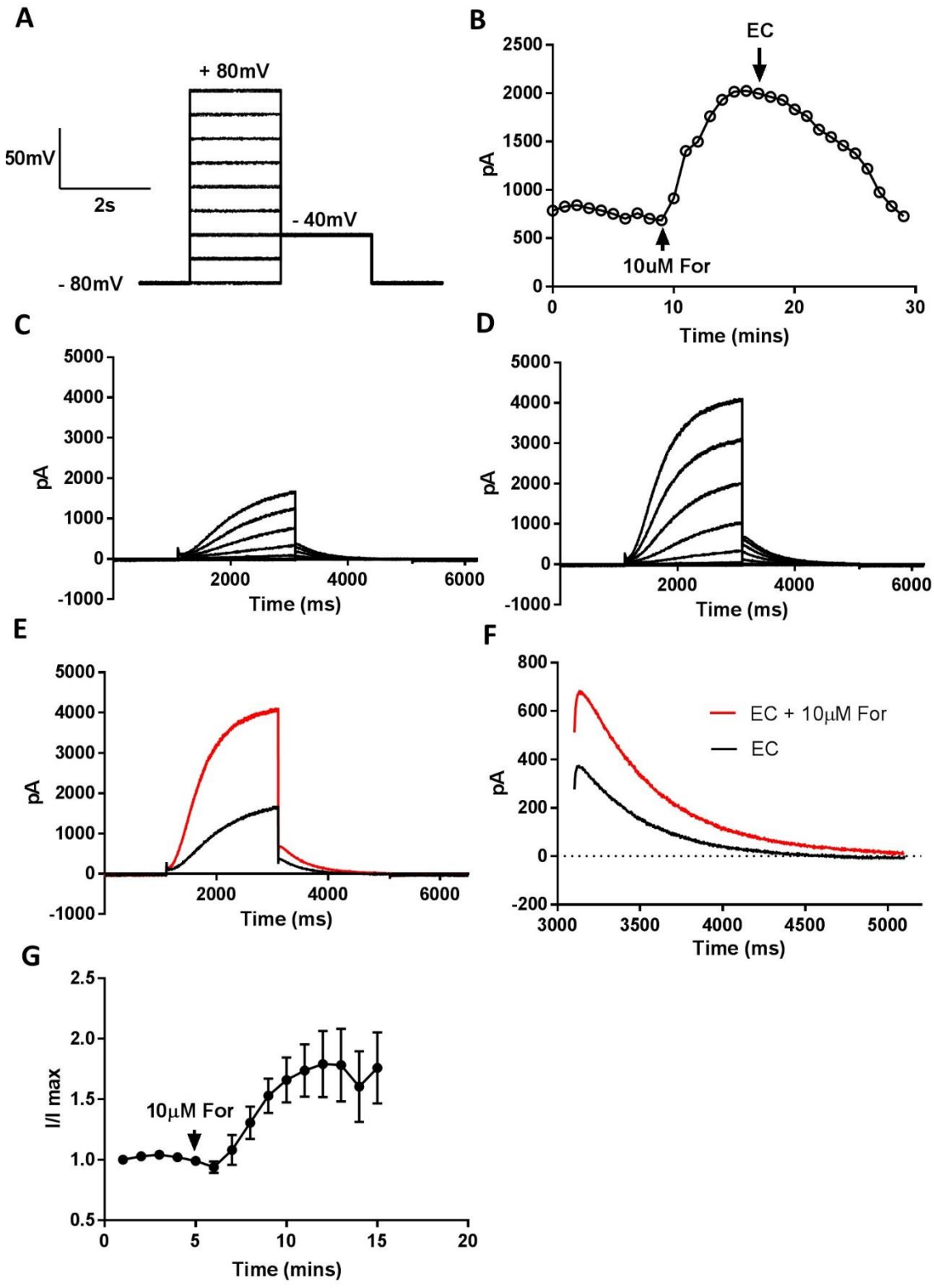


*Figure 4.4.* ***IKs current in HEK293 cells responds robustly to 10μM Forskolin treatment in perforated patch-clamp. A*** *One minute voltage protocol of nine 6.5 second sweeps continuously repeated during IKs recordings.* ***B*** *Representative current timecourse depicting time of forskolin treatment and subsequent washout.* ***C-D*** *Current-voltage profile before (C) and after (D) treatment of 10μM forskolin in HEK293 cells.* ***E*** *Representative trace of current recordings before (black) and after (red) treatment of 10μM forskolin at +40mV.* ***F*** *Enlarged tail current from (E) showing slow deactivation at -40mV after a +80mV step.* ***G*** *Mean time-course data from 7 cells showing peak current recorded at +40mV every minute for five minutes before treatment with forskolin and the effect of forskolin perfusion into the EC solution. Data are represented as current normalised to initial current level at t=1min. EC – Extracellular solution, For = Forskolin.*

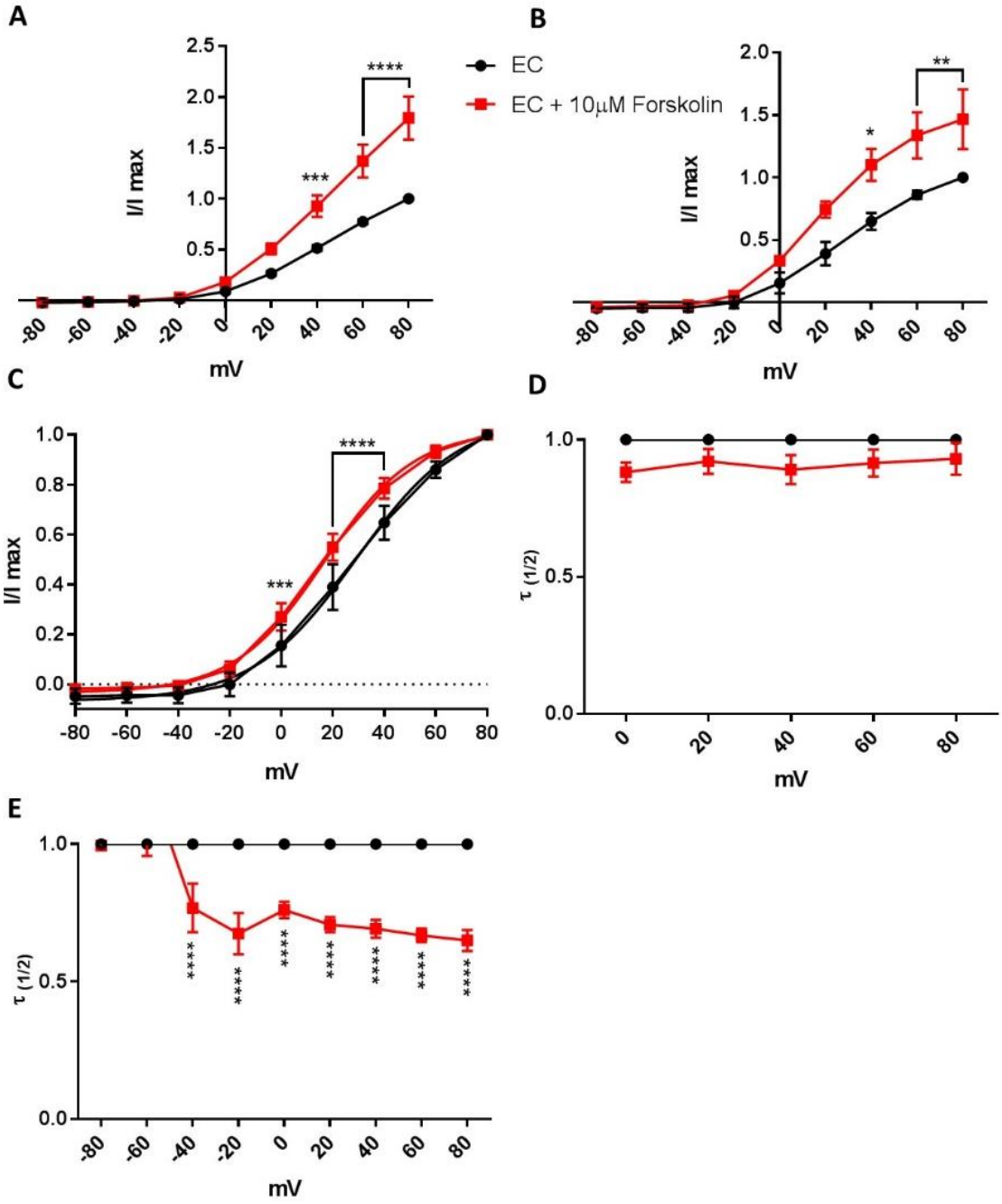


*Figure 4.5.* ***Analysis of IKs biophysics before and after treatment with forskolin. A-B*** *Normalised peak (A) and tail (B) current before (black) and after (red) forskolin treatment. Current normalised to average current before forskolin addition.* ***C*** *Boltzmann curve fitted to tail currents before (black) and after (red) forskolin treatment. Data are normalised to maximum average current before (black) and after (black) forskolin. Before forksolin: $V_{1/2}$ = 29.22mV slope = 20.1, after forskolin $V_{1/2}$ = 16.75mV slope = 17.49.* ***D-E*** *Deactivation (D) and activation (E) constants normalised to before (black) and after (red) forskolin treatment. Two-way ANOVA with Sidak's multiple comparison test **** - P<0.0001. EC – Extracellular solution.*

## 4.6 Analysing Adrenergic Response in KCNQ1/KCNE1 Transfected CHO-K1 Cells

Due to its previously unknown ability to couple adrenergic stimulation to increased KCNQ1\KCNE1 potassium current, we were unable to use our well characterised HEK293 cell line stably expressing KCNQ1-GFP/KCNE1. We therefore transiently transfected the CHO-K1 cell line (previously published to not respond to cAMP [131]) with KCNQ1-GFP/KCNE1 and used the perforated patch-clamp technique to record IKs current following addition of forskolin to the extracellular solution.

Transfected cells were initially incubated on glass-bottomed culture dishes for live confocal image analysis (Figure 4.6A). Protein was evenly distributed throughout the cytoplasm, in particular on the basal surface of the plasma membrane, there was a distinct lack of fluorescence in the centre of the cell – characteristics of a membrane associated protein. CHO-K1 cells were successfully transfected with KCNQ1-GFP/KCNE1, all but one GFP+ cell showed characteristic IKs current traces following establishment of electrical cytosol access (Data not shown). Using the perforated patch-clamp technique, stable currents were recorded with typical activation peaks and slowly deactivating tail currents (Figure 4.6B-C).

During perforated patch-clamp recordings, activation of PKA using forskolin did little to alter IKs current recorded, even after 5+ minutes of treatment (Figure 4.7A). This was in agreement to previous work by Kass et al. who used a cAMP analog (CPT-cAMP) to directly stimulate PKA [131]. Both tail and peak currents in cells changed little over the course of forskolin treatment in CHO-K1 cells expressing KCNQ1-GFP/KCNE1 (Figure 4.7E-F).

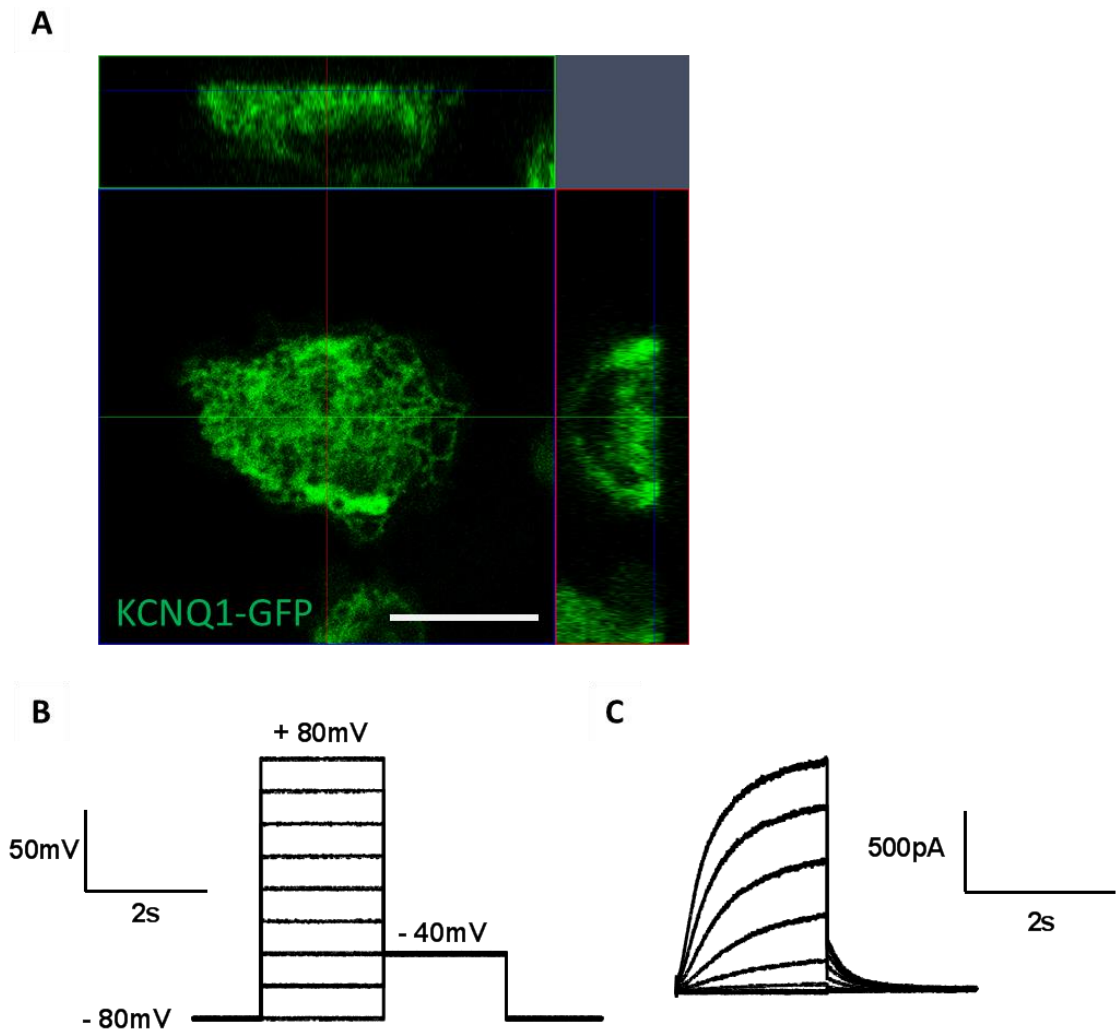


*Figure 4.6.* ***CHO-K1 cells transiently transfected with KCNQ1-GFP/KCNE1 display IKs current. A*** *Transiently transfected CHO-K1 cell live imaging of KCNQ1-GFP. Image is a composite of Z-stacked confocal images showing top-down view (main panel) and views from either angle (side panels). Cells were transfected into glass bottomed culture dishes before live confocal imaging on an LSM710 microscope. Scale bar is 5µm.* ***B*** *One minute voltage protocol of nine 6.5 second steps continuously repeated during CHO-K1 IKs recordings.* ***C*** *Representative current recording after membrane perforation showing typical slow activation followed by slowly deactivating tail current.*

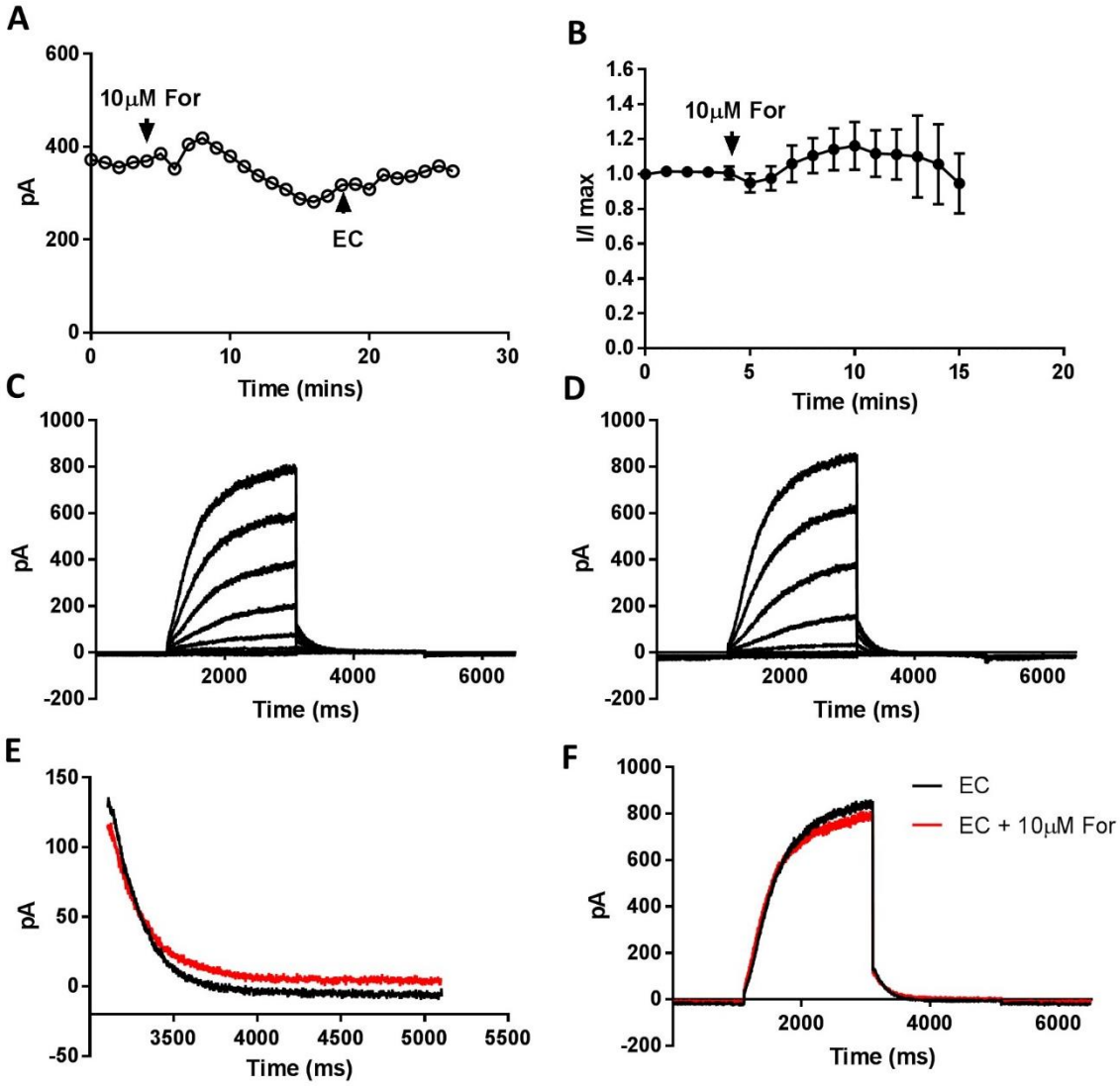


*Figure 4.7.* ***IKs in CHO-K1 cells does not respond to β-adrenergic stimulation. A*** *Representative trace of perforated patch-clamp recording of IKs in CHO-K1 cells during the application of 10μM forskolin after five minutes of stable current recording.* ***B*** *Mean timecourse data from 8 cells following forskolin treatment after five minutes of current recordings. These data are from peak recordings at +40mV.* ***C-D*** *Representative current-voltage relationship before (C) and after (D) 10μM forskolin.* ***E-F*** *Superimposed image of representative tail (E) and peak (F) current before (black) and after (red) forskolin treatment at the +80mV step. EC – Extracellular solution, For – Forskolin.*

## 4.7 Response to β-adrenergic Stimulation in CHO-K1 Cells Transfected with *AKAP9* or *Yotiao*

CHO-K1 cells were transiently transfected with 250ng *KCNQ1-GFP*, *KCNE1* and 500ng *AKAP9*. After 4-6 hours cells were split onto coverslips and incubated for at least 24 hours before perforated patch-clamp analysis of the resulting IKs current. In contrast to cells expressing purely KCNQ1-GFP/KCNE1, cells co-expressing AKAP9 responded to adrenergic stimulation with forskolin (Figure 4.8A). We also found that a cell transiently transfected with KCNQ1-GFP/KCNE1 and 500ng of a *Yotiao* expressing plasmid also responded to forskolin stimulation (Figure 4.8B).

Mean time course data of 12 cells showed a robust response to 10μM forskolin, with peak current at +40mV 2.05 ± 0.59 fold compared to initial current 15 minutes after forskolin treatment (Figure 4.8C). In contrast to forskolin treatment in HEK293 cells, while raw current increases were visible there was little change in the apparent shape of I-V relationships (Figure 4.8D-E). This confirmed that accessory proteins were required to couple IKs current expressed transiently in CHO-K1 cells with PKA activation via forskolin treatment.

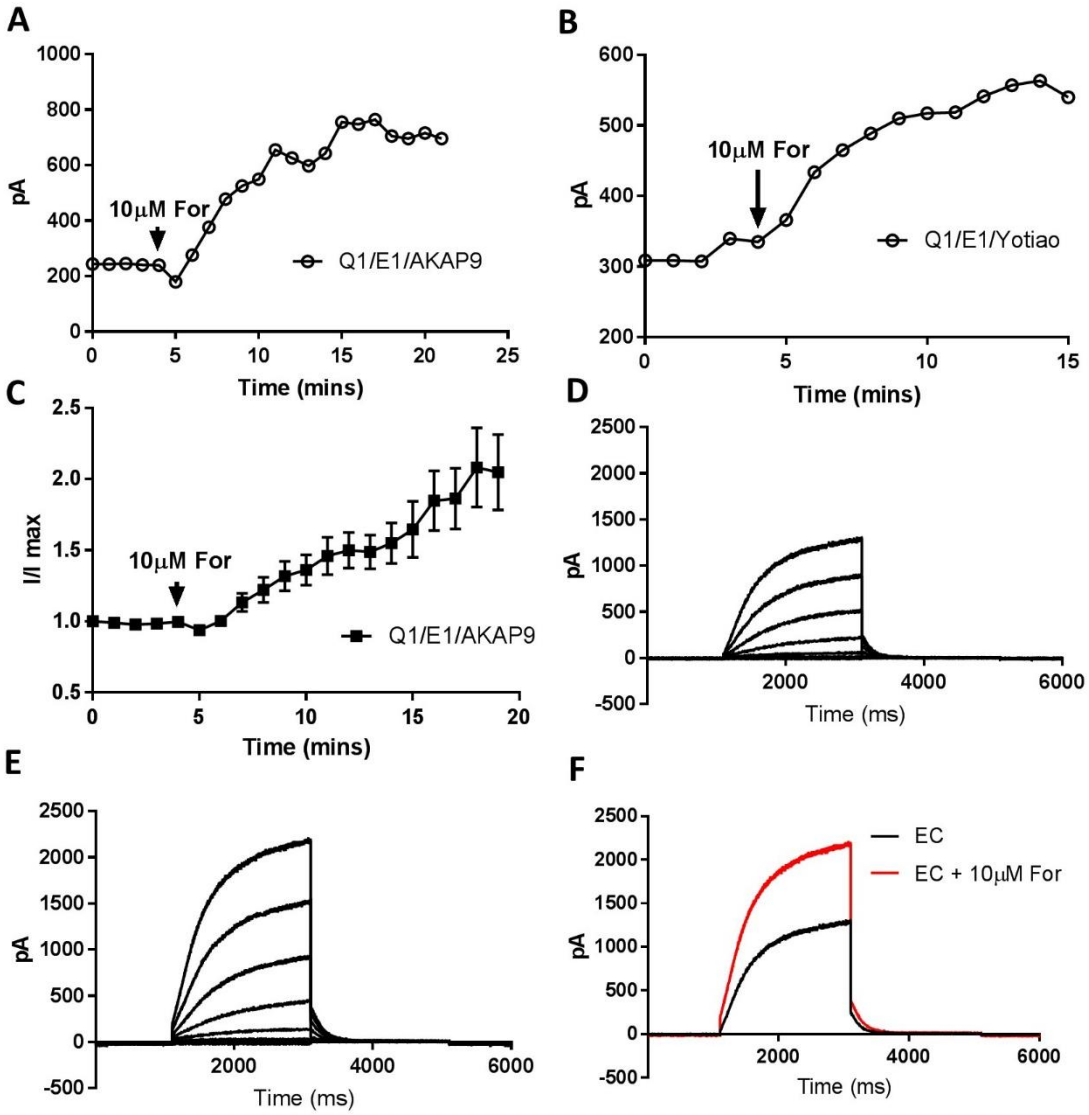


*Figure 4.8.* ***AKAP9 and Yotiao couple IKs to adrenergic drive in CHO-K1 cells. A*** *Representative time course trace of IKs in CHO-K1 cell co-transfected with AKAP9.* ***B*** *Representative time course trace of IKs in CHO-K1 cell co-transfected with Yotiao.* ***C*** *Mean data from 12 cells transiently transfected with KCNQ1-GFP/KCNE1/AKAP9. All timecourse data is recorded at +40mV.* ***D-E*** *Representative current-voltage relationship of IKs before (D) and after (E) forskolin treatment.* ***F*** *Superimposed traces at +80mV step before (black) and after (red) forskolin addition to extracellular solution. EC – Extracellular solution, For – Forskolin, Q1 – KCNQ1, E1 – KCNE1.*

## 4.8 Analysis of AKAP9's effect on Transfected IKs Current in CHO-K1 Cells following 10μM Forskolin Treatment

IKs responded robustly to forskolin treatment when co-expressing AKAP9. Further comparative analysis was carried out to identify the exact effect of AKAP9 transfection across a range of voltages following forskolin treatment. These cells underwent perforated patch-clamp analysis (Figure 4.7 & Figure 4.8). At both +40mV and +80mV peak current, there was clear divergence between cells transfected with KCNQ1-GFP/KCNE1 alone compared to those co-expressing AKAP9 (Figure 4.9A-B).

No significant difference between IKs peak current recorded before or after forskolin treatment was found at any voltages without AKAP9 co-transfection, the greatest difference being at +80mV (Figure 4.9C-D, two-way ANOVA, Sidak's multiple comparison, $P>0.36$). Correspondingly forskolin treatment did not significantly alter tail current in these cells, the largest observed effect was seen after a +40mV step (Figure 4.9D, two-way ANOVA, Sidak's multiple comparison, $P>0.83$). Conversely, when AKAP9 was co-expressed alongside IKs, peak current was significantly increased following forskolin treatment at voltage steps +40, +60 and +80mV (Figure 4.9E, two-way ANOVA, Sidak's multiple comparison, $P=0.0004$, $P<0.0001$ & $P<0.0001$ respectively). There was also an increase in relative peak tail current following adrenergic stimulation at -40mV following voltage steps +40, +60 and +80mV (Figure 4.9F, two-way ANOVA, Sidak's multiple comparison, $P=0.0047$, $P=0.0002$ & $P<0.0001$ respectively). In contrast to HEK293 data, analysis of Boltzmann fitted curves to the steady state of deactivation found no significant difference in $V_{1/2}$ or slope parameters, before or after forskolin treatment in AKAP9 transfected cells (Figure 4.9G).

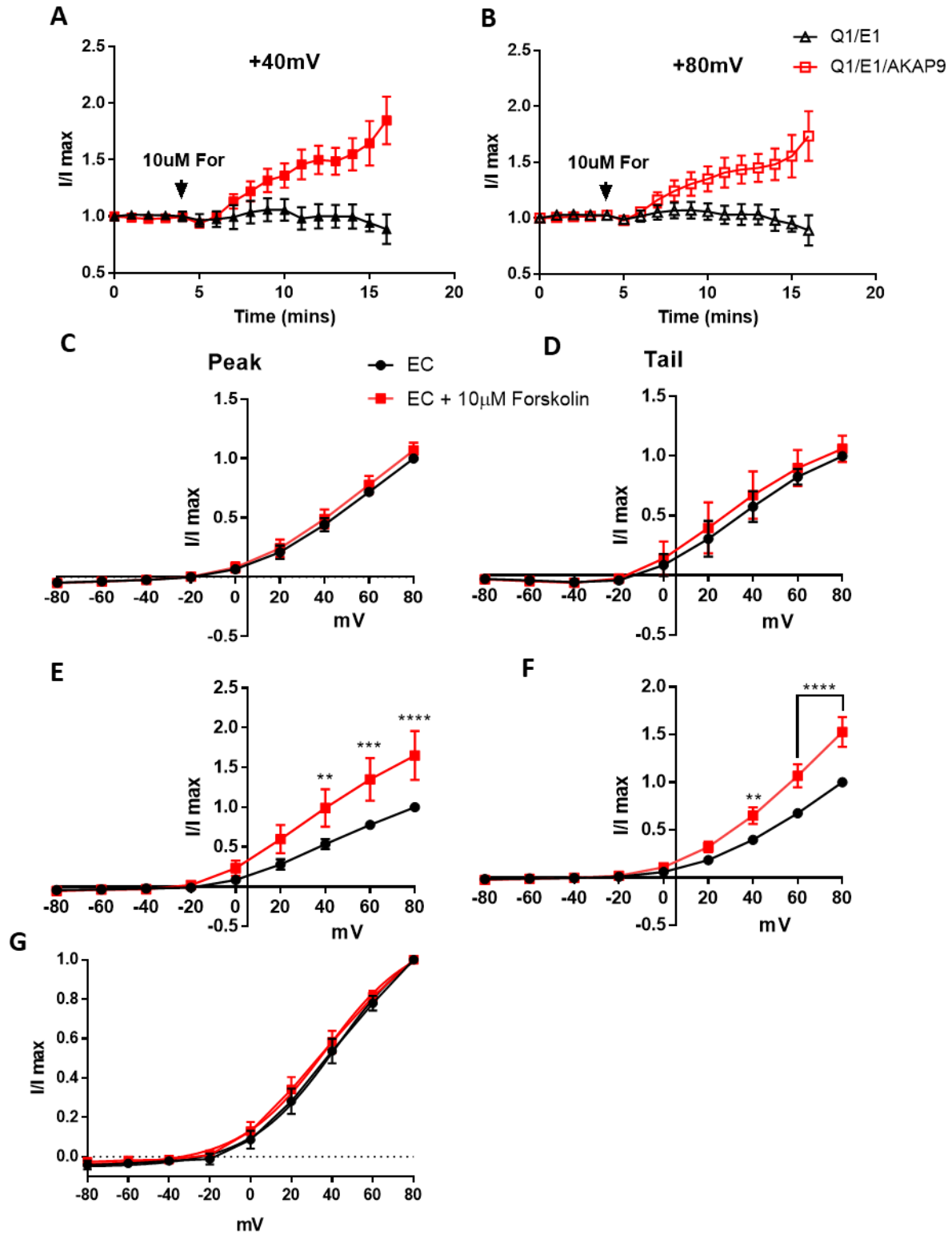


*Figure 4.9.* ***IKs responds to adrenergic stimulation in CHO-K1 cells when co-expressed alongside AKAP9. A-B*** *Mean normalised timecourse data from IKs current recorded during forskolin treatment at +40mV (A) and +80mV (B) voltage steps. Data from CHO-K1 cells transfected with AKAP9 (red) or without it (black) is shown.* ***C-D*** *Current-voltage relationships from CHO-K1 cells transfected with KCNQ1-GFP/KCNE1, recorded at peak (C) and tail (D) before (black) or after (red) treatment with 10μM forskolin.* ***E-F*** *Current-voltage relationships from CHO-K1 cells transfected with KCNQ1-GFP/KCNE1/AKAP9, recorded at peak (E) and tail (F) before (black) or after (red) treatment with 10μM forskolin. EC – Extracellular solution, Q1 – KCNQ1, E1 – KCNE1.* ***G*** *Boltzmann curve fitted to tail currents before (black) and after (red) forskolin treatment. Data are normalised to maximum average current before (black) and after (black) forskolin. Before forksolin: $V_{1/2}$ = 42.12mV slope = 21.35, after forskolin $V_{1/2}$ = 37.16mV slope = 21.39.*

## 4.9 Effect of p.D1507H on AKAP9's Ability to Couple β-adrenergic Stimulation to IKs

The first CICUS *AKAP9* variant tested was p.D1507H, it lies within 70 residues of the one known pathogenic LQT11 variant, p.S1570L [131]. This variant lies between two of the 13 coiled coil domains predicted to form in the AKAP9 protein. Interestingly, this variant is also less than 60 amino acids from the 'C-terminal binding site' of the smaller isoform *Yotiao*, also shown previously to interact with KCNQ1 [243].

We investigated whether the p.D1507H variant had an effect on the ability of AKAP9 to modulate IKs in response to adrenergic stimulation. CHO-K1 cells were transfected with KCNQ1-GFP/KCNE1 alongside p.D1507H *AKAP9* plasmid for 4-6 hours before being plated onto glass coverslips. After 24 hours cells underwent perforated patch-clamp analysis to measure IKs currents. After five minutes of stable recording, cells were perfused with extracellular solution with 10μM forskolin. Previous work on the smaller *AKAP9* isoform, *Yotiao*, has reported that a nearby p.S1570L mutation reduced its interaction with KCNQ1 [131].

Analysis of time-course I-V recordings at +40mV showed transfected CHO-K1 cells responded robustly to forskolin (Figure 4.10A-B). Although there was an apparent increase in currents recorded at voltage steps greater than +20mV, there was little noticeable change in the shape of I-V traces (Figure 4.10C-D). Superimposition of a representative traces looking at peak and tail currents clearly indicated the effect of forskolin treatment in increasing IKs activation and deactivation (Figure 4.10E-F).

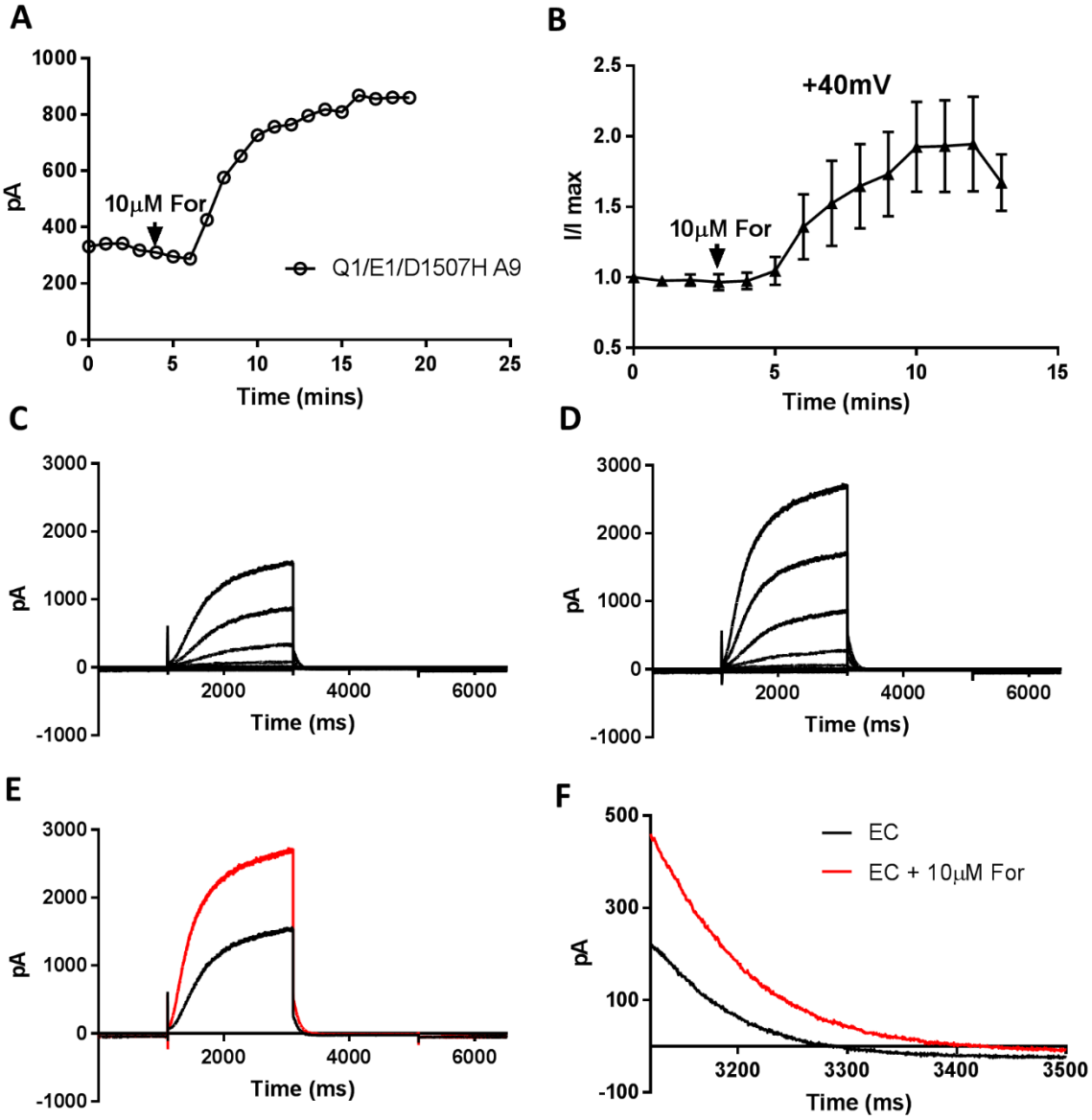


*Figure 4.10.* ***Transfection with p.D1507H AKAP9 allows IKs to respond to forskolin. A*** *Representative trace of IKs recording in CHO-K1 cell following KCNQ1-GFP/KCNE1/AKAP9 p.D1507H transfection, forskolin was added after five minutes of stable recording where indicated.* ***B*** *Mean time course data of IKs recorded at peak +40mV current from transiently transfected cells showing the effect of forskolin. Data is normalised to current observed five minutes before addition of drug. N = 8.* ***C-D*** *Current-voltage relationship from cell in (A) before (C) and after (D) 10 minutes of forskolin treatment.* ***E-F*** *Superimposed current traces from C/D at +80mV highlighting increase in peak (E) and tail (F) currents after addition of 10μM forskolin (red). EC – Extracellular solution, Q1 – KCNQ1, E1 – KCNE1.*

## 4.10 Effect of p.A3043T on AKAP9's Ability to Couple β-adrenergic Stimulation to IKs

We next investigated whether the p.A3043T mutation had an effect on the ability of AKAP9 to modulate IKs in response to adrenergic stimulation. This variant lies within 500 residues of the known PKA subunit binding domain at amino acids 2554-2567, and is close to a small coiled coil domain at residues 3065-3092.

CHO-K1 cells were transfected with KCNQ1-GFP/KCNE1 alongside the p.A3043T *AKAP9* plasmid. Cells were then being split onto glass coverslips 4-6 hours following transfection. After 24 hours cells underwent perforated patch-clamp analysis to measure IKs currents. After five minutes of stable recording, cells were perfused with extracellular solution containing 10μM forskolin.

Analysis of time-course I-V recordings at +40mV peak current steps showed transfected CHO-K1 cells did not respond to adrenergic stimulation (Figure 4.11A-B). Strikingly, at no voltage steps was there any noticeable increase or modulation of current recorded after forskolin treatment (Figure 4.11C-D). Peak current during the +80mV step showed no change following addition of 10μM forskolin (Figure 4.11E). There was no discernible effect on peak tail currents recorded at -40mV following an +80mV voltage step (Figure 4.11F).

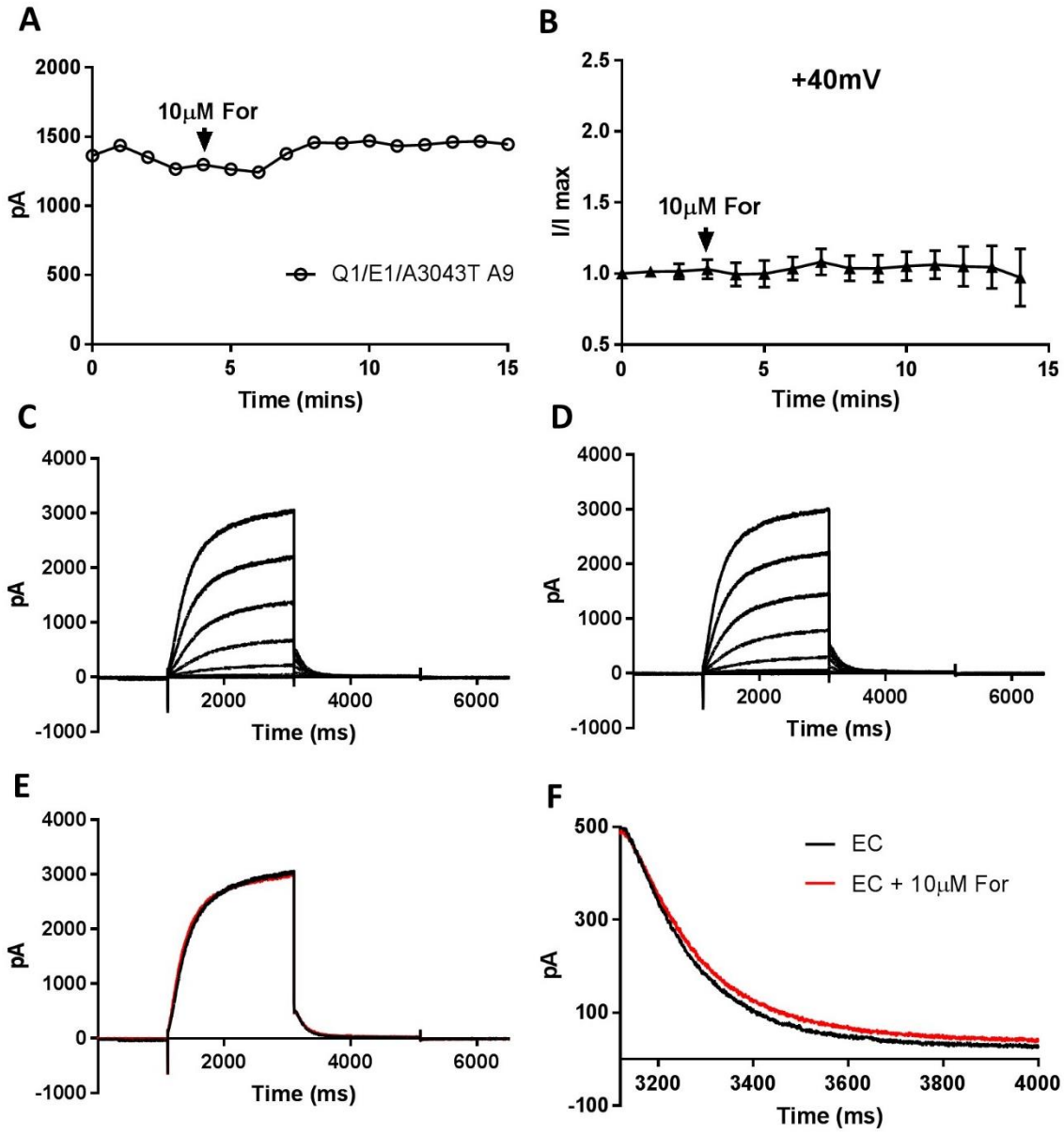


*Figure 4.11.* ***Transfection with p.A3043T AKAP9 does not allow IKs to respond to forskolin. A*** *Representative trace of IKs recording in CHO-K1 cell following KCNQ1-GFP/KCNE1/AKAP9 p.A3043T transfection, forskolin was added after five minutes of stable recording where indicated. N = 6.* ***B*** *Mean time course data of IKs recorded at peak +40mV current from transiently transfected cells indicating effect of forskolin. Data is normalised to current observed five minutes before addition of drug.* ***C-D*** *Current-voltage relationship from cell in (A) before (C) and after (D) 10 minutes of forskolin treatment.* ***E-F*** *Superimposed current traces from C/D at +80mV highlighting peak (E) and tail (F) currents after addition of 10μM forskolin (red). EC – Extracellular solution, For – Forskolin, Q1 – KCNQ1, E1 – KCNE1.*

## 4.11 Comparison of p.D1507H AKAP9 and p.A3043T AKAP9's Ability to Couple β-adrenergic Drive to Increased IKs Current

In addition to timecourse current measurements, the current-voltage relationship of IKs in CHO-K1 cells was investigated when co-expressed with p.D1507H or p.A3043T AKAP9. Current traces recorded at voltage steps between -80mV and +80mV were normalised to initial maximum current five minutes before forskolin treatment.

When compared to current recorded before 10μM forskolin treatment, normalised IKs was indistinguishable at all voltages after at least five minutes in KCNQ1-GFP/KCNE1/A3043T AKAP9 transfected cells (Figure 4.12A). Similarly, tail current recordings from these cells also showed a lack of response to forskolin treatment (Figure 4.12B). Conversely, in CHO-K1 cells transfected with IKs and p.D1507H AKAP9 a robust response in peak and tail current was observed at voltages >20mV and >0mV respectively. Normalised peak current in these cells was significantly greater at +40mV, +60mV and +80mV steps following 10μM forskolin treatment (Figure 4.12A, two-way ANOVA, Sidak's multiple comparison, $P=0.0017$, $P<0.0001$, $P<0.0001$ respectively). Correspondingly, peak tail current in these was significantly increased following adrenergic stimulation at -40mV following voltage steps at +20, +40, +60 and +80mV (Figure 4.12D, two-way ANOVA, Sidak's multiple comparison, $P=0.0022$, $P<0.0001$, $P>0.0001$ and $P>0.0001$ respectively).

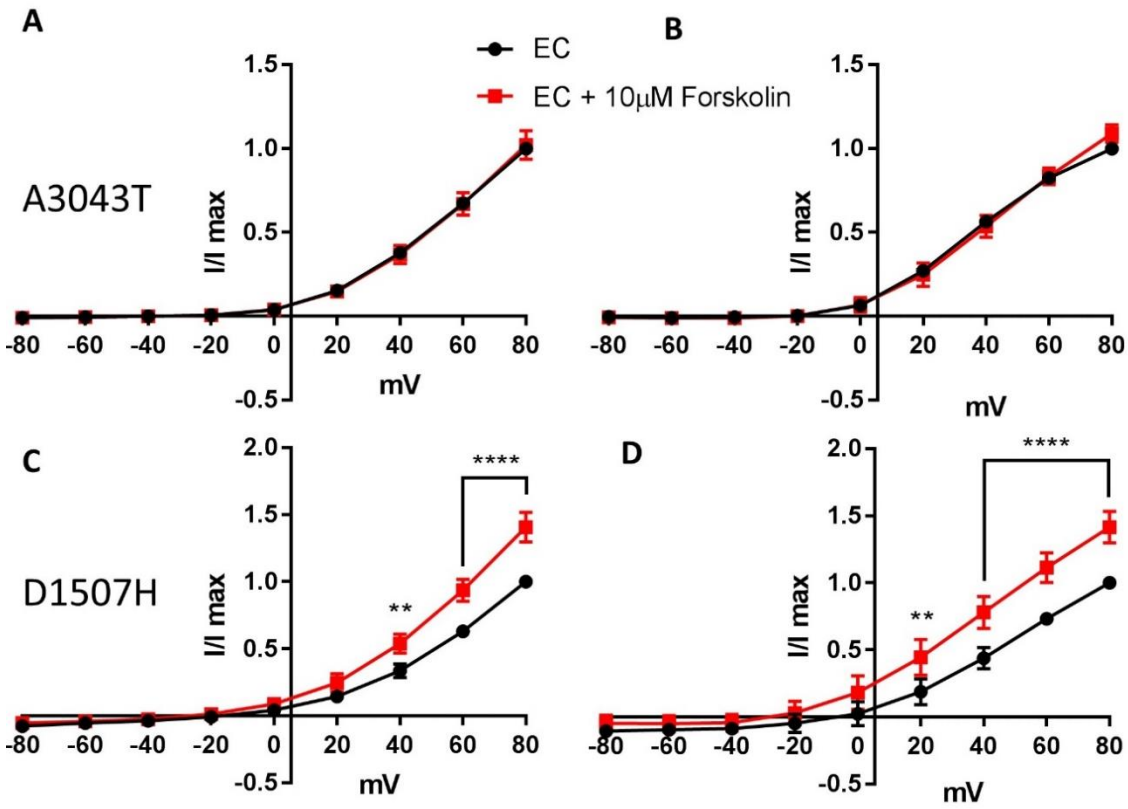


*Figure 4.12.* ***Comparison between the effects of p.D1507H and p.A3043T AKAP9 on IKs current following adrenergic stimulation with forskolin. A-B*** *Normalised IKs peak (A) and tail (B) current in CHO-K1 cells co-expressing p.A3043T AKAP9.* ***C-D*** *Normalised IKs peak (C) and tail (D) current in CHO-K1 cells co-expressing p.D1507H AKAP9. The two traces depict current with extracellular solution alone (black) or supplemented with 10μM forskolin. EC – Extracellular solution, Q1 – KCNQ1, E1 – KCNE1.N = 6-8.*

## 4.12 Relative Abundance of *AKAP9* Expression in the Human Heart

Previous experimental work in human myocardial tissue homogenates demonstrated the presence of Yotiao and its interaction with KCNQ1 [243]. Our data suggests a loss of function in p.A3043T AKAP9, however little is known about the abundance of the full length isoform in human myocardium. Therefore we wanted to investigate the expression of full length *AKAP9* expression in the human myocardium and discern the ratio of Yotiao : Full Length *AKAP9* present. Unfortunately, our laboratory lacks access to foetal myocardial tissue/RNA samples. Instead we investigated healthy adult human RNA samples available in our laboratory, to ascertain whether full length AKAP9 transcript can be seen in the human myocardium. Heart RNA samples were obtained from three males, aged 49, 65 and 69 who died of non-cardiovascular causes (obtained from Amsbio, UK). Each sample was split between the four heart chambers (Atria, Ventricles, Left and Right), allowing analysis of each separately. These RNA libraries were converted to cDNA by reverse transcription before qPCR analysis using probes targeting early and late *AKAP9* exons. The short probe spanned exons 5-6 (Ref: Hs01091034_m1) while the long probe targeted exon boundary 39-40 (Ref: Hs00323978_m1). The large isoform of *AKAP9* (NM_005751) contains both exon boundaries, therefore the 'short' probe measures expression of both short and long isoforms. All expression signals were normalised to the housekeeping gene GAPDH.

Full length *AKAP9* expression was highest in the left ventricle (4.5 ± 2.9% of GAPDH, Figure 4.13A). In both the left and right atrium expression was lower (1.8 ± 0.5% and 1.7 ± 0.8%, respectively), while the right ventricle showed the lowest levels of expression (1 ± 0.5%). The total expression of all *AKAP9* isoforms revealed a similar relationship between separate heart chambers (LV > LA > RA > RV, Figure 4.13B). A proportion of this total *AKAP9* signal, the proportion of full-length mRNA was highly consistent between the three hearts sampled (Figure 4.13C). In the left ventricle 35.3 ± 6.2% of total transcript contained the 39-40 exon boundary, whilst in the right ventricle this was slightly higher at 38.5 ± 2.8%. In atrial samples this

proportion was lower, with 32.5 ± 2.3% of right atrial *AKAP9* being full length, whereas this is only 26.7 ± 2.4% in the left atrium.

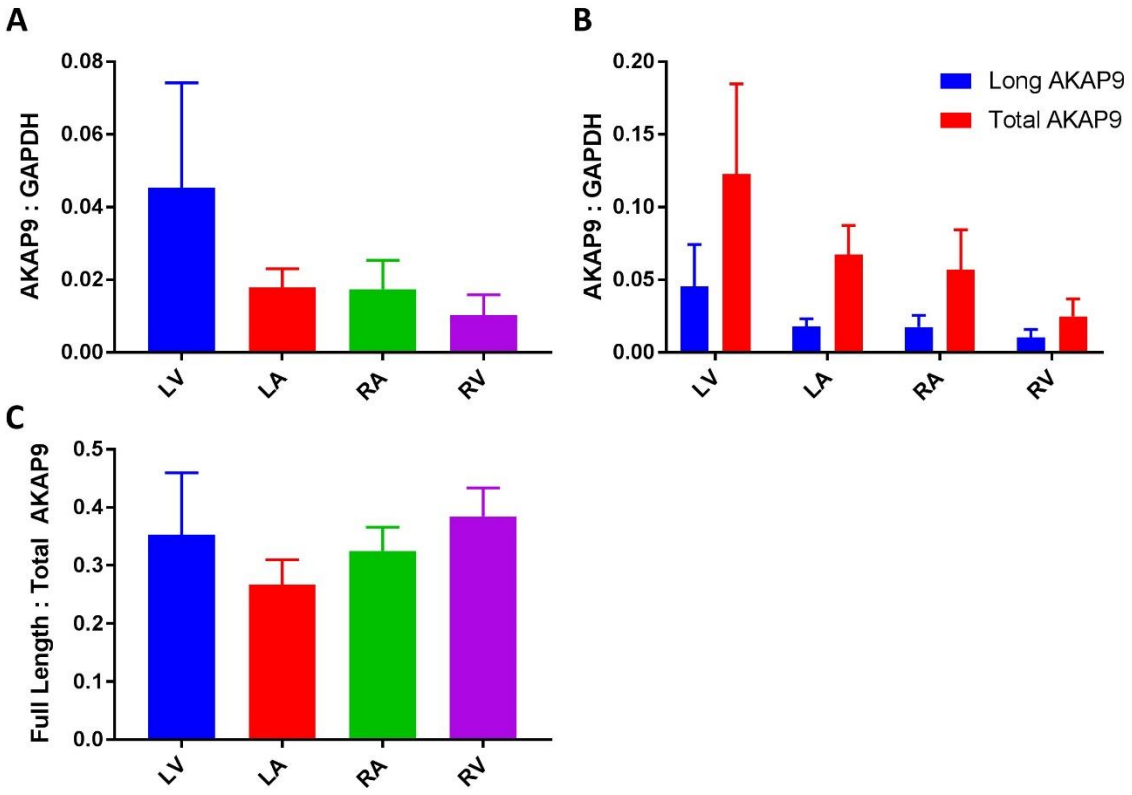


*Figure 4.13.* ***Human myocardial RNA AKAP9 expression levels. A*** *Full length AKAP9 expression from adult human heart chambers.* ***B*** *Addition of alternative probe signal to graph A. The short isoform probe targeted an exon found in all isoforms of AKAP9.* ***C*** *Comparison of long : total AKAP9 isoform signal observed in C between specific heart chambers. Total heart chamber RNA was harvested from three adult donors, divided into the four heart chambers. For each experiment n = 3. Data is shown as mean ± SEM. LV = Left Ventricle, LA = Left Atria, RA = Right Atria, RV = Right Ventricle.*

## 4.13 Testing for an Enrichment of Predicted Damaging Variants in the CICUS Study

We performed an enrichment analysis to investigate whether there was a significant increase in the number of predicted damaging variants found in CICUS cases compared with a healthy control population. This was to check for further evidence of association with stillbirth with the selected candidate gene. A control population consisting of 563 randomly chosen genomes from the 1000g database was used. This control population's ancestry was matched to that of the CICUS population; 69.6% European, 3.3% East Asian and 1.4% African with the remaining 25.7% randomly selected from the remaining samples in the 1000 Genomes project. All nonsynonymous SNVs from the CICUS and control populations were sorted based upon our variant prioritising methodology.

All variants from non-conserved residues were removed from the analysis as previously described for *AKAP9* and *TRPM7*. For the enrichment statistical test, we used a frequency cut-off point of 0.01% compared to 1% in prior analysis. We expect harmful variants that precipitate stillbirth in a population-based test to be very rare – below our initial 1% cut-off point to gather a sample of variants to test. We found 52 predicted damaging variants in 18 genes in the CICUS cases (Table 4.1). In the control population, we found 410 variants in these 18 genes.

Fisher's exact test was used to calculate whether there was a statistically significant difference in the number of cases or controls possessing a predicted damaging genetic variant. *TRPM7* showed a significant difference in the number of variants found between controls and cases. Of the 70 CICUS cases, four possessed *TRPM7* variants, compared to only 9 variants in 563 1000g controls (P = 0.047). Although it did not reach significance, there was nominal enrichment of putative damaging *CREBBP* variants in CICUS cases (P = 0.074). No significant enrichment for *AKAP9* predicted damaging variants was found between CICUS cases and the control population (P = 0.72).

| Gene | CICUS cases with a variant (%) | Controls with a variant (%) | P Value |
|---|---|---|---|
| *AKAP9* | 3 (4.2) | 18 (3.2) | 0.72 |
| *ANK2* | 2 (2.8) | 22 (3.9) | 1 |
| *BAZ2B* | 2 (2.8) | 13 (2.3) | 0.68 |
| *CACNA1C* | 2 (2.8) | 9 (1.6) | 0.35 |
| *CREBBP* | 5 (7.0) | 16 (2.8) | 0.074 |
| *KCNE1* | 0 | 2 (0.4) | 1 |
| *KCNE2* | 0 | 2 (0.4) | 1 |
| *KCNJ2* | 1 (1.4) | 1 (0.2) | 0.21 |
| *MKL2* | 0 | 5 (0.9) | 1 |
| *NDRG4* | 1 (1.4) | 4 (0.7) | 0.45 |
| *RYR2* | 3 (4.2) | 26 (4.6) | 1 |
| *SCN10A* | 3 (4.2) | 15 (2.7) | 0.44 |
| *SCN5A* | 2 (2.8) | 15 (2.7) | 1 |
| *SLC8A1* | 2 (2.8) | 5 (0.9) | 0.18 |
| *SMARCAD1* | 1 (1.4) | 1 (0.2) | 0.21 |
| *SRL* | 1 (1.4) | 6 (1.1) | 0.57 |
| *TRPM7* | 4 (5.6) | 9 (1.6) | 0.047* |

*Table 4.1.* ***Summary of rare predicted damaging variant enrichment found in the CICUS study cases compared to 563 controls from the 1000g database.*** *The total number of cases with variants is specific genes in shown alongside the population percentage for both cases and controls. Calculated Fisher's exact test p values are listed for each gene. * - P<0.05. Cases n = 70, Controls n = 563.*

## 4.14 Discussion

Protein Kinase A anchoring proteins are vital in the formation of large complexes that coordinate localised cAMP inputs with regulatory enzymes and their targets [316]. Yotiao or its larger isoform AKAP9 are thought to direct activated PKA molecules to phosphorylation of the KCNQ1 potassium channel. Coupling of adrenergic stimulation to increased slowly-rectifying potassium current output is required to shorten the action potential and repolarisation during periods of exercise or stress [54]. Maintaining PKA at the cell surface is believed to allow rapid translation of β-adrenergic stimulation, through cAMP and PKA to increase phosphorylated IKs at the cell surface. Under basal (low heart rate) conditions, IKs is likely unable to contribute significantly to hyperpolarisation due to its slowly activating kinetics. This was recently confirmed by the finding that in adult canine ventricular myocytes, KCNQ1 has been shown to largely reside in an intracellular reservoir under basal conditions [317]. Although acute stimulation was not investigated, chronic stress did boost IKs amplitude in this model, and represents the cells ability to increase KCNQ1 channel conductance at the membrane in response to exogenous factors. Despite initial data suggesting that in healthy human myocardium there was no slowly activating IKs potassium channel, IKs has been shown to activate slowly and deactivate rapidly in adult myocytes [318,319]. Therefore deleterious *AKAP9* variants may render IKs immune to adrenergic stimulation, promoting a pro-arrhythmogenic state due to delayed repolarisation during times of stress in the developing foetus.

The first stage of *in vitro* analysis of CICUS variants on the function of *AKAP9* was to acquire an expression vector for the gene and then insert the five different variants found in unexplained stillbirth cases into this DNA backbone. Despite several rounds of site-directed mutagenesis, only two CICUS variants could be grown using competent cells to a sufficient quantity to allow mammalian cell transfection. Both p.D1507H and p.A3043T transformed bacterial cells grew in larger 50ml bacterial cultures – sufficient for large-scale DNA harvesting. The other three variants (p.D155N, p.E2059G and p.S2186P) rarely grew colonies after

transformation and never grew to sufficient quantities in liquid cultures despite expanded (up to 72hours) incubation times. This is likely due to the large size of the *AKAP9* vector construct resulting in extremely long mutagenesis steps and the difficulty in competent cells firstly accepting the backbone and subsequently synthesising it in order to survive in an antibiotic environment. Despite this, p.D1507H and p.A3043T *AKAP9* transformations that did produce sizeable bacterial cultures, and were harvested in sufficient quantity and concentration (>400ng/µL) to allow a large number of mammalian cell transfections.

In order to examine the effect of β-adrenergic stimulation on the IKs current, we initially used the s5.3 cell line in our laboratory that stably expresses KCNQ1-GFP/KCNE1. These currents were measured using the whole-cell patch-clamp configuration, which confirmed classical IKs kinetics in these cells. Strikingly, in this cell line 1nM of isoprenaline added to the extracellular solution was capable of rapidly increasing IKs current without transfection of any vectors. Peak and peak tail currents measured following voltage steps over +10mV were significantly increased compared to cells incubated with extracellular solution alone.

However, although cAMP-dependent PKA phosphorylation of KCNQ1 occurs locally at the membrane, there is significant washout of intracellular components during dialysis after whole-cell access is acquired. Therefore we transitioned to using the perforated patch-clamp technique which would preserve the cytoplasmic environment of cells during recording. This would allow comparison of IKs currents before and after β-adrenergic stimulation, allowing paired comparisons of cells rather than independent grouped analysis. However, due to the prolonged nature of these experiments, where the pipette can be attached to cells for upwards of 90 minutes, the effect of isoprenaline was not predictable. Undiluted solutions of isoprenaline hydrochloride are stable at room temperature, nonetheless dilution of isoprenaline with extracellular solution leads to rapid oxidation of the drug. Although supplementation of isoprenaline containing solutions with ascorbic acid have been shown to increase stability, this requires pH adjustment to 2.8, which is not feasible in pH7.4 extracellular solutions [320]. Forskolin

which acts through direct stimulation of adenylyl cyclase was used as a PKA activator instead of isoprenaline.

Measuring IKs current in s5.3 cells following treatment with 10μM forskolin showed a robust response to adrenergic stimulation. Peak currents measured at +40mV steps showed currents almost doubled after five minutes of drug treatment. At voltage steps higher than +40mV, both peak and peak tail currents were significantly increased compared to baseline measurements. Fitting tail current, steady-state deactivation with a Boltzmann equation showed a $V_{1/2}$ leftward shift of 12.47mV, indicating that during channel deactivation, 50% of channels are still open at a lower voltage. There was no difference in the rate of deactivation observed following forskolin treatment, but at step voltages over -40mV, normalised activation constants were significantly reduced. This demonstrated that forskolin treatment was a preferred alternative to using isoprenaline to mimic adrenergic stimulation, as it reliably increased IKs amplitude while being stable at room temperature. Secondly, isoprenaline binds and activates both β1 and β2 adrenergic receptors on the cells surface while forskolin directly acts upon adenylyl cyclase to raise cytosolic cAMP levels. The predominant form of adrenoreceptors in the heart are β1, that when bound by a ligand increase adenylyl cyclase activity through the Gs effector protein [321,322]. This is the proposed mechanism by which AKAP9 regulates formation of the complex that oversees KCNQ1 phosphorylation. However, heterologous cells have been used to study adrenergic stimulation involving chiefly β2 related mechanisms [323,324].

When KCNQ1/KCNE1 were stably expressed in HEK293 cells, the IKs current was responsive to transient adrenergic stimulation. While not previously reported, this finding provided a barrier to accessing the function of AKAP9 as there is no data on what proteins are responsible for coupling adrenergic stimulation with increased IKs current in HEK293 cells. Previous work on the smaller *AKAP9* isoform Yotiao was conducted in CHO-K1 cells, therefore

we transiently transfected these cells with KCNQ1-GFP/KCNE1 and studied IKs current and its response to adrenergic stimulation [131].

After transfecting CHO-K1 cells with GFP tagged KCNQ1, we were able to measure typical IKs current using the perforated patch-clamp technique. In concordance with previous published data, adrenergic stimulation increased relative IKs current recordings after ~5 minutes [131,243]. Interestingly, initial studies by the Kass laboratory have used a cell permeable cAMP analog (CPT-cAMP) alongside okadaic acid to promote KCNQ1 phosphorylation by PKA instead of isoprenaline or forskolin [243]. Separate heterologous cell work by Baro et al. used 400µM CPT-cAMP and 10µM forskolin in combination to increase KCNQ1 phosphorylation in a mix of whole-cell and perforated patch-clamp techniques [325,326]. We were able to observe a rapid and reproducible increase in IKs current to treatment with forskolin alone, meaning adenylyl cyclase activation alone is capable of promoting significant channel phosphorylation without other signalling molecules.

The observed response in CHO-K1 cells was in stark contrast to HEK293 cells stably expressing KCNQ1-GFP/KCNE1, denoting a distinct lack of sufficient signalling/scaffolding proteins to allow PKA activation to lead to channel phosphorylation. Cells transfected with KCNQ1-GFP/KCNE1 and either full length *AKAP9* responded to forskolin treatment compared to those expressing KCNQ1-GFP/KCNE1 alone. After 10+ minutes of forskolin in solution, current at +40mV steps was almost doubled indicating that phosphorylation of KCNQ1-GFP at the membrane was capable of significantly increasing IKs conductance. Anecdotally, a cell transfected with small length AKAP9 isoform Yotiao alongside KCNQ1-GFP/KCNE1 were subjected perforated patch-clamp analysis. Although used extensively to characterize the one known LQT11 mutation (p.S1570L), this small isoform theoretically does not contain the single putative PKA-RII binding domain (2554-2567aa). Also of note, initial experiments in CHO-K1 cells looking at how Yotiao couples cellular responses to cAMP were done in the whole-cell patch-clamp configuration, using a dialysis step of 13 minutes [243]. This is likely to result in significant

current run-down and marked disruption to intracellular signalling pathways. When recording IKs in cells expressing KCNQ1-GFP/KCNE1 and Yotiao, we found that perfusing the extracellular solution with forskolin led to an immediate increase in current – indicating signal transduction and probable channel phosphorylation.

Further analysis in AKAP9 co-transfected cells showed significantly increased peak current and peak tail currents at voltage steps at and above +40mV, broadly in-line with the response to forskolin in HEK293 cells. This provided a preferable heterologous cell system to test whether CICUS variants in transiently transfected AKAP9 alter protein function compared to wild-type. Using the CHO-K1 cell system we were able to prove that PKA anchoring proteins alone are capable of coordinating PKA stimulation with increased IKs conductance.

Consequently, this allowed us to use the CHO-K1 cell system to interrogate the effect of CICUS *AKAP9* mutants may have in functionally influencing the coupling of β-adrenergic stimulation to increased IKs current through channel phosphorylation. The first variant to undergo this analysis was p.D1507H. This variant is within 70 amino acids of the one known LQT11 disease-causing mutation and lies in the centre of the AKAP9 protein. CHO-K1 cells were transfected with KCNQ1-GFP/KCNE1 alongside p.D1507H AKAP9 before undergoing perforated patch-clamp analysis. Under normal conditions CHO-K1 cells expressing IKs cannot couple treatment with forskolin to channel phosphorylation and increased conductance. However, when p.D1507H AKAP9 was co-transfected, we found that 10μM forskolin did result in an increase in IKs currents. This effect was observed within ~2minutes of treatment but persisted for 10+ minutes. Peak current at +80mV was noticeably increased, almost doubling whilst peak tail currents were noticeably increased. Further analysis of current-voltage relationships revealed significant peak current and peak tail current increases following adrenergic stimulation at voltages above +20mV. In summary, cells transfected with IKs and p.D1507H AKAP9 displayed similar responses to forskolin as those expressing wild-type AKAP9 protein. This data demonstrate that the p.D1507H variant sequenced in an unexplained stillbirth case

does not alter the ability of AKAP9 to couple β-adrenergic stimulation to increased IKs output. The gestation period for this case lasted 25 weeks, and the stillbirth was reported as occurring before or during birth (Intrapartum). The p.D1507H genetic variant occurs at very low frequency in both Esp6500 and 1000g (below 0.05% in both databases) and no predicted damaging genetic variants were found in any sequenced genes.

The effect of a second CICUS variant, p.A3043T, on AKAP9 was investigated using the CHO-K1 cell system. This genetic variant lies closer to the C-terminal region of AKAP9 than other variants we and others have studied. We transfected CHO-K1 cells with KCNQ1-GFP/KCNE1 alongside p.A3043T AKAP9 and measured IKs responses to 10μM forskolin using the perforated patch-clamp technique. We measured typical IKs currents with slowly activating currents in response to positive voltage steps (+20 to +80mV) and typical deactivating tail currents after these steps. In these cells, we found that activation of adenylyl cyclase using forskolin did not result in increased current after 10+ minutes of constant current recordings. Superimposed current traces before and after forskolin treatment were identical, indicating no interaction between forskolin addition and channel phosphorylation. Further analysis of I-V trace relationships showed that a complete lack of divergence between current recorded before or after forskolin treatment, indicating that transfected p.A3043T AKAP9 was not producing a functional macromolecular complex capable of functional KCNQ1 phosphorylation.

The first *AKAP9* CICUS mutant tested, p.D1507H represents a minor change in amino acid primary structure, as both aspartate and histidine are have charged side chains. While aspartate is usually listed as an 'acidic' amino acid, histidine is expected to be negatively charged at physiological pH (pKa around pH 6.5). Both amino acids, due to their charged side chains are commonly found in protein binding domains, representing a small physiological change. Therefore is not surprising to see a lack of functional effect between WT and p.D1507H AKAP9. The p.A3043T variant represents a more severe amino acid substitution, with the small non-polar alanine amino acid swapped for a polar threonine. While alanine contains a small and non-

reaction side-chain, the hydroxyl group of threonine is able to form hydrogen bonds to other polar substrates, alongside being a target for phosphorylation or glycosylation depending on it's neighbouring protein structure. This substitution may interfere with the folding of the AKAP9 protein due to steric hindrance during folding.

In the CICUS study we found two cases with p.A3043T *AKAP9* variants. The gestation period for the first case was 26 weeks, the second 40. The first case (identified as GOSH14M) was identified by a neonatal pathologist as "IUD with lesions" – growth restriction was observed, but no cause was found. Interestingly, data from the international mouse phenotyping consortium has shown significantly reduced body weight in both male and female mouse where one *AKAP9* gene has been silenced though exon deletion. The second case (identified as SHUT15) had increased foetal subcutaneous adipose tissue, but was classified as unexplained. The p.A3043T genetic variant occurs at very low frequency in both Esp6500 and 1000g (below 0.01% in both databases).

In both cases, predicted damaging variants were sequenced in cardiac ion channelopathy genes. Alongside the *AKAP9* variant found in GOSH14M, a novel p.H513Y nonsynonymous variant within the Ryanodine Receptor 2 gene (RYR2). This ion channel releases calcium from the sarcoplasmic reticulum in response to calcium influx, a fundamental step in cardiac muscle contraction. Several harmful variants in *RYR2* have been associated/attributed to causing CPVT, with the vast majority residing towards the 6 C-terminal transmembrane domains (amino acids 4282 – 4870) [156,327]. A predicted damaging variant in *SCN10A* was sequenced in the second case, SUHT15. This gene transcribes the α-subunit of sodium current $Na_v1.8$; most commonly associated with nociception. Interestingly, several GWAS have linked SNPs within the *SCN10A* gene to arrhythmogenesis [328]. More recent work has shown large numbers of BrS patients harbour *SCN10A* mutations, and that *SCN10A* expression increases $I_{Na}$ in cells expressing *SCN5A* or *SCN3B* – genes responsible for controlling cardiac depolarisation [104,149,329]. However, enrichment analysis of *SCN10A* variation in symptomatic BrS patients by a

different group has demonstrated a lack of significant enrichment [330]. This specific variant, p.A1235V, occurs rarely with a 0.001 frequency in the general population. It is positioned within the 5th transmembrane domain of the third pore forming unit, within 70 residues of a known gain-of-function mutation associated with hyperexcitability in neurons [331].

All *AKAP9* variants sequenced from the CICUS cases were heterozygous, these isoforms will be present alongside fully functional wild-type protein transcribed from the second allele. There are numerous examples of how genetic haploinsufficiency of potassium channels, specifically those regulated by PKA, can lead to disease. Work from Gouas et al. demonstrated how two heterozygous *KCNQ1* variants could be responsible for drug-induced arrhythmia amongst the general population [332]. Two variants, p.Y148X and p.ΔS276, reduced IKs current in COS-7 cells due to haploinsufficiency. The carriers showed borderline QT interval prolongation, however, during 24h ECG recording the p.Y148X carrier showed marked QT prolongation. In 1998 Shroeder et al. demonstrated that haploinsufficiency of heteromeric KCNQ2/KCNQ3 channels can cause epilepsy [333]. These channels were susceptible to PKA phosphorylation in HEK293 cells, showing significant current increases after PKA wash or cAMP treatment. Functional analysis of several epilepsy specific variants showed that a 25% reduction in channel expression was sufficient to cause electrical hyperexcitability in the brain.

Palmiter et al. showed in 1995 that mice incapable of synthesising noradrenaline or adrenaline died *in utero* which could be prevented by treatment with a noradrenaline precursor [334]. Although the authors postulated that death 'might be due to cardiovascular failure', this finding reinforces the importance of catecholamines to correct mammalian development. Mutant embryos showed a similar phenotype to previously published data investigating how catecholamines are required for correct heart development, with knock-out mice showing thin malformed atria and highly heterogeneous ventricular cardiomyocyte morphology [335]. Alongside this catecholamine dependence, data from the 1980's depicted clear responses to sympathetic drive in foetal rabbit and rat heart tissues [336,337]. Together, these data implicate clearly the

presence of sympathetic tone in the developing myocardium and show it is required for successful cardiovascular development and function.

While we did not have access to foetal heart RNA during the study, we did have access to an adult heart chamber specific RNA resource. These samples allowed us to measure *AKAP9* gene expression in the human myocardium. Alongside this, we investigated any chamber specific differences in *AKAP9* and calculated the ratio of short to long *AKAP9* isoform expression. We found full length *AKAP9* expression throughout the adult myocardium. Chamber specific analysis showed a bias toward greater levels of *AKAP* in the left ventricle, although this was not statistically significant. Other chambers when compared to the left ventricle were markedly lower, possibly influencing chamber specific differences in β-adrenergic stimulation. This is in contrast to the relative expression of *KCNQ1/KCNE1* found in human adult myocardium, which has been shown to be remarkably similar between the left atrium and ventricle [338].

We used a second *AKAP9* qPCR probe targeted between exons 5 and 6 to measure total mRNA expressed from the *AKAP9* gene. Interestingly, the relative amount of full length *AKAP9* was consistent throughout the four heart chambers, indicating that a regulatory mechanism ensures a specific proportion of full length *AKAP9* mRNA is transcribed. Controversially, protein based predictions have suggested that the putative PKA binding site of *AKAP9* is positioned at amino acids 2554-2567. Initial data suggested this makes up the 1600 N-terminal amino acids of the full length protein, theoretically unable to bind PKA. Our preliminary data however supports Kass's findings, as CHO-K1 cells expressing KCNQ1/KCNE1 alongside Yotiao respond to stimulation with Forskolin despite lacking this theoretical motif.

A-kinase anchoring proteins are found in a multitude of cardiac molecular scaffolds and have been shown to be indispensable in regulating hypertrophy, calcium cycling, repolarisation, cardiac rhythm, sarcomere contraction and organizing the cytoskeleton [316]. In particular, *AKAP9* couples PKA-dependent phosphorylation of the voltage-dependent outward rectifying potassium channel to regulation of cardiac repolarisation. Harmful genetic variants that prevent

PKA phosphorylation of KCNQ1 during periods of increased sympathetic tone are likely to be pathogenic due to prolongation of the cardiac action potential, a known cause of after depolarisations [64,250]. The *AKAP9* variant p.A3043T, sequenced in a case of unexplained stillbirth, could uncouple sympathetic drive to increased repolarisation, proving fatal to the developing foetus.

Burden testing has previously been used to analyse the occurrence of multiple rare coding variants in arrhythmia-associated genes in patients with BrS [330]. This analysis investigated the coding regions of 45 previously reported arrhythmia-susceptibility genes in 167 BrS cases compared to 167 healthy controls with no history of arrhythmia. Compared to the control population, only the *SCN5A* gene had an increased burden of rare predicted functionally damaging variants in BrS patients. This result confirmed the importance of variation at the *SCN5A* locus in causing BrS, and that dysfunctional sodium handling is likely the mechanism.

We further analysed our sequencing data to test for further evidence that variants within *TRPM7* or *AKAP9* may play a functional role in unexplained stillbirth. We calculated whether there was a significant enrichment of predicted damaging variants in CICUS cases for each candidate gene compared to a control population. The control population was comprised 563 genomes from the 1000g database roughly matched to the CICUS study in ethnicity. For this population based approach we used a more stringent allele frequency threshold of 0.01. We found a statistically significant enrichment of *TRPM7* variants in the CICUS study compared to healthy controls, highlighting a reduced frequency of predicted damaging variants in controls. Due to its ubiquitous cellular nature and involvement in multiple physiological processes, it is reasonable to assume in healthy individuals harmful *TRPM7* variants will be rarer [216,224,233].

Variant prioritisation relies upon accessing variant allele frequency in the 'general' population. During the variant annotation phase, both the 1000g and Esp6500 databases were used to provide frequency data for the CICUS studies. The amount of available sequencing data is constantly expanding. Novel variants highly likely to be predicted damaging can be sequenced

in healthy subjects and uploaded, changing allele frequencies attributed to the 'normal' population. Such dynamic changes to allele frequency will influence the number of predicted damaging variants in both case and control population studies that undergo secondary analysis. With the publication of the Exome Aggregation Consortium (ExAC) database, genetic variation in over 60,000 humans is publically available [339]. Indeed, one *TRPM7* predicted damaging novel genetic variant found in a CICUS case (p.E1205G) is now not novel, having been found 2 times in the ExAC population (Frequency: 0.000017). The second novel *TRPM7* variant identified in the CICUS cases, p.T860M still remains novel, but the ExAC database has found two alleles carrying a p.T860A mutation. These retrospective frequency changes make re-analysis of data increasingly more important. The relative frequency of predicted damaging variants can fluctuate dramatically as available sequencing data rapidly expands.

While we did find a significant enrichment for predicted damaging variants in *TRPM7* in the CICUS study cases, after adjusting for multiple testing we found no evidence of an enrichment of rare predicted damaging variants in any of the genes from our selected panel in CICUS stillbirth cases.

# 5 Results – TRPM7's Importance in Induced Pluripotent Stem Cell-Derived Cardiomyocyte Electrophysiology

## 5.1 Introduction

Advances in somatic cell reprogramming towards an induced pluripotent stem cell (iPSC) has greatly increased usefulness and availability of cellular models of development [254]. The recent progress in targeted cardiac differentiation has allowed the study of early human foetal-like cardiomyocytes using iPSCs [255]. These cells have been used extensively to study initial development *in vitro*, test new drugs or to model hereditary conditions such as LQTS [257,261,340,341]. While there is significant data documenting the importance of *TRPM7* expression throughout mouse development, little is known of its importance or presence during human cardiogenesis [212-214].

In the context of human disease, *TRPM7* is often associated with atrial myocytes, where it may significantly contribute to calcium signals in atrial fibrosis and fibrillation [237,342]. In the mouse, TRPM7 has been measured in adult/embryonic ventricular cardiomyocytes and SAN cells, where it is thought to determine automaticity [212,213].

By using *in vitro* cardiomyocyte differentiation from iPSCs to model cardiogenesis, our aim was to study the expression of *TRPM7* in iPSCs as they differentiate. After differentiation, single-cell patch-clamp analysis would allow us to investigate whether TRPM7 currents can be observed in a human model of cardiomyocyte development. Both *TRPM7* CICUS variants thought to be pathogenic, p.G179V and p.T860M appear to act through haploinsufficiency. By using siRNA to mimic reductions in *TRPM7* we hope to model haploinsufficiency in a physiological system and study any perturbations to cardiomyocyte electrophysiology.

## 5.2 Culturing Induced Human Pluripotent Stem Cells

Induced pluripotent stem cells can be differentiated toward a cardiomyocyte-like phenotype [255,257,261]. After optimising a recently published differentiation protocol, we used these cells to model early cardiac development and analyse the importance of TRPM7 in the process. Human pluripotent stem cells were generated in our laboratory by Duncan Miller from healthy donors and patients with Brugada syndrome [292]. These iPSCs were named HS1M cells (after the healthy donor) and were reprogrammed from fibroblasts using a lentiviral transduction of a polycistronic vector hSTEMCCA or nucleofection of three plasmids [290,291]. These stem cells underwent G-band staining, showing a normal karyotype. Immunofluorescent staining of differentiating embryoid bodies showed mesodermal, neuroectodermal and endodermal markers [292]. Frozen cell pellets were thawed and seeded onto Matrigel coated dishes without feeder cells (Figure 5.1A) [294]. These cells proliferated rapidly and were morphologically similar to published stem cell images (Figure 5.B-E) [291,343].

To ensure that these proliferative cells were pluripotent and capable of differentiation we analysed protein and mRNA transcripts from HS1Ms. Immunocytochemical staining of cells for the membrane protein TRA-1-60 using a mouse monoclonal antibody was successful (Figure 5.2). This cell surface antigen is widely used to confirm pluripotency in cells. All cells stained positively with heterogenous signal observed throughout the population as seen in other well documented iPSC populations [254,344,345]. Harvesting total RNA from iPSCs showed high levels of *Nanog*, *Oct4* and *SOX2* (Figure 5.3A), three key transcription factors crucial for maintaining pluripotency in stem cells [254,344,346].

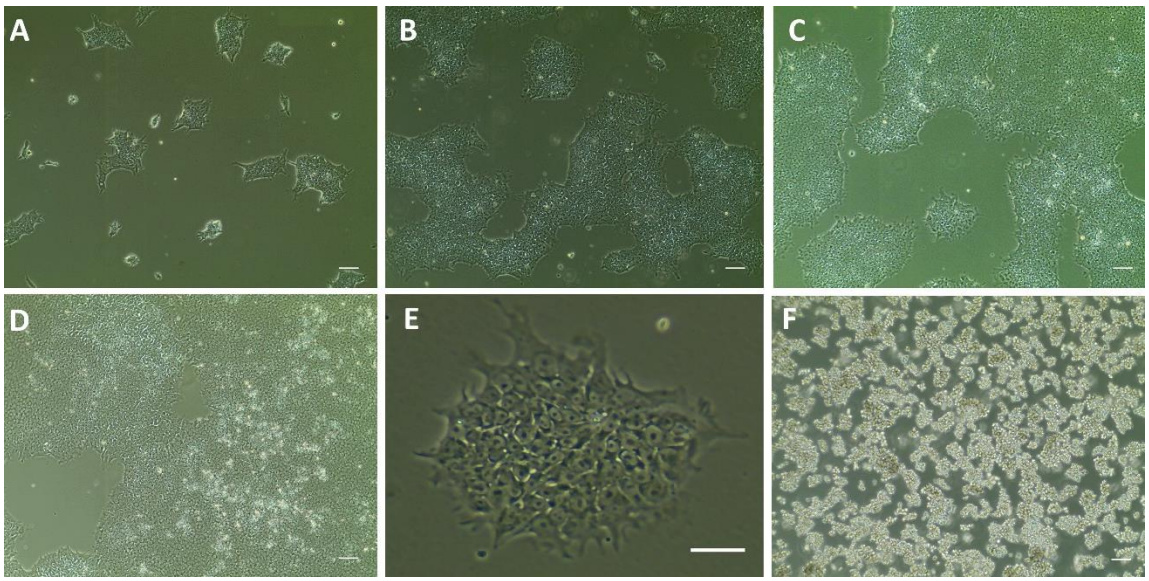


*Figure 5.1.* ***iPSC colonies maintained feeder free using mTESR1 and growth-factor reduced Matrigel. A*** *Pluripotent stem cells adhering to Matrigel one day after thawing, showing small colonies.* ***B-D*** *iPSCs colonies expand rapidly and become confluent in <6 days. Cells are shown at 3 (B), 4 (C) and 5 (D) days after initial seeding.* ***E*** *Magnified (x20) image of iPSC cell cluster depicting compact morphology.* ***F*** *Seven minutes of accutase treatment is sufficient to completely degrade Matrigel and allow cell resuspension. All images taken at x4 magnification apart from E, scale bar = 40µm.*

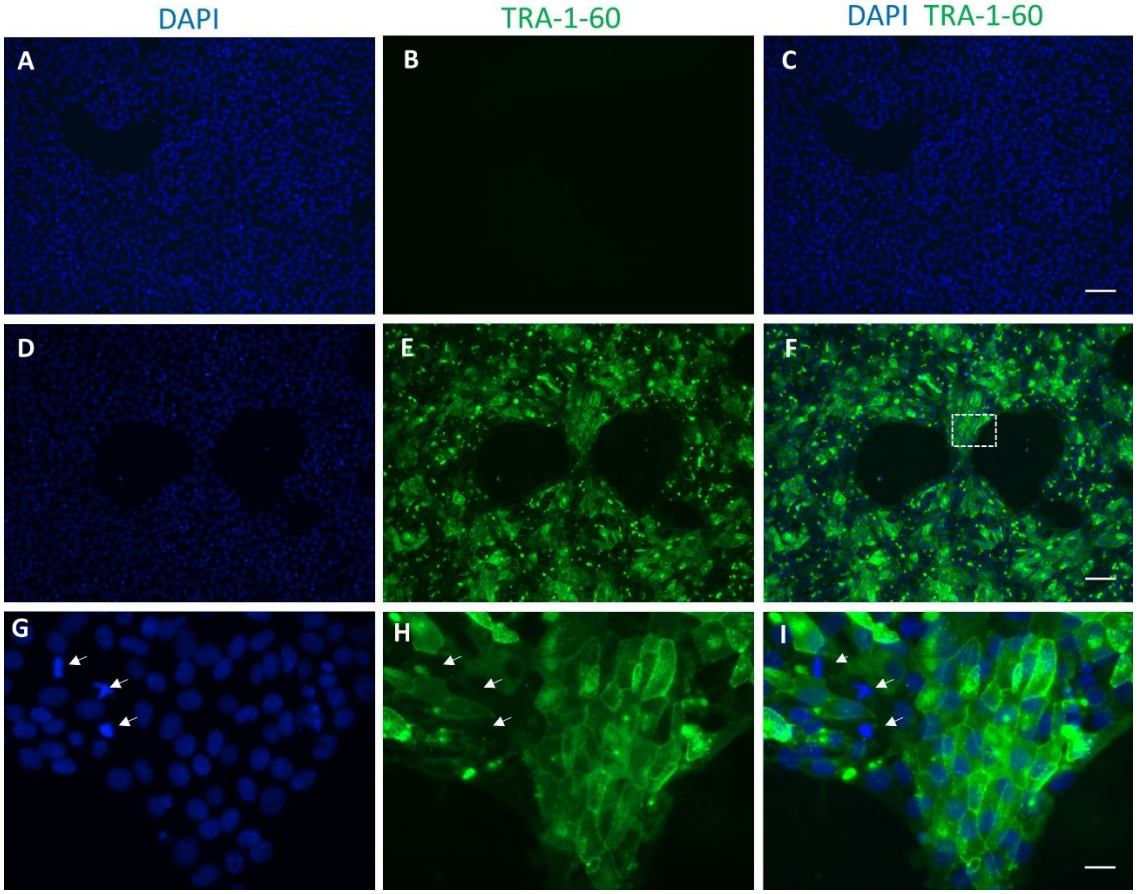


*Figure 5.2.* ***HS1-1M iPSC cells stain positively for the cell surface marker TRA-1-60. A-C*** *Negative control showing lack of positive staining when TRA-1-60 antibody is excluded from the protocol. Although significant numbers of cell nuclei stain positively for DAPI, there is a clear absence of background signal.* ***D-F*** *HS1M cells show marked heterogeneity for TRA-1-60.* ***G-I*** *Magnified image of dotted box from F, reduced TRA-1-60 signal corresponds to mitotic cells (white arrows). A, D, G – DAPI. B, E, H – Alexa Fluor 488. C, F, I – Composite Image. Scale bar A-F 40µm, G-I 10µm.*

## 5.3 Cardiomyocyte Differentiation from iPSCs

We used the previously published Burridge protocol to differentiate pluripotent stem cells toward a cardiomyocyte fate [255]. This method employs a basal media supplemented only with albumin and ascorbic acid. Two small molecular inhibitors CHIR99021 and C59, a Wnt activator and inhibitor respectively are added to the differentiation media at days 0-2 and days 2-4, respectively. Wnt activation sends cells toward a mesodermal lineage, while the subsequent Wnt inhibition produces cardiac mesodermal cells. To transcriptionally confirm differentiation from pluripotent cells, RNA samples were taken (days 0, 2, 4, 7, 14 & 21) for qPCR analysis. By day seven mRNA levels of *Nanog*, *Oct4* and *Sox2* were at 2.6, 3.8 and 1.6% respectively, of their expression levels before differentiation began (Figure 5.3A). Interestingly, *TRPM7* gene expression steadily increased as cells differentiated towards a more cardiac-like phenotype (Figure 5.3B). Expression peaked at day 4, with mRNA levels 2.6 times that observed in day 0, but was variable between seven differentiations (SEM = 2.78). Before differentiation, the expression of *Nanog*, *Oct4* and *Sox2* were higher than TRPM7 (Figure 5.3c). After seven days of differentiation, this had reversed, with significant reductions in *Oct4* and *Sox2* (two-way ANOVA, Sidak's multiple comparisons, $P<0.005$ and $P<0.0005$, respectively).

Alongside analysing the decrease in pluripotent specific transcription factors, we used a cardiomyocyte specific protein marker, cTnT, to ascertain successful differentiation. Cells began to contract spontaneously at days 7-10 following differentiation, indicating sufficient muscle protein structure to distort the cell membrane. Waves of contractility began to develop over the following week, whereupon any remaining non-beating cells would likely not develop contractions. Using a mouse monoclonal antibody to cTnT (ab8295), cells were fixed as a monolayer and underwent immunocytochemical staining. Contractile cells stained positively for cardiac troponin T after three weeks of differentiation (Figure 5.4). Differentiation was successful across the entire well, with large beating sheets clearly visible with light microscopy that stained positively for cTnT (Figure 5.4D).

To estimate the total area covered by cTnT positive, contractile cells, 18 random fluorescent images (by automated microscopy) were taken in individual wells from three independent differentiation batches (Figure 5.5A). Processing of these images using ImageJ software showed an average cTnT area coverage of 73.8±8.8%, 77.0±6.2% and 76.8±5.2% in three differentiations (Figure 5.5F).

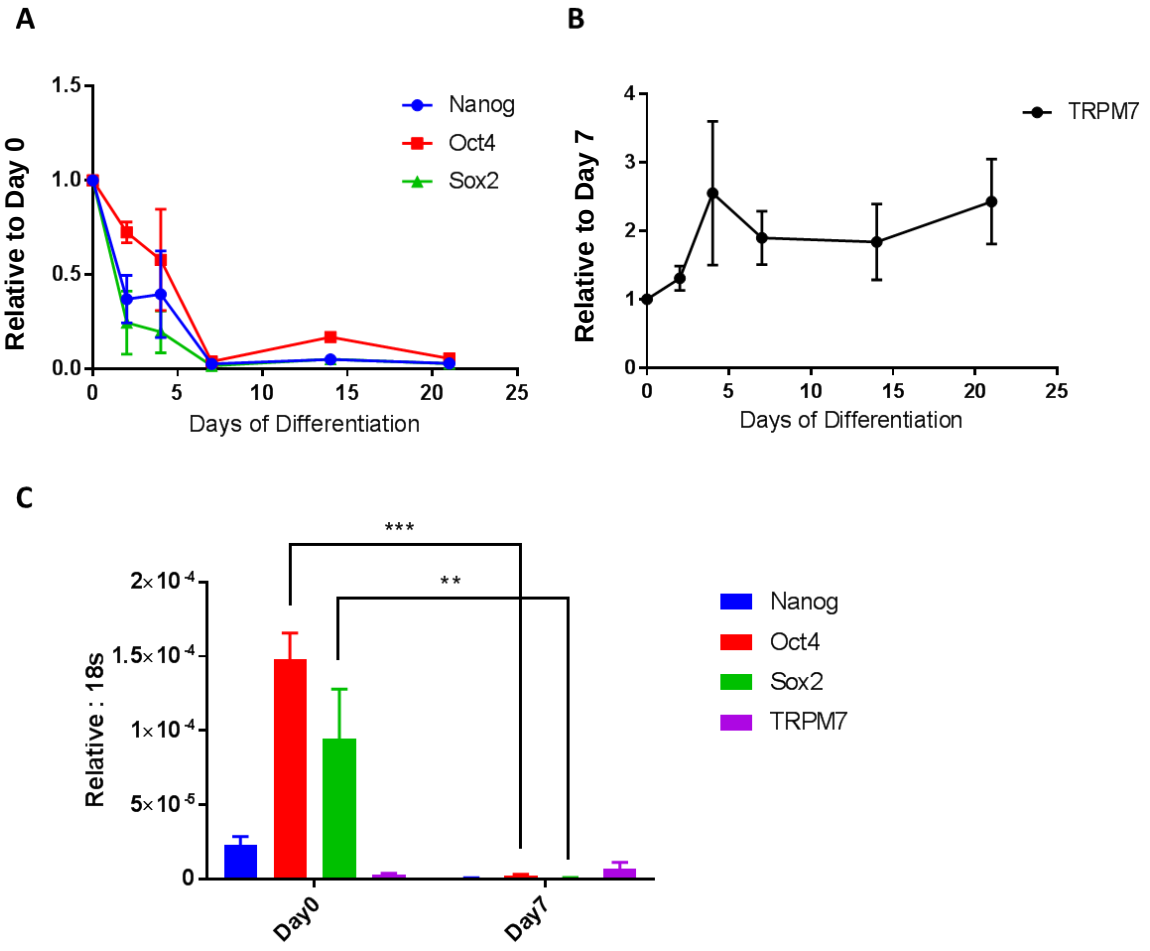


*Figure 5.3.* ***Quantitative PCR of pluripotency markers and TRPM7 during iPSC-cardiomyocyte differentiation. A*** *Quantification of pluripotent transcription factor mRNA signals at days 0, 2, 4, 7, 14 and 21 during differentiation.* ***B*** *Relative TRPM7 levels during monolayer cell differentiation towards a cardiac phenotype. All data was initially normalised to 18S RNA levels. Data is relative to signal observed in quiescent HS1M stem cells prior to differentiation.* ***C*** *Total mRNA gene expression of pluripotency factors and TRPM7 before differentiation (Day 0) and when the first beating clusters of cells become visible (Day7). ** = P<0.005, *** = P<0.0005. n = 3.*

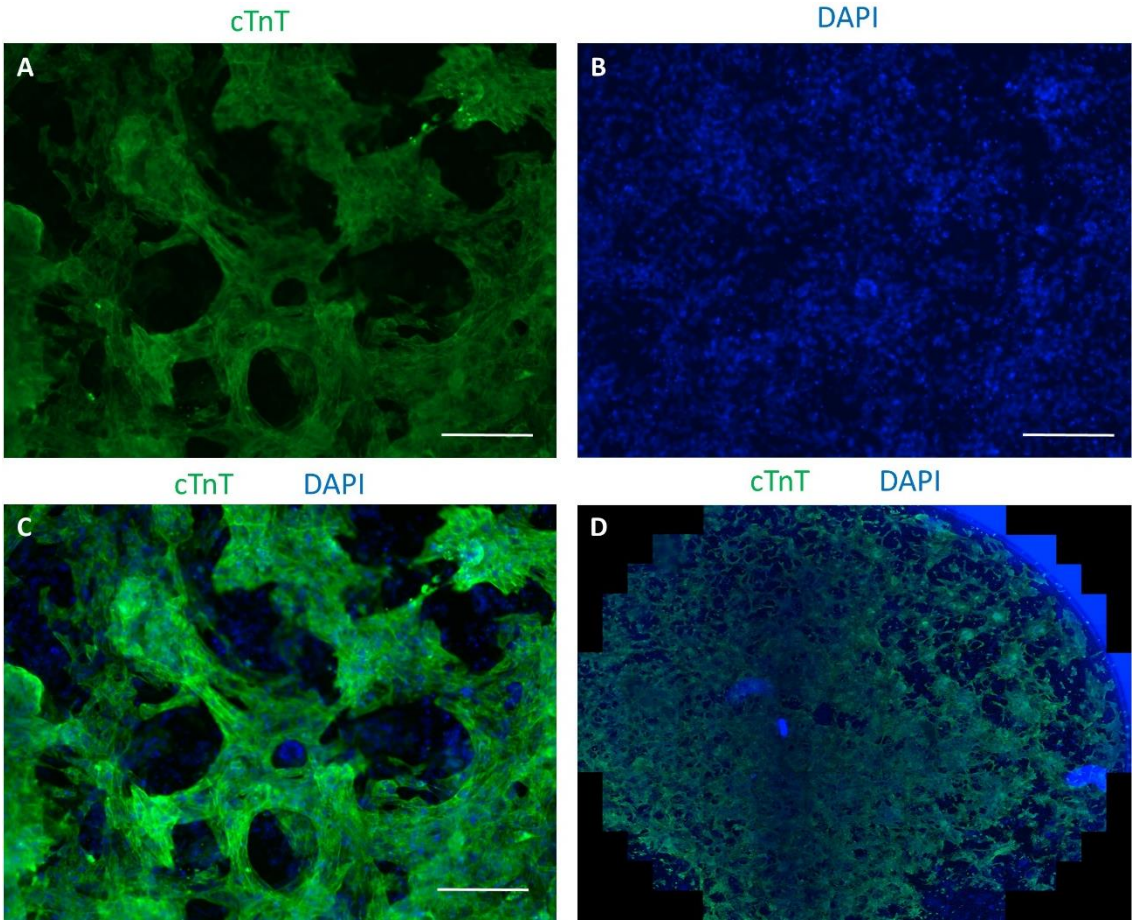


*Figure 5.4.* ***Cardiac Troponin T staining of human iPSC-derived cardiomyocytes 14 days after start of differentiation.*** ***A-C*** *Immunostaining of cTnT (A), DAPI (B) and a composite image (C) in previously contractile cell clusters following differentiation. Scale bar 80µm.* ***D*** *Stitched composite image of entire well from a 24-well plate (area = 1.9cm²) showing cardiac differentiation across the entire monolayer surface. Cells shown have been differentiating for 21 days.*

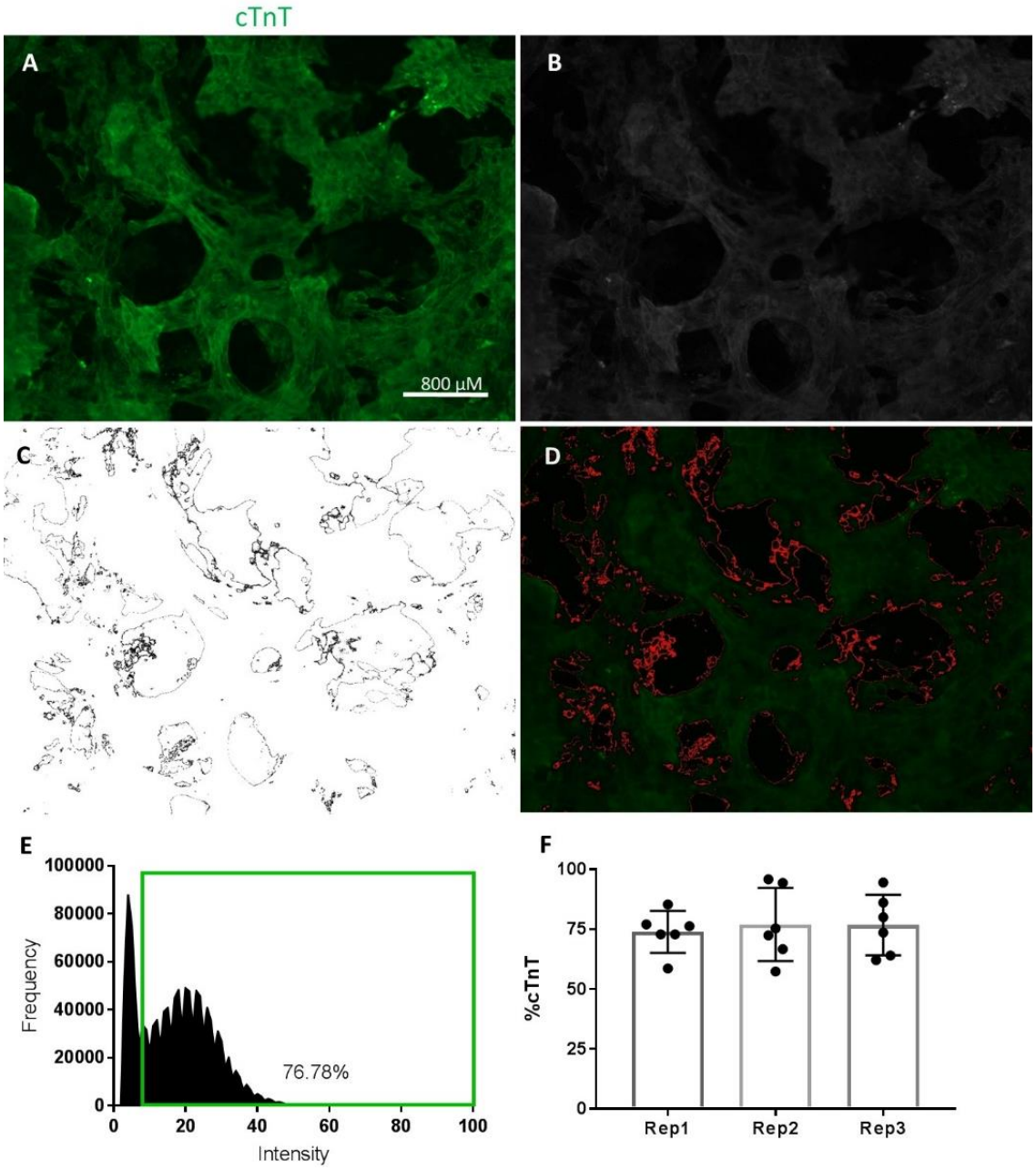


*Figure 5.5.* ***Quantification of cardiac purity following differentiation. A*** *Example image of cTnT staining used in Figure 5.4.* ***B*** *ImageJ converted black & white image.* ***C*** *Boundary of fluorescent intensity where positive staining meets negative.* ***D*** *Overlaid image showing positive cTnT staining (green) with automatic border (red) annotation.* ***E*** *Graphical representation of pixel fluorescent intensity, depicting positively stained fluorescent pixels (green box).* ***F*** *Six randomly taken images from each of three separate differentiations were assessed automatically for coverage of cTnT positive staining. Scale bar = 800µm. Cells shown have been differentiating for 21 days.*

## 5.4 Measuring a TRPM7-like Current in iPSC-CMs

After two weeks of differentiation, iPSC-CMs were dissociated and seeded onto glass coverslips. At 21-23 days post-differentiation cells underwent whole-cell patch-clamp analysis. Before cell-pipette contact was established, cells were perfused with Tyrode's solution to allow observation of spontaneous contraction, this allowed only cardiomyocyte-like cells to be patch-clamped. After establishing whole-cell electrical access, the extracellular solution was switched with a solution previously published to allow measurement of TRPM7 current in mouse cardiomyocytes (Methods 2.9.5) [213].

Linear, pA-currents were observed between -100mV and +100mV when recording began following membrane rupture. Similarly to heterologous cells transfected with *TRPM7*, after 5-10minutes of intracellular dialysis with EGTA/EDTA significant current-run up could be detected above +50mV (Figure 5.6A). At ±80mV, current density was significantly reduced by the addition of 10mM $Mg^{2+}$ to the extracellular solution (Figure 5.6B-C). Both 10mM $Mg^{2+}$ and 50µM 2-APB rapidly reduced outward current at +80mV to <5 pA/pF. Analysis of the effect of magnesium supplementation showed this inhibition was rapid and transient, with current density returning to its original peak when standard solution was returned to the bath (Figure 5.6D). Similarly, 50µM 2-APB present in the bath solution transiently attenuated current density at +80mV (Figure 5.6E).

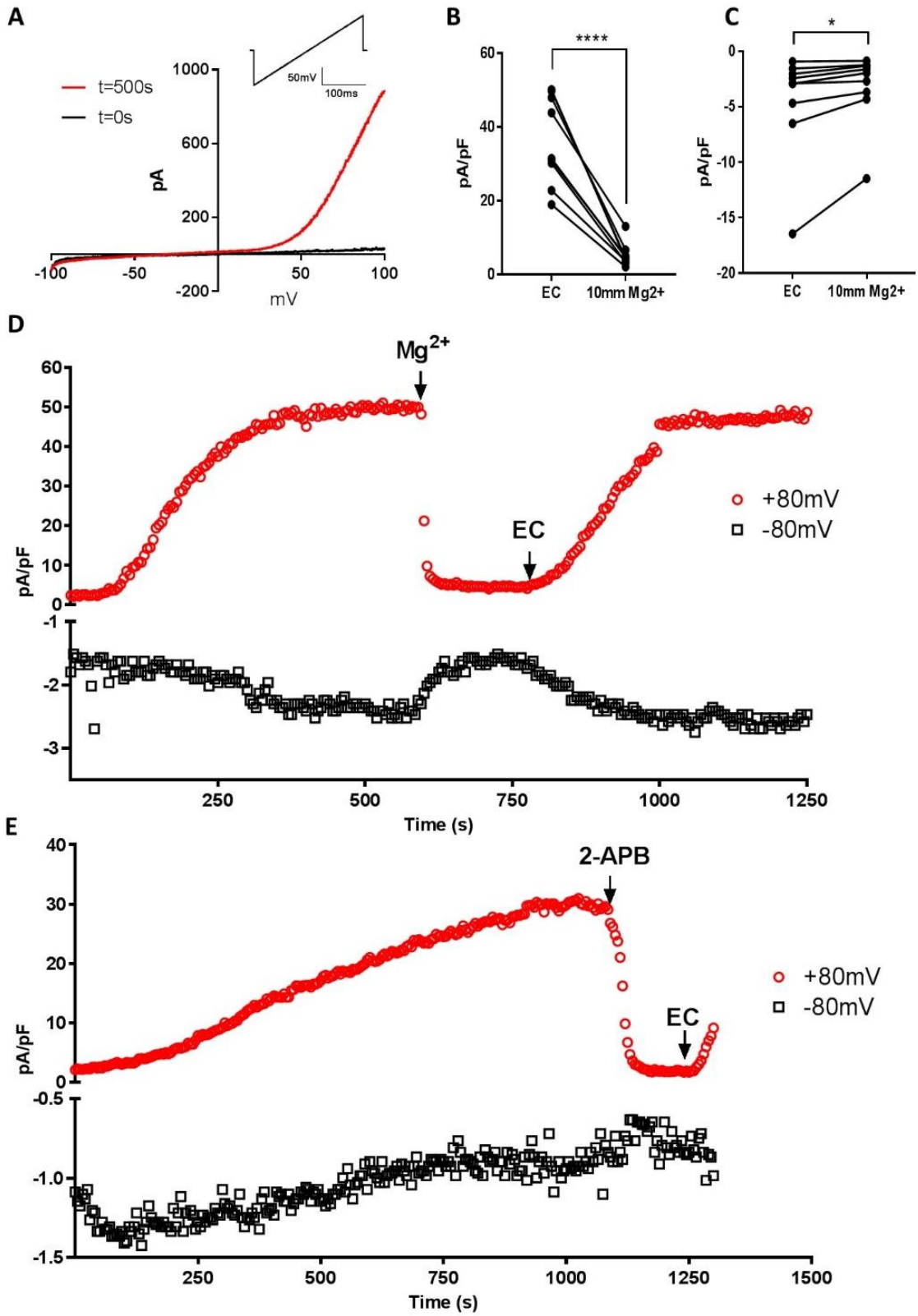


*Figure 5.6.* ***Measuring and characterising a TRPM7-like current in iPSC-CMs. A*** *Initial current recording (black) from cell following whole-cell membrane breakthrough in 21 day post differentiation iPSC-CM. Current measured after 500seconds of cell dialysis shows characteristic TRPM7 currents above +50mV. Inset -100mV to +100mV voltage ramp protocol.* ***B*** *Paired individual cell current measurements at +80mV peak during extracellular solution perfusion, and subsequent addition of 10mm $Mg^{2+}$.* ***C*** *Inward current recorded at -80mV in the same cells analysed in B.* ***D*** *Representative recording at ±80mV, showing current run-up and transient inhibition of 10mM $Mg^{2+}$.* ***E*** *Time course current measurements depicting the effect of 50μM 2-APB when included in the extracellular solution. All recordings were done in 20-23 day old iPSC-CMs at room temperature.*

## 5.5 iPSC-CM Electrophysiology and Analysing the Effect of TRPM7-siRNA Knockdown

To ascertain the electrical identity of contractile cells, cardiomyocytes derived from iPSCs after 21-23 days of differentiation were subjected to current-clamp analysis. Spontaneously contracting cells were identified using light microscopy before the whole-cell patch-clamp configuration was established. After recording spontaneous action potentials, action potentials were triggered at a frequency of 1Hz, using current pulses between 300-800pA for (depending on cell capacitance) over the course of one minute. The final action potential shape analysed was constructed from the final 10 action potentials recorded during the one minute protocol.

Electrophysiological analysis revealed that at days 21-23 post differentiation, the three main sub-types of human cardiomyocytes found in the heart were present (Figure 5.7D-F). The cellular identity of these cardiomyocytes appears similar to nodal-, atrial- and ventricular-like cardiomyocytes. These cells represent a board spectrum of contractile cellular identities due to the significant range of electrophysiological data, similar to that of previously published data [255]. These cells showed relative immaturity compared to adult cardiomyocytes, with small membrane capacitances (data not shown), disorganised structure and rounded shape (Figure 5.7A) and high resting membrane potentials (Figure 5.9D) [347]. Average APD was 138.7 ± 10.2ms, the lowest recorded at 68.3ms while the maximum was 238.5ms (Figure 5.7C).

To ascertain what role TRPM7 plays in mediating the electrophysiological development of cardiomyocytes, a TRPM7 targeting siRNA was transfected into iPSC-CMs at day 15 of differentiation before patch-clamp analysis. Current density in iPSC-CMs treated with TRPM7 siRNA was significantly reduced compared with control recordings at +80mV (Figure 5.8D, one-way ANOVA Tukey's comparison, $P<0.0001$). There was no significant difference between TRPM7 current at +80mV from wild-type iPSC-CMs treated with 10mM magnesium and those

transfected with TRPM7 siRNA (P=0.84). Although there was a decrease in average inward current measured at -80mV in cells transfected with TRPM7 siRNA, this was not statistically significant (Figure 5.8E, P=0.65).

Whole-cell current-clamp recordings were analysed from differentiated cells transfected with either a TRPM7 targeting siRNA or a scrambled siRNA. After gaining electrical access to the cell and allowing time for dialysis (2 minutes), triggered action potentials were recorded for one minute at a rate of 1Hz. From these recordings, action potential duration, resting membrane potential (RMP), minimum diastolic potential (MDP), peak voltage and upstroke velocity were calculated. Although there was an increase in mean APD following TRPM7 siRNA treatment compared to scrambled siRNA, this was not significant (P=0.89) due to the high variability of APD in transfected iPSCs: 196 ± 29.6ms (Figure 5.9A). There was no significant difference in RMP, MDP, peak voltage and upstroke velocity between wild-type iPSC-CMs and those treated with either scrambled or TRPM7 targeting siRNA (Figure 5.9B-E).

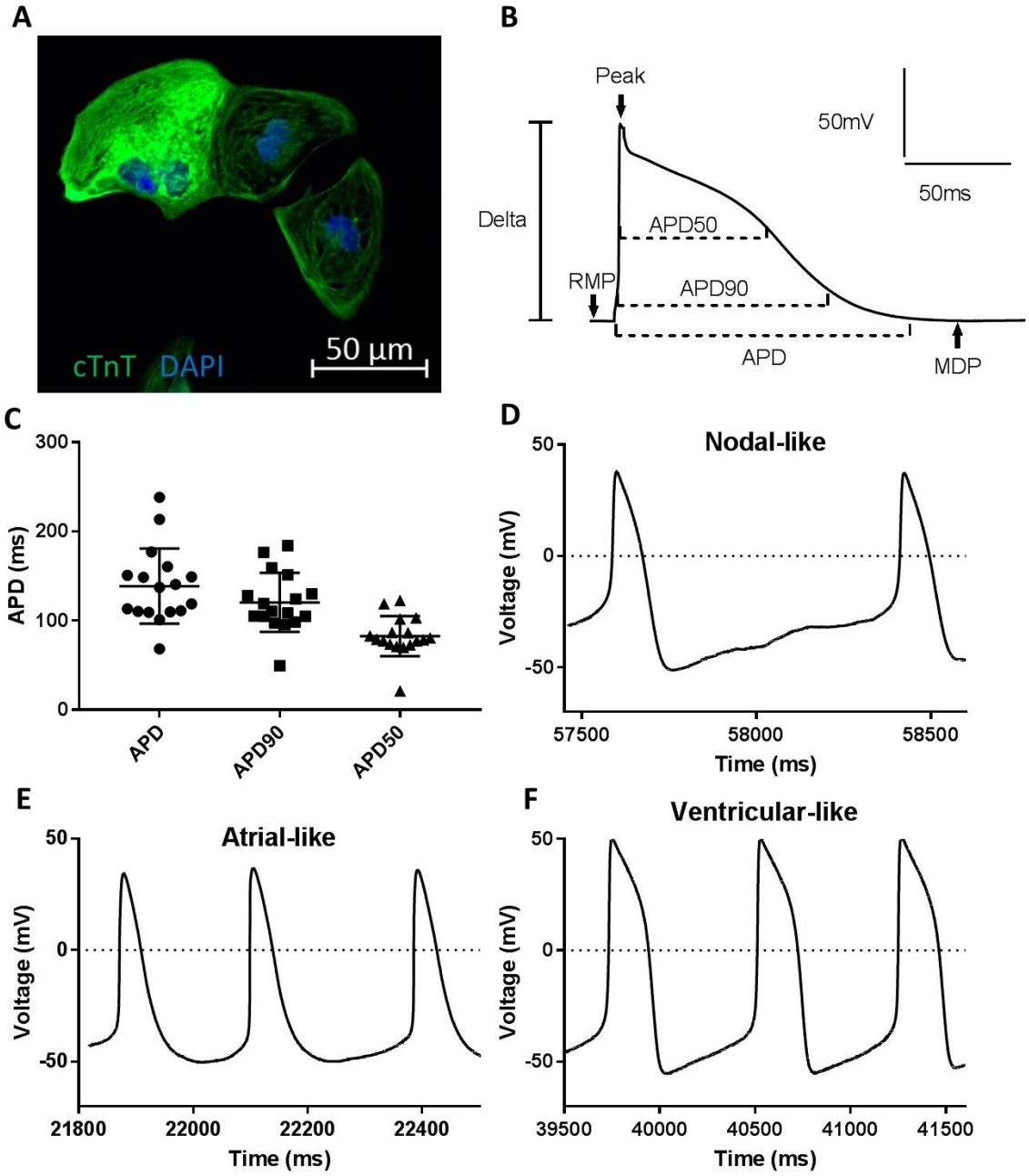


*Figure 5.7.* ***Appearance and electrophysiological properties of iPSC-CMs. A*** *Staining of iPSC-CMs at day 21 with cTnT and DAPI.* ***B*** *Schematic of where different measurements were obtained from action potential recordings. C Analysis of triggered action potential duration from three individual differentiations. Data shown as mean ±SEM. All recordings were done in 20-23 day old iPSC-CMs at room temperature.* ***D-F*** *Current-clamp recordings from spontaneously beating cells revealed a diverse array of action potential morphologies. We observed nodal, atrial and ventricular-like recordings. n = 17.*

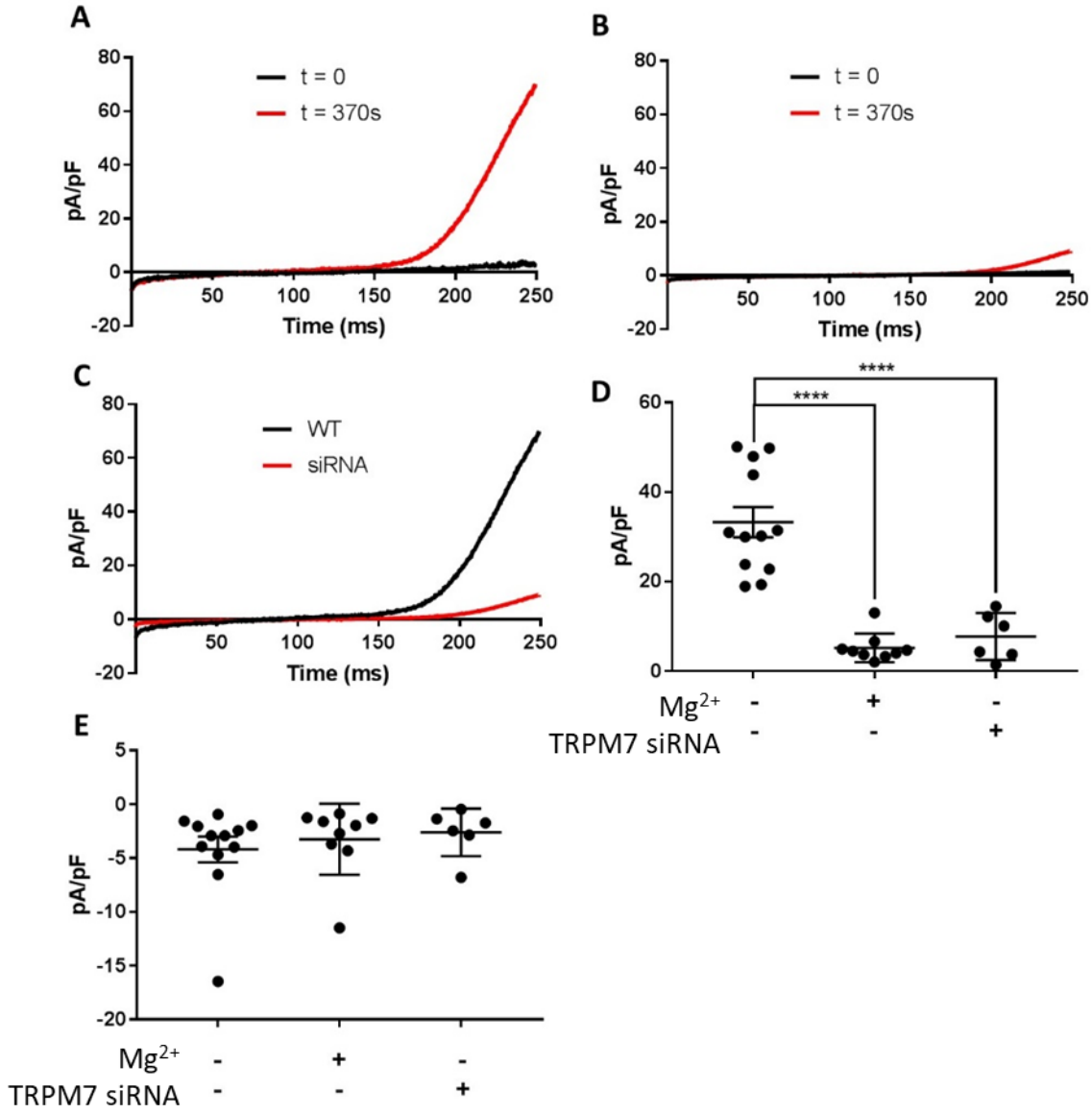


*Figure 5.8.* ***The effect of TRPM7 siRNA knockdown on TRPM7 current in iPSC-CMs. A*** *TRPM7 current trace from untransfected cell at membrane break-in (black) and after run-up (red).* ***B*** *Current recorded from iPSC-CM transfected with TRPM7 siRNA before (black) and after (red) run-up.* ***C*** *Comparison of TRPM7 currents after run-up in iPSC-CMs with (black) or without TRPM7 siRNA transfection (red).* ***D*** *TRPM7 current measured at +80mV following current run-up in control iPSC-CMs and the effect of magnesium addition or transfection with TRPM7 siRNA.* ***E*** *Inward -80mV current measured from the same cells as in D. **** = P<0.0001. Data shown as mean ±SEM. All recordings were done in 20-23 day old iPSC-CMs at room temperature. N = 6-12.*

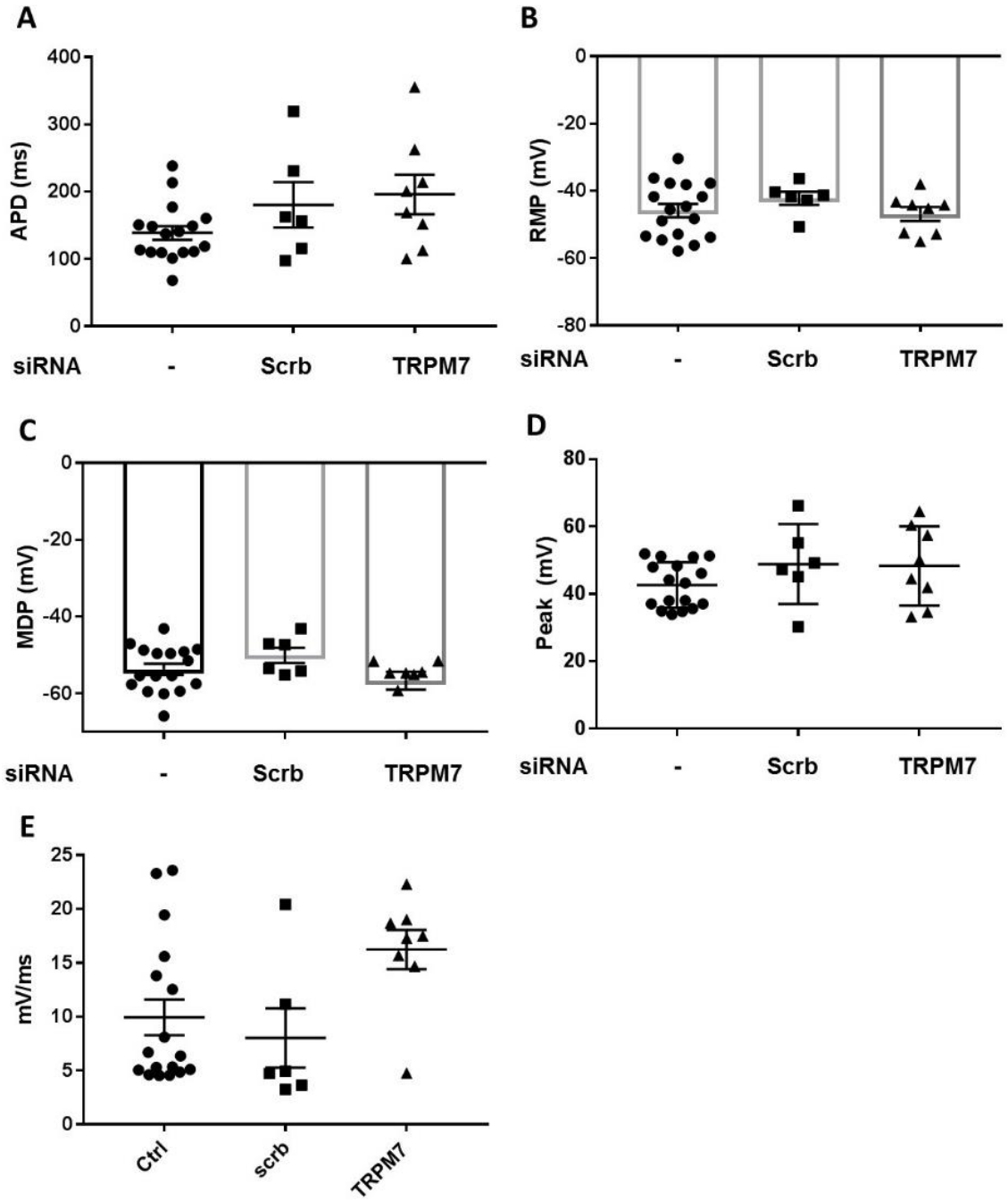


*Figure 5.9.* ***Action potential analysis of iPSC-CMs and the effect of TRPM7 siRNA knockdown. A*** *Triggered action potential duration in iPSC-CMs.* ***B*** *Resting membrane potential recorded immediately before triggered action potential.* ***C*** *Maximum diastolic potential.* ***D*** *Peak membrane voltage achieved following current pulse.* ***E*** *Upstroke velocity in control or transfected iPSC-CMs. Data shown as mean ±SEM. All recordings were done in 20-23 day old iPSC-CMs at room temperature. Scrb = Scrambled.*

## 5.6 Discussion

We used an *in vitro* model of cardiac development to confirm whether TRPM7 can be found in differentiating cardiomyocytes. Secondly, if present we wanted to attempt to model possible haploinsufficiency in this system, mimicking the effect of TRPM7 reduction due to the p.G179V and p.T860M variants.

Since 2001, cardiomyocyte differentiation protocols have existed to allow the targeted creation of these cells from stem cells [253]. These methods can range from embryoid body formation, protein supplementation, transfection or small molecule treatment [248,253,255,348]. The TRPM7 ion channel has been shown to be required for successful mouse cardiac development and maintaining automaticity [212,213]. We decided to use an iPSC-CM model of *in vitro* cardiac development to study the temporal expression of TRPM7 in 'human' cardiogenesis and record TRPM7 currents in immature cardiomyocytes. Lastly we wanted to ascertain the importance of *TRPM7* expression in the maturation of iPSC-CM electrophysiology.

We cultured iPSC cells using growth factor-reduced Matrigel for several weeks before adapting a recently published differentiation protocol to produce cardiomyocytes [255]. This procedure was relatively simple and inexpensive, using RPMI media supplemented with albumin and ascorbic acid alongside two small molecular interactors of the Wnt pathway. This is in contrast to other published differentiation techniques which require expensive hormone supplementation [254,296]. Reported extensively in the 1990s in the context of embryonal cancer, TRA-1-60 is a commonly used cell surface marker for pluripotency [346,349,350]. Immunocytochemical staining for TRA-1-60 using a monoclonal antibody showed all cells were positive, albeit in a highly heterogeneous manner. We found that reduced TRA-1-60 staining correlated with condensed DAPI staining, in-line with similar staining reported elsewhere in iPSCs derived from different cell lines [254,344,345]. These compact nuclei denote the early phases of mitotic cell division, before anaphase separates sister chromatids. Transcriptionally, cultured iPSCs were pluripotent due to their expression of *Nanog, Oct4* and *Sox2,* DNA-binding proteins

known to maintain cells in a quiescent, undifferentiated state [346]. Within seven days of differentiation transcription of these genes was clearly repressed, with significant reductions in mRNA levels. Of note, as cells differentiated, there was a notable increase in TRPM7 expression. TRPM7 has been investigated in mouse ESCs whilst investigating the function of the C-terminal kinase, but our data noted a clear trend for increased *TRPM7* transcription in differentiating human stem cells toward a cardiac phenotype [223].

Spontaneously beating cells were visible after seven days of differentiation, consistent with the published literature [255]. Over the course of two more weeks, beating clusters developed and synchronous waves of contraction were clearly visible across the cell monolayer surface. Initially we attempted to quantify the efficiency of cardiac differentiation by counting the proportion of cTnT positive cardiomyocyte cells in the population using flow cytometry. However due to the syncytial nature of the cell clusters, contractile clusters of cells rarely separated from the culture chamber or each other, despite extensive TrypLE treatment (>30minutes at 37˚C) and mechanical dissociation using a pipette. Non-contractile cells rapidly detached from the Matrigel surface, while previously beating clusters formed large clumps that could not be fed into the flow cytometer. Instead we used fluorescent analysis of cTnT stained cells using a microscope that randomly took four images per well. We found that cTnT positive cells covered over 75% of the culture surface, with only small areas of negative staining present with DAPI positive nuclei. This in in keeping with published literature showing that cardiac differentiation using CDM3 media produces relatively 'pure' populations of cardiac cells. This is likely due to iPSC-cardiomyocytes enduring conditions where metabolites are scarce, recently highlighted by their ability to survive in media depleted of glucose and glutamine but supplemented with lactate [351].

Cardiomyocytes seeded onto coverslips underwent whole-cell patch-clamp to measure TRPM7 current. In all contractile cells analysed, we found a characteristic 'run-up' of current over 5-10 minutes as the cell's magnesium was chelated by the intracellular solution. This

current was sensitive to inhibition by extracellular magnesium or 50μM 2-APB, confirming its identity as TRPM7. This result was in-line with our qPCR data that suggested *TRPM7* was expressed in these cells. Although TRPM7 current has been measured in the setting of the diseased adult myocardium or developing mouse heart, this iPSC-CM data suggest that that *TRPM7* is likely to be expressed during human heart development [213,237]. In chapter 3 we showed two CICUS *TRPM7* variants (p.G179V and p.T860M) that significantly reduced *TRPM7* protein expression and whole-cell ion channel conductance. Total knockout of *TRPM7* in mouse cardiomyocytes leads to embryonic lethality; haploinsufficiency due to reduced *TRPM7* ion channel expression could precipitate unexplained stillbirth.

Alongside TRPM7 current measurements, current-clamp recordings of contractile iPSC-CMs illustrated a heterogeneous mix of different electrophysiological identities. Even between cells differentiated on the same coverslips, we recorded atrial, ventricular and nodal-like action potentials. Our data found that all iPSC-CMs contain a TRPM7-like current, implicating the channels' presence in the development of all cardiomyocyte subtypes.

Transfection of cells with siRNA has been used extensively to test the effect of post-transcriptional knockdown of mRNA. We found that siRNA targeted to TRPM7 significantly reduced ion channel currents measured in cells but did not adversely affect differentiation of contractile cells and did not lead to a change action potential characteristics. While *TRPM7* knockout has been shown to significantly influence electrophysiology in developing mice, it is through transcriptional regulation of specific ion channels that its influence is seen, not through direct movement of ions across the plasma membrane. Only in the diseased atrial myocardium, where *TRPM7* gene expression increases, is it thought to contribute significantly to calcium ion influx in fibroblasts. We transfected cells with *TRPM7* siRNA 5-6 days before action potential and current measurements (day 20-22). We measured significantly lower TRPM7 current, demonstrating successful knockdown. However, action potentials from transfected cells were unchanged, it may be that the developmental timing of *TRPM7* knockdown is crucial in adversely

affecting the regulation of cardiomyocyte ion channel gene expression. Of importance, conditional knockout of *TRPM7* in embryonic mice before E9 is lethal to the embryo due to congestive heart failure, however deletion later than E13 produces viable mice with heart size and function similar to wild-type mice [213]. Although *TRPM7* knockout in adult mice has shown to dysregulate certain ion channel gene expression in SA nodal cells, these phenotypes are mild in comparison to the effect of early embryonic knockout. In the future, to test the role of *TRPM7* in regulating human cardiogenesis using an iPSC-CM model, siRNA transfection at specific time points post-differentiation would provide insights into when *TRPM7* is involved in human cardiac development, and how haploinsufficiency of *TRPM7* could adversely affect foetal gestation.

# 6 Conclusion - Remarks and Future Work

Unexplained stillbirth is classified as a baby born dead after 24 weeks of gestation, where no cause of death can be found after a full post-mortem analysis. Between 15-30% of stillbirths are ultimately classified as unexplained [9,20]. Previously, the CICUS study sequenced 35 genes in 70 unexplained stillbirth cases. Variants in these genes were known to cause LQTS or were either associated with cardiac ion channelopathies or discovered from GWASs of the QT interval in the general population. The CICUS study reported several predicted damaging genetic variants – four within the *TRPM7* gene, five within *AKAP9* [206]. TRPM7 is a non-selective ion channel expressed ubiquitously and is required for mammalian heart development [213]. AKAP9 is responsible for coupling β-adrenergic stimulation to increased outward potassium current in cardiomyocytes and damaging variation is thought to cause LQT11 [131]. The aim of this thesis was to test whether the nonsynonymous variants in *TRPM7* and *AKAP9* perturb the function of these WT proteins, potentially being a risk factor or cause of stillbirth.

Using both HEK293 and CHO-K1 heterologous cell lines, TRPM7 current was recorded and inhibited with both $Mg^{2+}$ and 2-APB. When transfected into CHO-K1 cells, p.G179V TRPM7 significantly decreased outward current density compared to wild-type channels. The second variant, p.R494Q, markedly increased both outward and inward currents. Two other variants, p.T860M and p.E1205G had no influence on current density recordings compared to wild-type. All four variants did not affect magnesium inhibition of the current. When transfected into HEK293 cells, both p.G179V and p.T860M significantly reduced outward current density, while p.R494Q current was similar to that recorded from wild-type TRPM7. Quantification of mRNA levels following transfection in HEK293 cells found equal levels of transcribed *TRPM7* mRNA despite large differences in recorded TRPM7 current. Western blot analysis of translated protein expression found full-length wild-type, p.R494Q and p.T860M channel present in transfected HEK293 cell lysates. Transfected HEK293 cells treated overnight with 26S proteosomal inhibitor MG132 revealed that p.T860M TRPM7 was being degraded rapidly, as after treatment a faint

band was present in western blots. To ascertain whether p.G179V or p.T860M showed a dominant negative effect on wild-type TRPM7 channel function we transfected both wild-type and variant channel simultaneously. No dominant negative effect was observed, leading us to believe that both variants lead to haploinsufficiency due to rapid proteosomal degradation in the case of p.T860M and lack of translation of p.G179V. Analysis of an apoptosis assay and confocal imaging following transfection with TRPM7 variants found no difference between mutants and wild-type channel. Further statistical analysis of rare predicted damaging variants in the CICUS study found that *TRPM7* contained a significantly greater number of predicted damaging variants compared to the number found in a randomly selected cohort from the 1000g study database.

These data point towards a pathogenic role of p.G179V and p.T860M TRPM7 by perturbing ion channel function. Both variants are very rare in public databases (<0.0001 allele frequency), while p.T860M resides within a key transmembrane domain. Whilst this suggests perturbed function of TRPM7 is due to these genetic variants, there are further opportunities to explore how this can lead to unexplained stillbirth. Recent papers have shown how important TRPM7 ion channels are in regulating zinc cellular homeostasis [223,305]. TRPM7 is now believed to be a key channel responsible for inward zinc uptake. Discovering whether these mutations influence TRPM7's ability to conduct zinc across the plasma membrane may give mechanistic insights into a possible pathogenic mechanism [226]. This is of importance in this setting, due to the increasing knowledge of how zinc affects heart physiology and pathology [305,352].

As mentioned previously, a large proportion of TRPM7 protein resides within unique intracellular vesicles [305]. Shown to act as an organelle that accumulates zinc, these vesicles release this zinc in response to reactive oxygen species. This may represent a network of protective membranes that buffer cytoplasmic zinc; TRPM7 may also allow the targeted release of zinc to specific cellular locations akin to how the sarcoplasmic reticulum sequesters and releases calcium in cardiomyocytes. This provides another possible setting to further investigate

how TRPM7 variants perturb the function of this ubiquitous ion channel. Genetic variants in *TRPM7* that do not perturb its expression or transport to the plasma membrane could disturb its ability to conduct zinc across the TRPM7 vesicle network. Alongside the central role zinc plays in allowing DNA binding protein to function; deficiency in zinc has been associated with DNA damage and apoptosis [353].

Apoptosis was investigated here under basal conditions, investigating whether transcription of mutant TRPM7 ion channels induces cell death. TRPM7 has been implicated in inducing apoptosis by activating multiple pathways in a cell-specific manner [235,354,355]. Ideally, stable cell-lines expressing *TRPM7* CICUS variants could be generated, and selective activation of apoptosis pathways using distinct mechanisms performed (Fas activation, reactive oxygen species exposure or serum deprivation for example). Spatial and temporal control of apoptosis during development (especially in the myocardium where uniform cellular orientation and connection are paramount) is vital to ensure the human foetus can survive gestation.

To analyse how full-length AKAP9 couples β-adrenergic stimulation to increased outward IKs current, and whether CICUS variants influenced this, we used a heterologous CHO-K1 cell system. All previously published cell data investigating LQT11 variant p.S1570L have involved the small *AKAP9* isoform *Yotiao*; no work as yet has focussed on the full-length protein. It has been shown in this thesis and elsewhere, that HEK293 cells expressing IKs respond to β-adrenergic stimulation (isoprenaline or forskolin) *in vitro* [244]. We found significant increases in peak and peak tail currents after forskolin treatment, a leftward shift in voltage activation and a slower rate of deactivation. Publically available data sets show that full length *AKAP9* mRNA is present in HEK293 cells, whilst peptides corresponding to the C-terminus of *AKAP9* are found in human foetal cardiac lysates. Future experiments using siRNA targeting short or full length AKAP9 (and other AKAPs) could help isolate the isoforms responsible for IKs β-adrenergic coupling in HEK cells. This response to β-adrenergic stimulation has been shown to mimic what is observed in cardiomyocytes [244]. Whilst robust and reproducible IKs currents were observed

from transiently transfected CHO-K1 cells, these did not respond to forskolin treatment. This data demonstrates that CHO-K1 cells lack the sufficient protein scaffolding/macro-molecular complex to couple activated PKA to IKs phosphorylation. Crucially, co-transfection with a full length *AKAP9* plasmid in these cells rendered IKs currents susceptible to β-adrenergic stimulation through forskolin treatment.

Unfortunately we were only able to generate two of the five *AKAP9* variants (p.D1507H and p.A3043T) sequenced from the CICUS project despite numerous rounds of site-directed mutagenesis. Following mutagenesis, bacterial transformation of the three remaining variants was attempted using three distinct strains of competent cells. This failure may be due to total DNA degradation during the reaction or failure to transform the resulting reaction. The *AKAP9* expression vector exceeds 17,000bp, presenting a large construct to manipulate. Future attempts to create the remaining three variants will require a different mutagenesis strategy. Either redesigning the primers (likely elongation), or using restriction endonucleases to remove the target fragment and conduct site-directed mutagenesis on a smaller section of DNA.

When CHO-K1 cells were transfected with *KCNQ1-GFP/KCNE1* alongside p.D1507H *AKAP9*, the IKs current remained responsive to treatment with 10μM forskolin. When p.A3043T *AKAP9* was co-transfected instead, IKs current in these cells did not respond to prolonged forskolin treatment in any cells that underwent perforated patch-clamp analysis. While the p.D1507H AKAP9 protein appears capable of coordinating activated catalytic PKA to KCNQ1/KCNE1 at the membrane, p.A3043T AKAP9 does not. This may either be due to a lack of expression, or the variant renders the protein incapable of co-ordinating PKA phosphorylation. Although the *AKAP9* vector was N-terminally FLAG tagged, western blots using a FLAG or AKAP9 specific antibody were unsuccessful after several attempts (data not shown). Proteins of this size (>400kDa) may find it difficult to migrate into the resolving gel, and subsequently exit the gel to bind the PVDF membrane for western analysis. The only published western blot data of full length AKAP9 was obtained using a non-commercially obtainable rabbit anti-AKAP9 antibody

in HUVEC cell lysates [356]. Despite having access to HUVEC protein lysates, we were unable to see any AKAP9 protein using western blot (not shown). Immunocytochemical analysis of transfected cells would provide data to support successful translation and also reveal the sub-cellular localisation of WT AKAP9. By overlaying KCNQ1-GFP and AKAP9 fluorescent signals in these cells, their localisation at the plasma membrane, and the possible perturbation of their interaction by p.A3043T could be investigated. Phosphorylation of KCNQ1 to augment IKs requires interaction with the cytoskeleton and AKAP9 deletion has been shown to affect microtubule dynamics [325,356]. The effect of colchicine treatment (inhibiting microtubule polymerisation) on CHO-K1 cells transfected with AKAP9 would demonstrate how important this interaction is when full length AKAP9 is present. Similar experiments in iPSC-CMs would provide a more physiologically relevant platform, but the well-documented diverse expression profiles of the ion channel genes in these immature cells make this a difficult prospect [255]. The expression of *KCNQ1* in iPSC-CM has been shown to be highly cell line dependant [287].

We demonstrated robust *AKAP9* gene expression in all four adult human heart chambers; where mRNA levels were highest in the left ventricle. Using two qPCR probes measuring both long isoform and total *AKAP9* gene expression we showed that in the human heart approximately 30% of mRNA is the full length 12471bp transcript. Therefore, while Kass et al. demonstrated the presence of Yotiao in human cardiac homogenates, here we show that the full length transcript is present in the human heart and is capable of coupling IKs to β-adrenergic stimulation. Further investigation into which *AKAP9* isoforms contribute to IKs/β-adrenergic coupling in the human cardiomyocyte is required. The majority of LQTS1 patients have cardiac events that occur during β-adrenergic stimulation, highlighting how this molecular coupling is a key component of cardiac arrhythmia [54]. Here we identified a loss-of-function genetic variant that uncouples this signalling pathway, representing not only a possible cause of unexplained stillbirth, but a second genetic variant that can cause fatal arrhythmia in this gene.

The importance of TRPM7 in mouse development has been well studied [213,214]. Using iPSC-derived cardiomyocytes we measured the temporal expression of TRPM7 during an *in vitro* model for cardiogenesis. One week after differentiation, the expression of *Nanog*, *Oct4* and *Sox2* was significantly reduced. As cells transitioned towards an immature cardiomyocyte-like, contractile phenotype, *TRPM7* gene expression increased, doubling by 21 days post-differentiation. We were able to measure characteristic TRPM7 currents when cells were subjected to whole-cell patch-clamp analysis. While these currents were not observed initially during membrane break-in; as divalent cations were chelated by EGTA/EGTA in the solution, characteristic currents were measured. These currents were inhibited by the addition of extracellular magnesium and 2-APB. Every cell had TRPM7 current that could be inhibited by either of these treatments.

Current-clamp recordings of action potentials in contractile cells revealed a diverse electrophysiological phenotype. Therefore, while cells may be nodal-like, atrial-like or ventricular-like, all subsets of developing immature cardiomyocytes have significant numbers of active TRPM7 channel present in the plasma membrane. We were able to show robust knockdown of TRPM7 using siRNA, but there was little evidence to suggest this significantly perturbed the action potential morphology of the iPSC-CMs analysed. Previous work in mice has shown how critical the timing of TRPM7 insufficiency has on successful cardiac embryonic gestation [213]. By transfecting siRNA at specific points of differentiation, the temporal importance of TRPM7 expression in cardiogenesis could be elucidated. Furthermore, CRISPR-cas9 knock-in or base editing technology could be used to genetically construct transgenic p.G179V and p.T860M *TRPM7* iPSC cell lines. This would provide a platform to ascertain how haploinsuffiency of *TRPM7* deleteriously influences gene expression, morphology and electrophysiology in the developing heart.

While this study focused on functionally investigating genetic variants found in the CICUS study within *AKAP9* and *TRPM7*, there were a large numbers of predicted damaging

variants in other genes. Many of these could warrant further follow-up experimentation to ascertain whether they are functionally damaging and potential genetic causes of unexplained stillbirth. For example, we identified a novel genetic variant in the cAMP response element binding protein – binding protein (*CREBBP*) gene, which we found in five unidentified stillbirth cases. The CREBBP protein is pivotal in the transcriptional regulation of numerous cAMP-responsive genes [357]. Harmful genetic mutations in *CREBBP* are known to cause Rubinstein-Taybi syndrome and acute lymphoblastic leukaemia [358-360]. We also found three novel variants in three separate cases within the *KCNAB2* gene. The gene encodes the voltage-gated, shaker-related potassium channel beta-2 subunit. Mice that do not express *KCNAB2* have been shown to have shortened lifespans, seizures and cold swim-induced tremors [361].

Unfortunately, during the sequencing stage of the CICUS study we were unable to obtain parental DNA access. Therefore it is impossible to know whether the variants found are inherited from the parents or are *de novo* mutations unique to the foetus. While we found deleterious genetic mutations in both *TRPM7* and *AKAP9*, interpreting the data in a clinical setting is difficult due to lacking parental genetic data. Genetic variation that causes unexplained stillbirth is more likely to occur *de novo*, as hereditary mutations that lead to stillbirth will struggle to persist from generation to generation.

All variants investigated in the CICUS study and throughout this thesis were nonsynonymous variants – they are amino acid altering changes within exons. The affordability of large scale whole-exome and whole-genome sequencing projects is rapidly increasing, and several papers have demonstrated the power of these approaches across a number of different fields [269,362]. Sequencing all transcribed exons from unexplained stillbirth cases would allow mutational analysis of missense variants in over 19,000 genes. This greatly increases the scope for detecting predicted damaging variants or copy-number variation in unexplained stillbirth cases. Recent work by Bagnall et al. found a clinically relevant cardiac mutation in 27% of unexplained SCD cases where exome-sequencing was performed [269]. The advantage of whole-

genome sequencing allows the identification of pathogenic synonymous variants. Non-coding variation has been implicated in reducing the incidence of ischaemic heart disease, increasing the risk of macular degeneration and can lead to congenital heart disease [363-365]. Intronic regions, especially promotors and enhancers can harbour genetic variation, however their effect is more difficult to predict as they do not directly alter protein structure, but instead act through DNA/RNA-binding protein interactions. Exome- and genome-wide studies are able to produce vast quantities of genetic data, however their usefulness is reduced by the lack of efficient methods to prioritise which variants are most likely to be damaging [366].

Future work in this field should sequence parental (if possible), alongside pro-band DNA, allowing the elimination of any inherited (and presumed non-causal) variants. This would limit the analysis to unique *de novo* variants, and greatly enhance the likelihood of identifying causal genetic variants that lead to unexplained stillbirth. Ideally this would be coupled with an increased number of sequenced cases, to find more predicted damaging mutations that can be functionally analysed.

# 7 References


1 Ronsmans, C. & Graham, W. J. Maternal survival 1 - Maternal mortality: who, when, where, and why. *Lancet* **368**, 1189-1200, doi:Doi 10.1016/S01406736(06)69380-X (2006).

2 Lawn, J. E., Cousens, S., Zupan, J. & Team, L. N. S. S. 4 million neonatal deaths: when? Where? Why? *The Lancet* **365**, 891-900 (2005).

3 Jones, G. *et al.* How many child deaths can we prevent this year?. *The Lancet* **362**, 65-71 (2003).

4 Norris, T., Manktelow, B. N., Smith, L. K. & Draper, E. S. Causes and temporal changes in nationally collected stillbirth audit data in high-resource settings. *Semin Fetal Neonatal Med* **22**, 118-128, doi:10.1016/j.siny.2017.02.003 (2017).

5 MacDorman, M. F., Kirmeyer, S. E. & Wilson, E. C. Fetal and perinatal mortality, United States, 2006. *Natl Vital Stat Rep* **60**, 1-22 (2012).

6 Lawn, J. E. *et al.* Stillbirths: Where? When? Why? How to make the data count? *The Lancet* **377**, 1448-1463 (2011).

7 Blencowe, H. *et al.* National, regional, and worldwide estimates of stillbirth rates in 2015, with trends from 2000: a systematic analysis. *Lancet Glob Health* **4**, e98-e108, doi:10.1016/S2214-109X(15)00275-2 (2016).

8 Zhu, J. *et al.* Sociodemographic and obstetric characteristics of stillbirths in China: a census of nearly 4 million health facility births between 2012 and 2014. *Lancet Glob Health* **4**, E109-E118, doi:10.1016/S2214-109x(15)00271-5 (2016).

9 Bukowski, R. *et al.* Causes of Death Among Stillbirths. *Jama-J Am Med Assoc* **306**, 2459-2468, doi:DOI 10.1001/jama.2011.1823 (2011).

10 Horn, L. C., Langner, A., Stiehl, P., Wittekind, C. & Faber, R. Identification of the causes of intrauterine death during 310 consecutive autopsies. *Eur J Obstet Gynecol Reprod Biol* **113**, 134-138, doi:10.1016/S0301-2115(03)00371-3 (2004).

11 Flenady, V. *et al.* Major risk factors for stillbirth in high-income countries: a systematic review and meta-analysis. *The Lancet* **377**, 1331-1340 (2011).

12 Feldman, G. B. Prospective risk of stillbirth. *Obstet Gynecol* **79**, 547-553 (1992).

13 Yudkin, P. L., Wood, L. & Redman, C. W. G. Risk of Unexplained Stillbirth at different gestational ages. *The Lancet* **1**, 1192-1194 (1987).

14 Flenady, V. *et al.* An evaluation of classification systems for stillbirth. *BMC Pregnancy Childbirth* **9**, 24, doi:10.1186/1471-2393-9-24 (2009).

15 Gravett, M. G., Rubens, C. E., Nunes, T. M. & Group, G. R. Global report on preterm birth and stillbirth (2 of 7): discovery science. *BMC Pregnancy Childbirth* **10 Suppl 1**, S2, doi:10.1186/1471-2393-10-S1-S2 (2010).

16 Silver, R. M. *et al.* Work-up of stillbirth: a review of the evidence. *Am J Obstet Gynecol* **196**, 433-444, doi:10.1016/j.ajog.2006.11.041 (2007).

17 Oyelese, Y. & Ananth, C. V. Placental abruption. *Obstet Gynecol* **108**, 1005-1016, doi:10.1097/01.AOG.0000239439.04364.9a (2006).

18 Gagnon, R. Placental insufficiency and its consequences. *Eur J Obstet Gyn R B* **110**, S99-S107, doi:10.1016/S0301-2115(03)00179-9 (2003).

19 Varli, I. H. *et al.* The Stockholm classification of stillbirth. *Acta Obstet Gynecol Scand* **87**, 1202-1212, doi:10.1080/00016340802460271 (2008).

20 Bring, H. S., Varli, I. A. H., Kublickas, M., Papadogiannakis, N. & Pettersson, K. Causes of stillbirth at different gestational ages in singleton pregnancies. *Acta Obstet Gyn Scan* **93**, 86-92, doi:10.1111/aogs.12278 (2014).

21 Parast, M. M., Crum, C. P. & Boyd, T. K. Placental histologic criteria for umbilical blood flow restriction in unexplained stillbirth. *Hum Pathol* **39**, 948-953, doi:10.1016/j.humpath.2007.10.032 (2008).

22 McPherson, E. Discovering the cause of stillbirth. *Curr Opin Obstet Gynecol* **25**, 152-156, doi:10.1097/GCO.0b013e32835e0f26 (2013).

23 Reddy, U. M. *et al.* Stillbirth Classification-Developing an International Consensus for Research Executive Summary of a National Institute of Child Health and Human Development Workshop. *Obstetrics and Gynecology* **114**, 901-914 (2009).

24 Froen, J. F. *et al.* Risk factors for sudden intrauterine unexplained death: epidemiologic characteristics of singleton cases in Oslo, Norway, 1986-1995. *Am J Obstet Gynecol* **184**, 694-702 (2001).

25 Mohsin, M., Bauman, A. E. & Jalaludin, B. The influence of antenatal and maternal factors on stillbirths and neonatal deaths in New South Wales, Australia. *J Biosoc Sci* **38**, 643-657, doi:10.1017/S002193200502701X (2006).

26 Stephansson, O., Dickman, P. W., Johansson, A. L. & Cnattingius, S. The influence of socioeconomic status on stillbirth risk in Sweden. *Int J Epidemiol* **30**, 1296-1301 (2001).

27 Smith, G. C., Pell, J. P. & Dobbie, R. Caesarean section and risk of unexplained stillbirth in subsequent pregnancy. *Lancet* **362**, 1779-1784 (2003).

28 Cotzias, C. S., Paterson-Brown, S. & Fisk, N. M. Prospective risk of unexplained stillbirth in singleton pregnancies at term: population based analysis. *Brit Med J* **319**, 287-288 (1999).

29 Deo, R. & Albert, C. M. Epidemiology and genetics of sudden cardiac death. *Circulation* **125**, 620-637, doi:10.1161/CIRCULATIONAHA.111.023838 (2012).

30 Chugh, S. S., Kelly, K. L. & Titus, J. L. Sudden cardiac death with apparently normal heart. *Circulation* **102**, 649-654 (2000).

31 Cote, A., Russo, P. & Michaud, J. Sudden unexpected deaths in infancy: what are the causes? *J Pediatr* **135** (1999).

32 Tester, D. J. & Ackerman, M. J. The role of molecular autopsy in unexplained sudden cardiac death. *Curr Opin Cardiol* **21**, 166-172, doi:10.1097/01.hco.0000221576.33501.83 (2006).

33 Fishman, G. I. *et al.* Sudden cardiac death prediction and prevention: report from a National Heart, Lung, and Blood Institute and Heart Rhythm Society Workshop. *Circulation* **122**, 2335-2348, doi:10.1161/CIRCULATIONAHA.110.976092 (2010).

34 Kong, M. H. *et al.* Systematic review of the incidence of sudden cardiac death in the United States. *J Am Coll Cardiol* **57**, 794-801, doi:10.1016/j.jacc.2010.09.064 (2011).

35 Byrne, R. *et al.* Multiple source surveillance incidence and aetiology of out-of-hospital sudden cardiac death in a rural population in the West of Ireland. *Eur Heart J* **29**, 1418-1423, doi:10.1093/eurheartj/ehn155 (2008).

36 deVreedeSwagemakers, J. J. M. *et al.* Out-of-hospital cardiac arrest in the 1990s: A population-based study in the Maastricht area on incidence, characteristics and

survival. *Journal of the American College of Cardiology* **30**, 1500-1505, doi:Doi 10.1016/S0735-1097(97)00355-0 (1997).

37 Zipes, D. P. & Wellens, H. J. Sudden cardiac death. *Circulation* **98**, 2334-2351 (1998).

38 Spain, M. D., Bradess, M. D. & Mohr, C. Coronary Atherosclerosis as a Cause of Unexpected and Unexplained Death. An Autopsy stdy from 1949-1959. *JAMA* **174**, 384-388 (1960).

39 Burke, A. P. *et al.* Coronary risk factors and plaque morphology in men with coronary disease who died suddenly. *The New England journal of medicine* **336**, 1276-1282, doi:10.1056/NEJM199705013361802 (1997).

40 Huikuri, H. V., Castellanos, A. & Myerburg, R. J. Medical progress: Sudden death due to cardiac arrhythmias. *New England Journal of Medicine* **345**, 1473-1482, doi:DOI 10.1056/NEJMra000650 (2001).

41 Stecker, E. C. *et al.* Population-based analysis of sudden cardiac death with and without left ventricular systolic dysfunction - Two-year findings from the Oregon sudden unexpected death study. *Journal of the American College of Cardiology* **47**, 1161-1166, doi:10.1016/j.jacc.2005.11.045 (2006).

42 Becker, L. B. *et al.* Racial differences in the incidence of cardiac arrest and subsequent survival. The CPR Chicago Project. *The New England journal of medicine* **329**, 600-606, doi:10.1056/NEJM199308263290902 (1993).

43 Kannel, W. B. & Schatzkin, A. Sudden death: lessons from subsets in population studies. *J Am Coll Cardiol* **5**, 141B-149B (1985).

44 Cowie, M. R., Fahrenbruch, C. E., Cobb, L. A. & Hallstrom, A. P. Out-of-hospital cardiac arrest: racial differences in outcome in Seattle. *Am J Public Health* **83**, 955-959 (1993).

45 Wannamethee, G., Shaper, A. G., Macfarlane, P. W. & Walker, M. Risk factors for sudden cardiac death in middle-aged British men. *Circulation* **91**, 1749-1756 (1995).

46 Cupples, L. A., Gagnon, D. R. & Kannel, W. B. Long- and short-term risk of sudden coronary death. *Circulation* **85**, I11-18 (1992).

47 Jouven, X., Zureik, M., Desnos, M., Guerot, C. & Ducimetiere, P. Resting heart rate as a predictive risk factor for sudden death in middle-aged men. *Cardiovascular Research* **50**, 373-378, doi:Doi 10.1016/S0008-6363(01)00230-9 (2001).

48 Iuliano, S. *et al.* QRS duration and mortality in patients with congestive heart failure. *Am Heart J* **143**, 1085-1091 (2002).

49 Kurl, S., Mäkikallio, T. H., Rautaharju, P., Kiviniemi, V. & Laukkanen, J. A. The Duration of QRS Complex in Resting Electrocardiogram is a Predictor of Sudden Cardiac Death in Men *Circulation* **125**, 2588-2594 (2012).

50 Garg, A., Finneran, W. & Feld, G. K. Familial sudden cardiac death associated with a terminal QRS abnormality on surface 12-lead electrocardiogram in the index case. *J Cardiovasc Electrophysiol* **9**, 642-647 (1998).

51 Sagie, A., Larson, M. G., Goldberg, R. J., Bengtson, J. R. & Levy, D. An improved method for adjusting the QT interval for heart rate (the Framingham Heart Study). *Am J Cardiol* **70**, 797-801 (1992).

52 Algra, A., Tijssen, J. G. P., Roelandt, J. R. T. C., Pool, J. & Lubsen, J. Qtc Prolongation Measured by Standard 12-Lead Electrocardiography Is an Independent Risk Factor for Sudden-Death Due to Cardiac-Arrest. *Circulation* **83**, 1888-1894 (1991).

53 Splawski, I. *et al.* Spectrum of mutations in long-QT syndrome genes. KVLQT1, HERG, SCN5A, KCNE1, and KCNE2. *Circulation* **102**, 1178-1185 (2000).

54 Schwartz, P. J. *et al.* Genotype-phenotype correlation in the long-QT syndrome: gene-specific triggers for life-threatening arrhythmias. *Circulation* **103**, 89-95 (2001).

55 Curran, M. E. *et al.* A molecular basis for cardiac arrhythmia: HERG mutations cause long QT syndrome. *Cell* **80**, 795-803 (1995).

56 Mohler, P. J. *et al.* Ankyrin-B mutation causes type 4 long-QT cardiac arrhythmia and sudden cardiac death. *Nature* **421**, 634-639, doi:10.1038/nature01335 (2003).

57 Wang, Q. *et al.* SCN5A mutations associated with an inherited cardiac arrhythmia, long QT syndrome. *Cell* **80**, 805-811 (1995).

58 Kapplinger, J. D. *et al.* Spectrum and prevalence of mutations from the first 2,500 consecutive unrelated patients referred for the FAMILION (R) long QT syndrome genetic test. *Heart Rhythm* **6**, 1297-1303, doi:10.1016/j.hrthm.2009.05.021 (2009).

59 Romano, C., Gemme, G. & Pongiglione, R. Rare cardiac arrythmias of the pediatric age. II. Syncopal attacks due to paroxysmal ventricular fibrillation. *La clinica pediatrica* **45**, 656 (1963).

60 Jervell, A. & Lange-Nielsen, F. Congenital deaf-mutism, functional heart disease with prolongation of the Q-T interval and sudden death. *Am Heart J* **54**, 59-68 (1957).

61 Arking, D. E. *et al.* A common genetic variant in the NOS1 regulator NOS1AP modulates cardiac repolarization. *Nat Genet* **38**, 644-651, doi:10.1038/ng1790 (2006).

62 Pfeufer, A. *et al.* Common variants at ten loci modulate the QT interval duration in the QTSCD Study. *Nature Genetics* **41**, 407-414, doi:10.1038/ng.362 (2009).

63 Arking, D. E. *et al.* Genetic association study of QT interval highlights role for calcium signaling pathways in myocardial repolarization. *Nat Genet* **46**, 826-836, doi:10.1038/ng.3014 (2014).

64 Weiss, J. N., Garfinkel, A., Karagueuzian, H. S., Chen, P. S. & Qu, Z. Early afterdepolarizations and cardiac arrhythmias. *Heart Rhythm* **7**, 1891-1899, doi:10.1016/j.hrthm.2010.09.017 (2010).

65 Schwartz, P. J. A Molecular Link between the Sudden Infant Death Syndrome and the Long-QT Syndrome. *The New England journal of medicine* **343**, 262-267 (2000).

66 Byard, R. W. & Krous, H. F. Suddent infant death syndrome: overview and update. *Pediatr Dev Pathol* **6**, 112-127 (2003).

67 Willinger, M., James, L. S. & Catz, C. Defining the sudden infant death syndrome (SIDS): deliberations of an expert panel convened by the National Institute of Child Health and Human Development. *Pediatr Pathol* **11**, 677-684, doi:10.3109/15513819109065465 (1991).

68 Côté, A., Russo, P. & Michaud, J. Sudden unexpected deaths in infancy: What are the causes? *The Journal of Pediatrics* **135**, 437-443 (1999).

69 Wedgwood, R. J. Review of USA experience. In: Camps FE, Carpenter RG, eds. Sudden and Unexpected Death in Infancy (Cot Deaths). *Wright*, 28 (1972).

70 Filiano, J. J. & Kinney, H. C. A perspective on neuropathologic findings in victims of the sudden infant death syndrome: the triple-risk model. *Biol Neonate* **65**, 194-197 (1994).

71 Rognum, T. O. & Saugstad, O. D. Biochemical and immunological studies in SIDS victims. Clues to understanding the death mechanism. *Acta Paediatr Suppl* **82 Suppl 389**, 82-85 (1993).

72 Guntheroth, W. G. & Spiers, P. S. The triple risk hypotheses in sudden infant death syndrome. *Pediatrics* **110**, e64 (2002).

73 Insolia, R., Ghidoni, A., Dossena, C., Mastanuono, E. & Schwartz, P. J. Sudden infant death syndrome and cardiac channelopathies: from mechanisms to prevention of avoidable tragedies. *Cardiogenetics* **1**, e6 (2011).

74 Haglund, B. & Cnattingius, S. Cigarette-Smoking as a Risk Factor for Sudden Infant Death Syndrome - a Population-Based Study. *American Journal of Public Health* **80**, 29-32 (1990).

75 Scragg, R. K. & Mitchell, E. A. Side sleeping position and bed sharing in the sudden infant death syndrome. *Ann Med* **30**, 345-349 (1998).

76 Markestad, T., Skadberg, B., Hordvik, E., Morild, I. & Irgens, L. M. Sleeping position and sudden infant death syndrome (SIDS): effect of an intervention programme to avoid prone sleeping. *Acta Paediatr* **84**, 375-378 (1995).

77 Dwyer, T., Ponsonby, A. L., Newman, N. M. & Gibbons, L. E. Prospective cohort study of prone sleeping position and sudden infant death syndrome. *Lancet* **337**, 1244-1247 (1991).

78 Mathews, T. J. & MacDorman, M. F. Infant mortality statistics from the 2004 period linked birth/infant death data set. *Natl Vital Stat Rep* **55**, 1-32 (2007).

79 Blair, P. S. *et al.* Smoking and the sudden infant death syndrome: results from 1993-5 case-control study for confidental inquiry into stillbirths and deaths in infancy. **313**, 195-198 (1996).

80 Alm, B. *et al.* Caffeine and alcohol as risk factors for sudden infant death syndrome. *Archives of Disease in Childhood* **81**, 107-111 (1999).

81 Ford, R. P. *et al.* Heavy caffeine intake in pregnancy and sudden infant death syndrome. New Zealand Cot Death Study Group. *Arch Dis Child* **78**, 9-13 (1998).

82 Weinburg, S. B. & Purdy, B. A. Postmortem leukocyte culture studies in sudden infant death. *Nature* **226**, 1264-1265 (1970).

83 Vege, A., Rognum, T. O., Scott, H., Aasen, A. O. & Saugstad, O. D. Sids Cases Have Increased Levels of Interleukin-6 in Cerebrospinal-Fluid. *Acta Paediatrica* **84**, 193-196, doi:DOI 10.1111/j.1651-2227.1995.tb13608.x (1995).

84 Froen, T. F., Aker, H., Stray-Pedersen, B. & Saugstad, O. D. Adverse effects of nicotine and interleukin-1 beta on autoresuscitation after apnea in piglets: Implications for sudden infant death syndrome. *Pediatrics* **105** (2000).

85 Blackwell, C. C. *et al.* Cytokine responses and sudden infant death syndrome: genetic, developmental, and environmental risk factors. *J Leukoc Biol* **78**, 1242-1254, doi:10.1189/jlb.0505253 (2005).

86 Moscovis, S. M., Hall, S. T., Gleeson, M., Scott, R. J. & Blackwell, C. C. Ethnicity, inflammation, stillbirths and SIDS. *13th Annual Conference, National SIDS Council of Australia* (2005).

87 Narita, N. *et al.* Serotonin transporter gene variation is a risk factor for sudden infant death syndrome in the Japanese population. *Pediatrics* **107**, 690-692, doi:DOI 10.1542/peds.107.4.690 (2001).

88 Weese-Mayer, D. E. *et al.* Sudden infant death syndrome: Case-control frequency differences at genes pertinent to early autonomic nervous system embryologic development. *Pediatr Res* **56**, 391-395, doi:10.1203/01.Pdr.0000136285.91048.4a (2004).

89 Burchell, A., Bell, J. E., Busuttil, A. & Hume, R. Hepatic microsomal glucose-6-phosphatase system and sudden infant death syndrome. *Lancet* **2**, 291-294 (1989).

90 Forsyth, L., Hume, R., Howatson, A., Busuttil, A. & Burchell, A. Identification of novel polymorphisms in the glucokinase and glucose-6-phosphatase genes in infants who died suddenly and unexpectedly. *J Mol Med (Berl)* **83**, 610-618, doi:10.1007/s00109-005-0666-0 (2005).

91 Keeton, B. R. *et al.* Cardiac conduction disorders in six infants with "near-miss" sudden infant deaths. *Br Med J* **2**, 600-601 (1977).

92 Schwartz, P. J. Cardiac sympathetic innervation and the sudden infant death syndrome. A possible pathogenetic link. *Am J Med* **60**, 167-172 (1976).

93 el-Sherif, N., Caref, E. B., Yin, H. & Restivo, M. The electrophysiological mechanism of ventricular arrhythmias in the long QT syndrome. Tridimensional mapping of activation and recovery patterns. *Circ Res* **79**, 474-492 (1996).

94 Maron, B. J., Clark, C. E., Goldstein, R. E. & Epstein, S. E. Potential role of QT interval prolongation in sudden infant death syndrome. *Circulation* **54**, 423-430 (1976).

95 Gordon, D. *et al.* Analysis of heart rate and respiratory patterns in sudden infant death syndrome victims and control infants. *Pediatr Res* **20**, 680-684, doi:10.1203/00006450-198607000-00021 (1986).

96 Southall, D. P., Arrowsmith, W. A., Stebbens, V. & Alexander, J. R. Qt Interval Measurements before Sudden-Infant-Death-Syndrome. *Archives of Disease in Childhood* **61**, 327-333 (1986).

97 Kelly, D. H., Shannon, D. C. & Liberthson, R. R. The Role of the QT interval in the SUdden Infant Death Syndrome. *Circulation* **55**, 633-635 (1976).

98 Schwartz, P. J. *et al.* The QT interval throughout the first 6 months of life: a prospective study. *Circulation* **66**, 496-501 (1982).

99 Sadeh, D. *et al.* Altered Cardiac Repolarization in Some Victims of Sudden-Infant-Death-Syndrome. *New England Journal of Medicine* **317**, 1501-1505, doi:Doi 10.1056/Nejm198712103172404 (1987).

100 Guntheroth, W. G. Theories of cardiovascular causes in sudden infant death syndrome. *J Am Coll Cardiol* **14**, 443-447 (1989).

101 Weinstein, S. L. & Steinschneider, A. QTc and RR intervals in victims of the sudden infant death syndrome. *American Journal of Diseases of Children* **139**, 987-990 (1985).

102 Schwartz, P. J. *et al.* Prolongation of the QT interval and the sudden infant death syndrome. *The New England journal of medicine* **338**, 1709-1714, doi:10.1056/NEJM199806113382401 (1998).

103 Schwartz, P. J. *et al.* Prevalence of the congenital long-QT syndrome. *Circulation* **120**, 1761-1767, doi:10.1161/CIRCULATIONAHA.109.863209 (2009).

104 Wedekind, H. *et al.* De novo mutation in the SCN5A gene associated with early onset of sudden infant death. *Circulation* **104**, 1158-1164 (2001).

105 Zaritsky, J. J., Eckman, D. M., Wellman, G. C., Nelson, M. T. & Schwarz, T. L. Targeted disruption of Kir2.1 and Kir2.2 genes reveals the essential role of the inwardly rectifying K(+) current in K(+)-mediated vasodilation. *Circ Res* **87**, 160-166 (2000).

106 Miake, J., Marban, E. & Nuss, H. B. Functional role of inward rectifier current in heart probed by Kir2.1 overexpression and dominant-negative suppression. *The Journal of clinical investigation* **111**, 1529-1536, doi:10.1172/JCI17959 (2003).

107 Dhar Malhotra, J. *et al.* Characterization of sodium channel alpha- and beta-subunits in rat and mouse cardiac myocytes. *Circulation* **103**, 1303-1310 (2001).

108 Patlak, J. B. & Ortiz, M. Slow Currents through Single Sodium-Channels of the Adult-Rat Heart. *J Gen Physiol* **86**, 89-104, doi:DOI 10.1085/jgp.86.1.89 (1985).

109 Oudit, G. Y. *et al.* The Molecular Physiology of the Cardiac Transient Outward Potassium Current (Ito) in Normal and Diseased Myocardium. *Journal of Molecular and Cellular Cardiology* **33**, 851-872 (2001).

110 Nerbonne, J. M. & Kass, R. S. Molecular physiology of cardiac repolarization. *Physiol Rev* **85**, 1205-1253, doi:10.1152/physrev.00002.2005 (2005).

111 Yue, L., Feng, J., Li, G. R. & Nattel, S. Characterization of an ultrarapid delayed rectifier potassium channel involved in canine atrial repolarization. *J Physiol* **496 ( Pt 3)**, 647-662 (1996).

112 Bers, D. M. Cardiac excitation–contraction coupling. *Nature* **415**, 198-205 (2002).

113 Arikkath, J. & Campbell, K. P. Auxiliary subunits: essential components of the voltage-gated calcium channel complex. *Curr Opin Neurobiol* **13**, 298-307 (2003).

114 Sanguinetti, M. C., Jiang, C., Curran, M. E. & Keating, M. T. A mechanistic link between an inherited and an acquird cardiac arrthytmia: HERG encodes the I Kr potassium channel. *Cell* **81**, 299-307 (1995).

115 McDonald, T. V. *et al.* A minK–HERG complex regulates the cardiac potassium current IKr. *Nature* **388**, 289-292 (1997).

116 Bryant, S. M., Wan, X., Shipsey, S. J. & Hart, G. Regional differences in the delayed rectifier current (IKr and IKs) contribute to the differences in action potential duration in basal left ventricular myocytes in guinea-pig. *Cardiovasc Res* **40**, 322-331 (1998).

117 Romey, G. *et al.* Molecular mechanism and functional significance of the MinK control of the KvLQT1 channel activity. *J Biol Chem* **272**, 16713-16716 (1997).

118 Jervell, A. & Lange-Nielsen, F. Congenital deaf-mutism, functional heart disease with prolongation of the QT interval, and sudden death. *American Heart Journal* **54**, 59-68 (1957).

119 Splawski, I., Timothy, K. W., Vincent, G. M. & Atkinson, D. Molecular basis of the long-QT syndrome associated with deafness. *New Engl J Med* **336**, 1562-1567 (1997).

120 Wollnik, B. *et al.* Pathophysiological mechanisms of dominant and recessive KVLQT1 K+ channel mutations found in inherited cardiac arrhythmias. *Hum Mol Genet* **6**, 1943-1949, doi:DOI 10.1093/hmg/6.11.1943 (1997).

121 Zareba, W. *et al.* Location of mutation in the KCNQ1 and phenotypic presentation of long QT syndrome. *J Cardiovasc Electrophysiol* **14**, 1149-1153 (2003).

122 Anderson, C. L. *et al.* Most LQT2 mutations reduce Kv11.1 (hERG) current by a class 2 (trafficking-deficient) mechanism. *Circulation* **113**, 365-373, doi:10.1161/Circulationaha.105.570200 (2006).

123 Zareba, W. *et al.* Influence of genotype on the clinical course of the long-QT syndrome. International Long-QT Syndrome Registry Research Group. *The New England journal of medicine* **339**, 960-965, doi:10.1056/NEJM199810013391404 (1998).

124 Wang, Q. *et al.* Positional cloning of a novel potassium channel gene: KVLQT1 mutations cause cardiac arrhythmias. *Nat Genet* **12**, 17-23, doi:10.1038/ng0196-17 (1996).

125 Splawski, I., Tristani-Firouzi, M., Lehmann, M. H., Sanguinetti, M. C. & Keating, M. T. Mutations in the hminK gene cause long QT syndrome and suppress IKs function. *Nat Genet* **17**, 338-340, doi:10.1038/ng1197-338 (1997).

126 Abbott, G. W. *et al.* MiRP1 forms IKr potassium channels with HERG and is associated with cardiac arrhythmia. *Cell* **97**, 175-187 (1999).

127 Plaster, N. M. *et al.* Mutations in Kir2.1 cause the developmental and episodic electrical phenotypes of Andersen's syndrome. *Cell* **105**, 511-519 (2001).

128 Splawski, I. *et al.* CaV1.2 Calcium Channel Dysfunction Causes a Multisystem Disorder Including Arrhythmia and Autism. *Cell* **119**, 19-31 (2004).

129 Vatta, M. *et al.* Mutant caveolin-3 induces persistent late sodium current and is associated with long-QT syndrome. *Circulation* **114**, 2104-2112, doi:10.1161/Circulationaha.106.635268 (2006).

130 Medeiros-Domingo, A. *et al.* SCN4B-Encoded Sodium Channel β4 Subunit in Congenital Long-QT Syndrome. *Circulation* **116**, 134-142 (2007).

131 Chen, L. *et al.* Mutation of an A-kinase-anchoring protein causes long-QT syndrome. *Proc Natl Acad Sci U S A* **104**, 20990-20995, doi:10.1073/pnas.0710527105 (2007).

132 Ueda, K. *et al.* Syntrophin mutation associated with long QT syndrome through activation of the nNOS-SCN5A macromolecular complex. *P Natl Acad Sci USA* **105**, 9355-9360, doi:10.1073/pnas.0801294105 (2008).

133 Yang, Y. *et al.* Identification of a Kir3.4 mutation in congenital long QT syndrome. *Am J Hum Genet* **86**, 872-880 (2010).

134 Crotti, L. *et al.* Calmodulin mutations associated with recurrent cardiac arrest in infants. *Circulation* **127**, 1009-1017, doi:10.1161/CIRCULATIONAHA.112.001216 (2013).

135 Limpitikul, W. B. *et al.* Calmodulin mutations associated with long QT syndrome prevent inactivation of cardiac L-type Ca2+ currents and promote proarrhythmic behavior in ventricular myocytes. *Journal of Molecular and Cellular Cardiology* **74**, 115-124, doi:10.1016/j.yjmcc.2014.04.022 (2014).

136 Moss, A. J. & Kass, R. S. Long QT syndrome: from channels to cardiac arrhythmias. *The Journal of clinical investigation* **115**, 2018-2024, doi:10.1172/JCI25537 (2005).

137 Mohler, P. J. *et al.* A cardiac arrhythmia syndrome caused by loss of ankyrin-B function. *Proc Natl Acad Sci U S A* **101**, 9137-9142, doi:10.1073/pnas.0402546101 (2004).

138 Nakajo, K., Ulbrich, M. H., Kubo, Y. & Isacoff, E. Y. Stoichiometry of the KCNQ1 - KCNE1 ion channel complex. *Proc Natl Acad Sci U S A* **107**, 18862-18867, doi:10.1073/pnas.1010354107 (2010).

139 Brugada, P. & Brugada, J. Right bundle branch block, persistent ST segment elevation and sudden cardiac death: a distinct clinical and electrocardiographic syndrome. A multicenter report. *J Am Coll Cardiol* **20**, 1391-1396 (1992).

140 Antzelevitch, C., Brugada, P., Brugada, J. & Brugada, R. Brugada syndrome: from cell to bedside. *Curr Probl Cardiol* **30**, 9-54, doi:10.1016/j.cpcardiol.2004.04.005 (2005).

141 Postema, P. G. About Brugada syndrome and its prevalence. *Europace* **14**, 925-928, doi:10.1093/europace/eus042 (2012).

142 Antzelevitch, C. Genetic basis of Brugada syndrome. *Heart Rhythm* **4**, 756-757, doi:10.1016/j.hrthm.2007.03.015 (2007).

143 Chen, Q. *et al.* Genetic basis and molecular mechanisms for idiopathic ventricular fibrillation. *Nature* **392**, 293-296 (1998).

144 Dumaine, R. *et al.* Ionic mechanisms responsible for the electrocardiographic phenotype of the Brugada syndrome are temperature dependent. *Circ Res* **85**, 803-809 (1999).

145 Bezzina, C. *et al.* A single Na+ channel mutation causing both long-QT and Brugada syndromes. *Circ Res* **85**, 1206-1213 (1999).

146 Antzelevitch, C. The Brugada syndrome: ionic basis and arrhythmia mechanisms. *J Cardiovasc Electrophysiol* **12**, 268-272 (2001).

147 London, B. *et al.* Mutation in glycerol-3-phosphate dehydrogenase 1 like gene (GPD1-L) decreases cardiac Na+ current and causes inherited arrhythmias. *Circulation* **116**, 2260-2268, doi:10.1161/CIRCULATIONAHA.107.703330 (2007).

148 Watanabe, H. *et al.* Sodium channel β1 subunit mutations associated with Brugada syndrome and cardiac conduction disease in humans. *The Journal of clinical investigation* **118**, 2260-2268 (2008).

149 Hu, D. *et al.* A mutation in the beta 3 subunit of the cardiac sodium channel associated with Brugada ECG phenotype. *Circ Cardiovasc Genet* **2**, 270-278, doi:10.1161/CIRCGENETICS.108.829192 (2009).

150 Cordeiro, J. M. *et al.* Accelerated inactivation of the L-type calcium current due to a mutation in CACNB2b underlies Brugada syndrome. *Journal of Molecular and Cellular Cardiology* **46**, 695-703, doi:10.1016/j.yjmcc.2009.01.014 (2009).

151 Beziau, D. M. *et al.* Complex Brugada syndrome inheritance in a family harbouring compound SCN5A and CACNA1C mutations. *Basic Res Cardiol* **109**, 446, doi:10.1007/s00395-014-0446-5 (2014).

152 Crotti, L. *et al.* Spectrum and Prevalence of Mutations Involving BrS1-Through BrS12-Susceptibility Genes in a Cohort of Unrelated Patients Referred for Brugada Syndrome Genetic Testing Implications for Genetic Testing. *Journal of the American College of Cardiology* **60**, 1410-1418, doi:10.1016/j.jacc.2012.04.037 (2012).

153 Reid, D. S., Tynan, M., Braidwood, L. & Fitzgerald, G. R. Bidirectional Tachycardia in a Child - Study Using His-Bundle Electrography. *Brit Heart J* **37**, 339-344 (1975).

154 Leenhardt, A., Denjoy, I. & Guicheney, P. Catecholaminergic Polymorphic Ventricular Tachycardia. *Circulation: Arrhythmia and Electrophysiology* **5**, 1044-1052 (2012).

155 Wilders, R. Cardiac ion channelopathies and the sudden infant death syndrome. *ISRN Cardiol* **2012**, 846171, doi:10.5402/2012/846171 (2012).

156 Kushnir, A. & Marks, A. R. The ryanodine receptor in cardiac physiology and disease. *Adv Pharmacol* **59**, 1-30, doi:10.1016/S1054-3589(10)59001-X (2010).

157 Priori, S. G. *et al.* Mutations in the cardiac ryanodine receptor gene (hRyR2) underlie catecholaminergic polymorphic ventricular tachycardia. *Circulation* **103**, 196-200 (2001).

158 Wehrens, X. H. *et al.* FKBP12.6 deficiency and defective calcium release channel (ryanodine receptor) function linked to exercise-induced sudden cardiac death. *Cell* **113**, 829-840 (2003).

159 Cerrone, M. *et al.* Arrhythmogenic mechanisms in a mouse model of catecholaminergic polymorphic ventricular tachycardia. *Circ Res* **101**, 1039-1048, doi:10.1161/CIRCRESAHA.107.148064 (2007).

160 Schimpf, R., Wolpert, C., Gaita, F., Giustetto, C. & Borggrefe, M. Short QT syndrome. *Cardiovasc Res* **3**, 357-366 (2005).

161 Brugada, R. *et al.* Sudden death associated with short-QT syndrome linked to mutations in HERG. *Circulation* **109**, 30-35, doi:10.1161/01.CIR.0000109482.92774.3A (2004).

162 Bellocq, C. *et al.* Mutation in the KCNQ1 gene leading to the short QT-interval syndrome. *Circulation* **109**, 2394-2397, doi:10.1161/01.CIR.0000130409.72142.FE (2004).

163 Gussak, I. *et al.* Idiopathic short QT interval: a new clinical syndrome? *Cardiology* **94**, 99-102, doi:47299 (2000).

164 Antzelevitch, C. *et al.* Loss-of-function mutations in the cardiac calcium channel underlie a new clinical entity characterized by ST-segment elevation, short QT intervals, and sudden cardiac death. *Circulation* **115**, 442-449, doi:10.1161/CIRCULATIONAHA.106.668392 (2007).

165 Templin, C. *et al.* Identification of a novel loss-of-function calcium channel gene mutation in short QT syndrome (SQTS6). *Eur Heart J* **32**, 1077-1088, doi:10.1093/eurheartj/ehr076 (2011).

166 Ferrer, M. I. The Sick Sinus Syndrome. *Hosp Pract* **15**, 79-89 (1980).

167 Benson, D. W. *et al.* Congenital sick sinus syndrome caused by recessive mutations in the cardiac sodium channel gene (SCN5A). *The Journal of clinical investigation* **112**, 1019-1028, doi:10.1172/JCI18062 (2003).

168 Kyndt, F. *et al.* Novel SCN5A Mutation Leading Either to Isolated Cardiac Conduction Defect or Brugada Syndrome in a Large French Family. *Circulation* **104** (2001).

169 Antzelevitch, C. & Yan, G. X. J wave syndromes. *Heart Rhythm* **7**, 549-558, doi:10.1016/j.hrthm.2009.12.006 (2010).

170 Osborn, J. J. Experimental hypothermia; respiratory and blood pH changes in relation to cardiac function. *Am J Physiol* **175**, 389-398 (1953).

171 Clements, S. D., Jr. & Hurst, J. W. Diagnostic value of electrocardiographic abnormalities observed in subjects accidentally exposed to cold. *Am J Cardiol* **29**, 729-734 (1972).

172 Kalla, H., Yan, G. X. & Marinchak, R. Ventricular fibrillation in a patient with prominent J (Osborn) waves and ST segment elevation in the inferior electrocardiographic leads: a Brugada syndrome variant? *J Cardiovasc Electrophysiol* **11**, 95-98 (2000).

173 Komiya, N. *et al.* Ventricular fibrillation in a patient with prominent j wave in the inferior and lateral electrocardiographic leads after gastrostomy. *Pacing Clin Electrophysiol* **29**, 1022-1024, doi:10.1111/j.1540-8159.2006.00481.x (2006).

174 Mehta, M. C. & Jain, A. C. Early repolarization on scalar electrocardiogram. *Am J Med Sci* **309**, 305-311 (1995).

175 Tikkanen, J. T. *et al.* Long-Term Outcome Associated with Early Repolarization on Electrocardiography. *New England Journal of Medicine* **361**, 2529-2537, doi:10.1056/NEJMoa0907589 (2009).

176 Antzelevitch, C. Genetic, molecular and cellular mechanisms underlying the J wave syndromes. *Circ J* **76**, 1054-1065 (2012).

177 Reinhard, W. *et al.* Heritability of early repolarization: a population-based study. *Circ Cardiovasc Genet* **4**, 134-138 (2011).

178 Medeiros-Domingo, A. *et al.* Gain-of-Function Mutation, S422L, in the KCNJ8-Encoded Cardiac KATP Channel Kir6.1 as a Pathogenic Substrate for J Wave Syndromes. *Heart Rhythm* **7**, 1466-1471 (2010).

179 Wu, S. N., Wu, A. Z. & Sung, R. J. Identification of two types of ATP-sensitive K+ channels in rat ventricular myocytes. *Life Sci* **80**, 378-387, doi:10.1016/j.lfs.2006.09.042 (2007).

180 Burashnikov, E. *et al.* Mutations in the cardiac L-type calcium channel associated with inherited J-wave syndromes and sudden cardiac death. *Heart Rhythm* **7**, 1872-1882, doi:10.1016/j.hrthm.2010.08.026 (2010).

181 Watanabe, H. *et al.* Electrocardiographic characteristics and SCN5A mutations in idiopathic ventricular fibrillation associated with early repolarization. *Circ Arrhythm Electrophysiol* **4**, 874-881, doi:10.1161/CIRCEP.111.963983 (2011).

182 Schott, J. J. *et al.* Cardiac conduction defects associate with mutations in SCN5A. *Nat Genet* **23**, 20-21, doi:10.1038/12618 (1999).

183 Tan, H. L. *et al.* A sodium-channel mutation causes isolated cardiac conduction disease. *Nature* **409**, 1043-1047, doi:10.1038/35059090 (2001).

184 Grundy, S. M. *et al.* Effect of potentially modifiable risk factors associated with myocardial infarction in 52 countries (the INTERHEART study): case-control study. *Circulation* **112**, 2735-2752 (2005).

185 Locati, E. H. *et al.* Age- and sex-related differences in clinical manifestations in patients with congenital long-QT syndrome: findings from the International LQTS Registry. *Circulation* **97**, 2237-2244 (1998).

186 Priori, S. G. *et al.* Natural history of Brugada syndrome: insights for risk stratification and management. *Circulation* **105**, 1342-1347 (2002).

187 Giustetto, C. *et al.* Short QT syndrome: clinical findings and diagnostic-therapeutic implications. *Eur Heart J* **27**, 2440-2447, doi:10.1093/eurheartj/ehl185 (2006).

188 Zareba, W. *et al.* Modulating effects of age and gender on the clinical course of long QT syndrome by genotype. *J Am Coll Cardiol* **42**, 103-109 (2003).

189 Herskowitz, I. Functional inactivation of genes by dominant negative mutations. *Nature* **329**, 219-222, doi:10.1038/329219a0 (1987).

190 Kagan, A., Yu, Z., Fishman, G. I. & McDonald, T. V. The dominant negative LQT2 mutation A561V reduces wild-type HERG expression. *J Biol Chem* **275**, 11241-11248 (2000).

191 Olson, T. M. *et al.* Kv1.5 channelopathy due to KCNA5 loss-of-function mutation causes human atrial fibrillation. *Hum Mol Genet* **15**, 2185-2191, doi:10.1093/hmg/ddl143 (2006).

192 Wang, P. *et al.* Functional dominant-negative mutation of sodium channel subunit gene SCN3B associated with atrial fibrillation in a Chinese GeneID population. *Biochem Biophys Res Commun* **398**, 98-104, doi:10.1016/j.bbrc.2010.06.042 (2010).

193 Mezghrani, A. *et al.* A destructive interaction mechanism accounts for dominant-negative effects of misfolded mutants of voltage-gated calcium channels. *J Neurosci* **28**, 4501-4511, doi:10.1523/JNEUROSCI.2844-07.2008 (2008).

194 Fialho, D. *et al.* Chloride channel myotonia: exon 8 hot-spot for dominant-negative interactions. *Brain* **130**, 3265-3274, doi:10.1093/brain/awm248 (2007).

195 Miller, T. E. *et al.* Recurrent third-trimester fetal loss and maternal mosaicism for long-QT syndrome. *Circulation* **109**, 3029-3034, doi:10.1161/01.CIR.0000130666.81539.9E (2004).

196 Bhuiyan, Z. A. *et al.* Recurrent Intrauterine Fetal Loss due to Near Absence of HERG: Clinical and Functional Characterization of a Homozygous Non-sense HERG mutation. *Heart Rhythm* **5**, 553-561 (2008).

197 Crotti, L. *et al.* Long QT syndrome-associated mutations in intrauterine fetal death. *JAMA* **309**, 1473-1482, doi:10.1001/jama.2013.3219 (2013).

198 Clarke, L. *et al.* The 1000 Genomes Project: data management and community access. *Nat Methods* **9**, 459-462, doi:10.1038/nmeth.1974 (2012).

199 Exome Variant Server NESPE, Seattle WA. http://evs.gs.washington.edu/EVS/. (2013).

200 National Heart, Lung, and Blood Institute Exome Sequencing Project (ESP). Exome variant server: Seattle GO. http://evs.gs.washington.edu/EVS. (2013).

201 Hedley, P. L. *et al.* The genetic basis of long QT and short QT syndromes: a mutation update. *Hum Mutat* **30**, 1486-1511, doi:10.1002/humu.21106 (2009).

202 Casimiro, M. C. *et al.* Targeted disruption of the Kcnq1 gene produces a mouse model of Jervell and Lange-Nielsen Syndrome. *Proc Natl Acad Sci U S A* **98**, 2526-2531, doi:10.1073/pnas.041398998 (2001).

203 Fu, W. *et al.* Analysis of 6,515 exomes reveals a recent origin of most human protein-coding variants. *Nature* **493**, 216-220 (2013).

204 Sotoodehnia, N. *et al.* Common variants in 22 loci are associated with QRS duration and cardiac ventricular conduction. *Nat Genet* **42**, 1068-1076, doi:10.1038/ng.716 (2010).

205 Tomasi, M. *et al.* Calsequestrin (CASQ1) rescues function and structure of calcium release units in skeletal muscles of CASQ1-null mice. *Am J Physiol Cell Physiol* **302**, C575-586, doi:10.1152/ajpcell.00119.2011 (2012).

206 Munroe, P. B. *et al.* Postmortem Genetic Testing for Cardiac Ion Channelopathies in Stillbirths. *Circ Genom Precis Med* **11** (2018).

207 Sesti, F. *et al.* A common polymorphism associated with antibiotic-induced cardiac arrhythmia. *Proc Natl Acad Sci U S A* **97**, 10613-10618, doi:10.1073/pnas.180223197 (2000).

208 Kääb S *et al.* A Large Candidate Gene Survey Identifies the KCNE1 D85N Polymorphism as a Possible Modulator of Drug-Induced Torsades de Pointes. *Circulation: Cardiovascular Genetics* **5**, 91-99 (2012).

209 Bendahhou, S. *et al.* Corticosteroid-exacerbated symptoms in an Andersen's syndrome kindred. *Hum Mol Genet* **16**, 900-906, doi:10.1093/hmg/ddm034 (2007).

210 Priori, S. G. *et al.* A novel form of short QT syndrome (SQT3) is caused by a mutation in the KCNJ2 gene. *Circ Res* **96**, 800-807, doi:10.1161/01.RES.0000162101.76263.8c (2005).

211 Xia, M. *et al.* A Kir2.1 gain-of-function mutation underlies familial atrial fibrillation. *Biochem Biophys Res Commun* **332**, 1012-1019, doi:10.1016/j.bbrc.2005.05.054 (2005).

212 Sah, R. *et al.* Ion channel-kinase TRPM7 is required for maintaining cardiac automaticity. *P Natl Acad Sci USA* **110**, E3037-E3046, doi:DOI 10.1073/pnas.1311865110 (2013).

213 Sah, R. *et al.* Timing of myocardial trpm7 deletion during cardiogenesis variably disrupts adult ventricular function, conduction, and repolarization. *Circulation* **128**, 101-114, doi:10.1161/CIRCULATIONAHA.112.000768 (2013).

214 Jin, J. *et al.* Deletion of Trpm7 Disrupts Embryonic Development and Thymopoiesis Without Altering Mg2+ Homeostasis. *Science* **322**, 756-760 (2008).

215 de Villiers, C. P. *et al.* AKAP9 Is a Genetic Modifier of Congenital Long-QT Syndrome Type 1. *Circ-Cardiovasc Gene* **7**, 599-606, doi:10.1161/Circgenetics.113.000580 (2014).

216 Clapham, D. E. TRP channels as cellular sensors. *Nature* **426**, 517-524, doi:10.1038/nature02196 (2003).

217 Hardie, R. C. & Minke, B. The trp gene is essential for a light-activated Ca 2+ channel in Drosophila photoreceptors. *Neuron* **8**, 643-651 (1992).

218 Stowers, L., Holy, T. E., Meister, M., Dulac, C. & Koentges, G. Loss of sex discrimination and male-male aggression in mice deficient for TRP2. *Science* **295**, 1493-1500, doi:10.1126/science.1069259 (2002).

219 Schilling, T., Miralles, F. & Eder, C. TRPM7 regulates proliferation and polarisation of macrophages. *J Cell Sci* **127**, 4561-4566, doi:10.1242/jcs.151068 (2014).

220 Runnels, L. W., Yue, L. & Clapham, D. E. TRP-PLIK, a bifunctional protein with kinase and ion channel activities. *Science* **291**, 1043-1047, doi:10.1126/science.1058519 (2001).

221 Fonfria, E. *et al.* Tissue distribution profiles of the human TRPM cation channel family. *J Recept Signal Transduct Res* **26**, 159-178, doi:10.1080/10799890600637506 (2006).

222 Perraud, A. L., Zhao, X., Ryazanov, A. G. & Schmitz, C. The channel-kinase TRPM7 regulates phosphorylation of the translational factor eEF2 via eEF2-k. *Cell Signal* **23**, 586-593, doi:10.1016/j.cellsig.2010.11.011 (2011).

223 Krapivinsky, G., Krapivinsky, L. & Clapham, D. The TRPM7 chanzyme is cleaved to release a chromatin-modifying kinase. *Cell* **157**, 1061-1072 (2014).

224 Visser, D., Middelbeek, J., van Leeuwen, F. N. & Jalink, K. Function and regulation of the channel-kinase TRPM7 is health and disease. *European journal of cell biology* **93**, 455-465 (2014).

225 Penner, R. & Fleig, A. The Mg2+ and Mg(2+)-nucleotide-regulated channel-kinase TRPM7. *Handb. Exp. Pharmacol.* **179**, 313-328 (2007).

226 Monteilh-Zoller, M. K. *et al.* TRPM7 provides an ion channel mechanism for cellular entry of trace metal ions. *J Gen Physiol* **121**, 49-60, doi:10.1085/jgp.20028740 (2003).

227 Demeuse, P., Penner, R. & Fleig, A. TRPM7 channel is regulated by magnesium nucleotides via its kinase domain. *J Gen Physiol* **127**, 421-434, doi:10.1085/jgp.200509410 (2006).

228 Runnels, L. W., Yue, L. X. & Clapham, D. E. The TRPM7 channel is inactivated by PIP2 hydrolysis. *Nature Cell Biology* **4**, 329-336, doi:Doi 10.1038/Ncb781 (2002).

229 Oancea, E., Wolfe, J. T. & Clapham, D. E. Functional TRPM7 channels accumulate at the plasma membrane in response to fluid flow. *Circ Res* **98**, 245-253, doi:10.1161/01.RES.0000200179.29375.cc (2006).

230 Qin, X. *et al.* Sphingosine and FTY720 are potent inhibitors of the transient receptor potential melastatin 7 (TRPM7) channels. *Br J Pharmacol* **168**, 1294-1312, doi:10.1111/bph.12012 (2013).

231 Li, M., Jiang, J. & Yue, L. Functional characterization of homo- and heteromeric channel kinases TRPM6 and TRPM7. *J Gen Physiol* **127**, 525-537, doi:10.1085/jgp.200609502 (2006).

232 Schmitz, C. *et al.* Regulation of vertebrate cellular Mg 2+ homeostasis by TRPM7. *Cell* **114**, 191-200 (2003).

233 Ryazanova, L. V. *et al.* TRPM7 is essential for Mg2+ homeostasis in mammals. *Nat Commun* **1**, doi:ARTN 109

10.1038/ncomms1108 (2010).

234 Aarts, M. *et al.* A key role for TRPM7 channels in anoxic neuronal death. *Cell* **115**, 863-877, doi:Doi 10.1016/S0092-8674(03)01017-1 (2003).

235 Desai, B. N. *et al.* Cleavage of TRPM7 releases the kinase domain from the ion channel and regulates its participation in Fas-induced apoptosis. *Dev Cell* **22**, 1149-1162, doi:10.1016/j.devcel.2012.04.006 (2012).

236 Waring, P. & Mullbacher, A. Cell death induced by the Fas/Fas ligand pathway and its role in pathology. *Immunol Cell Biol* **77**, 312-317, doi:DOI 10.1046/j.1440-1711.1999.00837.x (1999).

237 Du, J. *et al.* TRPM7-mediated Ca2+ signals confer fibrogenesis in human atrial fibrillation. *Circ Res* **106**, 992-1003, doi:10.1161/CIRCRESAHA.109.206771 (2010).

238 Tomasek, J. J., Gabbiani, G., Hinz, B., Chaponnier, C. & Brown, R. A. Myofibroblasts and mechano-regulation of connective tissue remodelling. *Nat Rev Mol Cell Biol* **3**, 349-363, doi:10.1038/nrm809 (2002).

239 Volders, P. G. *et al.* Probing the contribution of IKs to canine ventricular repolarization: key role for beta-adrenergic receptor stimulation. *Circulation* **107**, 2753-2760, doi:10.1161/01.CIR.0000068344.54010.B3 (2003).

240 Duchatelle-Gourdon, I., Hartzell, H. C. & Lagrutta, A. A. Modulation of the delayed rectifier potassium current in frog cardiomyocytes by beta-adrenergic agonists and magnesium. *J Physiol* **415**, 251-274 (1989).

241 Lei, M., Brown, H. F. & Terrar, D. A. Modulation of delayed rectifier potassium current, iK, by isoprenaline in rabbit isolated pacemaker cells. *Exp Physiol* **85**, 27-35 (2000).

242 Wong, W. & Scott, J. D. AKAP signalling complexes: focal points in space and time. *Nat Rev Mol Cell Biol* **5**, 959-970, doi:10.1038/nrm1527 (2004).

243 Marx, S. O. *et al.* Requirement of a macromolecular signaling complex for beta adrenergic receptor modulation of the KCNQ1-KCNE1 potassium channel. *Science* **295**, 496-499, doi:10.1126/science.1066843 (2002).

244 Imredy, J. P., Penniman, J. R., Dech, S. J., Irving, W. D. & Salata, J. J. Modeling of the adrenergic response of the human IKs current (hKCNQ1/hKCNE1) stably expressed in

HEK-293 cells. *Am J Physiol Heart Circ Physiol* **295**, H1867-1881, doi:10.1152/ajpheart.433.2008 (2008).

245 Consortium, E. P. The ENCODE (ENCyclopedia Of DNA Elements) Project. *Science* **306**, 636-640, doi:10.1126/science.1105136 (2004).

246 Kim, M. S. *et al.* A draft map of the human proteome. *Nature* **509**, 575-581, doi:10.1038/nature13302 (2014).

247 Bergmann, O. *et al.* Evidence for cardiomyocyte renewal in humans. *Science* **324**, 98-102, doi:10.1126/science.1164680 (2009).

248 Laflamme, M. A. *et al.* Cardiomyocytes derived from human embryonic stem cells in pro-survival factors enhance function of infarcted rat hearts. *Nat Biotechnol* **25**, 1015-1024, doi:10.1038/nbt1327 (2007).

249 Hasenfuss, G. Animal models of human cardiovascular disease, heart failure and hypertrophy. *Cardiovasc Res* **39**, 60-76 (1998).

250 Edwards, A. G. & Louch, W. E. Species-Dependent Mechanisms of Cardiac Arrhythmia: A Cellular Focus. *Clin Med Insights Cardiol* **11**, 1179546816686061, doi:10.1177/1179546816686061 (2017).

251 Knollmann, B. C. *et al.* Isoproterenol exacerbates a long QT phenotype in Kcnq1-deficient neonatal mice: possible roles for human-like Kcnq1 isoform 1 and slow delayed rectifier K+ current. *J Pharmacol Exp Ther* **310**, 311-318, doi:10.1124/jpet.103.063743 (2004).

252 Schwartz, P. J. *et al.* The Jervell and Lange-Nielsen syndrome: natural history, molecular basis, and clinical outcome. *Circulation* **113**, 783-790, doi:10.1161/CIRCULATIONAHA.105.592899 (2006).

253 Kehat, I. *et al.* Human embryonic stem cells can differentiate into myocytes with structural and functional properties of cardiomyocytes. *Journal of Clinical Investigation* **108**, 407-414, doi:Doi 10.1172/Jci12131 (2001).

254 Takahashi, K. *et al.* Induction of pluripotent stem cells from adult human fibroblasts by defined factors. *Cell* **131**, 861-872, doi:10.1016/j.cell.2007.11.019 (2007).

255 Burridge, P. W. *et al.* Chemically defined generation of human cardiomyocytes. *Nat Methods* **11**, 855-860, doi:10.1038/nmeth.2999 (2014).

256 Gao, L. *et al.* Myocardial Tissue Engineering With Cells Derived From Human-Induced Pluripotent Stem Cells and a Native-Like, High-Resolution, 3-Dimensionally Printed Scaffold. *Circ Res* **120**, 1318-1325, doi:10.1161/CIRCRESAHA.116.310277 (2017).

257 Karakikes, I., Ameen, M., Termglinchan, V. & Wu, J. C. Human induced pluripotent stem cell-derived cardiomyocytes: insights into molecular, cellular, and functional phenotypes. *Circ Res* **117**, 80-88, doi:10.1161/CIRCRESAHA.117.305365 (2015).

258 DeLaughter, D. M. *et al.* Single-Cell Resolution of Temporal Gene Expression during Heart Development. *Dev Cell* **39**, 480-490, doi:10.1016/j.devcel.2016.10.001 (2016).

259 Ribeiro, M. C. *et al.* Functional maturation of human pluripotent stem cell derived cardiomyocytes in vitro - Correlation between contraction force and electrophysiology. *Biomaterials* **51**, 138-150, doi:10.1016/j.biomaterials.2015.01.067 (2015).

260 Moretti, A. *et al.* Patient-specific induced pluripotent stem-cell models for long-QT syndrome. *The New England journal of medicine* **363**, 1397-1409, doi:10.1056/NEJMoa0908679 (2010).

261 Itzhaki, I. *et al.* Modelling the long QT syndrome with induced pluripotent stem cells. *Nature* **471**, 225-229, doi:10.1038/nature09747 (2011).

262 Wang, Z. *et al.* Functional effects of mutations in KvLQT1 that cause long QT syndrome. *J Cardiovasc Electr* **10**, 817-826, doi:DOI 10.1111/j.1540-8167.1999.tb00262.x (1999).

263 Nakajima, T. *et al.* Novel mechanism of HERG current suppression in LQT2: shift in voltage dependence of HERG inactivation. *Circ Res* **83**, 415-422 (1998).

264 Davis, R. P. *et al.* Cardiomyocytes derived from pluripotent stem cells recapitulate electrophysiological characteristics of an overlap syndrome of cardiac sodium channel disease. *Circulation* **125**, 3079-3091, doi:10.1161/CIRCULATIONAHA.111.066092 (2012).

265 Yazawa, M. *et al.* Using iPS cells to investigate cardiac phenotypes in patients with Timothy Syndrome. *Nature* **471**, 230-234 (2011).

266 Gilissen, C., Hoischen, A., Brunner, H. G. & Veltman, J. A. Disease gene identification strategies for exome sequencing. *Eur J Hum Genet* **20**, 490-497, doi:10.1038/ejhg.2011.258 (2012).

267 Pennisi, E. Genomics. 1000 Genomes Project gives new map of genetic diversity. *Science* **330**, 574-575, doi:10.1126/science.330.6004.574 (2010).

268 Davydov, E. V. *et al.* Identifying a High Fraction of the Human Genome to be under Selective Constraint Using GERP plus. *Plos Comput Biol* **6**, doi:ARTN e1001025 (2010).

269 Bagnall, R. D. *et al.* A Prospective Study of Sudden Cardiac Death among Children and Young Adults. *New England Journal of Medicine* **374**, 2441-2452, doi:10.1056/NEJMoa1510687 (2016).

270 Genomes Project, C. *et al.* A global reference for human genetic variation. *Nature* **526**, 68-74, doi:10.1038/nature15393 (2015).

271 Adzhubei, I. A. *et al.* A method and server for predicting damaging missense mutations. *Nat Methods* **7**, 248-249, doi:10.1038/nmeth0410-248 (2010).

272 Ng, P. C. & Henikoff, S. SIFT: predicting amino acid changes that affect protein function. *Nucleic Acids Research* **31**, 3812-3814, doi:10.1093/nar/gkg509 (2003).

273 Sanger, F., Nicklen, S. & Coulson, A. R. DNA sequencing with chain-terminating inhibitors. *Proc Natl Acad Sci U S A* **74**, 5463-5467 (1977).

274 Thomas, P. & Smart, T. G. HEK293 cell line: a vehicle for the expression of recombinant proteins. *J Pharmacol Toxicol Methods* **51**, 187-200, doi:10.1016/j.vascn.2004.08.014 (2005).

275 Gamper, N., Stockand, J. D. & Shapiro, M. S. The use of Chinese hamster ovary (CHO) cells in the study of ion channels. *Electrophysiological Methods in Neuropharmacology* **51**, 177-185 (2005).

276 Kim, T. K. & Eberwine, J. H. Mammalian cell transfection: the present and the future. *Anal Bioanal Chem* **397**, 3173-3178, doi:10.1007/s00216-010-3821-6 (2010).

277 Towbin, H., Staehelin, T. & Gordon, J. Electrophoretic Transfer of Proteins from Polyacrylamide Gels to Nitrocellulose Sheets - Procedure and Some Applications. *P Natl Acad Sci USA* **76**, 4350-4354, doi:DOI 10.1073/pnas.76.9.4350 (1979).

278 Hodgkin, A. L. & Huxley, A. F. A Quantitative Description of Membrane Current and Its Application to Conduction and Excitation in Nerve (Reprinted from Journal of Physiology, Vol 117, Pg 500-544, 1952). *B Math Biol* **52**, 25-71, doi:Doi 10.1007/Bf02459568 (1990).

279 Ling, G. & Gerard, R. W. The normal membrane potential of frog sartorius fibers. *J Cell Physiol* **34**, 383-396 (1949).

280 Sakmann, B., Patlak, J. & Neher, E. Single Acetylcholine-Activated Channels Show Burst-Kinetics in Presence of Desensitizing Concentrations of Agonist. *Nature* **286**, 71-73, doi:DOI 10.1038/286071a0 (1980).

281 Linley, J. E. Perforated whole-cell patch-clamp recording. *Methods Mol Biol* **998**, 149-157, doi:10.1007/978-1-62703-351-0_11 (2013).

282 Horn, R. & Marty, A. Muscarinic activation of ionic currents measured by a new whole-cell recording method. *J Gen Physiol* **92**, 145-159 (1988).

283 Rae, J., Cooper, K., Gates, P. & Watsky, M. Low Access Resistance Perforated Patch Recordings Using Amphotericin-B. *Journal of Neuroscience Methods* **37**, 15-26, doi:Doi 10.1016/0165-0270(91)90017-T (1991).

284 de Kruijff, B., Gerritsen, W. J., Oerlemans, A., Demel, R. A. & van Deenen, L. L. Polyene antibiotic-sterol interactions in membranes of Acholeplasma laidlawii cells and lecithin liposomes. I. Specificity of the membrane permeability changes induced by the polyene antibiotics. *Biochim Biophys Acta* **339**, 30-43 (1974).

285 Sarantopoulos, C., McCallum, J. B., Kwok, W. M. & Hogan, Q. Beta-escin diminishes voltage-gated calcium current rundown in perforated patch-clamp recordings from rat primary afferent neurons. *J Neurosci Methods* **139**, 61-68, doi:10.1016/j.jneumeth.2004.04.015 (2004).

286 Schmittgen, T. D. & Livak, K. J. Analyzing real-time PCR data by the comparative CT method. *Nat Protoc* **3**, 1101-1108 (2008).

287 Liu, Q. *et al.* Genome-Wide Temporal Profiling of Transcriptome and Open Chromatin of Early Cardiomyocyte Differentiation Derived From hiPSCs and hESCs. *Circ Res* **121**, 376-391, doi:10.1161/CIRCRESAHA.116.310456 (2017).

288 Wijsman, J. H. *et al.* A new method to detect apoptosis in paraffin sections: in situ end-labeling of fragmented DNA. *J Histochem Cytochem* **41**, 7-12, doi:10.1177/41.1.7678025 (1993).

289 Porrello, E. R. *et al.* MiR-15 family regulates postnatal mitotic arrest of cardiomyocytes. *Circ Res* **109**, 670-679, doi:10.1161/CIRCRESAHA.111.248880 (2011).

290 Somers A *et al.* Generation of transgene-free lung disease-specific human induced pluripotent stem cells using a single excisable lentiviral stem cell cassette. *Stem Cell* **28**, 1728-1740 (2010).

291 Okita, K. *et al.* A more efficient method to generate integration-free human iPS cells. *Nat Methods* **8**, 409-412, doi:10.1038/nmeth.1591 (2011).

292 Miller, D. C. *et al.* Ajmaline blocks I-Na and I-Kr without eliciting differences between Brugada syndrome patient and control human pluripotent stem cell-derived cardiac clusters. *Stem Cell Res* **25**, 233-244, doi:10.1016/j.scr.2017.11.003 (2017).

293 Watanabe, K. *et al.* A ROCK inhibitor permits survival of dissociated human embryonic stem cells. *Nat Biotechnol* **25**, 681-686, doi:10.1038/nbt1310 (2007).

294 Xu, C. *et al.* Feeder-free growth of undifferentiated human embryonic stem cells. *Nat Biotechnol* **19**, 971-974, doi:10.1038/nbt1001-971 (2001).

295 Blauwkamp, T. A., Nigam, S., Ardehali, R., Weissman, I. L. & Nusse, R. Endogenous Wnt signalling in human embryonic stem cells generates an equilibrium of distinct lineage-specified progenitors. *Nat Commun* **3**, 1070, doi:10.1038/ncomms2064 (2012).

296 Lian, X. J. *et al.* Directed cardiomyocyte differentiation from human pluripotent stem cells by modulating Wnt/beta-catenin signaling under fully defined conditions. *Nat Protoc* **8**, 162-175, doi:10.1038/nprot.2012.150 (2013).

297 Guo, S. & Kemphues, K. J. Par-1, a Gene Required for Establishing Polarity in C-Elegans Embryos, Encodes a Putative Ser/Thr Kinase That Is Asymmetrically Distributed. *Cell* **81**, 611-620, doi:Doi 10.1016/0092-8674(95)90082-9 (1995).

298 Fire, A. *et al.* Potent and specific genetic interference by double-stranded RNA in Caenorhabditis elegans. *Nature* **391**, 806-811, doi:10.1038/35888 (1998).

299 Zamore, P. D., Tuschl, T., Sharp, P. A. & Bartel, D. P. RNAi: Double-stranded RNA directs the ATP-dependent cleavage of mRNA at 21 to 23 nucleotide intervals. *Cell* **101**, 25-33, doi:Doi 10.1016/S0092-8674(00)80620-0 (2000).

300 Hermosura, M. C. *et al.* A TRPM7 variant shows altered sensitivity to magnesium that may contribute to the pathogenesis of two Guamanian neurodegenerative disorders. *Proceedings of the National Academy of Sciences* **102**, 11510-11515 (2005).

301 Dorovkov, M. V. & Ryazanov, A. G. Phosphorylation of annexin I by TRPM7 channel-kinase. *J Biol Chem* **279**, 50643-50646, doi:10.1074/jbc.C400441200 (2004).

302 Kerschbaum, H. H., Kozak, J. A. & Cahalan, M. D. Polyvalent cations as permeant probes of MIC and TRPM7 pores. *Biophys J* **84**, 2293-2305, doi:Doi 10.1016/S0006-3495(03)75035-8 (2003).

303 Chokshi, R., Fruasaha, P. & Kozak, J. A. 2-Aminoethyl diphenyl borinate (2-APB) inhibits TRPM7 channels through an intracellular acidification mechanism. *Channels* **6**, 362-369, doi:10.4161/chan.21628 (2012).

304 Romani, A. M. P. Cellular magnesium homeostasis. *Archives of Biochemistry and Biophysics* **512**, 1-23, doi:10.1016/j.abb.2011.05.010 (2011).

305 Abiria, S. A. *et al.* TRPM7 senses oxidative stress to release Zn2+ from unique intracellular vesicles. *Proc Natl Acad Sci U S A* **114**, E6079-E6088, doi:10.1073/pnas.1707380114 (2017).

306 Flockerzi, V. *et al.* Specific detection and semi-quantitative analysis of TRPC4 protein expression by antibodies. *Pflug Arch Eur J Phy* **451**, 81-86, doi:10.1007/s00424-005-1443-1 (2005).

307 Meissner, M. *et al.* Lessons of studying TRP channels with antibodies. (2011).

308 Chubanov, V. *et al.* Disruption of TRPM6/TRPM7 complex formation by a mutation in the TRPM6 gene causes hypomagnesemia with secondary hypocalcemia. *Proc Natl Acad Sci U S A* **101**, 2894-2899, doi:10.1073/pnas.0305252101 (2004).

309 Su, L. T. *et al.* TRPM7 regulates cell adhesion by controlling the calcium-dependent protease calpain. *J Biol Chem* **281**, 11260-11270, doi:10.1074/jbc.M512885200 (2006).

310 Furukawa, T. *et al.* Major SNP (Q141K) variant of human ABC transporter ABCG2 undergoes lysosomal and proteasomal degradations. *Pharm Res* **26**, 469-479, doi:10.1007/s11095-008-9752-7 (2009).

311 Kruse, M. *et al.* Impaired endocytosis of the ion channel TRPM4 is associated with human progressive familial heart block type I. *Journal of Clinical Investigation* **119**, 2737-2744, doi:10.1172/Jci38292 (2009).

312 Tipler, C. P. *et al.* Purification and characterization of 26S proteasomes from human and mouse spermatozoa. *Mol Hum Reprod* **3**, 1053-1060 (1997).

313 Lee, A. V., Gooch, J. L., Oesterreich, S., Guler, R. L. & Yee, D. Insulin-like growth factor I-induced degradation of insulin receptor substrate 1 is mediated by the 26S proteasome and blocked by phosphatidylinositol 3 '-kinase inhibition. *Mol Cell Biol* **20**, 1489-1496, doi:Doi 10.1128/Mcb.20.5.1489-1496.2000 (2000).

314 Ficker, E. *et al.* Retention in the endoplasmic reticulum as a mechanism of dominant-negative current suppression in human long QT syndrome. *Journal of Molecular and Cellular Cardiology* **32**, 2327-2337, doi:10.1006/jmcc.2000.1263 (2000).

315 Seamon, K. B., Padgett, W. & Daly, J. W. Forskolin: unique diterpene activator of adenylate cyclase in membranes and in intact cells. *Proc Natl Acad Sci U S A* **78**, 3363-3367 (1981).

316 Diviani, D., Dodge-Kafka, K. L., Li, J. & Kapiloff, M. S. A-kinase anchoring proteins: scaffolding proteins in the heart. *Am J Physiol Heart Circ Physiol* **301**, H1742-1753, doi:10.1152/ajpheart.00569.2011 (2011).

317 Jiang, M., Wang, Y. & Tseng, G. N. Adult Ventricular Myocytes Segregate KCNQ1 and KCNE1 to Keep the IKs Amplitude in Check Until When Larger IKs Is Needed. *Circ Arrhythm Electrophysiol* **10**, e005084 (2017).

318 Iost, N. *et al.* Delayed rectifier potassium current in undiseased human ventricular myocytes. *Cardiovasc Res* **40**, 508-515 (1998).

319 Virag, L. *et al.* The slow component of the delayed rectifier potassium current in undiseased human ventricular myocytes. *Cardiovasc Res* **49**, 790-797 (2001).

320 Smith, G., Hasson, K. & Clements, J. A. Effects of ascorbic acid and disodium edetate on the stability of isoprenaline hydrochloride injection. *J Clin Hosp Pharm* **9**, 209-215 (1984).

321 Bristow, M. R. *et al.* Beta-1-Adrenergic-Receptor and Beta-2-Adrenergic-Receptor Subpopulations in Nonfailing and Failing Human Ventricular Myocardium - Coupling of Both Receptor Subtypes to Muscle-Contraction and Selective Beta-1-Receptor down-Regulation in Heart-Failure-. *Circ Res* **59**, 297-309 (1986).

322 Minneman, K. P., Hegstrand, L. R. & Molinoff, P. B. The pharmacological specificity of beta-1 and beta-2 adrenergic receptors in rat heart and lung in vitro. *Mol Pharmacol* **16**, 21-33 (1979).

323 Friedman, J., Babu, B. & Clark, R. B. β2-Adrenergic Receptor Lacking the Cyclic AMP-Dependent Protein Kinase Consensus Sites Fully Activates Extracellular Signal-Regulated Kinase 1/2 in Human Embryonic Kidney 293 Cells: Lack of Evidence for Gs/Gi Switching. *Molecular Pharmacology* **62**, 1094-1102 (2002).

324 Daaka, Y., Luttrell, L. M. & Lefkowitz, R. J. Switching of the coupling of the β2-adrenergic receptor to different G proteins by protein kinase A. *Nature* **390**, 88-91 (1997).

325 Nicolas, C. S. *et al.* IKs response to protein kinase A-dependent KCNQ1 phosphorylation requires direct interaction with microtubules. *Cardiovasc Res* **79**, 427-435, doi:10.1093/cvr/cvn085 (2008).

326 Potet, F., Scott, J. D., Mohammad-Panah, R., Escande, D. & Baro, I. AKAP proteins anchor cAMP-dependent protein kinase to KvLQT1/IsK channel complex. *Am J Physiol Heart Circ Physiol* **280**, H2038-2045 (2001).

327 Medeiros-Domingo, A. *et al.* The RYR2-encoded ryanodine receptor/calcium release channel in patients diagnosed previously with either catecholaminergic polymorphic ventricular tachycardia or genotype negative, exercise-induced long QT syndrome: a

comprehensive open reading frame mutational analysis. *J Am Coll Cardiol* **54**, 2065-2074, doi:10.1016/j.jacc.2009.08.022 (2009).

328 Chambers, J. C. *et al.* Genetic variation in SCN10A influences cardiac conduction. *Nat Genet* **42**, 149-152, doi:10.1038/ng.516 (2010).

329 Hu, D. *et al.* Mutations in SCN10A are responsible for a large fraction of cases of Brugada syndrome. *J Am Coll Cardiol* **64**, 66-79, doi:10.1016/j.jacc.2014.04.032 (2014).

330 Le Scouarnec, S. *et al.* Testing the burden of rare variation in arrhythmia-susceptibility genes provides new insights into molecular diagnosis for Brugada syndrome. *Hum Mol Genet* **24**, 2757-2763, doi:10.1093/hmg/ddv036 (2015).

331 Faber, C. G. *et al.* Gain-of-function Nav1.8 mutations in painful neuropathy. *Proc Natl Acad Sci U S A* **109**, 19444-19449, doi:10.1073/pnas.1216080109 (2012).

332 Gouas, L. *et al.* New KCNQ1 mutations leading to haploinsufficiency in a general population; Defective trafficking of a KvLQT1 mutant. *Cardiovasc Res* **63**, 60-68, doi:10.1016/j.cardiores.2004.02.011 (2004).

333 Schroeder, B. C., Kubisch, C., Stein, V. & Jentsch, T. J. Moderate loss of function of cyclic-AMP-modulated KCNQ2/KCNQ3 K+ channels causes epilepsy. *Nature* **396**, 687-690, doi:10.1038/25367 (1998).

334 Thomas, S. A., Matsumoto, A. M. & Palmiter, R. D. Noradrenaline Is Essential for Mouse Fetal Development. *Nature* **374**, 643-646, doi:DOI 10.1038/374643a0 (1995).

335 Zhou, Q. Y., Quaife, C. J. & Palmiter, R. D. Targeted Disruption of the Tyrosine-Hydroxylase Gene Reveals That Catecholamines Are Required for Mouse Fetal Development. *Nature* **374**, 640-643, doi:DOI 10.1038/374640a0 (1995).

336 Okuda, H., Nakanishi, T., Nakazawa, M. & Takao, A. Effect of isoproterenol on myocardial mechanical function and cyclic AMP content in the fetal rabbit. *J Mol Cell Cardiol* **19**, 151-157 (1987).

337 Shigenobu, K., Tanaka, H. & Kasuya, Y. Changes in sensitivity of rat heart to norepinephrine and isoproterenol during pre- and postnatal development and its relation to sympathetic innervation. *Dev Pharmacol Ther* **11**, 226-236 (1988).

338 Bendahhou, S. *et al.* In vitro molecular interactions and distribution of KCNE family with KCNQ1 in the human heart. *Cardiovasc Res* **67**, 529-538, doi:10.1016/j.cardiores.2005.02.014 (2005).

339 Lek, M. *et al.* Analysis of protein-coding genetic variation in 60,706 humans. *Nature* **536**, 285-291, doi:10.1038/nature19057 (2016).

340 Sala, L. *et al.* A new hERG allosteric modulator rescues genetic and drug-induced long-QT syndrome phenotypes in cardiomyocytes from isogenic pairs of patient induced pluripotent stem cells. *EMBO Mol Med* **8**, 1065-1081, doi:10.15252/emmm.201606260 (2016).

341 Anderson, D. J. *et al.* NKX2-5 regulates human cardiomyogenesis via a HEY2 dependent transcriptional network. *Nat Commun* **9**, 1373, doi:10.1038/s41467-018-03714-x (2018).

342 Zhang, Y. H. *et al.* Evidence for functional expression of TRPM7 channels in human atrial myocytes. *Basic Res Cardiol* **107**, 282, doi:10.1007/s00395-012-0282-4 (2012).

343 Yu, J., Chau, K. F., Vodyanik, M. A., Jiang, J. & Jiang, Y. Efficient feeder-free episomal reprogramming with small molecules. *PLoS One* **6**, e17557, doi:10.1371/journal.pone.0017557 (2011).

344 Zhao, Y. *et al.* Two supporting factors greatly improve the efficiency of human iPSC generation. *Cell Stem Cell* **3**, 475-479, doi:10.1016/j.stem.2008.10.002 (2008).

345 Seki, T. *et al.* Generation of induced pluripotent stem cells from human terminally differentiated circulating T cells. *Cell Stem Cell* **7**, 11-14, doi:10.1016/j.stem.2010.06.003 (2010).

346 Kashyap, V. *et al.* Regulation of stem cell pluripotency and differentiation involves a mutual regulatory circuit of the NANOG, OCT4, and SOX2 pluripotency transcription factors with polycomb repressive complexes and stem cell microRNAs. *Stem Cells Dev* **18**, 1093-1108, doi:10.1089/scd.2009.0113 (2009).

347 Yang, X., Pabon, L. & Murry, C. E. Engineering adolescence: maturation of human pluripotent stem cell-derived cardiomyocytes. *Circ Res* **114**, 511-523, doi:10.1161/CIRCRESAHA.114.300558 (2014).

348 Ieda, M. *et al.* Direct Reprogramming of Fibroblasts into Functional Cardiomyocytes by Defined Factors. *Cell* **142**, 375-386, doi:10.1016/j.cell.2010.07.002 (2010).

349 Jorgensen, N. *et al.* Expression of immunohistochemical markers for testicular carcinoma in situ by normal human fetal germ cells. *Lab Invest* **72**, 223-231 (1995).

350 Badcock, G., Pigott, C., Goepel, J. & Andrews, P. W. The human embryonal carcinoma marker antigen TRA-1-60 is a sialylated keratan sulfate proteoglycan. *Cancer Res* **59**, 4715-4719 (1999).

351 Tohyama, S. *et al.* Glutamine Oxidation Is Indispensable for Survival of Human Pluripotent Stem Cells. *Cell Metab* **23**, 663-674, doi:10.1016/j.cmet.2016.03.001 (2016).

352 Turan, B. & Tuncay, E. Impact of Labile Zinc on Heart Function: From Physiology to Pathophysiology. *Int J Mol Sci* **18**, doi:10.3390/ijms18112395 (2017).

353 Ho, E., Courtemanche, C. & Ames, B. N. Zinc deficiency induces oxidative DNA damage and increases p53 expression in human lung fibroblasts. *J Nutr* **133**, 2543-2548, doi:10.1093/jn/133.8.2543 (2003).

354 Cao, R. *et al.* Decreased TRPM7 inhibits activities and induces apoptosis of bladder cancer cells via ERK1/2 pathway. *Oncotarget* **7**, 72941-72960, doi:10.18632/oncotarget.12146 (2016).

355 Lange, I., Espinoza-Fuenzalida, I., Ali, M. W., Serrano, L. E. & Koomoa, D. T. FTY-720 induces apoptosis in neuroblastoma via multiple signaling pathways. *Oncotarget* **8**, 109985-109999, doi:10.18632/oncotarget.22452 (2017).

356 Sehrawat, S. *et al.* AKAP9 regulation of microtubule dynamics promotes Epac1-induced endothelial barrier properties. *Blood* **117**, 708-718, doi:10.1182/blood-2010-02-268870 (2011).

357 Chrivia, J. C. *et al.* Phosphorylated CREB binds specifically to the nuclear protein CBP. *Nature* **365**, 855-859, doi:10.1038/365855a0 (1993).

358 Bartsch, O. *et al.* DNA sequencing of CREBBP demonstrates mutations in 56% of patients with Rubinstein-Taybi syndrome (RSTS) and in another patient with incomplete RSTS. *Human Genetics* **117**, 485-493, doi:DOI 10.1007/s00439-005-1331-y (2005).

359 Roelfsema, J. H. *et al.* Genetic heterogeneity in Rubinstein-Taybi syndrome: Mutations in both the CBP and EP300 genes cause disease. *Am J Hum Genet* **76**, 572-580, doi:Doi 10.1086/429130 (2005).

360 Mullighan, C. G. *et al.* CREBBP mutations in relapsed acute lymphoblastic leukaemia. *Nature* **471**, 235-239, doi:10.1038/nature09727 (2011).

361 McCormack, K. *et al.* Genetic analysis of the mammalian K+ channel β subunit Kvβ2 (Kcnab2). *Journal of Biological Chemistry* **277**, 13219-13228 (2002).

362 Norton, N. *et al.* Genome-wide Studies of Copy Number Variation and Exome Sequencing Identify Rare Variants in BAG3 as a Cause of Dilated Cardiomyopathy. *Am J Hum Genet* **88**, 273-282, doi:10.1016/j.ajhg.2011.01.016 (2011).

363 Maller, J. *et al.* Common variation in three genes, including a noncoding variant in CFH, strongly influences risk of age-related macular degeneration. *Nat Genet* **38**, 1055-1059, doi:10.1038/ng1873 (2006).

364 Ono, K. *et al.* A promoter variant of the heme oxygenase-1 gene may reduce the incidence of ischemic heart disease in Japanese. *Atherosclerosis* **173**, 315-319, doi:10.1016/j.atherosclerosis.2003.11.021 (2004).

365 Smemo, S. *et al.* Regulatory variation in a TBX5 enhancer leads to isolated congenital heart disease. *Hum Mol Genet* **21**, 3255-3263, doi:10.1093/hmg/dds165 (2012).

366 Cooper, G. M. & Shendure, J. Needles in stacks of needles: finding disease-causal variants in a wealth of genomic data. *Nat Rev Genet* **12**, 628-640, doi:10.1038/nrg3046 (2011).